

The vesicular trafficking protein PRA1  
domain family member 2 (PRAF2) is a  
novel cellular binding partner of the  
papillomavirus E5 proteins

David James Kealy

Submitted in accordance with the requirements for the degree of  
Doctor of Philosophy

The University of Leeds

School of Molecular and Cellular Biology

September 2019

The candidate confirms that the work submitted is his own and that appropriate credit has been given where reference has been made to the work of others.

This copy has been supplied on the understanding that it is copyright material and that no quotation from the thesis may be published without proper acknowledgement.

© 2019, The University of Leeds, David James Kealy

The right of David James Kealy to be identified as author of this work has been asserted by him in accordance with the Copyright, Designs and Patents Act 1988.

## Acknowledgements

Thank you to my supervisor Dr Andrew Macdonald for advice and guidance throughout my PhD and giving me freedom to pursue my research. I would also like to thank my co-supervisor Professor Nic Stonehouse for all her support, for acting as a second port of call, proofreading and helping arrange my PIPs. Thanks also go to Professor Eric Blair, for acting as my assessor, and always being available for a chat, coffee and biscuit. I also thank those who I have worked with throughout my PhD. Dr Stuart Armstrong of the University of Liverpool for performing the mass spectroscopy and its analysis, Dr Sally Boxall for invaluable help with flow cytometry and microscopy, and Dr Sally Roberts of the University of Birmingham for technical expertise, without which my primary cell work would not have been possible. Thanks also to Dr Toby Tuthill, Dr Lidia Lasecka, Dr Joseph Newman and Dr Jess Swanson, who made my PIPs at The Pirbright Institute a fun and fulfilling experience. I would also like to thank the University of Leeds and my funding body, the BBSRC, for allowing me to undertake this research.

To the current members of the Macdonald group, Michaella Antoni, Molly Patterson, Dr Ethan Morgan, Gemma Swinscoe and Corinna Brockhaus, for making the lab an enjoyable place to be. To the Greek from the East, Michaella, you have been a constant source of fun and valuable advice, both in and out of the lab! Thank you for putting up with me! Molly, never a dull day! To Ethan, thank you for the experimental help, advice and laughs. Corinna, I have enjoyed our conversations about Japan. I would also like to thank past members of the group, Dr Margarita Panou, Aniek Meijers and Dr Marietta Müller. I would also like to thank my past housemates Jim, Sophie, Dan, Raymond and Christian. You made life in Leeds much more interesting, thank you for all the shared laughs over the years.

A heartfelt thanks go to my family; Dad, Mum, Andrew, Tom, Gus and Gemma. Mum and Dad, thank you for putting up with the late-night phone calls, for always believing in me and being proud of me. I owe a large part of who I am to you. I would also like to thank my girlfriend

Emma. You have been a constant source of inspiration. Without you, I would not have made it through this PhD. Thank you for always listening to me, and for putting up with PhD induced grumpiness! I look forward to our future together.

## Abstract

Human papillomaviruses (HPVs) infect the epithelium and are responsible for a wide range of diseases, including nearly all cases of cervical cancer (CC) worldwide, and are increasingly recognised as aetiological agents for head and neck cancers. HPV encodes three oncoproteins, E5, E6 and E7. The E5 protein is known to be important in the HPV lifecycle, however, there remains a great deal to be elucidated about the E5 protein. A mass spectroscopy screen identified PRA1 Domain Family Member 2 (PRAF2) as a putative cellular binding partner of E5. Overexpression of PRAF2 is associated with a negative prognosis in hepatocellular carcinoma, glioblastoma and neuroblastoma and PRAF2 interacts with the anti-apoptotic Bcl-XL and Bcl-2 proteins.

I have used immunoprecipitation to confirm interaction between PRAF2 and E5, and the binding of PRAF2 to HPV-18E5 was mapped. PRAF2 expression was elevated in HPV-16 CC cells and HPV-16 positive CC biopsies; and loss of PRAF2 in HPV-16 CC cells resulted in a reduction in colony formation and migration, suggesting a possible role for PRAF2 as an oncogene. PRAF2 expression increased upon differentiation in normal human keratinocytes and those harbouring either wild type HPV-18 or E5 knockout genome. PRAF2 overexpression reduced the thickness of stratified epithelium in HPV-18 rafts and caused loss of HPV-18E1<sup>E4</sup> in E5 knockout rafts, suggesting E5-PRAF2 interaction is important to the viral lifecycle. The proapoptotic function of PRAF2 was investigated in CC cells, with conflicting results. A putative PRAF2 cellular interactome was established through a proximity dependent biotinylation for the first time, with many of the proteins identified also identified as putative HPV E5 protein interactors. These data may illuminate further studies into the function of the PRAF2 protein, and also help determine the nature of the interaction between E5 and PRAF2 and shed light on the cellular functions of E5 proteins.

## Table of Contents

|  |           |
|--|-----------|
| <b>Acknowledgements .....</b>  | <b>2</b>  |
| <b>Abstract.....</b>   | <b>4</b>  |
| <b>Table of Contents .....</b>                                       | <b>5</b>  |
| <b>List of Tables.....</b>   | <b>12</b> |
| <b>List of Figures .....</b>   | <b>13</b> |
| <b>Abbreviations .....</b>   | <b>18</b> |
| <b>Chapter 1 Introduction.....</b>                                   | <b>22</b> |
| <i>1.1 Papillomaviridae .....</i>                                    | <i>22</i> |
| 1.1.1 The natural history of papillomaviruses .....                  | 22        |
| 1.1.2 The classification of papillomaviruses .....                   | 23        |
| <i>1.2 HPV associated diseases .....</i>                             | <i>25</i> |
| 1.2.1 Cutaneous lesions .....  | 25        |
| 1.2.2 Mucosal lesions.....   | 27        |
| 1.2.3 Benign mucosal lesions.....                                    | 27        |
| 1.2.4 Malignant mucosal lesions.....                                 | 28        |
| <i>1.3 Transmission of HPV .....</i>                                 | <i>31</i> |
| 1.3.1 Cutaneous transmission.....                                    | 31        |
| 1.3.2 Mucosal transmission .....                                     | 31        |
| <i>1.4 Epidemiology of HPV.....</i>                                  | <i>32</i> |
| <i>1.5 Prevention and treatment of HPV associated diseases .....</i> | <i>35</i> |
| 1.5.1 Prevention.....  | 35        |
| 1.5.2 Treatment .....  | 38        |
| <i>1.6 Papillomavirus Virology .....</i>                             | <i>39</i> |
| 1.6.1 Genome organisation.....                                       | 39        |
| 1.6.2 Normal Epithelial Development.....                             | 41        |
| 1.6.3 The HPV lifecycle.....   | 48        |
| <i>1.7 Papillomavirus proteins .....</i>                             | <i>52</i> |
| 1.7.1 The E1 and E2 regulatory proteins.....                         | 52        |
| 1.7.2 The L1 and L2 structural proteins .....                        | 55        |

|                  |   |           |
|------------------|---|-----------|
| 1.7.3            | The E4 protein.....                               | 57        |
| 1.7.4            | The E6 protein.....                               | 58        |
| 1.7.5            | The E7 protein.....                               | 62        |
| 1.8              | <i>The E5 protein</i> .....                       | 65        |
| 1.8.1            | The natural history of E5.....                    | 65        |
| 1.8.2            | The cellular functions of E5.....                 | 66        |
| 1.9              | <i>The PRA family</i> .....                       | 73        |
| 1.9.1            | PRAF1.....  | 73        |
| 1.9.2            | PRAF3.....  | 76        |
| 1.9.3            | PRAF2.....  | 78        |
| 1.10             | <i>Project Aims</i> .....                         | 79        |
| <b>Chapter 2</b> | <b>Materials and Methods</b> .....                | <b>81</b> |
| 2.1              | <i>Bacterial Cell Culture</i> .....               | 81        |
| 2.1.1            | Bacterial cell growth.....                        | 81        |
| 2.1.2            | Preparation of chemically competent bacteria..... | 81        |
| 2.1.3            | Transformation of Bacteria.....                   | 81        |
| 2.1.4            | Miniprep (small scale).....                       | 82        |
| 2.1.5            | Maxiprep (large scale).....                       | 82        |
| 2.1.6            | Production of Glycerol Stocks.....                | 82        |
| 2.1.7            | Quantification of Plasmid DNA.....                | 83        |
| 2.2              | <i>Molecular cloning</i> .....                    | 83        |
| 2.2.1            | Plasmid DNA vectors and oligonucleotides.....     | 83        |
| 2.2.2            | PCR (Q5).....                                     | 83        |
| 2.2.3            | Agarose Gel Electrophoresis.....                  | 83        |
| 2.2.4            | Restriction endonuclease digest.....              | 84        |
| 2.2.5            | Shrimp alkaline phosphatase treatment.....        | 84        |
| 2.2.6            | DNA ligation.....                                 | 84        |
| 2.2.7            | Gibson assembly reaction.....                     | 85        |
| 2.2.8            | Screening of Clones.....                          | 85        |
| 2.2.9            | Sequencing.....                                   | 85        |
| 2.2.10           | Basic Bioinformatics.....                         | 86        |
| 2.3              | <i>Protein biochemistry</i> .....                 | 86        |
| 2.3.1            | Cell lysis.....                                   | 86        |

|        |  |    |
|--------|--|----|
| 2.3.2  | Protein bicinchoninic acid assay (BCA) for protein concentration ..... | 86 |
| 2.3.3  | Extraction of protein from cytology samples.....                       | 87 |
| 2.3.4  | SDS polyacrylamide gel electrophoresis (SDS-PAGE).....                 | 88 |
| 2.3.5  | Western Blotting .....   | 88 |
| 2.3.6  | Densitometry .....   | 89 |
| 2.4    | <i>Mammalian cell culture</i> .....                                    | 89 |
| 2.4.1  | Cell Culture.....  | 89 |
| 2.4.2  | Culture of transformed and cancer cell lines.....                      | 90 |
| 2.4.3  | Selection of the HEK293TT cell line.....                               | 90 |
| 2.4.4  | Selection of the Phoenix A cell line .....                             | 90 |
| 2.4.5  | Freezing of cell lines.....  | 90 |
| 2.4.6  | Thawing of cell lines.....   | 91 |
| 2.4.7  | Transient transfection with polyethylenimine (PEI) .....               | 91 |
| 2.4.8  | Transient transfection with Lipofectamine 2000.....                    | 91 |
| 2.4.9  | Transfection of siRNA with Lipofectamine 2000.....                     | 92 |
| 2.4.10 | Production of retrovirus.....  | 92 |
| 2.4.11 | Production of 2 <sup>nd</sup> generation lentivirus .....              | 93 |
| 2.4.12 | Production of 3 <sup>rd</sup> generation lentivirus.....               | 93 |
| 2.4.13 | Infection with virus .....   | 94 |
| 2.4.14 | Production of polyclonal cell lines .....                              | 94 |
| 2.4.15 | Production of monoclonal cell lines.....                               | 94 |
| 2.5    | <i>Culture of Primary Keratinocytes</i> .....                          | 95 |
| 2.5.1  | Culture of normal human keratinocytes.....                             | 95 |
| 2.5.2  | Freezing of NHKs .....   | 96 |
| 2.5.3  | Thawing NHKs .....   | 96 |
| 2.5.4  | Thawing of J2 3T3.....   | 96 |
| 2.5.5  | Culture of J2 3T3 mouse fibroblasts .....                              | 96 |
| 2.5.6  | Mitomycin C treatment of J2 3T3 mouse fibroblasts.....                 | 97 |
| 2.5.7  | Freezing of J2 3T3 mouse fibroblasts.....                              | 98 |
| 2.5.8  | Production of HPV positive primary keratinocytes.....                  | 98 |
| 2.5.9  | Culture of HPV positive primary keratinocytes.....                     | 98 |
| 2.5.10 | Freezing of HPV positive primary keratinocytes .....                   | 99 |
| 2.5.11 | Thawing of HPV positive primary keratinocytes.....                     | 99 |
| 2.5.12 | Keratinocyte monolayer high-calcium differentiation.....               | 99 |

|        |   |     |
|--------|---|-----|
| 2.5.13 | Lysis of HPV positive primary keratinocytes .....                         | 100 |
| 2.6    | <i>Raft Cultures</i> .....  | 100 |
| 2.6.1  | Production of PRAF2 overexpression primary cell lines .....               | 100 |
| 2.6.2  | Production of PRAF2 knockdown primary cell lines .....                    | 100 |
| 2.6.3  | Production of collagen plugs.....   | 101 |
| 2.6.4  | Seeding of collagen plugs with primary keratinocytes and rafting.....     | 101 |
| 2.7    | <i>Immunofluorescence</i> .....   | 102 |
| 2.7.1  | Cell growth on coverslips .....   | 102 |
| 2.7.2  | Fixation and permeabilisation of cells .....                              | 102 |
| 2.7.3  | Immuno-labelling .....  | 102 |
| 2.7.4  | Microscopy.....   | 102 |
| 2.7.5  | Colocalisation analysis .....   | 103 |
| 2.8    | <i>Immunofluorescent immunohistochemistry</i> .....                       | 103 |
| 2.8.1  | ALTER (Agitated low temperature epitope retrieval) antigen retrieval..... | 103 |
| 2.8.2  | Raft section staining for immunofluorescence .....                        | 103 |
| 2.9    | <i>Co-immunoprecipitation</i> .....                                       | 104 |
| 2.9.1  | Cell lysis for co-immunoprecipitation .....                               | 104 |
| 2.9.2  | GFP-trap co-immunoprecipitation.....                                      | 104 |
| 2.10   | <i>Flow cytometry</i> .....   | 104 |
| 2.10.1 | Determination of cell cycle phase by propidium iodide staining.....       | 104 |
| 2.10.2 | Cell surface EGFR assay.....  | 105 |
| 2.11   | <i>Cancer cell assays</i> .....   | 105 |
| 2.11.1 | Colony formation assays .....   | 105 |
| 2.11.2 | Soft agar assays.....   | 106 |
| 2.11.3 | Growth curve assays .....   | 106 |
| 2.11.4 | Wound healing assays.....   | 106 |
| 2.12   | <i>Apoptosis assays</i> .....   | 106 |
| 2.12.1 | DNA laddering.....  | 106 |
| 2.12.2 | Active caspase-3 staining .....   | 108 |
| 2.12.3 | Annexin V staining assay .....  | 108 |
| 2.13   | <i>BiOD</i> .....   | 109 |
| 2.13.1 | Generation of BiOD cell lines.....  | 109 |

|   |  |            |
|---|--|------------|
| 2.13.2  | Induction of biotinylation .....   | 109        |
| 2.13.3  | Visualisation of biotinylated proteins by Streptavidin HRP .....   | 110        |
| 2.13.4  | Visualisation of biotinylated proteins by immunofluorescence .....   | 110        |
| 2.13.5  | BioID pulldown .....   | 111        |
| 2.14  | <i>Mass spectroscopy (MS)</i> .....  | 112        |
| 2.14.1  | On bead digestion .....  | 112        |
| 2.14.2  | TMT labelling.....   | 114        |
| 2.14.3  | LC MS/MS analysis .....  | 114        |
| 2.14.4  | Analysis of MS data .....  | 115        |
| <b>Chapter 3 The interaction of PRAF2 with HPV .....</b>              |  | <b>116</b> |
| 3.1   | <i>Introduction</i> .....  | 116        |
| 3.1.1   | The E5 protein.....  | 116        |
| 3.1.2   | The PRAF2 protein .....  | 117        |
| 3.1.2   | The localisation of PRAF2.....   | 118        |
| 3.2   | <i>Results</i> .....   | 120        |
| 3.2.1   | Confirming the interaction of PRAF2 and HPV18E5 .....  | 120        |
| 3.2.2   | The amino acids 135-160 are essential for PRAF2 binding to HPV18E5 .....   | 122        |
| 3.2.3   | PRAF2 localises to primarily to the ER .....   | 126        |
| 3.2.4   | Mutation of PRAF2 and its effect on subcellular localisation .....   | 129        |
| 3.2.5   | Mutation of PRAF2 does not alter co-localisation with GFP-18E5 .....   | 134        |
| 3.2.6   | The subcellular localisation of PRAF1 and PRAF3 .....  | 139        |
| 3.2.7   | The interaction of HPV18E5 is conserved between PRAF family members .....  | 142        |
| 3.2.8   | The interaction of PRAF2 and E5 is conserved across Papillomavirus types .....   | 144        |
| 3.2.9   | PRAF2 did not interact with other HPV18 early proteins .....   | 146        |
| 3.2.10  | HPV18 oncoproteins do not affect PRAF2 protein expression levels .....   | 149        |
| 3.2.11  | HPV16 positive cancer cell lines maintain PRAF2 expression and it is lost in HPV18<br>positive cancer cell lines ..... | 150        |
| 3.3   | <i>Discussion</i> .....  | 151        |
| <b>Chapter 4 PRAF2, cancer and keratinocyte differentiation .....</b> |  | <b>157</b> |
| 4.1   | <i>Introduction</i> .....  | 157        |
| 4.1.1   | PRAF2 and cancer .....   | 157        |
| 4.1.2   | The PRAF family- trafficking and signalling .....  | 159        |
| 4.1.3   | The PRAF proteins and differentiation .....  | 160        |

|  |  |            |
|--|--|------------|
| 4.2  | <i>Results</i> .....   | 162        |
| 4.2.1  | PRAF2 did not alter EGFR cell surface expression in cervical cancer cell lines .....                                     | 162        |
| 4.2.2  | PRAF2 did not alter cell cycle progression in cervical cancer cell lines .....   | 168        |
| 4.2.3  | Loss of PRAF2 expression impaired the ability of SiHa to form colonies.....  | 172        |
| 4.2.4  | PRAF2 overexpression enhanced proliferation in C33A cells .....  | 174        |
| 4.2.5  | PRAF2 knockdown impairs wound closure by SiHa cells .....  | 175        |
| 4.2.6  | PRAF2 protein expression was increased in high grade HPV-16 positive cervical lesions.....                               | 177        |
| 4.2.7  | PRAF2 expression was increased upon differentiation in monolayer culture of HPV negative and positive keratinocytes..... | 179        |
| 4.2.8  | PRAF2 localisation and expression was not altered by the loss of HPV-18E5 in organotypic raft cultures .....             | 182        |
| 4.2.9  | PRAF2 overexpression reduced raft thickness in both WT18 and E5KO rafts.....   | 186        |
| 4.2.10   | PRAF2 overexpression resulted in the loss of E1 <sup>E4</sup> expression in E5KO organotypic rafts .....                 | 190        |
| 4.2.11   | PRAF2 overexpression and knockdown did not alter the expression and distribution of CK10.....                            | 191        |
| 4.3  | <i>Discussion</i> .....  | 194        |
| <b>Chapter 5 Investigation of the role of PRAF2 in apoptosis .....</b> |  | <b>200</b> |
| 5.1  | <i>Introduction</i> .....  | 200        |
| 5.1.1  | The PRAF proteins and Apoptosis.....   | 200        |
| 5.2  | <i>Results</i> .....   | 203        |
| 5.2.1  | PRAF2 titration into keratinocytes resulted in PARP cleavage in a dose-dependent manner .....                            | 203        |
| 5.2.2  | Induction of apoptosis could not be demonstrated by other methods .....  | 205        |
| 5.2.3  | GFP-18E5 co-expression abrogates PRAF2 mediated PARP cleavage .....  | 209        |
| 5.2.4  | PRAF2 knockdown and overexpression is tolerated by stable cell lines .....   | 211        |
| 5.2.5  | The localisation of PRAF2 and changes to cellular morphology .....   | 212        |
| 5.3  | <i>Discussion</i> .....  | 216        |
| <b>Chapter 6 Investigating the PRAF2 interactome by BioID .....</b>    |  | <b>222</b> |
| 6.1  | <i>Introduction</i> .....  | 222        |
| 6.1.1  | The PRAF2 interactome .....  | 222        |
| 6.2  | <i>Results</i> .....   | 225        |

|                           |  |            |
|---------------------------|--|------------|
| 6.2.1                     | Fusion of PRAF2 to GFP does not alter subcellular localisation.....                        | 225        |
| 6.2.2                     | Myc-BioID2-PRAF2 does not display altered localisation relative to GFP fusions             | 226        |
| 6.2.3                     | The Myc-BioID2-PRAF2 fusion is functional and displays the ability to biotinylate<br>..... | 228        |
| 6.2.4                     | Streptavidin Immunoprecipitation successfully precipitated biotinylated proteins<br>.....  | 234        |
| 6.2.5                     | Mass spectroscopy successfully identifies putative proximal partners for PRAF2             | 236        |
| 6.3                       | <i>Discussion</i> .....  | 241        |
| 6.3.1                     | The proximal protein interactors of PRAF2 .....  | 241        |
| <b>Chapter 7</b>          | <b>Final discussion and summary .....</b>  | <b>252</b> |
| <b>Appendices</b> .....   |  | <b>256</b> |
|                           | <i>Appendix A Supplementary reagent tables</i> .....                                       | 256        |
|                           | <i>Appendix B Supplementary methods</i> .....  | 266        |
| B.1                       | Mitochondrial staining with Mitotracker CMXRos .....                                       | 266        |
|                           | <i>Appendix C Supplementary figures</i> .....  | 267        |
| <b>Bibliography</b> ..... |  | <b>270</b> |

## List of Tables

|            |  |     |
|------------|--|-----|
| Table 2.1  | List of components in complete E-media.....  | 97  |
| Table 6.1  | Potential PRAF2 proximal interaction partners determined by TMT MS. ....             | 239 |
| Table 6.2  | Comparison of BioID2-PRAF2 hits to DNA tumour virus oncoprotein TAP-MS data<br>..... | 251 |
| Table A. 1 | Cloning of constructs used in this study.....  | 256 |
| Table A. 2 | Primers for triple FLAG tagging .....  | 258 |
| Table A. 3 | Plasmids used in this study. ....  | 259 |
| Table A. 4 | Antibody reagents used in this study.....  | 262 |
| Table A. 5 | Secondary antibody reagents and fluorescent conjugates used in this study...         | 264 |
| Table A. 6 | Cell lines used in this study .....  | 264 |
| Table A. 7 | TMT sample labels.....   | 265 |

## List of Figures

|             |  |     |
|-------------|--|-----|
| Figure 1.1  | The phylogeny of human papillomaviruses (adapted from (Mühr et al., 2018)).  | 24  |
| Figure 1.2  | Number of cancer cases attributable to HPV worldwide in 2012 by anatomical site. ....  | 29  |
| Figure 1.3  | Histological images of CIN progression from CIN1 through to CIN3 adapted from (Cubie, 2013). ....  | 30  |
| Figure 1.4  | Age standardised rates of incidence and mortality of cervical cancer 2018, all sexes and ages. Adapted from (Ferlay et al., 2018). ....  | 33  |
| Figure 1.5  | Age standardised rates of incidence for oesophagus, oropharynx, larynx, lip, oral cavity and salivary gland cancers, all sexes and ages 2018, adapted from (Ferlay et al., 2018). .... | 35  |
| Figure 1.6  | Genome organisation of HPV18. ....   | 40  |
| Figure 1.7  | The epidermal differentiation programme of a basal keratinocyte (adapted from (Fuchs, 2008)). ....   | 41  |
| Figure 1.8  | Schematic model of asymmetric division within the epithelium, and the possible mechanism. ....   | 43  |
| Figure 1.9  | Cell signalling events crucial to epithelial development. ....   | 45  |
| Figure 1.10 | Schematic of Notch signalling in the keratinocyte. ....  | 47  |
| Figure 1.11 | Schematic of the epithelial stratification and HPV lifecycle and HPV gene expression. ....   | 51  |
| Figure 1.12 | Schematic diagram of the high-risk HPV-16 E6 oncoprotein (from (Tomaić, 2016))<br>.....  | 59  |
| Figure 1.13 | Schematic diagram of the high-risk HPV-16 E7 oncoprotein (from (Tomaić, 2016))<br>.....  | 63  |
| Figure 3.1  | Co-immunoprecipitation confirmed the interaction between PRAF2 and HPV18E5<br>.....  | 121 |

|             |   |     |
|-------------|---|-----|
| Figure 3.2  | Schematic of the PRAF2 truncation mutants .....   | 123 |
| Figure 3.3  | PRAF2 requires amino acids 135-160 to bind to HPV18E5 .....   | 125 |
| Figure 3.4  | Subcellular organelle marker localisation in untreated HeLa cells .....   | 126 |
| Figure 3.5  | Subcellular localisation of overexpressed PRAF2-3HA in HeLa cells .....   | 128 |
| Figure 3.6  | Co-localisation of C-terminal PRAF2 mutants with calnexin .....   | 130 |
| Figure 3.7  | Co-localisation of C-terminal PRAF2 mutants with GM130 .....  | 131 |
| Figure 3.8  | Co-localisation of N-terminal PRAF2 mutants with calnexin .....   | 132 |
| Figure 3.9  | Co-localisation of N-terminal PRAF2 mutants with GM130 .....  | 133 |
| Figure 3.10 | GFP-18E5 co-localises with the ER marker calnexin .....   | 135 |
| Figure 3.11 | GFP-18E5 did not appear to co-localise with GM130 .....   | 136 |
| Figure 3.12 | Co-localisation of amino-terminal PRAF2 mutants with GFP-18E5 .....   | 137 |
| Figure 3.13 | Co-localisation of C-terminal PRAF2 mutants with GFP-18E5 .....   | 138 |
| Figure 3.14 | PRAF1 and PRAF3 localise with the ER marker calnexin .....  | 140 |
| Figure 3.15 | PRAF1 and PRAF3 co-localise with the cis-Golgi marker GM130 .....   | 141 |
| Figure 3.16 | Localisation of PRAF1 and PRAF3 with the trans-Golgi marker TGN46 .....   | 142 |
| Figure 3.17 | PRAF1 and PRAF3 co-localise with GFP-18E5 .....   | 142 |
| Figure 3.18 | The interaction of HPV-18E5 with the PRA family is conserved .....  | 143 |
| Figure 3.19 | The interaction between PRAF2 and E5 is conserved amongst E5 types and genera<br>.....  | 146 |
| Figure 3.20 | The interaction of PRAF2 is limited to only E5 of the E-proteins .....  | 147 |
| Figure 3.21 | HPV-18E5 is the only HPV-18 oncoprotein interacting partner of PRAF2 .....  | 148 |
| Figure 3.22 | Overexpression of GFP-tagged HPV18 Oncoproteins and did not alter<br>endogenous PRAF2 expression .....  | 149 |
| Figure 3.23 | PRAF2 is expressed by HPV negative and HPV-16 positive cervical cancer cell<br>lines but not HPV-18 positive cervical cancer cell lines ..... | 150 |
| Figure 4.1  | EGFR levels are unaffected by changes in PRAF2 in cervical cancer cell lines. ...   | 163 |

|             |   |     |
|-------------|---|-----|
| Figure 4.2  | Flow cytometry detected cell surface EGFR in a specific manner .....  | 165 |
| Figure 4.3  | Cell surface EGFR expression was not altered by changes in PRAF2 expression   | 167 |
| Figure 4.4  | PRAF2 knockdown in C33A and SiHa cells did not alter cyclin expression .....  | 168 |
| Figure 4.5  | Transiently and stably expressed PRAF2 did not alter cyclin expression in C33A<br>and HeLa cells.....                                       | 170 |
| Figure 4.6  | Alterations in PRAF2 expression did not alter cell cycle progression in cervical<br>cancer cell lines. ....                                 | 171 |
| Figure 4.7  | Colony formation of SiHa but not C33A or HeLa cells was impaired by alterations<br>to PRAF2 expression.....                                 | 173 |
| Figure 4.8  | PRAF2 knockdown did not affect C33A or SiHa cell growth rates, however<br>overexpression increased growth in C33A but not HeLa cells.....   | 175 |
| Figure 4.9  | Wound healing was impaired in SiHa cells but not C33A or HeLa cells by<br>alterations to PRAF2 expression .....                             | 177 |
| Figure 4.10 | PRAF2 protein expression is increased in high grade cervical lesions positive for<br>HPV-16.....  | 178 |
| Figure 4.11 | PRAF2 expression increases with high calcium mediated differentiation in NHKs,<br>WT18 and E5KO keratinocyte cell lines.....                | 180 |
| Figure 4.12 | PRAF2 expression and distribution was not altered by the loss of HPV-18E5 in<br>HPV18 positive raft cultures.....                           | 183 |
| Figure 4.13 | Reduced PRAF2 staining was detected in WT18 and E5KO shRNA raft sections  | 185 |
| Figure 4.14 | FLAG was successfully detected in the basal and suprabasal layers of 3xFLAG-<br>PRAF2 rafts .....   | 186 |
| Figure 4.15 | A significant increase in the thickness of the stratified epithelium was observed<br>in both WT18 and E5KO shPRAF2 raft sections. ....      | 187 |
| Figure 4.16 | A significant reduction in the thickness of the stratified epithelium was observed<br>in both WT18 and E5KO 3xFLAG-PRAF2 raft sections..... | 189 |

|             |   |     |
|-------------|---|-----|
| Figure 4.17 | NHK rafts exhibited a failure to stratify as determined by H&E staining.....  | 190 |
| Figure 4.18 | HPV-18E1 <sup>E4</sup> staining was lost in 3xFLAG-PRAF2 E5KO raft sections .....   | 191 |
| Figure 4.19 | No changes in CK10 staining were observed between WT18 PRAF2 knockout and overexpression rafts when compared to controls. ....                                  | 192 |
| Figure 4.20 | Increased CK10 staining was observed in PRAF2 overexpression but not knockdown in E5KO raft sections.....   | 193 |
| Figure 5.1  | PRAF2-3HA expression induces PARP cleavage in a dosage dependent manner .....   | 204 |
| Figure 5.2  | PRAF2-3HA overexpression failed to induce detectable caspase-3 cleavage....   | 206 |
| Figure 5.3  | Active caspase-3 antibody stained the nuclei of non-apoptotic HeLa cells.....   | 207 |
| Figure 5.4  | DNA laddering and Annexin V assays did not detect a significant increase in cell death between pcDNA3 and PRAF2 transfected cells .....                         | 208 |
| Figure 5.5  | Coexpression of GFP-18E5 with PRAF2-3HA prevented PARP cleavage.....  | 210 |
| Figure 5.6  | Stable overexpression of PRAF2 in C33A cells did not increase levels of PARP cleavage and PRAF2 knockdown did not desensitise C33A cells to staurosporine ..... | 212 |
| Figure 5.7  | High levels of GFP-PRAF2 expression result in the redistribution of calnexin to puncta.....   | 213 |
| Figure 5.8  | PRAF2 staining in mitomycin C treated 3T3 cells resembles mitochondrial staining in C33A cells.....   | 214 |
| Figure 6.1  | GFP fusion of PRAF2 did not alter its subcellular localisation.....   | 225 |
| Figure 6.2  | Schematic of the BioID workflow .....   | 226 |
| Figure 6.3  | Myc-BioID2-PRAF2 colocalised with the ER marker PDI .....   | 227 |
| Figure 6.4  | Myc-BioID2-PRAF2 colocalised with the ER marker calnexin .....  | 228 |
| Figure 6.5  | The BioID2 fusion protein retained the ability to bind HPV-18E5 and was able to biotinylate proximal proteins.....  | 230 |

|             |  |     |
|-------------|--|-----|
| Figure 6.6  | The addition of 50 $\mu$ M biotin resulted in biotinylation of proteins and the biotinylated proteins co-localised with their respective BioID2 constructs ..... | 232 |
| Figure 6.7  | Biotinylated proteins colocalised with the BioID2 constructs .....   | 233 |
| Figure 6.8  | Biotin titration into C33A BioID cell lines resulted in increased biotinylation until saturation at 0.1 $\mu$ M biotin .....                                     | 234 |
| Figure 6.9  | Biotinylated proteins were successfully immunoprecipitated by streptavidin pulldowns .....   | 236 |
| Figure 6.10 | Protein intensity clustering of BioID2 samples .....   | 238 |
| Figure 6.11 | Schematic of the BioID2-PRAF2 protein fusion biotinylating proximal proteins   | 242 |
| Figure 6.12 | STRING analysis of proximal interactors of PRAF2 identified by BioID2 .....  | 244 |
| Figure A. 1 | PRA family protein sequence alignment .....  | 267 |
| Figure A. 2 | Alignment of PRAF2 mutants against the WT PRAF2 sequence .....   | 268 |
| Figure A. 3 | Endogenous PRAF2 was not detected by immunofluorescence in a specific manner by the PRAF2 antibody.....  | 268 |
| Figure A. 4 | Proteins from the Ras family could immunoprecipitate PRAF2.....  | 269 |

## Abbreviations

|                   |   |
|-------------------|---|
| °C                | Degrees Celsius                             |
| A                 | Amp   |
| ALTER             | Agitated low temperature epitope retrieval  |
| AsO <sub>3</sub>  | Arsenic trioxide                            |
| ATM               | Ataxia-telangiectasia mutated               |
| BCA               | Bicinchoninic acid                          |
| BER               | Base excision repair                        |
| BLAST             | Basic local alignment search tool           |
| BM                | Basement membrane                           |
| Bp                | Base pair                                   |
| BS                | Binding site                                |
| BSA               | Bovine serum albumin                        |
| Ca                | Calcium                                     |
| CaCl <sub>2</sub> | Calcium Chloride                            |
| CBM               | Cyclin binding motif                        |
| CC                | Cervical cancer                             |
| c-Cbl             | c-Casitas B-Linageage Lymphoma              |
| CDK2              | Cyclin dependent kinase 2                   |
| CIN               | Cervical intraepithelial neoplasia          |
| CK                | Cytokeratin                                 |
| CO <sub>2</sub>   | Carbon Dioxide                              |
| cSCC              | Cutaneous squamous cell carcinoma           |
| C-terminus        | Carboxyl-terminus                           |
| CTL               | Cytotoxic T-lymphocytes                     |
| Da                | Daltons                                     |
| DAPI              | 4',6-diamidino-2-phenylindole               |
| DBD               | DNA binding domain                          |
| DKK1              | Dickkopf WNT signalling pathway inhibitor 1 |
| DMEM              | Dulbecco's modified Eagle's medium          |
| DMSO              | Dimethyl sulfoxide                          |
| DNA               | Deoxyribonucleic acid                       |
| dNTP              | Deoxyribonucleotide triphosphate            |
| ds                | Double stranded                             |
| DTI               | Defined trypsin inhibitor                   |
| DTT               | Dithiothreitol                              |
| E                 | Early                                       |
| E5KO              | E5 knockout                                 |
| EAAC1             | Excitatory amino-acid carrier-1             |
| EBV               | Epstein-Barr Virus                          |
| EDTA              | Ethylenediamine tetraacetic acid            |
| EE                | Early endosomes                             |
| EGF               | Epidermal growth factor                     |
| EGFR              | Epidermal growth factor receptor            |
| EMT               | Epithelial-to-mesenchymal                   |
| ER                | Endoplasmic reticulum                       |
| ERK               | Extracellular-signal-regulated kinase       |
| EV                | Epidermodysplasia verruciformis             |
| FA                | Focal adhesion                              |
| FABP5             | Fatty acid binding protein-5                |

|                  |  |
|------------------|--|
| FAK              | Focal adhesion kinase                              |
| FBS              | Fetal bovine serum                                 |
| FCS              | Fetal calf serum                                   |
| FGFR             | Fibroblast growth factor receptor                  |
| G                | Growth   |
| GA               | Golgi apparatus                                    |
| GDE1             | Glycerophosphodiester Phosphodiesterase 1          |
| gDNA             | Genomic DNA  |
| GFP              | Green fluorescent protein                          |
| GW               | Genital warts                                      |
| H <sub>2</sub> O | Water  |
| HBSS             | Hanks balanced salt solution                       |
| HEPES-BSS        | HEPES-buffered saline solution                     |
| HIV              | Human immunodeficiency virus                       |
| HNC              | Head and neck cancer                               |
| HPV              | Human papillomavirus                               |
| Hsc70            | Heat shock cognate protein 70                      |
| HSIL             | High-grade squamous intraepithelial lesion         |
| HSPG             | Heparan sulphate proteoglycans                     |
| HUVEC            | Human umbilical vein endothelial cell              |
| Hygro            | Hygromycin   |
| ICTV             | International Committee on Taxonomy of Viruses     |
| IFN              | Interferon   |
| ILV              | Intralumenal vesicle                               |
| ISG              | Interferon stimulated genes                        |
| ISH              | Fluorescent <i>in situ</i> hybridisation           |
| Kb               | Kilobase   |
| KBM              | Keratinocyte basal medium                          |
| kDa              | Kilodaltons  |
| KGFR             | Keratinocyte growth factor receptor                |
| KGM              | Keratinocyte growth medium                         |
| KLK8             | Kallikrein-8                                       |
| L                | Late   |
| LB               | Luria-Bertani                                      |
| LC               | Liquid chromatography                              |
| LCR              | Long coding region                                 |
| LE               | Late endosomes                                     |
| LIC              | Low-income countries                               |
| LL/NETZ          | Loop or needle excision of the transformation zone |
| LSIL             | Low-grade squamous intraepithelial lesion          |
| M                | Mitosis  |
| M                | Molar  |
| MAM              | Mitochondrially associated ER membrane             |
| MAPKK            | Mitogen activated kinase kinase                    |
| MDM2             | Mouse double minute 2 homologue protein            |
| Mg               | Milligram  |
| MHC              | Major histocompatibility complex                   |
| min              | Minutes  |
| ml               | Millilitres  |
| mM               | Millimolar   |
| MMPs             | Matrix metalloproteinases                          |

|            |  |
|------------|--|
| mRNA       | Messenger RNA  |
| MS         | Mass spectrometry  |
| MSM        | Men who have sex with men  |
| MSP        | Major sperm protein  |
| MVB        | Multivesicular body  |
| Mya        | Million years ago  |
| NaCl       | Sodium Chloride  |
| NDRG       | N-myc downstream regulated gene  |
| NE         | Nuclear envelope   |
| NES        | Nuclear export signal  |
| ng         | Nanogram   |
| NGS        | Normal goat serum  |
| NHK        | Normal human keratinocytes   |
| NICD       | Notch intracellular domain   |
| NK         | Natural killer   |
| NLS        | Nuclear localisation signal  |
| nM         | Nanomolar  |
| N-terminus | Amino-terminus   |
| OPSCC      | Oropharyngeal squamous cell carcinoma  |
| ORF        | Open reading frame   |
| <i>Ori</i> | Origin of replication  |
| PANTHER    | Protein annotation through evolutionary relationship   |
| PBS        | Phosphate buffered saline  |
| PDZ        | Post synaptic density protein, drosophila disc large tumour suppressor, zonula occuldens-1 protein |
| PE         | Early promoter   |
| PFA        | Paraformaldehyde   |
| PHE        | Public Health England  |
| PI         | Propidium iodide   |
| PI3K       | Phosphatidylinositol 3-kinase  |
| PID        | Primary immunodeficiency   |
| PKA        | Protein kinase A   |
| PL         | Late promoter  |
| PML        | Promyelocytic leukaemia protein  |
| pmol       | Picomoles  |
| PRAF       | Prenylated rab acceptor family   |
| Puro       | Puromycin  |
| PV         | Papillomaviruses   |
| R.T.       | Room temperature   |
| Rb         | Retinoblastoma   |
| RNA        | Ribonucleic acid   |
| RNA-seq    | RNA-sequencing   |
| ROS        | Reactive oxygen species  |
| RRP        | Recurrent respiratory papillomatosis   |
| RTK        | Receptor tyrosine kinase   |
| S          | Synthesis  |
| SCC        | Squamous cell carcinoma  |
| SCJ        | Squamocolumnar junctions   |
| SDS        | Sodium dodecyl sulfate   |
| SDS PAGE   | Sodium dodecyl sulfate polyacrylamide gel electrophoresis  |
| shNTC      | Short hairpin non targeting control  |

|               |  |
|---------------|--|
| shPRAF2       | Short hairpin against the PRAF2 gene           |
| shRNA         | Short hairpin RNA                              |
| siRNA         | Small interfering RNA                          |
| ss            | Single stranded                                |
| Stbd1         | Starch-binding domain-containing protein 1     |
| TA            | Transactivation                                |
| TAE           | Tris-acetate-EDTA                              |
| TAP-MS        | Tandem affinity purification mass spectroscopy |
| TBS-T         | Tris Buffered Saline                           |
| TCA           | Trichloroacetic acid                           |
| TEAB          | Tetraethylammonium bromide                     |
| TFA           | Trifluoroacetic acid                           |
| TGF- $\beta$  | Transforming growth factor- $\beta$            |
| TGN           | Trans-Golgi network                            |
| TLR           | Toll-like receptor                             |
| TMT           | Tandem mass tag                                |
| TNF- $\alpha$ | Tumour necrosis factor- $\alpha$               |
| URR           | Upstream regulatory region                     |
| UTR           | Untranslated region                            |
| UV            | Ultraviolet                                    |
| V             | Volt   |
| v/v           | Volume/volume                                  |
| vDNA          | Viral DNA                                      |
| VLP           | Virus-like particle                            |
| w/v           | Weight/volume                                  |
| WT            | Wild type                                      |
| xg            | Times gravity                                  |
| $\mu$ l       | Microlitre                                     |
| $\mu$ m       | Micrometer                                     |

## Chapter 1 Introduction

### 1.1 *Papillomaviridae*

#### 1.1.1 The natural history of papillomaviruses

Papillomaviruses (PVs) are one of the most successful viruses infecting vertebrates, with 221 human and 211 non-human papillomaviruses recorded to date (Van Doorslaer et al., 2017; PaVE, 2016). The PVs infect a diverse range of hosts across both amniotes and anamniotes, from Humans through to Gilthead Bream (López-Bueno et al., 2016), which puts the emergence of PVs back to at least 550 million years ago (mya). If like humans, animals also have hundreds of papillomaviruses, which is likely, then the total 'Papillomasphere' could number in the tens of millions (Rector and Van Ranst, 2013). Papillomaviruses seem to have emerged separately from the other large dsDNA virus families that infect Eukaryotes, such as *Adenoviridae* and *Herpesvirales* which may have arisen from the dsDNA bacteriophages *Tectiviridae* and *Caudovirales* respectively (Koonin et al., 2015). Instead PVs possibly share origins with the *Polyomaviridae*, another family of small dsDNA viruses, with which they share a region of homology between the PV helicase E1 and the polyomavirus T-antigen (Bernard et al., 2010). Current theories suggest that PVs arose from an ancient recombination event between a positive sense ssRNA bacteriophage and a rolling circle plasmid. This then gave rise to a ssDNA virus which eventually resulted in the dsDNA virus ancestral to PVs (Krupovic, 2013). This is evidenced by ssDNA and small dsDNA viruses sharing the 'jelly roll' capsid protein structure with positive sense ssRNA viruses.

Due to the PVs harnessing their host's DNA replication machinery, the rate of nucleotide substitution for mammalian PVs is slow, with  $1.95 \times 10^{-8}$  nucleotide substitutions per site per year (Rector et al., 2007). This results in PVs diverging at a rate of about 2% per million years (Buck et al., 2016) giving a rate of evolution about 5 times faster than that of their hosts (Van Doorslaer, 2013).

It is thought that PVs co-speciated with their hosts. However, the huge variety of PV types cannot be explained solely through this as HPVs are split into 5 different genera, and animal PVs are intermingled with HPVs. If PVs co-speciated closely with their hosts this would not be the case (Van Doorslaer, 2013). The current dogma is that an ancestral generalist PV underwent an initial radiation event (as evidenced by the 5 major clades of the PV phylogenetic tree), giving rise to PVs with more specific niches. This was then followed by niche adaptation, resulting in further radiation and co-speciation with the host. Additional to co-evolution, cross species infection, recombination and virus duplication are thought to have played a role minor in PV evolution (Shah et al., 2010; Gottschling et al., 2007; Gottschling et al., 2011).

### **1.1.2 The classification of papillomaviruses**

The PV classification system differs from that of the International Committee on Taxonomy of Viruses (ICTV), due to the particularity of PV biology (de Villiers, 2013). Due to the high host and niche speciality of PVs they are difficult to culture in cell culture and animal models, making initial isolation difficult. Further to this, PV infections often do not generate a humoral response, preventing PV classification via serology. The old phylogenetic system for PV classification used the L1, E6 and E7 genes to classify a new type. However, this was found wanting, when PVs which had <90% identity in their L1 and E6 genes were found, but greater than 90% similarity in their E7 genes (de Villiers et al., 2004; Bernard et al., 2010; de Villiers, 2013). The current classification system was set out in full by the Reference Centre for Papillomaviruses, Heidelberg, Germany (de Villiers, 2013); however, since 2012 its curation has moved to the Karolinska Institute in Sweden (Bzhalava et al., 2015). To be recognised as a new isolate, for Human PV (HPV) the cloned full length genome, as well as sequence data must be submitted to the reference centre, for non-human PVs they are accepted solely on sequence data (de Villiers, 2013).

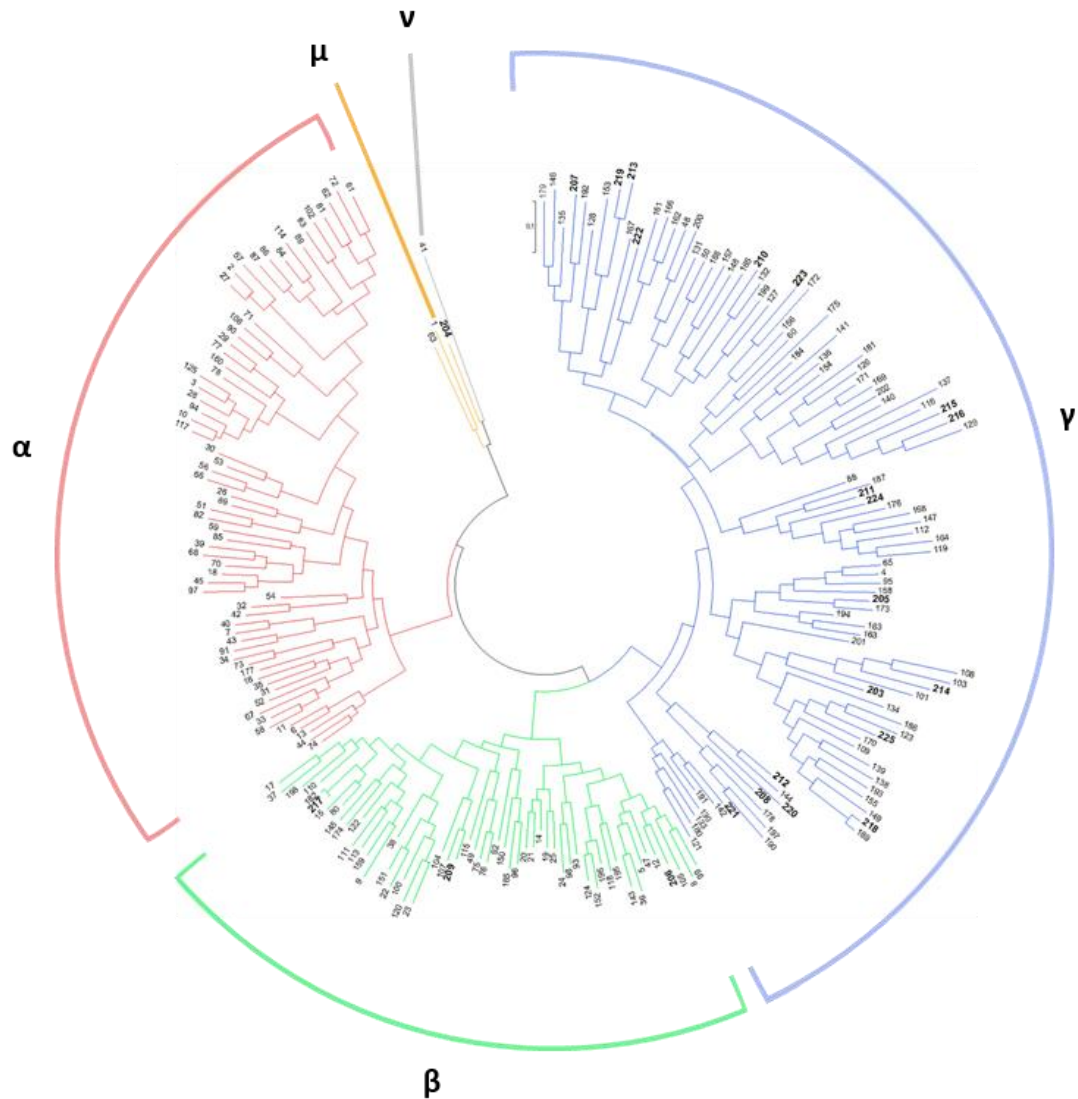


**Figure 1.1** *The phylogeny of human papillomaviruses (adapted from (Mühr et al., 2018))*

*The HPV types are divided into genera based upon the sequence identity of their L1 capsid proteins. The five HPV genera are Alpha ( $\alpha$ ), Beta ( $\beta$ ), Gamma ( $\gamma$ ), Mu ( $\mu$ ) and Nu ( $\nu$ ). Bold numbers classification pending approval by the ICTV.*

Currently classification of PVs is based off the L1 open reading frame (ORF), to sort PVs into genera, a PV isolate must have <60% nucleotide identity in its L1 ORF to other PVs to qualify to be a new PV genera (de Villiers et al., 2004). Additionally, the complete genome must have >23% but <43% sequence identity to others. Following this, species within a genus must share between 60-70% nucleotide identity. Within a species, to be considered a new PV type, there

must be >10% difference, but between 71-89% shared nucleotide identity. After this, 2-10% variation is considered a subtype, and <2% variation a variant. The HPVs are currently split between five genera: Alpha ( $\alpha$ ), Beta ( $\beta$ ), Gamma ( $\gamma$ ), Mu ( $\mu$ ) and Nu ( $\nu$ ). Of these, there are currently 65 $\alpha$ , 54 $\beta$ , 98 $\gamma$ , 3 $\mu$  and 1 $\nu$  (Müher et al., 2018). The  $\gamma$ -genera currently comprise the largest HPV grouping (44.3%), and most of these have been recently discovered by next generation sequencing and metagenomics (Bzhalava et al., 2015). Of the HPVs, the  $\alpha$ -genus is responsible for the greatest clinical disease burden (Bernard et al., 2010; de Villiers, 2013; Doorbar et al., 2015).

## **1.2 HPV associated diseases**

### **1.2.1 Cutaneous lesions**

Infections of the cutaneous epithelium are caused largely by the  $\beta$  and  $\gamma$ -genera, and is also the site of  $\mu$  and  $\nu$ -HPV genera (Gheit, 2019). The  $\alpha$ -genus does also infect the cutaneous epithelium, largely in the form of HPV-2, 3 and 10. Of the HPVs that infect the cutaneous epithelium, most can be considered to be commensal organisms, mostly causing asymptomatic infection in immunocompetent individuals (Cubie, 2013). However, cutaneous HPV infection can give rise to warts, benign lesions characterised by exhibiting dermal hypertrophy. These display acanthosis (thickening), papillomatisation (folding) and hyperkeratosis (expansion of the cornified layer of skin) of the skin (Cubie, 2013).

Common warts are generally located on the hands and face, and range in size, generally between 2-10 mm in diameter, and are most commonly caused by HPV-2 (Cubie, 2013) and are especially persistent. Common warts are also caused by HPV-5 and 7. Other than being unsightly, they are mostly harmless. Planar warts are smaller and not as rough as common warts, and generally occur in groups on the face and hands, and are predominantly caused by HPV 3, 10 and 28. Plantar warts (also known as verrucas) are large warts, often found in the plantar aspect of the foot (Witchey et al., 2018), primarily caused by HPV-1, they can also be caused by HPV-2,

3, 4, 27, 29, 57, 60, 63, 65, 66 and 69. Due to their position under pressure, the developing wart is often forced inwards, which can lead to severe discomfort (Cubie, 2013). Interestingly, HPV-1, 2 and 3 are predominant in children between the ages of 5-15, with HPV-4 more commonly found in older children (Mammas et al., 2014). With cutaneous lesions, they generally are self-resolving within 2 years, regressing in 65-78% of cases (Witchev et al., 2018).

The condition epidermodysplasia verruciformis (EV) is a rare, lifelong condition characterised by cutaneous lesions and an abnormal predisposition to infection by HPV of the  $\beta$ -genus, most commonly HPV-5 and 8 (Przybyszewska et al., 2017), but also HPV-17, 20 and 47. These patients are particularly susceptible to non-melanoma skin cancer, predominantly of a squamous cell carcinoma (SCC) in ultraviolet (UV) exposed areas (Cubie, 2013; Fox and Elston, 2016), with 30-70% of patients progressing to cancer. EV is a primary immunodeficiency (PID), which in ~75% of cases arises from the mutation of the genes *EVER1* and *EVER2* (also known as TMC6 and TMC8) (Kalińska-Bienias et al., 2016). These genes encode integral membrane proteins of the endoplasmic reticulum (ER), that are responsible for regulation of intracellular  $Zn^{2+}$  levels. They are important for the induction of tumour necrosis factor (TNF)- $\alpha$ , and for antigen presentation (Przybyszewska et al., 2017). Recently studies have demonstrated that *EVER2* loss results in HPV-5 long coding region (LCR) activation and a resulting increase in viral replication (Vuillier et al., 2014), enabling viral persistence.

Additionally, in immunosuppressed individuals, such as those suffering from severe HIV immunosuppression, EV can manifest itself as Acquired EV (AEV) (Rogers et al., 2009; Pohthipornthawat et al., 2018). Recently, mutations in the genes *RHOH* (Crequer et al., 2012b), *MST-1* (Crequer et al., 2012a), *CORO1A* (Stray-Pedersen et al., 2014) and *IL-7* (Horev et al., 2015) have been reported as causing EV. Broadly speaking, individuals with these mutations suffer from reduced T-cell levels and responsiveness, impairing their ability to defend against HPV infection (Przybyszewska et al., 2017).

The role of  $\beta$ -genus HPV in cutaneous SCC (cSCC) has recently come under increased investigation. It has been found that there is a higher incidence of  $\beta$ -genus HPV DNA in cSCC relative to the skin of the general population (Rollison et al., 2019). In cSCC, UV radiation is a key risk factor, and  $\beta$ -HPV can influence the networks controlled by retinoblastoma (Rb) and p53, through E6 and E7, which would facilitate the accumulation of UV induced DNA damage. Indeed, over-expression of HPV-38 E6/E7 in transgenic mice expressing results in an increased level of UV induced DNA mutations post UV treatment (Viarisio et al., 2018).  $\beta$ -HPV have also been demonstrated to impair Toll-like receptor (TLR-9) UV damage sensing (Pacini et al., 2017). Together, the evidence for  $\beta$ -HPV in driving UV induced skin lesions is growing.

### **1.2.2 Mucosal lesions**

#### **1.2.3 Benign mucosal lesions**

Infection at mucosal sites associated with  $\alpha$ -HPV types is more common than at cutaneous sites (Cubie, 2013) and a majority of these infections are asymptomatic. The most common sites for symptomatic  $\alpha$ -HPV infection are the oropharyngeal tract and genital mucosa. HPV-6 and 11 are responsible for ~90% of genital warts (GWs, also known as condylomata acuminata) (Flores-Díaz et al., 2017), and the lifetime risk of the acquisition of GW is 10% (Stanley, 2016). In oral condylomata acuminata, the HPV types 6 and 11 have been detected in 75-85% of lesions (Bharti et al., 2013). GW tend to occur in regions that have been abraded by sexual intercourse, such as the glans penis, labia, clitoris and vulva (Cubie, 2013). HPV-6 and 11 infections rarely give rise to cervical cancers and are considered 'low-risk'. Of condylomata acuminata's ~30% undergo spontaneous regression within the first four months of infection, however, 30% will also recur, even after appropriate treatment (Yanofsky et al., 2012).

HPV-6 and 11 infection is also associated with the condition recurrent respiratory papillomatosis (RRP) (Derkay, 2001), which affects both adults and juveniles. RRP is the most common benign neoplasm of the larynx amongst children. It occurs *in utero* or at birth and is

associated with mothers with GWs (Gillison, M.L. et al., 2012). It is a hard to treat condition, and presents with hoarseness, stridor and can result in obstruction of the airway (Cubie, 2013), which is life-threatening. In ~2% of cases in a case study it was found to progress to malignancy (Dedo and Yu, 2001). Treatment is through repeated surgeries, and the condition can be lifelong, or go through stages of remission and relapse. (Cubie, 2013).

The rare condition focal epithelial hyperplasia or Heck's disease is characterised by small benign lesions of the oral mucosa, whitish or normal in colour in the oral cavity. The disease primary occurs in children and is caused by HPV-13 and 32 (Bassioukas et al., 2000; Ozden et al., 2011).

#### **1.2.4 Malignant mucosal lesions**

High risk HPV types cause malignant cancers of several anatomical sites, most commonly the anogenital region and the head and neck (Figure 1.2) (Bouvard et al., 2009). HPV infection at mucosal sites is one of the greatest factors for cancers of the uterine cervix, penis, vagina, vulva, anus and oropharynx (Doorbar et al., 2015). Cervical cancer, and increasingly head and neck cancers are the most studied HPV related cancers. In 2008 the Nobel prize for physiology or medicine went to Professor Harold Zu Hausen, for identifying the link between HPV and cervical cancers (Dürst et al., 1983).

Currently, HPV types 16, 18, 31, 34, 33, 35, 39, 42, 44, 45, 51, 52, 56, 58 and 66 are considered to be high risk (Burd, 2003), with HPV-16 and 18 accounting for ~70% of cervical cancers (Gupta et al., 2018). Most HPV infections of the cervix are asymptomatic and self-resolve, indeed in one study 85.7% of cervical lesions self-resolved within 5.5 months (Winer et al., 2005), however, persistent infection can lead to cervical intraepithelial neoplasia (CIN),

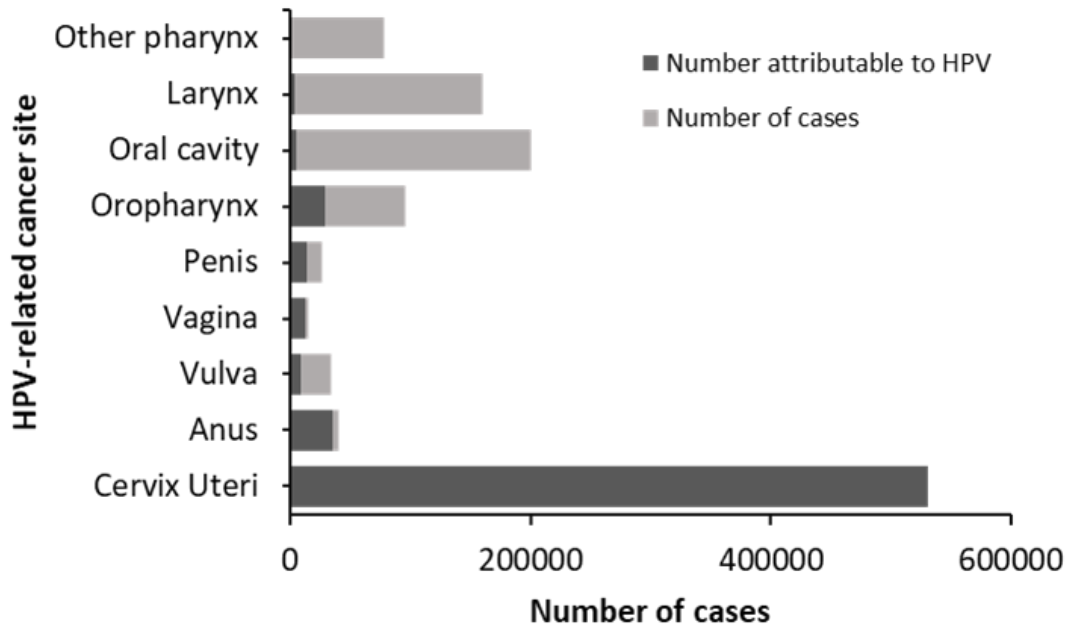


**Figure 1.2** Number of cancer cases attributable to HPV worldwide in 2012 by anatomical site.

Data from (de Martel et al., 2017).

indeed, in the aforementioned study, 8.9% of the patients followed went onto develop higher grade CIN. CIN is graded from 1 to 3 (Figure 1.3) with CIN1 infections considered productive, and permitting the full viral lifecycle to be completed, whereas CIN grades 2-3 are considered to be 'abortive' infections, in which the virus is no longer able to complete its lifecycle (Doorbar, 2006).

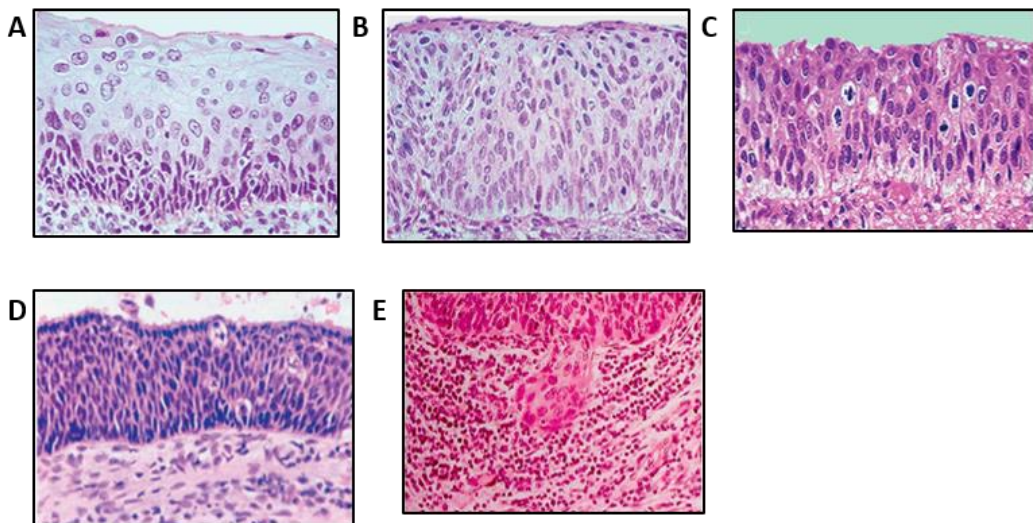


**Figure 1.3** *Histological images of CIN progression from CIN1 through to CIN3 adapted from (Cubie, 2013).*

A. *Histological classification CIN1, displaying mild dysplasia and abnormal cells in 1 in 3 layers (also known as low-grade squamous intraepithelial lesion (LSIL)). B. Histological classification CIN2, displaying moderate dysplasia and abnormal cells in 2 in 3 layers. Stratification and differentiation of the epidermis is lost (also known as a high-grade intraepithelial lesion (HSIL)). C-D Histological classification CIN3, displaying severe dysplasia and abnormal cells in all epithelial layers, complete loss of stratification. Carcinoma in situ, HSIL E. Histological classification CIN3 with microinvasion of surrounding tissue by carcinoma. Carcinoma has progressed to invasive cancer.*

Cervical cancers can arise from different anatomical sites, those which arise from the transformation zone known as squamous cell carcinoma, and those that generally arise in the endocervical glands known as adenocarcinomas (Crosbie et al., 2013). These various forms of carcinoma are generally associated with different types of HPV, with HPV16 responsible for a great majority of SSC's (54.38%), whilst HPV18 is more prevalent within adenocarcinomas (37.3% of HPV-positive cervical adenocarcinoma) (Doorbar et al., 2012).

HPV can also cause cancers of the head and neck (HNC), and recently cases of HPV positive HN cancer have been increasing (Marur et al., 2010), whilst the incidence of other forms of HC cancer has fallen. However, the anatomical site of HNCs appears to play an important role in whether it is HPV positive or not. HPV DNA was found to be present in 35% of oropharyngeal SCC (OPSCC), but in only 24% of laryngeal SCC. It was found that HPV DNA was detected in 90% of OPSCC that arose from the tonsil (Gillison, M.L. et al., 2012). It has also been found that HPV-16 is the dominant type of HPV in HNCs, responsible for 90% of cases, with HPV 18, 31, 33 and 35 largely responsible for the remainder.

HPV can also cause cancers at other sites in the anogenital tract, and is responsible for 48% of penile cancers (Stratton and Culkin, 2016), 90% of anal cancers (Stier et al., 2016), 39.7% of vulvar cancers (Faber et al., 2017) and 78% of vaginal cancers (de Martel et al., 2017). In all of these cancers, HPV-16 is responsible for the greatest number of cancers (de Martel et al., 2017).

## **1.3 Transmission of HPV**

### **1.3.1 Cutaneous transmission**

Transmission of cutaneous HPV types occurs by shedding of the virus via desquamated epithelial cells (Mammas et al., 2014), which can contain high viral load. The HPV virus can be passed via direct person to person contact (Cubie, 2013), which is particularly common in children, owing to high frequency of person to person contact, and lack of handwashing practice. HPV can also be spread by indirect contact, with HPV capable of surviving months to years on contaminated surfaces such as flooring, socks, shoes, toys and sports equipment (Witchev et al., 2018). Re-inoculation and auto-inoculation is also common amongst children (Cubie, 2013). Infection occurs via access to the cells of the basal epithelium through microabrasions (Sancllemente and Gill, 2002).

### **1.3.2 Mucosal transmission**

HPV is the most commonly sexually transmitted infection in the world (Egawa et al., 2015). Mucosal infection is dominated by HPV of the  $\alpha$ -genus (Cubie, 2013). As with cutaneous infections, mucosal HPVs gain entry to the basal layer of the epidermis resulting from microabrasions. The primary method of mucosal HPV transmission is through direct or indirect sexual contact. Skin to skin contact, not penetration, is more important to transmission (Stanley, 2010), and can also occur via oral sex (D'Souza and Dempsey, 2011).

Mucosal HPVs can also be transmitted horizontally through non-penetrative sex, with inoculation via fingertips (Moscicki et al., 2012) and sex toy use (Anderson et al., 2014). Mucosal

HPVs can also be transferred between family members via digital contact and kissing (Sabeena et al., 2017). Autoinoculation, through genital scratching is also possible (Houlihan et al., 2019). Fomites are also a source of infection, and these are particularly problematic in GUM clinics, with vaginal ultrasound probes and colposcopes hosting fomites that may be resistant to disinfection by standard methods (Meyers et al., 2014; Ryndock and Meyers, 2014), this is also problematic in the home, with fomites on sex toys resistant to standard disinfectant methods (Anderson et al., 2014).

Vertical transmission is also possible for mucosal HPV. Intrauterine transmission can occur through microtears in foetal membranes, or via the placenta if the mother has genital HPV (Armbruster-Moraes et al., 1994). Perinatal transmission is also possible at the time of delivery, through direct contact with the infected maternal genital tract (Sabeena et al., 2017). However, the risk is low, and generally infants have cleared the HPV by 6 months of age, so it may not represent a true infection (Park et al., 2012).

## **1.4 Epidemiology of HPV**

The disease burden of HPV associated cancers is large. The greatest incidence of HPV associated cancers is that of cervical cancer, which in 2018 was responsible for 570,000 cases (Figure 1.4 A) and 311,000 deaths worldwide (Bray et al., 2018). Cervical cancer is the fourth most frequently diagnosed cancer and the fourth highest cause of cancer deaths in women. Indeed, it is the leading cause of cancer death in 42 countries, most of which are in sub-Saharan Africa and South Eastern Asia (Figure 1.4 B) (Bray et al., 2018), with 76.2% of cases diagnosed in Africa and Asia (Ferlay et al., 2018), likely due to the lack of vaccination programmes and protective contraceptive use. Additionally, the high incidence of HIV in areas such as sub Saharan Africa increases the prevalence and persistence of HPV, further increasing the risk of cervical cancer (Menon et al., 2018). Worldwide it is estimated that 4.5% of new cancer cases are HPV

related (de Martel et al., 2017), in 2012 it was estimated that 630,000 cancers were attributable to HPV.

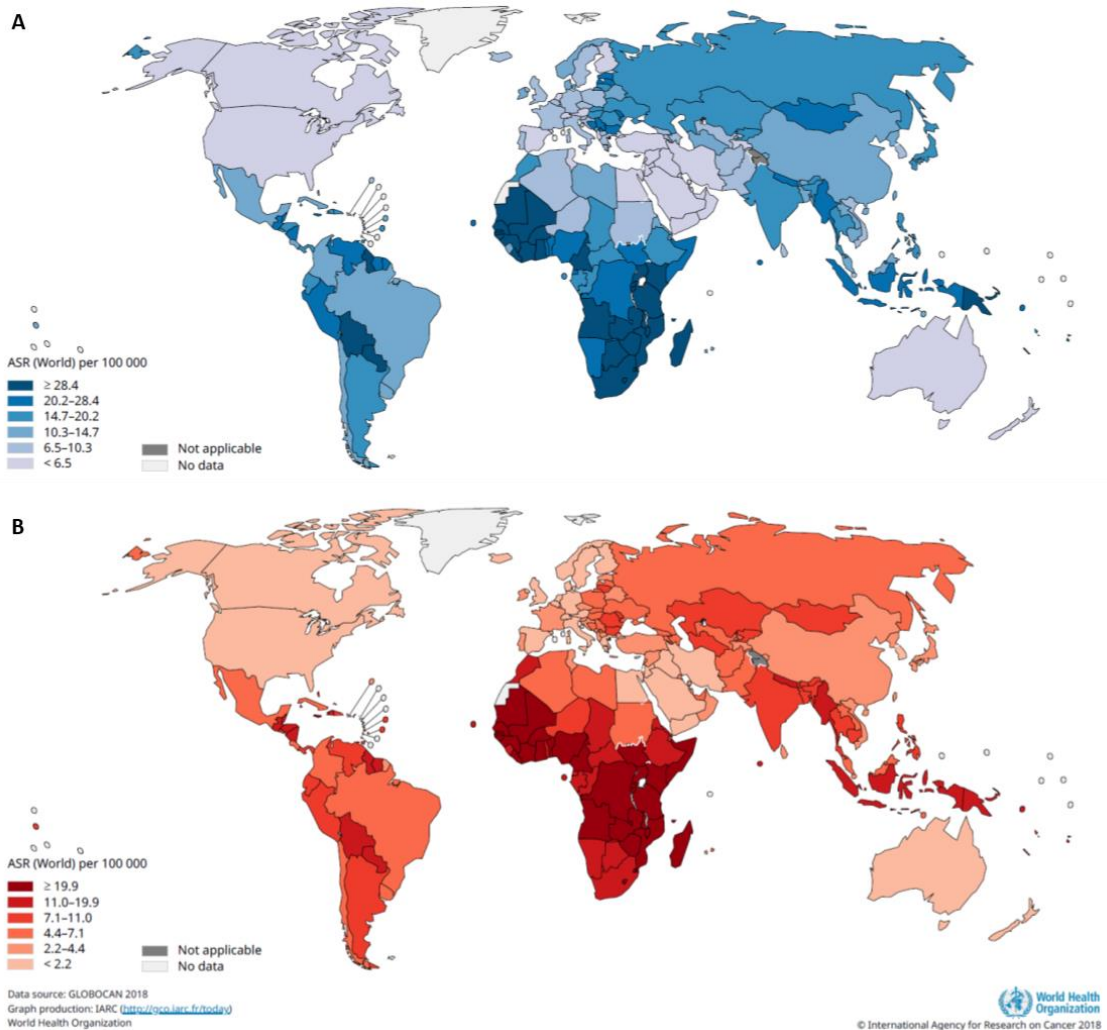


**Figure 1.4** Age standardised rates of incidence and mortality of cervical cancer 2018, all sexes and ages. Adapted from (Ferlay et al., 2018).

A. Worldwide age standardised incidence rates for cervical cancer 2018. B. Worldwide age standardised mortality rates for cervical cancer 2018.

Whilst the incidence of cervical cancer has declined in Western Europe, North America, Australia and New Zealand owing to screening and vaccination (Bray et al., 2018), there have been rapid increases in the incidence and mortality of cervical cancer in the ex-Soviet countries of Eastern Europe and Central Asia. HPV16 is the most prevalent type found within cervical

cancers, responsible for 61.35% of invasive cervical cancers, with HPV18 causing the second greatest incidence, with 10.28% (Doorbar et al., 2012; de Sanjose et al., 2010).

As stated previously, HPV is also responsible for cancers at other sites such as the anus. In 2018 there were 48,541 cases diagnosed, accounting for 0.3% of the global cancer burden, of these cases, 41.6% were in men and 58.4% in women (Bray et al., 2018) of which 88-90% are attributable to HPV (Stier et al., 2016; de Martel et al., 2017). Interestingly, anal cancer incidence is increasing greatest in more developed regions, such as Australia, Canada, Denmark, England, the USA, Scotland and Sweden (Kang et al., 2019). Penile cancer was responsible for 0.2% of global cancer burden in 2018 (Bray et al., 2018), of which HPV is responsible for 48% (de Martel et al., 2017). The rates of penile cancer worldwide are seen to correlate with that of cervical cancer, and are higher in developing countries (Kidd et al., 2017).

When considered together, oesophageal, lip, oral cavity, pharyngeal, laryngeal and salivary gland cancer were responsible for 1,459,688 cases of cancer in 2018 (8.57% of the total cancer burden). When considered together, HNCs were responsible for fourth biggest grouping of cancers diagnosed in 2018 (Bray et al., 2018; Ferlay et al., 2018). Key risk factors for the development of HNC include smoking, alcohol consumption, HPV infection and poor dental hygiene (Gillison, 2008). Interestingly, increased risk of HPV cancers was associated with increased numbers of oral sex partners, and increased use of marijuana. However, whether marijuana use, or behaviours associated with it are to blame is yet to be determined.

The area of origin for HNC cancer has a large influence on whether it is likely to be HPV positive, with 70% of pharyngeal cancers HPV positive, but only 1% of oral cavity cancers HPV positive (Mehanna et al., 2013). Incidence of HNC is highest in Europe, China and the Indian subcontinent (Figure 1.5), however, the causes differ. In Asian countries, HPV negative HNC is more prevalent, whereas in Europe and North America HPV positive HNC is more prevalent. Indeed, in Europe 73% of oropharyngeal cancer cases are positive for HPV, and the proportion

of those positive for HPV is increasing over time (Mehanna et al., 2013). Cancer risk is greatest in those with more past sexual partners, people who became sexually active at a younger age and men who have sex with men (MSM) (Heck et al., 2010). In oropharyngeal SCC, HPV-16 is the predominant type, responsible for 86.7% of cases (Kreimer et al., 2005), with HPV-18 only detected in 2.8% of cases. This contrasts with other sites of SCC, for example oral and laryngeal SCC in which HPV-18 was responsible for 34.1% and 17% of cases respectively. However, HPV-16 was still the predominant type detected in these SCC.

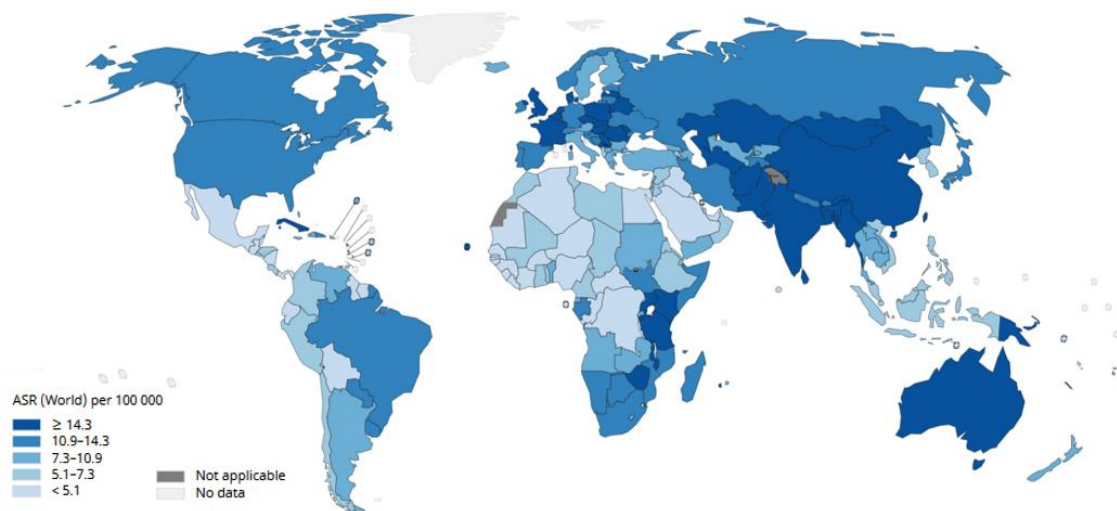


**Figure 1.5** *Age standardised rates of incidence for oesophagus, oropharynx, larynx, lip, oral cavity and salivary gland cancers, all sexes and ages 2018, adapted from (Ferlay et al., 2018).*

## 1.5 Prevention and treatment of HPV associated diseases

### 1.5.1 Prevention

There are currently prophylactic vaccinations available against HPV infection. All current HPV vaccinations are based on virus-like particle (VLP) technologies, using the L1 capsid protein of HPV. The first generation of HPV vaccines were Cervarix<sup>®</sup> by GlaxoSmithKline and Gardasil<sup>®</sup> by Merck. Cervarix<sup>®</sup> is effective at preventing infection by HPV-16 and 18 which account for ~70% of cervical cancers (Egawa et al., 2015), whereas Gardasil<sup>®</sup> also protects against the

primary causative agents for 90% GWs HPV-6 and 11 (Yanofsky et al., 2012). Since its initial release, a second generation of the Gardasil® VLP vaccine has been developed, Gardasil®9 which protects against HPV-31, 33, 45, 52 and 58, which account for ~20% of cervical cancers (Harper and DeMars, 2017), in addition to HPV-6, 11, 16 and 18.

Since 2008 a vaccination programme against HPV has been running in the UK, with girls aged 12-13 receiving a dose of HPV vaccine, with follow up doses 6-12 months later. The programme initially used Cervarix® as it offered greater protection against HPV-16 and 18, however from 2012 the programme switched to using Gardasil®. From September 2019, the vaccination programme has been expanded to include boys aged 12-13 (Kmietowicz, 2018). Since the programme has started in the UK, there has been a 86% reduction in HPV-16 and 18 infection in young women, with a 71% reduction in CIN seen in women and the diagnosis of GWs between 2009-2017 has fallen by 90% and 70% in 15-17 year old females and males respectively (Mesher et al., 2018).

Getting vaccination programmes up and running in low-income countries (LICs), where there is a great need for HPV vaccination has not been without issue. The issues encountered include the logistical issues such as the requirement for cold storage of the vaccine, cost associated with manufacture, the requirement for multiple doses, age of vaccination and manpower for distribution (Wigle et al., 2013; Kumar et al., 2015). There are also social issues, such as the fact that the immediate benefit of the vaccine is not seen, versus vaccines such as measles and polio, in which there are obvious immediate effects (Wigle et al., 2013). There are also technical issues: the vaccination is prophylactic and not therapeutic and highly type specific (Kumar et al., 2015).

However, these odds may not be insurmountable and there is a great deal of research ongoing into overcoming these obstacles. Recent research suggests that one dose of vaccine may be enough to provide a long-lasting humoral response (Brotherton et al., 2019). Other

research is ongoing into improving the vaccines temperature stability to remove the need for cold storage (Hassett et al., 2015). Attempts are also being made at reducing cost barriers, such as work into piggybacking the immunogen onto existing live attenuated vaccines such as measles (Schiller and Müller, 2015). There is also hope for a pan-type HPV vaccine, based upon an L2 capsid immunogen (Karanam et al., 2009), and work is ongoing on developing a therapeutic vaccine based on E6 and E7, owing to their ongoing expression throughout the viral lifecycle and in cancer (Massa et al., 2019). Aside from vaccination, condom usage is the most effective method of prevention for cervical cancer (Hatcher, 1982).

Currently, these vaccines are of no use to those already infected with the virus, and there is a lack of specific anti-virals that treat the virus infection, preventing infection or treating the condition as it progresses to cancer. Currently, screening programmes exist for cervical cancer based upon the cytology-based Pap smear and liquid based cytology assays, which detect abnormalities in cells of the cervix. Cervical cancer screening has been ongoing in the UK since 1988, and the current guidelines call for screening of individuals between the ages of 25-49 every three years, and individuals between the ages of 50-64 every five years. It is predicted that 80% of cervical cancer deaths are prevented in this manner, and there has been a steady decrease in cervical cancer over the past 30 years (Peto et al., 2004; Castanon et al., 2018). In 2019, the uptake of screening in those aged 25-49 was 70.2% and 76.45% for those aged 50-64 (PHE, 2019). If cervical screening shows signs of abnormalities, a further biopsy is taken and screened for the presence of HPV DNA or RNA (Santesso et al., 2016). Cervical screening programmes are not present in many LICs, which contributes to the risk of cervical cancer in these countries (Catarino et al., 2015). There are currently no screening programmes for other HPV associated cancers. Current UK general dental council guidelines require examination for signs of HNC, however this is purely visual and tactile in nature and down to the skill of the clinician, further to this, early stage HNC will be difficult to detect by this method (Gibson, 2018).

### 1.5.2 Treatment

Treatment of HPV varies depending on the site and type of lesion. For benign cutaneous lesions, such as common warts, generally no treatment is recommended as the lesions are self-resolving. However, in cases with recalcitrant warts, those causing discomfiture or in immunosuppressed individuals, treatment may be required. Treatment is usually by topical salicylic acid application, which promotes removal through the inflammatory response and debridement, alternatively cryotherapy with liquid nitrogen may be pursued (Witchey et al., 2018).

Treatment of GW is generally focussed on removing the growth and not eliminating the underlying viral infection and does not result in long term eradication. Treatments include topical application of the immunomodulatory agent Imiquimod, which is believed to act through triggering the inflammatory response via TLR activation (Yanofsky et al., 2012), which achieves clearance in 56% of patients (Edwards et al., 1998). Other treatments are application of Trichloroacetic acid (TCA) to chemically burn and cauterise the lesion, and cryotherapy, electrosurgery, surgical excision or CO<sub>2</sub> laser therapy (Yanofsky et al., 2012).

Treatment of mucosal lesions of the cervix will depend on the CIN classification. Often with CIN1 lesions no treatment is required as the lesion will self-resolve (Cubie, 2013), however depending on colposcopy investigation, treatment may be decided upon for the lesion. If cytology and colposcopy suggest moderate to severe changes, and biopsies suggests CIN2 or CIN3 grade changes then treatment will be required. Treatment either involves direct destruction of the abnormal cells by laser ablation, cold coagulation or cryotherapy (PHE, 2016). Alternatively, removal of the transformation zone of the cervix may be performed either by large loop or needle excision of the transformation zone (LL/NETZ) whereby electrical current is used to cut and cauterise away the tissue (Khan, M.J. and Smith-McCune, 2014; PHE, 2016). Alternatively, if further examination of the removed tissue is required a cone biopsy may be

performed to remove the transformation zone. In those suffering from recurrent or severe abnormalities to the cervix, hysterectomy may be performed (PHE, 2016). In cases of invasive cervical cancer treatment by hysterectomy and chemoradiotherapy may be pursued (Peralta-Zaragoza et al., 2012).

In HPV positive HNC treatment prognosis is generally better than HPV negative HNC, whilst standard surgery and chemoradiotherapy may be pursued, HPV positive HNC have been demonstrated to be sensitive to lower doses of radiation and respond well to radiation treatment combined with the epidermal growth factor receptor (EGFR) inhibitor cetuximab (Kobayashi et al., 2018).

## **1.6 Papillomavirus Virology**

### **1.6.1 Genome organisation**

The HPV genome is circular and double-stranded, and usually between 7.3-8Kb in size (Figure 1.6) (Doorbar et al., 2012). The genome is associated with cellular histones inside virions, forming a chromatin like structure, packaged within a icosahedral capsid of ~60 nm diameter (Zheng and Baker, 2006; Cardone et al., 2014). The average HPV genome encodes 8 major ORFs, which are expressed as multiple transcripts from at least two promoters, with multiple splicing events (Hebner and Laimins, 2006). The ORFs encode early proteins (E) E1, E2, E4, E5, E6 and E7, and occasionally the protein E8 as well as late proteins (L) L1 and L2 (Doorbar et al., 2012; Hebner and Laimins, 2006). HPV encodes more than 8 gene products, as further products are generated by alternative splicing (figure 2). High risk HPV types (e.g. HPV16 and 18) contain two major viral promoters, the early (PE) and late (PL) (Doorbar et al., 2012; Hebner and Laimins, 2006; Longworth and Laimins, 2004). The PE is located in a region called the long control region (LCR)/upstream regulatory region (URR), upstream of the E6 ORF (Doorbar et al., 2012), which also contains the origin of replication (*ori*). In HPV18 this promoter is known as the p105 (p97 in

HPV-16 and 31) (Wang, X. et al., 2011), and possesses binding sites for cellular factors, more specifically, a keratinocyte specific enhancer region. The transcript produced is expressed prior to productive replication, and generally encodes the proteins E1, E2, E6 and E7. The second major promoter PL is the differentiation dependent promoter, p765, p811 or p829 in HPV18 (p670 in HPV-16 and p742 in HPV-31), which is contained within the E7 ORF, and initiates during productive replication, driving the transcription of E1, E2, E4 and E5 as well as the capsid genes L1 and L2 (Doorbar et al., 2012; Hebner and Laimins, 2006).

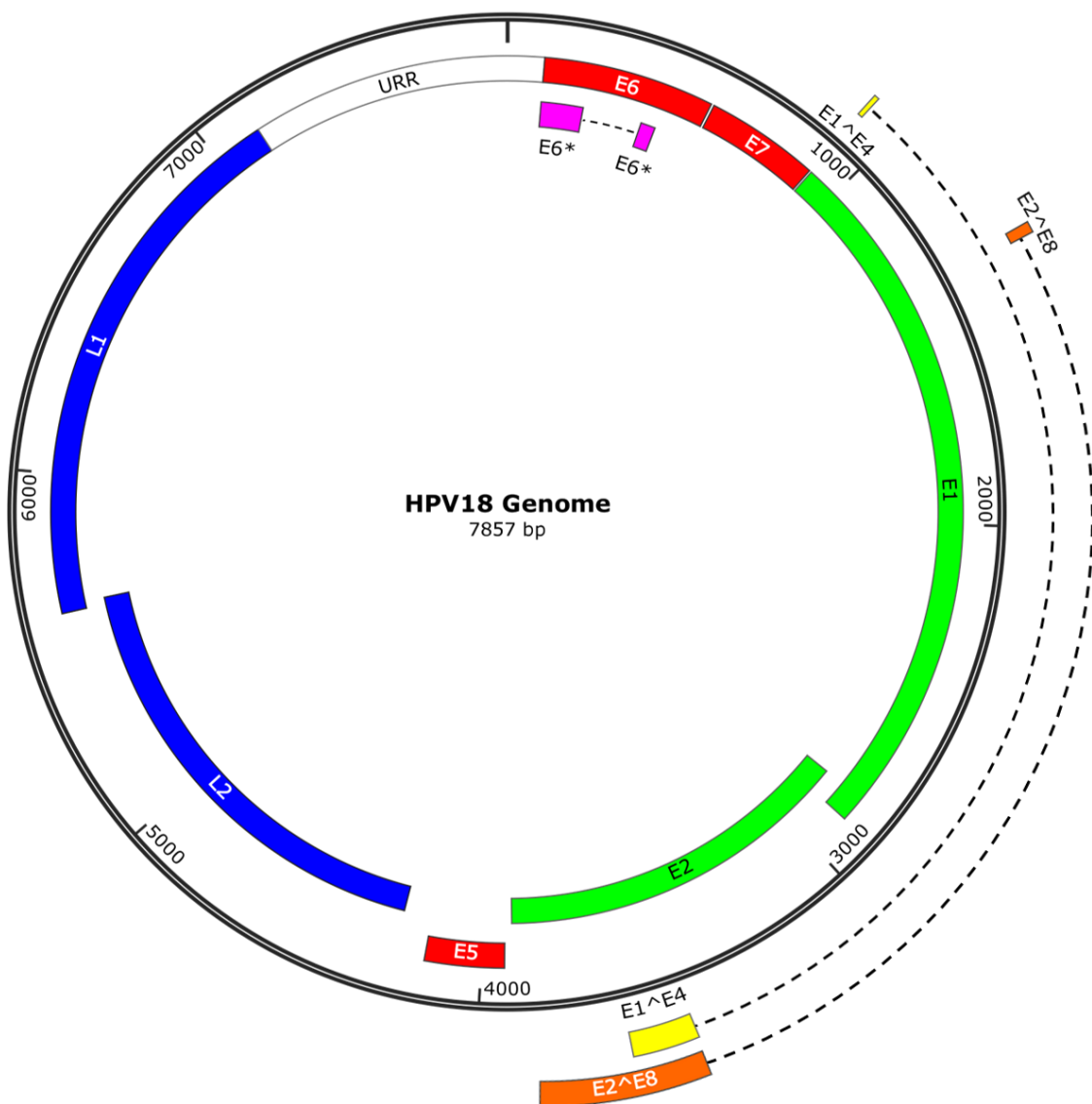


**Figure 1.6** Genome organisation of HPV18.

A circular genome, comprised of the LTR and eight major genes L1, L2, E1, E2, E4, E5, E6 and E7, as well as additional spliced products such as E6\*, E1^E4 and E8^E2. The early promoter p105 is located within the LTR/URR, and the late (differentiation dependent) promoter p811 within the E7 ORF. Drawn in Snapgene.

### 1.6.2 Normal Epithelial Development

The epidermis is a stratified structure, starting at the basement membrane and ending at the tough cornified outer surface. The structure of the epidermis can be divided into a basal layer that sits atop the basement membrane, followed by the suprabasal layers, spinous layer, granular layer and finally the stratum corneum. Each layer possesses a distinct set of morphological and biochemical characteristics, which can be used to distinguish them (Fuchs, 2007; Fuchs, 2008) (Figure 1.7).

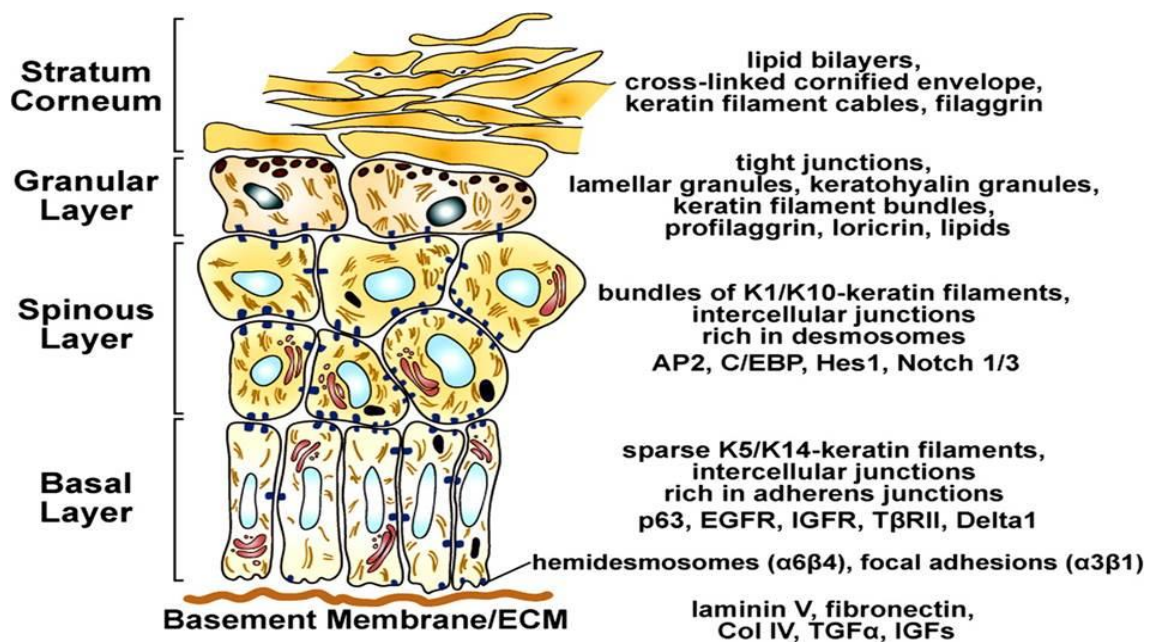


**Figure 1.7** The epidermal differentiation programme of a basal keratinocyte (adapted from (Fuchs, 2008)).

The different stages of epidermal stratification are shown on the left, and the key molecular markers of these transitions on the right. In normal epidermal development, the basal layer is the only mitotically active zone. In the suprabasal layers, proliferation should not occur. The transition from basal to suprabasal is marked by the expression of keratins 1 and 10, as well as

*various changes to cell signalling such a reduction in TBR1 signalling and an increase Notch signalling.*

The basement membrane (BM) separates the epithelium from the endothelium and is an important region for anchorage and signalling. It is an extracellular matrix, whose major components are collagen IV, laminin, perlecan and nidogen/entactin (Fuchs, 2008; LeBleu et al., 2007). The BM not only serves as an attachment substrate for cells but can also directly signal to the cells. For example, laminin 5 signalling through  $\alpha3\beta1$ -rich focal adhesions (FAs) leading to stimulation of the Ras-MAPK pathway through focal adhesion kinase (FAK), which can lead to epidermal migration (Fuchs, 2008). Finally, the BM proteoglycans can capture growth factors, such as transforming growth factor- $\beta$  (TGF- $\beta$ ) and epidermal growth factor (EGF) which serve as important regulators of epidermal proliferation (Fuchs, 2008; Guasch et al., 2007; Wang, Y. et al., 2002).

The basal layer of the epidermis contains the epidermal stem cells. However, debate exists as to whether all cells contained within are stem cells (Fuchs, 2008; Clayton et al., 2007), and whether the basal cells are a mix of stem cells and transit-amplifying cells (committed cells, that will divide several times before exiting the basal layer). This layer is the only mitotically active part of the skin, with cells dividing to replenish those lost from the upper layers (Blanpain and Fuchs, 2006; Clayton et al., 2007). Keratins are expressed by epidermal cells, which possess a structural role in the cell, forming intermediate filaments. In basal cells, keratins 5 and 14 are expressed, and can be used as a marker for basal cells (Blanpain and Fuchs, 2006). Periodically, basal cells will cease the cell cycle, delaminate, and then exit the basal layer for the suprabasal layers.

It has been suggested that asymmetric cell division is required for the stratification and differentiation of the epithelia (Clayton et al., 2007; Williams et al., 2011; Lechler and Fuchs, 2005). Two possible mechanisms for asymmetric division and subsequent differentiation have

been proposed (figure 1.8 A and 1.8 B), that enable cells to exit the basal layer. One mechanism proposes a reorientation of cell divisions, so that the daughter cell is perpendicular to the basement membrane, and then receives a reduced level of receptor tyrosine kinases (RTKs) and integrins via asymmetrical division, resulting in one daughter cell that retains a strong affinity for the BM and proliferation (figure 1.8 B), and the other daughter with a reduced affinity and a spinous character (Fuchs, 2008; Lechler and Fuchs, 2005; Williams et al., 2011). The other proposed model is an asymmetrical partitioning of the cell signalling molecule Notch in the daughter cells (figure 1.8 B); with the committed cell receiving a greater Notch signal (Clayton et al., 2007; Fuchs, 2008; Lechler and Fuchs, 2005; Williams et al., 2011). Notch has been suggested to be the gatekeeper of cell lineage commitment in epidermal cells, so a stronger signal would result in the cell leaving the basal layer (Williams et al., 2011).

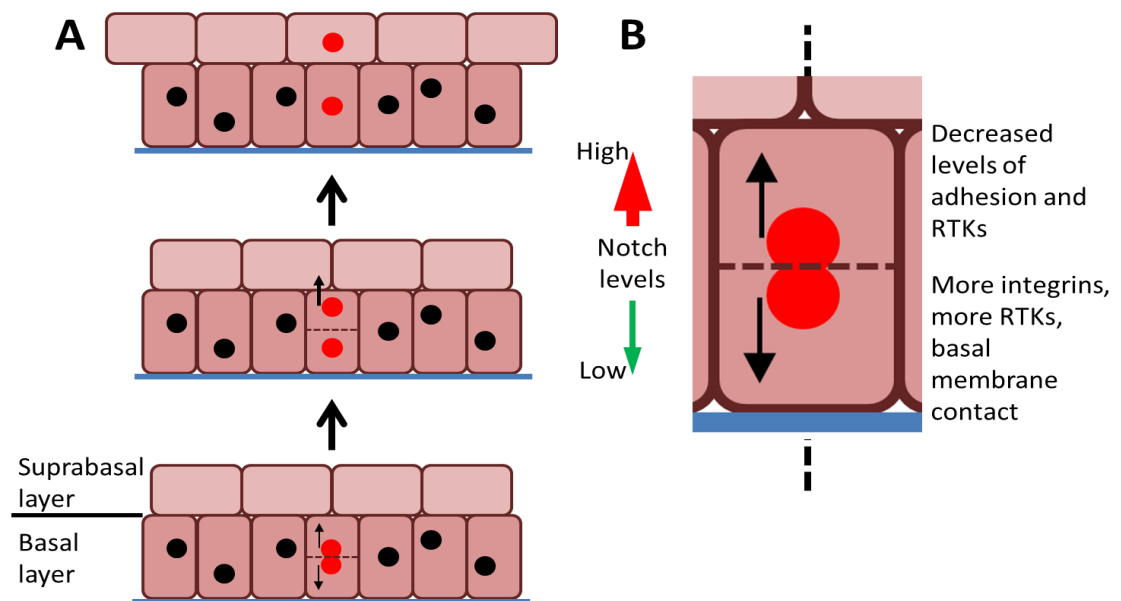


**Figure 1.8** *Schematic model of asymmetric division within the epithelium, and the possible mechanism.*

*A. Asymmetrical division enables cells to exit the basal layer for the suprabasal layers. This is achieved through a rearrangement of the mitotic spindle apparatus, permitting one daughter cell to remain in the basal microenvironment. B. Schematic of possible influences on the*

*developing keratinocyte during asymmetrical division, where altered signalling from the microenvironment primes one cell to remain and the other to exit the compartment.*

Upon leaving the basal layer, the cell starts to express the keratinocyte specific markers keratins 1 and 10 (Blanpain and Fuchs, 2006), and changes from adherens junction rich to desmosome rich to better maintain cell-cell contacts. Additionally, the expression of involucrin is initiated, and will be maintained as the cell progresses through the granular layer. Upon entry to the granular layer, profilaggrin and loricrin are synthesised, and the keratins bundled (Watt, 1983). Finally, upon entry to the stratum corneum, the cells become enucleated, keratin filaments are cross linked, filaggrin is mature and the lipid bilayer is extruded (Watt, 1983; Fuchs, 2008; Blanpain and Fuchs, 2006), forming the final, tough layer of the epidermis. Crucial cell signalling events underpin the transformation of an epidermal stem cell.

EGFR signalling is crucial to the development of the stratified epithelium. EGFR signalling has been implicated in proliferation, survival and cell migration in the basal epithelium (Fuchs, 2008; Wang, Y. et al., 2002). EGFR is a receptor tyrosine kinase (RTK), and its activation occurs through the binding of EGF which results in trans-autophosphorylation, enabling the binding of signalling proteins with phosphotyrosine binding domains. Some important examples are SHC and phosphatidylinositol 3-kinase (PI3K). Binding of SHC enables signalling through the Ras pathway (figure 1.9), which results in the stimulation of Raf, and hence mitogen activated kinase kinase (MAPKK, also known as MEK, mitogen/extracellular signal regulated kinase) and extracellular-signal-regulated kinase (ERK), activating transcription factors c-fos and c-jun (Wang, Y. et al., 2002). ERK signalling has been shown to be required for G2/M cell cycle transition in epithelial cells (Dumesic et al., 2009); its regulation of c-fos levels sustains cyclin B1 expression, enabling the G2/M transition (Dumesic et al., 2009; Wang, Y. et al., 2002). Cells lacking functional ERK1/2, and hence a functional EGFR pathway are hypoproliferative. Thus, EGFR signalling is important to cellular proliferation. EGFRs effects on PI3K signalling have been implicated in cellular survival, through the stimulation of the Akt pathway (figure 1.9) (Wang, Y.

et al., 2002). Additionally, EGFR signalling has been shown to act as a negative regulator of Notch signalling, thereby preventing keratinocyte differentiation (Blanpain et al., 2006; Kolev et al., 2008). Once activated, the EGFR receptor is rapidly internalised through endocytosis, followed by lysosome mediated degradation. However, endocytosis of the active EGFR complex does not abrogate signalling, and it has been shown that endocytosed EGFR is still capable of stimulating Ras, ERK1/2 and Akt up until degradation (Wang, Y. et al., 2002).

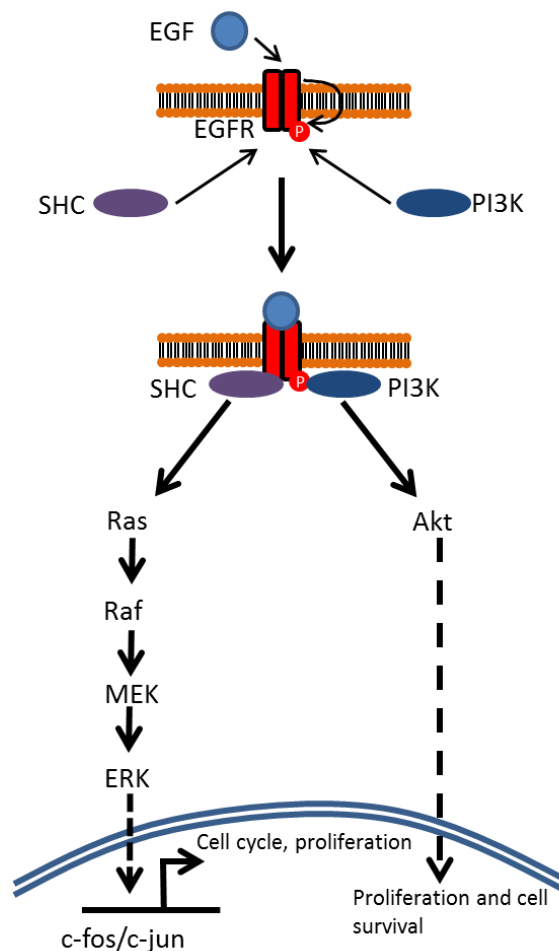


**Figure 1.9** Cell signalling events crucial to epithelial development.

*EGFR signalling through Ras and Akt is crucial for correct epithelial development, controlling proliferation of the basal keratinocytes and ensuring cellular survival.*

Through the transcription factor STAT3, EGFR signalling possesses a crucial role in the control of the important director of epidermal cell fate, p63 (Yoh and Prywes, 2015). p63 is a p53 homologue and possesses at least six different isoforms generated through alternative

splicing (Yoh and Prywes, 2015). These can be split into two classes; transactivating (TA) which possesses the N-terminal TA domain and  $\Delta N$ , which lacks the TA domain. These are then further divided into  $\alpha$ ,  $\beta$  and  $\gamma$ . Knockout mice deficient in p63 display a severely impaired ability to generate epidermis (Mills et al., 1999). It appears that  $\Delta Np63$  is preferentially expressed in basal epidermal cells (Fuchs, 2008), as demonstrated by FISH (Laurikkala et al., 2006) and immunostaining (Wasson, et al, unpublished) and that it is crucial to epithelial development and differentiation. Epidermal specific knockout of  $\Delta Np63$  results in epidermis which is highly defective, lacking stratification (Koster et al., 2007) and suffering from erosion and impaired terminal differentiation (Romano et al., 2012). In primary keratinocytes it has been shown that shRNA knockdown of  $\Delta Np63$  results in smaller colonies that display reduced proliferation (Fuchs, 2008). P63 also possesses interactions with the Notch signalling pathway. The relationship between notch and p63 is an intimate one. As basal cells undergo the basal to suprabasal (spinous) transition, the levels of p63 fall, and the levels of Notch rise. This demonstrates p63s importance in maintaining cell proliferation in the basal layer, but not in the superabasal layers.  $\Delta Np63$  can activate Notch related gene expression (Yoh and Prywes, 2015), and Notch has been shown to suppress p63 expression in keratinocytes (Nguyen et al., 2006), as well as being able to cause proteosomal degradation of p63 through the activation of IRF6 regulated genes (Yoh and Prywes, 2015).

Notch signalling promotes keratinocyte differentiation. Upon signal activation, Notch is cleaved, releasing the Notch intracellular domain (NICD) which interacts with its signalling partner RBP-J (figure 1.10) (Blanpain et al., 2006), which then activate Hes and Hey. Epidermal specific knockout of the signalling partner RBP-J causes a much thinner epidermis in mice, which lacks keratin filament bundles, and shows a reduction in both spinous and granular layer markers. However, basal layer markers appear relatively unaffected. This suggests that a functional Notch pathway is critical for the basal-suprabasal switch, and is required for correct terminal differentiation (Blanpain et al., 2006). Consistent with an important role in

differentiation and spinous layer development, constitutively active Notch 1 NICD in mouse epithelium resulted in great expansion of the spinous layer relative to control (Blanpain et al., 2006). This reinforces the importance of Notch signalling in keratinocyte differentiation. However, it should be noted that granular layer development was impaired in this model, suggesting that Notch may play a greater role in cell fate specification than in terminal differentiation.

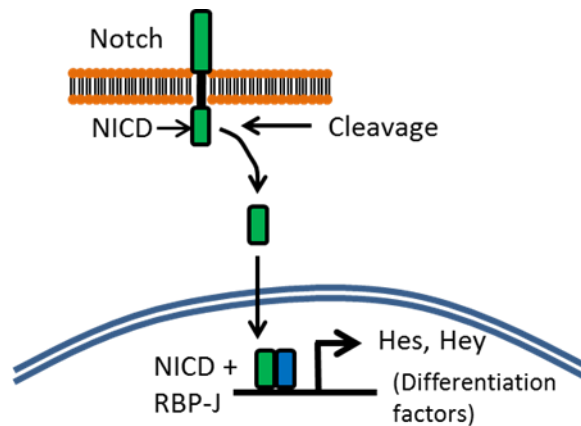


**Figure 1.10** Schematic of Notch signalling in the keratinocyte.

*Notch signalling possesses a crucial role in keratinocyte differentiation, through the effects of NICD and its binding partner RBP-J.*

Studies have also demonstrated the interplay between EGFR signalling and Notch. EGFR signalling has the ability to negatively regulate Notch, as demonstrated by the chemical inhibition of EGFR resulting in decreased activity of ERK1/2, c-jun and Elk and induction of Notch target genes (Kolev et al., 2008). It appears the EGFRs effects on Notch are p53 related, as Notch is a transcriptional target of p53. When EGFR is inhibited, c-jun is no longer able to negatively regulate p53 gene expression, which in turn results in increased Notch signalling and hence cellular differentiation (Kolev et al., 2008). In the basal layer EGFR signalling levels are maintained, resulting in cellular proliferation, however, upon division and the asymmetrical partitioning of the Notch signal (Williams et al., 2011) coupled with decreased levels of EGFR, the daughter cell can respond to the Notch signal, enabling differentiation (Fuchs, 2008).

An under reported, but nevertheless important signal in maintaining correct epidermal stratification is TGF- $\beta$ . TGF- $\beta$  signals through T $\beta$ RII, activating Smad 2/3, which upregulates p15 and p21 expression whilst downregulating c-myc levels, thereby blocking the cell cycle and preventing excessive proliferation of keratinocytes in the basal layers (Guasch et al., 2007; Wakefield and Stuelten, 2007). Loss of TGF- $\beta$  signalling has been associated with invasive cell migration (Zi et al., 2012), and aberrant T $\beta$ RII expression is often seen in cancer. Epidermal specific knockout of T $\beta$ RII in mouse epithelial tissue resulted in spontaneous formation of SSCC in the anogenital region, suggesting that TGF- $\beta$  signalling is particularly important in controlling keratinocyte proliferation in this region (Guasch et al., 2007). It seems that the role of T $\beta$ RII signalling in the basal layer is directly opposed to that of EGFR, and the two signalling pathways share downstream signal cascades such as the Ras ERK1/2 pathway (Guo and Wang, 2009), so it is possible that the two possess direct antagonistic actions on the other. Indeed LRIG1, an inhibitor of EGFR (Fuchs, 2008), shares downstream targets such as c-myc (Jensen and Watt, 2006; Kou et al., 2015) with T $\beta$ RII, so it is possible that these pathways work in concert to modulate EGFR signalling.

### **1.6.3 The HPV lifecycle**

The HPV life cycle is intimately linked with epithelial differentiation. However, the normal keratinocyte life cycle is ill suited to viral replication owing to exiting the cell cycle upon leaving the basal layer (Doorbar et al., 2012). As a result, the virus must be able to perturb the normal cell cycle in order to effectively replicate. The first hurdle HPV needs to overcome is cellular entry.

For the virus to gain entry to the host cell it requires a host receptor. HPVs are known to use heparan sulphate proteoglycans (HSPG) as the primary attachment receptor (Sapp and Bienkowska-Haba, 2009) and this binding is mediated by capsid protein L1 (Raff et al., 2013). For example, it has been demonstrated that in COS-7 cells depleted of HSPG that HPV-16 and 33

pseudovirions were incapable of causing infection (Giroglou et al., 2001; Sapp and Bienkowska-Haba, 2009). It has also been proposed that HPVs may undergo specific interactions after HSPG binding and prior to viral entry, resulting in a conformation change to the capsid. Binding of HSPG has been demonstrated to result in a conformation change to L1, enabling cleavage by the trypsin-like serine protease kallikrein-8 (KLK8), which may enable further enzymatic access to the capsid proteins (Cerqueira et al., 2015; Becker et al., 2018). Further conformation changes are generated by Cyclophilin B/protein convertase furin mediated L2 cleavage, resulting in L2 N-terminus exposure (Raff et al., 2013), known as the RG-1 epitope. The conformational change results in reduced affinity for HSPG, enabling interactions with the secondary receptor and hence viral entry (Raff et al., 2013; Selinka et al., 2003). Currently, the identity of the secondary receptor is unclear, however the tetraspanin CD151 has been proposed (Day and Schelhaas, 2014; Scheffer et al., 2013) as have  $\alpha 6$  integrins (Raff et al., 2013) and annexin A2 heterotetramer (Day and Schelhaas, 2014). Studies with HPV16 and keratinocyte cell lines suggest that HPV initiates growth factor signalling prior to entry, through a HSPG/Growth factor receptor/virus complex, possibly paving the way for successful infection (Raff et al., 2013). Following receptor interactions, the virion is endocytosed. However, it appears that HPV endocytosis is Clathrin, calveolin and lipid independent and recent studies have suggested that it may occur via its own novel pathway (Day and Schelhaas, 2014; Scheffer et al., 2013).

HPV infects the keratinocytes of the epithelium, and this is thought to occur through micro-wounding (Figure 1.11), which enables virions to infect the basal cells of the epithelium. It has been suggested that the wound healing response contributes to the ability of HPVs to infect the host cell, possibly owing to the induction of mitosis providing a more hospitable environment for the virus (Doorbar et al., 2012). However, it is important to think laterally of the epidermis. The epidermis covers a wide range of body areas, and as a result undergoes changes between tissue types, from stratified squamous epithelium to columnar epithelium (Herfs et al., 2012). These junctions are known as squamocolumnar junctions (SCJs) and are

located near the transformation zone, and are found at the cervical, ano-rectal and gastroesophageal junctions. SCJs possess specific markers, which are often seen in high grade CIN2/3 lesions, suggesting that these cells could be the progenitors for neoplasms, with most cervical cancers arising in this region (Herfs et al., 2012; Herfs et al., 2013).

Upon endocytosis, the acidification of the endosome results in viral uncoating, with the viral genome remaining in complex with the L2 protein ensuring that correct entry to the nucleus occurs (Doorbar, 2006; Doorbar et al., 2012). Post uncoating, the egress from endosomes and transit to the trans-Golgi network (TGN) appears to require the retromer complex, in addition to Rab9a, Rab7a and Rab7b (Day and Schelhaas, 2014; Siddiqi et al., 2018). To enter the nucleus, the viral DNA (vDNA) then requires cell cycle progression, as breakdown of the nuclear envelope (NE) is required. Once in the nucleus the vDNA localises to promyelocytic leukaemia protein (PML) bodies.

Initial infection appears to require a mitotically active cell, which enables the amplification of the genome (Doorbar et al., 2012; Longworth and Laimins, 2004). Stable establishment of the episomal tethered genome and initial amplification appears to require viral proteins E1 and E2, with a stable copy number of 20-100 genomes per cell being produced (Longworth and Laimins, 2004; Doorbar et al., 2012). After initial replication, asymmetric cell division (Figure 1.8) ensures that a daughter cell remains in the basal layer to act as a reservoir for viral episomes. Initial infection also involves the production of viral proteins E6 and E7 (Figure 1.11), which drive the proliferation of the cells upon exit into the suprabasal layer, maintain an active cell cycle, expanding the pool of infected cells and enabling genome amplification. These proteins will target a variety of cellular proteins, such as Rb, p53, p21 and p27 with the aim of preventing cell cycle arrest, apoptosis and immune detection (Doorbar et al., 2012; Roman and Munger, 2013; Vande Pol and Klingelutz, 2013).

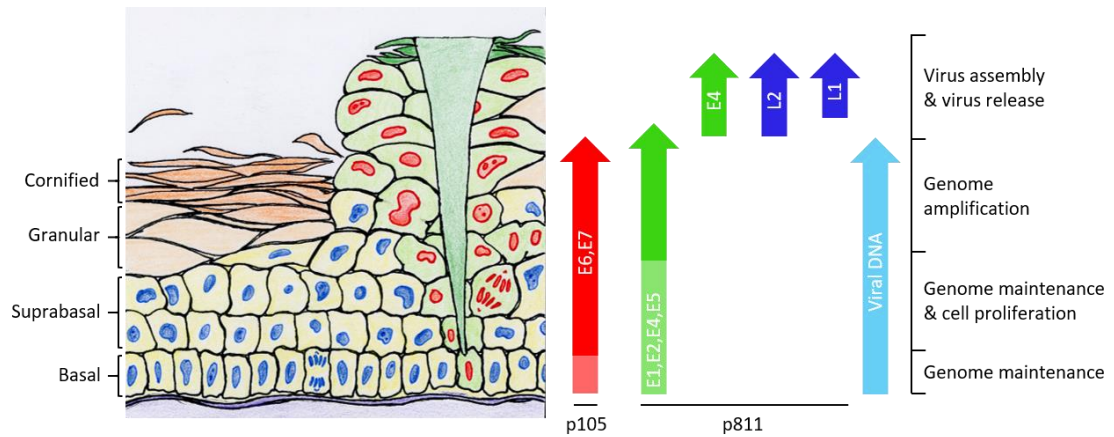


**Figure 1.11** *Schematic of the epithelial stratification and HPV lifecycle and HPV gene expression.*

*Schematic of the architecture of the stratified epithelium in normal and HPV infected skin. Infected cells shown in green with red nuclei. Infection occurs via micro wounding, enabling access to the basal layer and establishment of HPV infection. Stages of the viral lifecycle and HPV gene expression are outlined.*

As the infected keratinocyte progresses into the suprabasal layer transcription occurs from the late promoter, which is believed to be triggered by differentiation signals from the surrounding microenvironment. Resulting in entry into an S-like phase in which both viral and cellular DNA will be amplified (Doorbar et al., 2012; Longworth and Laimins, 2004; Fehrmann et al., 2003). The infected keratinocytes will respond to the differentiation signals, for example through the production of Keratins 1 and 10, yet will also display cellular markers of cell cycling such as MCM, cyclin E and A expression, as well as the retention of the nucleus (Doorbar et al., 2012). Towards the end of the viral life cycle, capsid proteins L1 and L2 will begin to accumulate as well as E1 and E4. Assembly of the virion requires E2, and L2 is recruited to areas of genome amplification (Doorbar et al., 2012; Doorbar, 2005; Deng et al., 2004; McBride, 2013). The protein E4 begins to form amyloid fibrils that disrupt the keratin structure of the cell and prevent cornification. Finally, as the keratinocyte begins to mature, the cellular environment becomes oxidising, causing the formation of disulphide bonds between the L1 capsid proteins, resulting

in the formation of a robust virion (Doorbar et al., 2012). Finally, the virus is then shed, to establish further infections.

## **1.7 Papillomavirus proteins**

### **1.7.1 The E1 and E2 regulatory proteins**

The E1 protein is the only PV protein with enzymatic activity, and it is the most highly conserved protein of the PVs (Bergvall et al., 2013). The E1 protein is capable of self-oligomerising and forms a double hexameric DNA helicase. The E1 protein is highly regulated through different mechanisms, including caspase cleavage, phosphorylation, SUMOylation and ubiquitination (Mechali et al., 2004; Moody et al., 2007; Knight et al., 2011; Bergvall et al., 2013). In PV infected cells the levels of the E1 protein are very low, this is due to the instability of the protein and its degradation via the ubiquitin-proteasome pathway (Mechali et al., 2004).

The key roles of the E1 proteins are to establish an increased level of viral episomes in the basal keratinocyte immediately post infection, then to maintain a constant level of episomes in the dividing cells as they migrate up through the epithelia, and finally to amplify the genome copy numbers during the productive phase of infection (Bergvall et al., 2013). In undifferentiated cells, E1 replicates the viral genome via a bidirectional replication fork. However, in differentiating cells a switch in the method of replication occurs and replication occurs via a rolling circle mechanism, allowing rapid amplification of the viral genome (Flores and Lambert, 1997). The cleavage of the N-terminal region of the E1 protein by caspases is believed to support this switch (Moody et al., 2007).

The E1 protein has three distinct domains. The first domain is the N-terminal domain, which is the least conserved region. However, key functional motifs are conserved such as the bipartite nuclear localisation signal (NLS), the crm1 dependent nuclear export signal (NES) and the cyclin binding motif (CBM). The NES acts as a dominant nuclear export signal, however this

is prevented by interactions with the cyclins A/E in complex with the cyclin dependent kinase (CDK2), which phosphorylates the N-terminus of E1 to ensure retention during S-phase (Deng et al., 2004; Fradet-Turcotte et al., 2010). This ensures that vDNA replication is synchronised with that of the host DNA. Further regulation by phosphorylation of E1 is achieved by ERK and JNK2 phosphorylation of serine residues in the NLS. Additionally, the C-terminus of E1 possesses two MAPK docking sites, which further promote nuclear import (Yu et al., 2007).

The second key domain of E1 is its DNA binding domain (DBD), which recognises the specific sequence of the PV *ori* which is found in the URR. The *ori* has six E1 binding sites (BS), with a consensus sequence of 5'-ATTGTT-3' (Titolo et al., 2003), the first four E1BS orchestrate the association of E1 double trimers, which are a key intermediate for the formation of the functional double E1 hexamer required for DNA replication (Schuck and Stenlund, 2005). *In vivo* the recognition of the *ori* by E1 requires the PV protein E2, which will act as a loading factor for E1 by binding to the E1 protein and E2 binding sites. This is required as E1 has only a moderate affinity *in vivo* for its E1BS and association with E2 avoids non-specific binding to host DNA. The binding of the E2 transactivating domain to the C-terminal helicase domain of E1 produces a E1-E2-ternary complex, and acts as a tether to the *ori* (Titolo et al., 2003; Titolo et al., 1999; Müller, F. and Sapp, 1996).

The helicase domain of E1 is the final domain, containing an AAA+ ATPase domain and the oligomerisation domain, enabling assembly into the double hexamer in the presence of ATP and the *ori*, or a hexamer in the presence of ssDNA (Hughes and Romanos, 1993). This domain also contains the C-terminal brace, that plays a role in stabilisation of the hexamer, maintaining its oligomeric state during conformational changes wrought by ATP binding and hydrolysis during DNA unwinding (Whelan et al., 2012).

The E2 protein is essential to all PV and possesses the ability to homodimerize. Several spliced forms of E2 exist such as E2<sup>E8</sup>, which function as viral transcription and replication

repressors (McBride, 2013). The E2 protein is important for controlling the transcription of viral genes, through the recruitment of host and viral proteins, which can activate or suppress viral gene transcription.

The E2 proteins contain three domains, the transactivation domain, hinge region and DNA binding and dimerization domain. The TA domain is important in genome replication through its association with E1 (Titolo et al., 1999), as well as for its role in tethering the viral genome to host chromatin through association with host cell factors such as Brd4 and ChIR1, to ensure that the viral episomes are partitioned upon cellular division (Abbate et al., 2006; Parish et al., 2006a; Chang, S.W. et al., 2014). The hinge region, whilst poorly conserved is important for nuclear localisation and association with host chromatin through phosphorylation (Chang, S.W. et al., 2014). The C-terminal domain is the DNA binding and oligomerisation domain (McBride, 2013), which recognises the sequence ACCN<sub>6</sub>GGT which is in the URR of the PV genome (Hawley-Nelson et al., 1988). This region is also targeted for phosphorylation by the host cell factor CDK2.

The E2 proteins are localised to the nucleus by means of an NLS, and additionally by a tract of basic residues located in the hinge region. The E2 proteins are unstable, with a half-life of 40 minutes observed for the full-length protein, and shorter for the spliced forms (Hubbert et al., 1988), with the N-terminus of E2 a target for proteasomal degradation (Bellanger et al., 2001). E2 proteins are regulated by phosphorylation, acetylation and SUMOylation (Wu, Y.C. et al., 2009; Chang, S.W. et al., 2014; Quinlan et al., 2013), as well by as protein-protein interactions. These interactions can destabilise or stabilise E2, for example association with the host chromatin adaptor protein Brd4 stabilises the E2 protein (Chang, S.W. et al., 2014). The E2 ORF is transcribed from both the early and late promoters, depending on lifecycle stage. The E2 protein is also able to associate with the viral capsid protein L2, this interaction has been shown

to be required for the establishment of initial viral replication and infection (Holmgren et al., 2005).

At low concentrations the E2 protein promotes viral transcription; however, E2 possesses the ability to self-regulate. There are four E2 BS adjacent to the early promoter from which E2 is transcribed, and at high concentrations it can bind these sites, and prevent any further initiation of this promoter, hence suppressing its own transcription (Stubenrauch and Laimins, 1999), this allows a stable copy number of episomes to be established. Upon initiation from the late promoter, transcription of both E1 and E2 resumes, but the late promoter is unaffected by E2 inhibition, enabling genome amplification.

The E2 region is often found mutated or integrated in cancer, resulting in the loss of transcriptional repression of the oncoproteins E6 and E7, leading to their uncontrolled transcription which aids in cellular transformation (Collins et al., 2009).

E2 and E1 are responsible for the initiation and maintenance of viral replication from the *ori*, with the E1-E2-ternary complex ensuring that E1 binds to the palindromic E1BS, followed by the assembly of an E1 double trimer in a head to head configuration (Enemark et al., 2002). This melts the DNA at the *ori*, in an ATP dependent manner (Schuck and Stenlund, 2011). This enables the formation of the double hexamer, which unwinds the DNA further. Viral DNA is then replicated by recruitment of host replication machinery, such as replication protein A and topoisomerase I (Han, Y. et al., 1999; Clower et al., 2006).

### **1.7.2 The L1 and L2 structural proteins**

The PV capsid is composed of the major structural protein L1 and the minor structural protein L2. L1 is a protein of ~55kDa size (Buck et al., 2013), L2 is also predicted to be ~55kDa in size yet runs at 64-74kDa on SDS-PAGE gels (Wang, J.W. and Roden, 2013). The mature virion is ~60nm in diameter and composed of 72 pentameric capsomeres. The mature virion is composed of 360 L1 proteins, and possibly up to 72 L2 proteins, it is predicted that the ratio of L1 to L2 is

5:1, however, the exact number still is up for debate (Buck et al., 2008). The L1 protein makes up the external face of the capsid, with its N- and C-termini facing the viral lumen, the L2 buried within the capsid pentamers.

L1 facilitates entry via its interaction with HSPG as the primary attachment receptor (Sapp and Bienkowska-Haba, 2009; Raff et al., 2013). Binding of HSPG results in a confirmation change to L1, enabling cleavage by the trypsin-like serine protease KLK8, possibly enabling further enzymatic access to the capsid proteins (Cerqueira et al., 2015; Becker et al., 2018). Further confirmation changes are generated by Cyclophilin B and furin mediated L2 cleavage, resulting in L2 N-terminus exposure (Raff et al., 2013). This enables interactions with the secondary receptor and viral entry (Raff et al., 2013; Selinka et al., 2003). The identity of the secondary receptor remains unknown, however CD151,  $\alpha 6$  integrins and annexin A2 have been proposed (Day and Schelhaas, 2014; Scheffer et al., 2013; Raff et al., 2013).

Upon entry, the virus is trafficked via the endocytic pathway, sorting to early endosomes, which then mature to late endosomes (LE), the formation of the LE results in multivesicular bodies (MVBs), these MBVs contain intraluminal vesicles (ILVs), ILVs are formed with the help of the endosomal sorting complex (Siddiqa et al., 2018). One of the components of this is the protein Alix which forms a complex with CD63 and syntenin-1, which controls PV trafficking into multivesicular endosomes, where capsid disassembly can occur (Gräßel et al., 2016). Endosome acidification is thought to be crucial here, where cyclophilin B mediates the separation of the L2-vDNA complex from the L1 capsid proteins (Bienkowska-Haba et al., 2012).

The C-terminus of L2 contains a membrane destabilising peptide that enables access of the L2 protein to the cytoplasm (Kämper et al., 2006). This C-terminus has been demonstrated to interact with the Retromer complex, formed of VPS26, VPS29 and VPS35, and this interaction is thought to enable endosomal exit to the TGN (Popa et al., 2015; Siddiqa et al., 2018). The L2-vDNA complex is then trafficked to the nucleus via the molecular motor protein dynein

(Schneider et al., 2011). Final entry to the nucleus then requires breakdown of the nuclear envelope during mitosis. The central region of L2 has also been demonstrated to enable viral genome tethering to chromosomes, thereby enabling the establishment of infection (Aydin et al., 2017).

L1 and L2 are transcribed from the late promoter during the productive stage of the lifecycle. L1 and L2 are produced in the cytoplasm. L1 forms pentamers in the cytoplasm which are then imported into the nucleus. The nuclear import of L1 is mediated by a polybasic patch at the C-terminus (Zhou, J. et al., 1991). L2 also possesses nuclear localisation signals, at both its N and C-terminus, and complexing with heat shock cognate protein 70 (Hsc70) has been shown to be required for L2 nuclear import (Florin, L. et al., 2004). Assembly into the virion occurs in the nucleus, and to finally mature the virion, disulphide bonds are formed, ensuring capsid stability and infectivity (Cardone et al., 2014; Campos and Ozbun, 2009).

### **1.7.3 The E4 protein**

The E4 ORF is located within the ORF for the E2 protein, and it is a spliced RNA product, which includes the first five codons of the E1 protein. The overlap with the E2 protein corresponds to the flexible hinge region of the protein, this protein is referred to as the E1<sup>E4</sup> protein and is the primary gene product of the E4 gene and is what is commonly referred to as the E4 protein (Doorbar, 2013). The E4 gene product is generally expressed prior to the production of the structural proteins L1 and L2 (Florin, Luise et al., 2002), and its expression occurs from the late promoter, when the switch from maintenance viral DNA replication to vegetative viral DNA replication occurs (Ozbun and Meyers, 1997). The E4 protein is expressed at high levels in the productive lifecycle of the PV virus, in cells that are undergoing or have undergone genome amplification, and as a result is often considered a good biomarker for a productive infection (Griffin et al., 2012). The E4 protein can cause a G2/M arrest, through

binding to active Cdk complexes and cyclins A/B1 through its RXL tripeptide motif (Knight et al., 2011), promoting viral amplification.

The E4 protein is post translationally modified by the action of kinases and proteases (Doorbar, 2013), and these modifications are key to the proteins' activity. The E4 protein has been demonstrated to associate with and disrupt the cyokeratin network of cells, through E4 multimerization to produce amyloid-like fibres (McIntosh et al., 2008) which associate with keratins, and cleavage by the cellular protease calpain has been shown to be crucial to this (Khan, J. et al., 2011). Phosphorylation of the E4 protein by ERK MAPK stabilises the protein and enhances its association with cyokeratin (Wang, Q. et al., 2009). Association with keratin has been demonstrated to trigger keratin hyperphosphorylation, which results in the activation of p38 MAPK and JNK (McIntosh et al., 2010). In organotypic raft cultures, the knockout of the E4 protein has been shown to delay genome amplification and L1 expression, and that HPV-16 is affected worse than HPV-18. It was found that the delay in genome amplification was due to the loss of cytoplasmic active JNK triggered by the activity of E4 (Egawa et al., 2017). The E4 protein has also been demonstrated to retain cytoplasmically active Cdk1/Cyclin B1 complexes (Davy et al., 2005), which drive HPV-16E1 accumulation in the nucleus and increase E2 stability through phosphorylation, thereby enhancing E1/E2 *ori* dependent replication (Egawa et al., 2017). Loss of the E4 protein in the infectious lifecycle of the virus has been demonstrated to reduce the titre and infectivity of produced virus, impacting the maturation of virions and decreasing the stability of the virions formed (Biryukov et al., 2017).

#### **1.7.4 The E6 protein**

The  $\alpha$ -HPV E6 protein is generally around 150 amino acids in length and contains two zinc fingers composed of CXXC motifs (Figure 1.12), which are highly conserved. High risk HPV E6 proteins also contain a PDZ (post synaptic density protein, drosophila disc large tumour suppressor, zonula occuldens-1 protein) binding motif at their C-terminus (Tomaić, 2016). The

subcellular localisation of the E6 protein varies depending on HPV type, with high-risk type HPV E6 localised to both nucleus and cytoplasm, and low-risk type HPV E6 localises to the nucleus (Stewart et al., 2005).

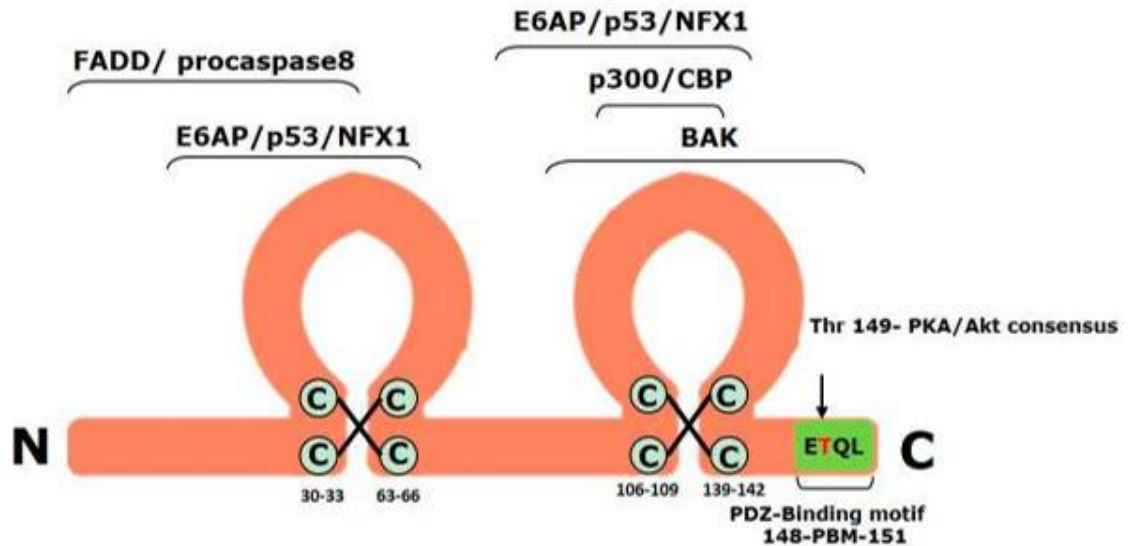


**Figure 1.12** Schematic diagram of the high-risk HPV-16 E6 oncoprotein (from (Tomaić, 2016))

The location of the motifs important for E6 activity and structure are shown. The E6 protein contains two zinc fingers, based around CXXC motifs, regions of the protein responsible for interactions with cellular proteins are indicated e.g. p300/CBP. The C-terminal PDZ binding motif is indicated in green and the PKA phosphorylated Threonine indicated in red.

The primary cellular target of high-risk HPV E6 proteins is the tumour suppressor protein p53. In normal cells, the transcription factor p53 is regulated through its interactions with the mouse double minute 2 homologue protein (MDM2), which is a ubiquitin ligase that mediates the degradation of p53 via the proteasome. When cells are under stress the p53 protein undergoes phosphorylation or acetylation, activating it and preventing its MDM2 mediated degradation (Moll and Petrenko, 2003). P53 can then exert effects such as cell cycle arrest and apoptosis through its downstream effectors, such as by increasing p21 expression, thereby preventing entry into S phase or M phase and arresting the cell cycle.

The E6 protein can cause the degradation of p53 through its ability to associate with host proteins containing LXXLL motifs via its zinc finger motifs (Zanier et al., 2013). This is achieved through complexing with the ubiquitin ligase E6AP (also known as ubiquitin protein ligase E3A, UBE3A) LXXLL motif, which then can bind and mediate the ubiquitin-proteasomal degradation of p53 (Scheffner et al., 1993). The binding of E6AP changes the conformation of E6, enabling it to interact with p53, additionally the E6 protein is stabilised by its interaction with E6AP (Tomaić et al., 2009). The ability of E6 to degrade p53 is important, as the actions of the HPV E7 protein stimulate increased p53 levels through the degradation of pRb and the induction of the DNA damage response, which would lead to cell cycle arrest and/or apoptosis (Hong and Laimins, 2013). The E6 protein is also able to regulate levels of p53 in a proteasome independent manner, through its ability to associate with p300 (Figure 1.12) and prevent p300-mediated p53 acetylation, this results in decreased p53 stability and reduced transcriptional activity of p53 target genes such as p21 (Patel et al., 1999; Zimmermann et al., 1999; Thomas, M.C. and Chiang, 2005). The low-risk HPV E6 proteins can bind to the E6AP protein and stimulate its ubiquitin ligase activity, however this does not result in the degradation of p53. The low risk E6 proteins do modulate p53 through preventing its p300-mediated acetylation (Thomas, M.C. and Chiang, 2005). Both high-risk and low-risk HPV E6 proteins are able to bind E6AP and mediate the degradation of the PDZ adapter protein NHERF1, consequently activating WNT/ $\beta$ -catenin signalling, thereby promoting cell growth and proliferation (Drews et al., 2019).

The high-risk HPV E6 proteins are characterised by their possession of class-I PDZ binding motifs (PBM). The PDZ protein binding domain is located at the C-terminus (Figure 1.12), and has the consensus motif of X-T/S-X-L/V. This enables the degradation of PDZ domain containing proteins such as the tumour suppressor proteins Dlg and Scribble (Nakagawa and Huibregtse, 2000; Kiyono et al., 1997). Interestingly, there seems to be a correlation between the oncogenic potential of an HPV and the number of proteins bound by its PBM (Thomas, M. et al., 2016). The protein Dlg1 was found to be a common interactor for all PBMs, whereas the ability to bind the

target Scribble was found to correlate with oncogenic potential. Many of the PDZ containing proteins targeted for proteasome mediated degradation by the PBM of E6 are scaffold proteins, which assemble signalling complexes at regions of cell junction contact (Tomaić, 2016), and when lost the integrity of tight junctions is lessened.

The binding preference of the PBM of E6 seems to vary between HPV types, with HPV-18 possessing stronger affinity to Dlg1 and MAGI-1 than HPV-16, which binds Scribble more strongly. This affinity can be altered by swapping the last residue of the PBM of HPV-16E6 for that of HPV-18E6's PBM (Thomas, M. et al., 2001). The HPV-16 and 18 PBM is also able to be regulated by phosphorylation and is sensitive to protein kinase A (PKA) phosphorylation. PKA phosphorylation of the E6 PBM prevents PDZ association, yet confers the ability to interact with 14-3-3 $\zeta$ , which helps maintain E6 levels (Boon and Banks, 2013). Loss of the PBM in the HPV-31 lifecycle was shown to slow growth and reduce viral copy numbers (Lee, C. and Laimins, 2004), with similar results observed in HPV-18 (Delury et al., 2013), however, disruption of the PKA recognition site resulted in increased growth and hyperplasia.

The E6 protein is also able to regulate apoptosis through a variety of means. The E6 protein can degrade Fas-associated death domain (FADD) and procaspase 8 through interacting with their death effector domains (DED) via the C-terminus of E6 (Figure 1.12), targeting them for degradation (Tungteakkhun et al., 2010; Filippova et al., 2004). E6 can also degrade the pro-apoptotic protein Bak via E6AP mediated proteasomal degradation (Thomas, M. and Banks, 1998), and can upregulate the expression of the pro-survival protein survivin (Borbély et al., 2006).

E6 can also promote survival through activation of the signal transducer and activator of transcription-3 (STAT3). Growth factors and cytokines binding cell surface receptors activate receptor activated kinases e.g. JAK or RTKs e.g. EGFR which then activate STAT3 through phosphorylation of its Y705. It can also be phosphorylated at its S727 residue. Active STAT3

translocates to the nucleus and initiates gene expression programs, such as those involved in survival. Active STAT3 also drives epithelial proliferation and prevents differentiation, and it is often constitutively active in cervical cancers. E6 has been demonstrated to cause phosphorylation of Y705 and S727, and thereby increasing STAT3 activity, and this has been observed in cervical cancer biopsies, and STAT3 activity has been shown to be required for the HPV lifecycle (Morgan et al., 2018). Recently, the mechanism behind this was shown to be through E6 mediated IL-6 production via NF- $\kappa$ B signalling. IL-6 then signals in an autocrine manner to drive STAT3 phosphorylation, driving proliferation and survival (Morgan and Macdonald, 2019). Absence of active STAT3 in cervical cancer induces apoptosis, therefore E6 enhances cervical cancer survival through its actions on STAT3.

### **1.7.5 The E7 protein**

The E7 protein is the major transforming protein of high-risk HPV. E7 proteins are small, generally around 100 amino acids in length and highly acidic, localising primarily to the nucleus of the cell, but also shuttling between the nucleus and cytoplasm. The E7 protein contains both nuclear localisation and nuclear export signals (Knapp et al., 2009). The E7 protein possesses three conserved domains. The flexible N-terminus of the E7 protein contains two conserved regions (CR), CR1 and CR2, which are separated by a non-conserved stretch of amino acids. CR1 and CR2 possess some similarities to the simian vacuolating virus 40 (SV40) large T antigen and the adenovirus E1A protein in their amino acid motifs. The C-terminus of E7 is also a conserved domain, containing two CXXC motifs, which act as zinc binding sites (Roman and Munger, 2013) (Figure 1.13).

The CR2 domain contains the LXCXE motif, this mediates binding to the cellular proteins pRb, p105 and p130, stimulating their degradation. The degradation of the pRb occurs through the

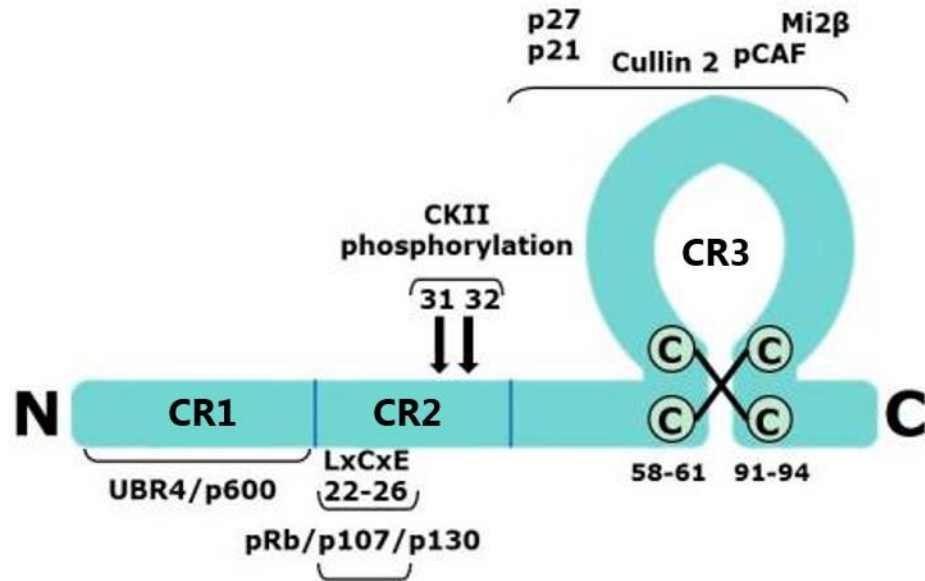


**Figure 1.13** Schematic diagram of the high-risk HPV-16 E7 oncoprotein (from (Tomaić, 2016))

The location of the motifs important for E7 activity and structure are shown. The E7 protein contains three conserved regions (CR1-3). The zinc finger is shown (CR3) as well as the LXCXE motif responsible for pRb binding. Casein Kinase II (CKII) phosphorylation sites are also indicated.

association of the pRb/E7 protein complex with the cullin 2 ubiquitin ligase complex, thereby leading to the ubiquitination of pRb and proteasomal degradation (Huh et al., 2007). pRb functions as a suppressor of the transcription factor E2F, the loss of pRb binding mediated by E7 results in the release of E2F (Helt and Galloway, 2001), this enables HPV to overcome the checkpoint R, bypassing G1/S. E2F is then able to constitutively activate DNA synthesis and cell proliferation, through increasing the expression of proteins such as Cyclin E and A (Martin et al., 1998; Zerfass et al., 1995). The E7 protein is also able to directly bind to E2F, thereby enhancing its function. The CR2 domain is also phosphorylated by the cellular kinase casein kinase II (CKII) at serine 31 and serine 32 in HPV-16 (serine's 32 and 34 in HPV-18) (Tomaić, 2016), this phosphorylation enhances the binding affinity of E7 for E2F, which is important in driving S-phase entry (Chien et al., 2000). E7 proteins usually have a short half-life of less than one hour (Selvey et al., 1994), however HPV-16E7 phosphorylation at threonines 5 and 7 located in the

CR1 domain by dual-specificity tyrosine phosphorylation-regulated kinase 1A (DYRK1A) enhances the stability of the E7 protein by interfering with its 26S proteasome-dependent degradation (Liang, Y.J. et al., 2008). The increased stability of E7 results in enhanced degradation of pRb, thereby enhancing cellular proliferation and transformation ability. Low-risk HPV E7 lack the high affinity for pRb seen in high risk types. High risk E7 proteins also possess the ability to override growth arrest through binding to and inactivating the Cdk inhibitors p21<sup>Cip1</sup> and p27<sup>KIP1</sup> (Shin, M.K. et al., 2009; Zerfass-Thome et al., 1996), preventing CDK2 inhibition and removing the block on CDK2-Cyclin complexes, enabling the bypassing of the G1/S checkpoint. The E7 protein is also able to directly activate CDK2 through binding via CR1 and CR2, enabling the promotion of S-phase onset (He et al., 2003). Through its action E7 can maintain cellular proliferation, and therefore DNA synthesis, enabling HPV genome replication.

The E7 protein is also able to aid in immune evasion by HPV. The HPV E7 protein associates with the MHC class I promoter and impairs the expression of the MHC heavy chain, it also suppresses antigen processing, via repression of TAP2 and LMP2 expression thereby reducing immune detection (Georgopoulos et al., 2000; Li, H. et al., 2009). Further to this, E7 has been demonstrated to reduce levels of the TLR-9 protein, by downregulating its transcription and impairing innate immune sensing (Hasan et al., 2007).

HPV E7 also dysregulates processes that increase the future risk of cellular transformation. For example, in response to DNA damage in HPV-16E7 expressing cells, the DNA replication initiating factor Chromatin licencing and DNA replication 1 (Cdt1) is seen to be overexpressed (Fan et al., 2013). This enables the process of re-replication, whereby cells arrest at G2 and undergo repeated rounds of DNA replication without undergoing mitosis, which results in genomic instability. It has also been shown that E7 induces STAT5 activation, which activates the ataxia-telangiectasia mutated (ATM) protein DNA damage response, again leading to genome instability (Hong and Laimins, 2013), thereby promoting the chance of HPV genome

integration. This combined with E7s ability to downregulate the anti-proliferative miRNA203 (Melar-New and Laimins, 2010) and promoting expression of matrix metalloproteinases (MMPs) (Cardeal et al., 2012; Smola-Hess et al., 2005) further predispose cells to cancer.

## 1.8 The E5 protein

### 1.8.1 The natural history of E5

The enigmatic E5 oncoprotein is the least well understood HPV gene product. The E5 protein is considered to be the 'minor' oncoprotein of high risk alpha HPV, which contrasts to other known E5 proteins, such as BPV E5 in which it is the major oncoprotein (Rodriguez et al., 2000). The E5 protein is not present in all HPVs, but is well conserved and maintained in many, such as the high-risk types (Wetherill et al., 2012). Considering the small size of the HPV genome, it is unlikely that the gene would be retained if it was not required for productive infection. The HPV E5 proteins are small (HPV18 78 amino acids, HPV16 83 amino acids), highly hydrophobic membrane integrated proteins (Wetherill et al., 2012).

The E5 proteins are not encoded by all PVs, however, those which are expressed can be divided into six main families of evolutionarily related proteins,  $\alpha$ ,  $\beta$ ,  $\gamma$ ,  $\delta$ , A and B. The E5 families A and B are found in ungulates, and do not group with the other E5 families. The high-risk HPV types 16, 18 and 31 all possess an  $\alpha$ -family E5, characterised by a global hydrophobic pattern with three hydrophobic regions which are conserved within the family, even though the amino acids sequences are not. The  $\beta$ -family E5 do not possess sequence similarity with those of the  $\alpha$ -family E5, however, the sequence similarity is high within the family. Cutaneous  $\alpha$ -HPV, such as HPV-2 often encode  $\beta$ -family E5, and this family of E5 proteins possesses only one hydrophobic domain, localised at the proteins C-terminus.

The  $\gamma$ -family E5 are highly hydrophobic, possessing three putative transmembrane domains. Low-risk HPV types 6 and 11 both possess a  $\gamma$ -family E5, however, they also possess E5

of the  $\delta$ -family. These E5 proteins are well conserved, with greater than 50% sequence homology and 80% amino acid similarity, and this conservation is observed both in human and non-human E5s of this family suggesting that the  $\gamma$ -E5 is important to the lifecycle of these viruses. The  $\delta$ -family E5 possess only one putative transmembrane domain, located at the proteins N-terminus, which is well conserved between  $\delta$ -E5.

The shared characteristics of E5 proteins are that they are highly hydrophobic, that they possess high Ile-Leu-Val content and that they possess transmembrane regions. Due to the spread of E5 types, if they all arose from a common ancestor, this ancestor would have to predate the split between apes and ungulates ~75 mya. Interestingly, the E5 protein is the PV early protein which has diverged the most, and its divergence is greatest in those HPV types with high oncogenic potential, suggesting that it is under high evolutionary pressure.

### **1.8.2 The cellular functions of E5**

When transfected into primary keratinocytes HPV16 E5 localises to the endoplasmic reticulum (ER) (Disbrow et al., 2003), and has also been shown to localise to the Golgi apparatus (GA) and perinuclear region (Wetherill et al., 2012). The E5 protein possesses the ability to homo-oligomerise, forming dimers and oligomers that are visible on SDS PAGE gels (Wetherill et al., 2012), this is indicative of a strong interaction between E5 oligomers.

When transfected into murine fibroblasts HPV-16E5 demonstrated the ability to induce cellular proliferation in response to EGF (Pim et al., 1992), furthermore HPV-16E5 was able to induce anchorage independent growth and weakly transform murine fibroblasts (Straight, Samuel W. et al., 1993). The E5 protein has been demonstrated to interact with a number of membrane interacting partners including YIPF4, Bap31, calpactin I, A4, karyopherin  $\beta$ 3 and the 16kDa subunit of the vacuolar H<sup>+</sup> ATPase (Halavaty et al., 2014; Krawczyk et al., 2008; Krawczyk et al., 2011; Muller et al., 2015; Regan and Laimins, 2008; Rodriguez et al., 2000). Most of these partners were identified through yeast two-hybrid (Y2H) screening which can give false

positives. However, they are supported by immunofluorescence, co-localisation and co-immuno-precipitation experiments.

One of the key targets of the E5 proteins is EGFR signalling. E5 has been shown to facilitate the *in vitro* transformation of cells through its actions on EGFR (Pim et al., 1992; Leechanachai et al., 1992; Tomakidi et al., 2000), and *in vivo* mouse studies where E5 is expressed under the control of the cytokeratin-14 (CK14) promoter have demonstrated that EGFR is crucial to E5 mediated tumour formation (Genther Williams et al., 2005). Increased levels of EGFR are often seen in HPV related cancers such as cervical and anal cancer (Schrevel et al., 2011; Wechsler et al., 2018), however E6 and E7 are also able to upregulate EGFR expression (Akerman et al., 2001). The mechanisms by which E5 acts on the EGFR pathway are however still under investigation.

Studies have suggested that HPV-16E5 can complex with EGFR (Hwang et al., 1995), however another study suggested that HPV-6E5 but not HPV-16E5 was able to do so (Conrad et al., 1994). However, whether this interaction effected the activities of EGFR was not shown. An initial model for the ability of E5 to hyperactivate EGFR was thought to be through its ability to influence endosome acidification, and therefore prevent degradation of EGFR and increase recycling. HPV-16E5 had been demonstrated to associate with the 16kDa subunit of the vacuolar proton ATP-ase (Straight, S. W. et al., 1995), and in keratinocytes overexpressing HPV-16E5 simulated with EGFR, endosomal acidification had been demonstrated to be delayed fourfold. However, later studies suggested that whilst HPV-16E5 was able to bind and disrupt the vacuolar ATPase (Briggs et al., 2001), the residues responsible for its binding and EGFR activation were distinct, and mutants could be made that were able to bind the ATPase but not overactivate EGFR (Rodríguez et al., 2000). Further studies suggested that HPV-16E5 did inhibit endosomal acidification, but only associated with a small proportion of endosomes positive for the vacuolar ATPase, therefore making it unlikely that this was the reason for the delay in acidification

(Supryniewicz et al., 2010). It was suggested that the inhibition of EGFR trafficking and resulting overactivation of EGFR was occurring via a pH-independent inhibition of vesicle fusion. Recent studies have shown that HPV-18E5 and 16E5 possess viroporin activity (Wetherill et al., 2018; Wetherill et al., 2012), this channel forming ability could provide a potential mechanism for the decrease in acidification observed. Additionally, these viroporins proved sensitive to inhibition by the viroporin inhibitor Rimantadine, as well as alkyl-imino sugars (Wetherill et al., 2018), resulting in reduced ERK-MAPK signalling and reduced cyclin B1 expression, key downstream targets of EGFR. This suggests that the endosome acidification step is important to the overactivation of EGFR by E5.

Alternative mechanisms have been proposed for the enhanced signalling through EGFR via E5. The E3 ubiquitin ligase c-Casitas B-Linageage Lymphoma (c-Cbl) associates with the active form of EGFR, targeting it for proteasomal degradation. However, in the presence of HPV-16E5 less c-Cbl is found in complex with EGFR, and less ubiquitinated EGFR is detected, suggesting that E5 prevents EGFR degradation, enabling extended duration of signalling and greater recycling to the cell surface (Zhang, B. et al., 2005).

Studies have been carried out to investigate the loss of the E5 protein on the HPV lifecycle in high risk HPV types. The method for producing knockout genomes is common to the studies on HPV-16, 18 and 31, and involves putting a stop codon early in the HPV E5 ORF (Position 11 in 16, 2 in 18 and 3 and 7 in 31), preventing the production of E5 (Fehrmann et al., 2003; Genter et al., 2003b; Wasson et al., 2017). The HPV-31 study also altered the start codon of the E5 ORF and saw the same effects as placing a stop codon. Loss of E5 has been shown to have no effect on the maintenance of the HPV genome in undifferentiated cells in any of the HPV types studied. However, type specific differences are observed. In HPV-16 and HPV-18, no loss of viral late gene expression is observed, with late gene L1 and E1<sup>E4</sup> comparable to cells maintaining the wild type (WT) genome (Genter et al., 2003b; Wasson et al., 2017), which

contrasts with findings for HPV-31, where a significant reduction in the levels of E1<sup>E4</sup> were observed, in addition to reduced late gene transcription (Fehrmann et al., 2003). No reduction in the number of cells supporting viral genome amplification was observed in HPV-16 or 18 either, however this was impacted in the HPV-31 model. However, the findings in HPV-31 are based upon methylcellulose differentiation, whereas the findings in HPV-16 and 31 are based upon viral genome *in situ* hybridisation (ISH) in organotypic raft cultures, which could possibly account for this. However, it has been observed previously that loss of the E1<sup>E4</sup> protein results in reduced genome amplification (Biryukov et al., 2017), and HPV-31E5 loss was shown to reduce levels of E1<sup>E4</sup>, therefore it is likely that had viral genome *in situ* hybridisation been carried out, similar results would have been observed.

In HPV-16 and 18 E5 knockout cell lines a decrease in unscheduled suprabasal DNA synthesis was observed in organotypic rafts, suggesting that E5 is required to drive cell cycle re-entry in the suprabasal layers (Genther et al., 2003a; Wasson et al., 2017). In HPV-18 it has been observed that there is a reduction in the levels of cyclin B1 in E5 knockout organotypic rafts. Whilst organotypic rafts were not stained for cyclin B1 in other HPV types, it has been observed that in HPV-31 there is a reduction in the levels of cyclin A and cyclin B1 observed in methylcellulose differentiation (Fehrmann et al., 2003). Taken together this indicates that E5 is required to drive cell cycle re-entry in the suprabasal layers. Interestingly, whilst no gross morphological changes were evident in any of the E5 knockout rafts, earlier differentiation was evident in HPV-18E5 knockout cells grown in high calcium (Wasson et al., 2017). However, in transgenic mice expressing HPV-16E5 under the control of the CK-14 promoter, no changes were observed in the expression of the early marker cytokeratin-10 (CK-10) or late differentiation marker filaggrin in the presence of E5, however CK-14, a marker usually restricted to basal cells persisted in the suprabasal layers (Genther Williams et al., 2005). This is also in agreement with observations about the differentiation status of HPV-16 knockout rafts, in which no change was observed in the distribution of markers CK-10 or filaggrin (Genther et al., 2003b).

In HPV-16 and HPV-31 E5 knockout cell lines, no changes were observed in the levels or activity of EGFR (Fehrmann et al., 2003; Genther et al., 2003b), which contrasts to the findings in HPV-18, where EGFR expression was not maintained upon differentiation in monolayer, and levels of suprabasal EGFR were reduced in E5 knockout rafts comparison to WT (Wasson et al., 2017). It should be noted that the HPV-16 knockout study did not investigate the levels of EGFR in differentiated cells or rafts. However, a recent, separate study utilising HPV-16E5 knockout cell lines saw a reduction in the basal levels of EGFR expressed relative to WT in undifferentiated cells, which is contradictory (Scott et al., 2018).

E5 has also been demonstrated to alter the expression and action of other growth factor receptors. A splice variant of the fibroblast growth factor receptor (FGFR), keratinocyte growth factor receptor (KGFR/FGFR2b) has its expression altered by HPV-16E5. The expression of HPV-16E5 was seen to downregulate the levels of KGFR transcript and protein in addition to altering its degradation pathway to increase its recycling (Belleudi et al., 2011), resulting a reduced response to KGF stimulation. HPV-16E5 has also been shown to be responsible for the KGFR depletion mediated decrease in expression of the early differentiation marker cytokeratin-1 (CK-1)(Purpura et al., 2013). This agrees with findings in HPV-18, in which an increase in CK-1 levels are observed upon differentiation upon E5 loss, with a corresponding increase in the expression of KGFR (Wasson et al., 2017). It was also shown that increased EGFR signalling via E5 was responsible for the suppression of KGFR expression. Interestingly, mice lacking the epidermal expression of KGFR develop papillomas, and are sensitised to chemical mutagens (Grose et al., 2007), which is a similar phenotype to that seen in mice expressing HPV-16E5 under the control of the CK14 promoter (Maufort et al., 2007), which have been demonstrated to have overactive EGFR. Additionally, HPV-16E5 has been shown to promote the switch from FGFR2b (KGFR) expression to FGFR2c expression, via downregulation of the epidermal splicing regulatory proteins (ESRC) 1 and 2, responsible for governing the splicing of KGFR (Ranieri et al., 2015). It has also been shown that this E5 driven switch in FGFR expression results in responsiveness to

FGF2, which drives an epithelial-to-mesenchymal (EMT) switch. E5 has also been shown to down regulate the expression of T $\beta$ R11, attenuating responsiveness to TGF- $\beta$ 1 and reducing SMAD signalling, a key regulator of cell proliferation (French et al., 2013).

E5 has also been shown to modulate the immune response. E5 proteins from BPV were originally shown to be able to downregulate plasma membrane surface expression of the major histocompatibility complex (MHC) class I, by retention of the MHC class I in the GA, and also by decreasing the light and heavy chains of the receptor (Ashrafi et al., 2002). It was later found that the ability of E5 to downregulate surface MHC class I was a common function, as it was observed in HPV-2, 6, 16 and 83 (Cartin and Alonso, 2003; Ashrafi et al., 2005; Ashrafi et al., 2006a). Like BPV E5, the HPV E5 proteins caused retention of MHC Class I in the GA, however, unlike BPV they did not downregulate expression of the components of MHC class I. The interaction between HPV-16E5 and MHC class I was found to be mediated by interactions between the di-leucine motifs of E5 and the heavy chain of MHC class I (Ashrafi et al., 2006b; Cortese et al., 2010), and that the interaction was specific to HLA-A and B, which are responsible for presentation of viral antigens to cytotoxic T-lymphocytes (CTLs), but not HLA-C or E which are responsible for the inhibition of killing by natural killer (NK) cells (Ashrafi et al., 2005). Indeed, it has been shown that by downregulating HLA-A2 in an E5 dependent manner, cells are able to evade HPV specific CD8+ T-cell mediated killing (Campo et al., 2010). It was also found that the motif of HPV-16E5 responsible for its interaction with MHC class I was required for its interaction with calnexin, and the interaction with calnexin was required for E5 association with and prevention of MHC class I traffic from the ER (Gruener et al., 2007). Interestingly, a known E5 binding partner Bap31 (Regan and Laimins, 2008) is known to associate with MHC class I, and Bap31 controls the exit of peptide loaded MHC class I from the ER (Abe et al., 2009), perhaps this represents a mechanism by which E5 is able sequester MHC class I in order to enable HPV immune evasion.

HPV-16E5 has also been demonstrated to downregulate the surface expression of MHC class II in response to IFN- $\gamma$  treatment. This could be linked to the impairment of endosomal acidification observed in HPV-16E5 positive cells (Supryniewicz et al., 2010), as this is required for the degradation of the invariant chain of MHC class II and subsequent maturation of the complex, and was demonstrated to be inhibited in HPV-16E5 expressing cells (Zhang, B. et al., 2003). This prevents peptide presentation. Additionally, HPV-16E5 has been demonstrated to downregulate the surface expression of the NK recognition ligand CD1d, by causing ER retention and proteasomal degradation (Miura et al., 2010), providing another mechanism by which E5 contributes to immune evasion of HPV.

Recently it has been demonstrated that the E5 protein is also important for the suppression of the immune response in stromal fibroblasts. It was observed that when HPV-16E5 was knocked out, that interferon stimulated genes (ISGs) such as IFIT1, RSAD2, OASL, IFI44L and CCL7 were upregulated in the stromal fibroblasts (Raikhy et al., 2019). And that whilst the presence of WT HPV resulted in the suppression of ISGs, loss of E5 restored expression of many to uninfected levels. It was also found that conditioned media from E5 knockout cells resulted in levels of ISG stimulation in primary fibroblasts similar to that of uninfected cells (Raikhy et al., 2019), suggesting that E5 was controlling secretion of some form of soluble factor.

More needs to be done to establish what the cellular interactome of the E5 proteins are. With this in mind, a study utilising the oncoproteins of DNA tumour viruses to elucidate cancer interactomes was of great interest (Rozenblatt-Rosen et al., 2012). This study included the E5 proteins of HPV-6B, 11, 16 and 18, and identified interactors by TAP-MS. Many putative interactions were identified, for example the TAP-MS of HPV-16E5 identified 152 and HPV-18E5 identified 256. A protein that piqued our interest was PRAF2, however at the time relatively little was known about it.

## 1.9 The PRA family

The prenylated rab acceptor family (PRAF) is composed of three proteins in humans PRAF1, PRAF2 and PRAF3 (Figure A.1). The first family member characterised was PRAF1 back in 1997 as an interactor for Rab1 and Rab3a in a Y2H screen (Martincic et al., 1997), the next family member PRAF3 was identified as an interactor for ARL-6 in a Y2H screen (Ingley et al., 1999), and the last family member to be discovered was PRAF2 as an interactor for the CCR5 protein (Schweneker et al., 2005). PRAF family proteins are evolutionarily conserved, with a PRAF1 homologue (Yip3) found in yeast (Fo et al., 2006). Broadly speaking, PRAF proteins are small, hydrophobic transmembrane proteins, which are characterised by the possession of a PRA1 domain (Martincic et al., 1997; Fo et al., 2006).

### 1.9.1 PRAF1

The PRAF1 protein (also known as PRA1, RABAC1 and YIP3) is a protein of 20.6kDa in mass, and is broadly expressed throughout the tissues of the body (Bucci et al., 2001; Martincic et al., 1997) and is primarily localised to the GA (Liang, Z. et al., 2004; Abdul-Ghani et al., 2001), and possesses the ability to dimerise. The protein was originally predicted to be an extrinsic membrane protein, due to its extraction from membranes with buffer and urea (Hutt et al., 2000). However, later studies demonstrated that the protein was an integral membrane protein with four transmembrane domains, with its N and C-terminus as well as linker domains orientated cytoplasmically (Lin, J. et al., 2001). Studies also demonstrated that the C-terminal 10 amino acids were crucial to its localisation to the GA, specifically an acidic DXEE motif, with loss resulting in ER accumulation (Liang, Z. and Li, 2000; Liang, Z. et al., 2004; Abdul-Ghani et al., 2001). Interestingly a single point mutation of the valine at position 185 was sufficient to prevent PRAF1 trafficking along the exocytic pathway to the GA, resulting in ER retention (Liang, Z. et al., 2004). The V185 and C-terminal 10 amino acid deletion PRAF1 mutants were also incapable of dimerising.

The PRAF1 protein was originally identified as an interactor for proteins involved in synaptic vesicle traffic such as Rab1, Rab3a and VAMP2 via Y2H screen, and that its N-terminal residues 30-54 and C-terminal 10 amino acids were required for these interactions (Martincic et al., 1997), it was also found that its interactions with Rab proteins required their prenylation, hence the protein families name. Further Y2H studies expanded the repertoire of Rab proteins bound to include Rab4a, 4b, 5a, 5c, 6, 7, 17 and 22 (Bucci et al., 1999), it was also found that PRAF1 was capable of binding other small GTPases such as H-Ras, RhoA, TC21 and Rap1a in a prenylation dependent manner (Figueroa et al., 2001). PRAF1 was also found to interact with the GDP dissociation inhibitor (GDI) (Hutt et al., 2000), a protein which binds to prenylated GDP bound inactive Rabs and extracts them from membranes (Müller, M.P. and Goody, 2018). PRAF1 can bind to GDI and inhibit its function as well as compete for Rab binding (Hutt et al., 2000; Sivars et al., 2003), suggesting that PRAF1 is important for the regulation of membrane traffic.

Other proteins involved in trafficking that interact with PRAF1 are Rheb,  $\alpha$ -synuclein and the N-myc downstream regulated gene (NDRG) family of proteins (Li, Y. et al., 2007; Lee, H.J. et al., 2011; Hunter et al., 2005; Kim, J.T. et al., 2012; Kachhap et al., 2007).  $\alpha$ -synuclein has been demonstrated to be important for synaptic vesicle trafficking (Lee, H.J. et al., 2011) and NDRG proteins are required for transport vesicle formation at the GA and interact with Rab and SNARE proteins. NRDG proteins have also been demonstrated to be important for vesicular E-cadherin recycling. The established interacting network of PRAF1 strongly implicates it as part of the trafficking machinery of the cell. This is also supported by data from alterations of expression and mutations of Arabidopsis homologues of PRAF1, which result in anterograde trafficking defects (Jung et al., 2011; Lee, M.H. et al., 2011). Interestingly, in Arabidopsis the C-terminal acidic motif and valine are also required for correct PRAF1 localisation, suggesting that PRAF1 plays a conserved role across the kingdoms of life.

Knockdown of PRAF1 resulted in upregulation of proteins such as caveolin-1, fatty acid binding protein-5 (FABP5) and TIP46, which are involved in lipid homeostasis, as well as integrins and annexins which are involved in cellular migration (Liu, H.P. et al., 2011). This upregulation was likely due to the accumulation of cellular cholesterol, suggesting that PRAF1 may play a role in lipid trafficking. This could be through its binding partner VAMP2, which is a known binding partner of VAPA and VAPB, which control the transport of lipids from the ER to the GA via their interactions with lipid binding proteins (Weir et al., 2001; Gkogkas et al., 2008; Santos et al., 2018; Mao, D. et al., 2019).

PRAF1 has also been demonstrated to interact with viral proteins from diverse backgrounds. The PRAF1 protein has been shown to interact with the envelope gp41 glycoprotein from a variety of lentiviruses such as SIV and HIV (Evans et al., 2002). PRAF1 has also been shown to bind Rotavirus VP4 (Enouf et al., 2003), with a possible role in its trafficking and localisation. PRAF1 also interacts with proteins from DNA viruses, for example the Epstein-Barr Virus (EBV) BHRF1. BHRF1 is a virally encoded mimic of the anti-apoptotic protein Bcl-2, which interacts with PRAF1 using the same residues as required for the PRAF1/Rab interaction (Li, L.Y. et al., 2001). The interaction with PRAF1 impairs the anti-apoptotic ability of BHRF1. Interestingly PRAF1 has also been shown to interact with the anti-apoptotic BCL2A1 protein and inhibit its effects as well (Kim, J.T. et al., 2019). PRAF1 overexpression enhances LMP-1 induced NF- $\kappa$ B activation (Liu, H.P. et al., 2006). PRAF1 knockdown or expression of the V185 mutant results in a disruption to LMP-1 trafficking and its retention in the ER, suggesting that it is important for correct LMP-1 traffic, and subsequently impairs LMP-1 mediated NF- $\kappa$ B activation.

PRAF1 has been shown to be a regulator of the Wnt signalling pathway. PRAF1 overexpression has been shown to inhibit proliferation, migration and invasion of cancer cells (Kim, J.T. et al., 2006; Kim, J.T. et al., 2019), through binding to  $\beta$ -catenin (Kim, J.T. et al., 2006) and its interactor NDRG2 (Kim, J.T. et al., 2012), to prevent  $\beta$ -catenin translocation to the

nucleus, resulting in decreased T-cell factor (TCF) transcriptional activity. This has been shown to result in decreased levels of ERK1/2 and GSK-3 $\beta$  phosphorylation and reduced levels of cyclin D1, suggesting that PRAF1 could play a role in regulating cellular signalling.

### **1.9.2 PRAF3**

The PRAF3 protein (also known as JWA, ARL6IP5, GTRAP3-18 and Yip6b) is a protein of 21.6kDa in mass, and like PRAF1 is broadly expressed throughout the body, is evolutionarily conserved and possesses the ability to oligomerise (Lin, C.I. et al., 2001; Butchbach et al., 2002). Expression of PRAF3 can be induced by treatment with retinoic acid (Lin, C.I. et al., 2001) or morphine (Ikemoto et al., 2002). PRAF3 localises to the ER, and this is governed by its C-terminus (Abdul-Ghani et al., 2001). PRAF3 was initially identified in a Y2H screen of ARL-6 (Ingley et al., 1999), and then further characterised by its interaction with the excitatory amino-acid carrier-1 (EAAC1) (Lin, C.I. et al., 2001; Butchbach et al., 2002). PRAF3 was shown to associate with EAAC1 and reduce its affinity for glutamate, resulting in reduced glutamate uptake (Watabe et al., 2007). PRAF3 overexpression delays the ER exit of EAAC1 and other EAAC family members to the GA, suggesting that it can act as a regulator of ER protein trafficking (Ruggiero et al., 2008). PRAF3 overexpression has also been shown to delay transport of VSV-G-ts045 from the ER to the Golgi. The delay is mediated by PRAF3 binding Rab1a, and reducing the cargo concentration in transport complexes, therefore slowing protein export from the ER (Maier et al., 2009). Knockdown of PRAF3 in osteoblasts has been demonstrated to result in the accumulation of unfolded proteins in the ER, possibly due to impaired ER export, resulting in ER-stress mediated apoptosis (Wu, Y. et al., 2014). The PRAF3 protein has been shown to mediate the ER exit of RANKL from osteoblasts, with PRAF3 overexpression resulted in RANKL retention in the ER, suppressing osteoclast formation (Wu, Y. et al., 2015), further evidence that PRAF3 is involved in protein trafficking.

Compared to PRAF1, there is far less data about its interactions with Rab family proteins, as only Rab1a and 3a have been demonstrated to interact (Abdul-Ghani et al., 2001; Maier et al., 2009). However, PRAF3 also possesses the PRA1 domain, so is likely to associate with other prenylated GTPases, enabling it to act as a regulator of trafficking. The interaction between PRAF3 and Rab1a has recently been demonstrated to prevent PRAF3 mediated toxicity in the SH-SY5Y neuroblastoma cell line (Oshikane et al., 2018), perhaps Rab1a ensures proteins can exit the ER in transport complexes, thereby preventing ER-stress mediated apoptosis.

Most research into PRAF3 has focussed on its role as a tumour suppressor. Mutations in PRAF3 are associated with increased risk of oesophageal, gastric and bladder cancer (Tang, W.Y. et al., 2007; Li, C.P. et al., 2007). Knockdown of PRAF3 has been shown in melanoma, breast cancer, oesophageal and hepatocellular cancer cell lines to promote migration, invasion and proliferation (Bai et al., 2010; Lu et al., 2013; Chen, X. et al., 2015; Shi et al., 2012; Wu, X. et al., 2014), whilst its overexpression has reduced migration, invasion and proliferation, suggesting that it can act as a tumour suppressor.

Additionally, PRAF3 seems to exert a proapoptotic effect, with its overexpression resulting in apoptosis via caspase-8 and caspase-9 dependent pathways (Shi et al., 2012), and PRAF3 expression sensitises cancer cells to apoptosis via chemically induced reactive oxygen species, for example via cisplatin or AsO<sub>3</sub> treatment (Xu, W. et al., 2014; Wang, Q. et al., 2017; Zhou, J. et al., 2008; Shen et al., 2011). Interestingly, PRAF3 has been reported as a novel protein in DNA damage repair, localising to the nucleus with the DNA base excision repair proteins XRCC1, PARP1 and DNA ligase III upon DNA damage (Wang, S. et al., 2009) and is required for double strand break repair upon cisplatin treatment (Xu, W. et al., 2014). This suggests that there may be more to the PRAF proteins than just modulation of protein trafficking.

### 1.9.3 PRAF2

The PRAF2 protein (also known as JM4 and Yip6a) is a protein of 19.3kDa in mass, and is expressed throughout the tissues of the body, however its greatest expression is seen in the central nervous system and tissues of the male reproductive organ (Borsics et al., 2010; Fo et al., 2006; Thul et al., 2017; Uhlen et al., 2017). Like PRAF1 and PRAF3, PRAF2 is also predicted to be an integral membrane protein with four transmembrane domains, with its N and C-terminus cytoplasmically orientated (Fo et al., 2006). PRAF2 is known form homodimers, as well as heterodimers with PRAF3 (Vento et al., 2010).

PRAF2 is known to localise to membranes, and has been detected in the ER (Schweneker et al., 2005; Borsics et al., 2010), endosomes (Schweneker et al., 2005; Geerts et al., 2007), exosomes (He et al., 2019), NE (Borsics et al., 2010) and synaptic vesicles (Koomoa et al., 2008). PRAF2 has also been detected as a dimer in the cytoplasmic fraction of cells, suggesting that dimerization may enable it to conceal its hydrophobic domain and exist in the cytosol (Borsics et al., 2010). Whilst a member of the prenylated Rab acceptor family, there have been no studies demonstrating a direct interaction with Rabs or other small GTPases in the literature. However, PRAF2 possesses the PRA1 domain, so it is likely that it does. Additionally, in a screen to dissect the role of Rab proteins in Golgi-to-ER trafficking, PRAF2 was identified as an important regulator of Golgi-to-ER traffic. Pairwise depletion of PRAF2 with Rab1b, Rab11a and Rab21 was found to have a significant impact on retrograde traffic, suggesting that there may be an interaction between Rab proteins and PRAF2 (Galea et al., 2015). PRAF2 has been shown to influence the exit of the GABA<sub>B</sub> receptor from the ER, acting as a gatekeeper (Doly et al., 2016), and also the cell surface expression of the G-protein coupled receptors CCR5 and CXCR4 (Fo et al., 2006), suggesting that PRAF2 may play an active role in protein transport. PRAF2 expression in colorectal cancer has also been found to promote exosome secretion (He et al., 2019), suggesting an additional form of trafficking that PRAF2 contributes to.

PRAF2 has also been identified as an interactor for viral proteins by TAP-MS. The TAP-MS screen of DNA tumour virus oncoproteins suggested that PRAF2 was a putative interactor for HPV E5 proteins, EBV BHRF1, EBV BALF1, EBV BDLF4, EBV BNLF2A, Adenovirus-5 E1B19K, Merkel cell polyomavirus Small-T antigen and Human polyomavirus 607A Large-T antigen (Rozenblatt-Rosen et al., 2012). Additionally, PRAF2 was downregulated by Dengue Virus-2 infection (Chiu et al., 2014), suggesting that it is a target of several viruses. The PRAF2 protein is upregulated by cerulenin mediated apoptosis (Geerts et al., 2007), and can bind the antiapoptotic Bcl-2 and Bcl-xL proteins, and when overexpressed induces cell death (Vento et al., 2010), suggesting that PRAF2 can act as a tumour suppressor.

However, PRAF2 is overexpressed in several cancers, such as glioblastoma, neuroblastoma, hepatocellular carcinoma, oesophageal squamous cell carcinoma and colorectal cancer (Borsics et al., 2010; He et al., 2019; Qian et al., 2019; Wang, C.H. et al., 2018; Yco et al., 2013). PRAF2 overexpression in these cancers predicts a poor prognosis, with overexpression of PRAF2 promoting proliferation, metastasis, invasion and migration, and depletion of PRAF2 often reducing these effects. This suggests that the role of PRAF2 in cancers may be more as an oncogene than as a tumour suppressor.

## **1.10 Project Aims**

The goal of this thesis is to expand the knowledge available about the PRAF2 protein, both on a cellular basis and with regards to its interaction with the E5 protein of HPV, and its role in the lifecycle of HPV. A further goal was to determine whether PRAF2 acted as a tumour suppressor or as an oncogene in cervical cancer. Specifically, I aim to investigate:

- 1) To validate the interaction between PRAF2 and the HPV E5 proteins and to determine the nature of the interaction between PRAF2 and HPV-18E5.
- 2) To perform cancer cell assays to determine whether PRAF2 is functioning as an oncogene or tumour suppressor in cervical cancer.

- 3) To investigate the role of PRAF2 in the lifecycle of HPV-18, using primary cell culture and the organotypic raft system.
- 4) To determine whether PRAF2 can act as a proapoptotic protein in cervical cancers
- 5) To elucidate the cellular interactome of the PRAF2 protein

## Chapter 2 Materials and Methods

### 2.1 Bacterial Cell Culture

#### 2.1.1 Bacterial cell growth

The *Escherichia coli* strain DH5 $\alpha$  was used to host DNA vectors. *E. Coli* were grown on LB agar plates (1% NaCl (w/v), 1% tryptone (w/v), 0.5% yeast extract (w/v) and 1.5% agar (w/v)) and in LB media (1% NaCl (w/v), 1% tryptone (w/v) and 0.5% yeast extract (w/v)). Selection antibiotics ampicillin (100  $\mu\text{g}/\mu\text{l}$ ) and kanamycin (50  $\mu\text{g}/\mu\text{l}$ ) were used where appropriate.

#### 2.1.2 Preparation of chemically competent bacteria

DH5 $\alpha$  were streaked out onto a LB agar plate containing no antibiotics and incubated a 37°C overnight. A single colony was picked and inoculated into 20 ml 2xYT media (1% NaCl (w/v), 1.6% Tryptone (w/v), 1% yeast extract (w/v)) and grown with shaking. After 6 hours this culture was used to inoculate 200ml of 2xYT media and grown overnight at 18°C with shaking. Once the OD reached 0.75 the culture was placed into an ice-water bath for 10 min, then centrifuged at 2000xg for 10 min at 4°C to pellet cells. Cells were then resuspended into 80 ml of ice-cold transformation buffer (10mM PIPES KOH (pH6.7), 15mM CaCl<sub>2</sub>, 250mM KCl and 55mM MnCl<sub>2</sub>) and placed in an ice water bath at 4°C overnight. Cells were then centrifuged at 2000xg for 10 min at 4°C to pellet, and then resuspended in 18.6 ml ice cold transformation buffer. 1.4 ml of DMSO was then added slowly with gentle stirring, followed by an incubation on ice for 10 min. Cells were then aliquoted and snap frozen in liquid nitrogen, then stored at -80°C.

#### 2.1.3 Transformation of Bacteria

Chemically competent DH5 $\alpha$  were thawed on ice. 5 $\mu\text{l}$  of DNA containing no more than 100ng of DNA was placed in a 1.5ml Eppendorf tube on ice to chill. 50 $\mu\text{l}$  of DH5 $\alpha$  were then added to the DNA and mixed by flicking, then the tube returned to incubate on ice for 30 min. The transformations were then transferred to a 42°C heat block and incubated for 45 seconds,

then returned to ice for a further 2 min. 200µl of LB broth was then added and transformations grown at 37°C with shaking for 45 min. Transformations were then spread onto LB agar plates with the required antibiotics and grown at 37°C for 18 hours.

#### **2.1.4 Miniprep (small scale)**

To purify plasmid DNA on a small scale, 10 ml of LB media with selection antibiotic was inoculated with a single colony grown on a LB Agar plate with selection antibiotic. The culture was grown with shaking at 37°C for 16 hours. Cells were harvested by centrifugation at 17000xg for 30 seconds. 1.5 ml of culture was harvested for high copy number plasmids and 5 ml for low copy number plasmids. The plasmid DNA was then purified using the alkaline lysis method through the use of the Monarch<sup>®</sup> Plasmid DNA Miniprep Kit (NEB, T1010) as per the manufacturer's protocol. DNA was eluted in 30 µl of DNA elution buffer (NEB, T1016).

#### **2.1.5 Maxiprep (large scale)**

To purify plasmid DNA on a large scale, a starter culture was prepared by inoculating 5 ml of LB media with selection antibiotic with a single colony grown on a LB Agar plate with selection antibiotic. The culture was grown with shaking at 37°C for 8 hours, then 500 µl was used to inoculate 100 ml of LB media with selection antibiotic. The culture was then grown with shaking at 37°C for 16 hours. The culture was then harvested by centrifugation at 2000xg for 10 min at 4°C. The plasmid DNA was then purified through the use of the QIAGEN Plasmid Maxi Kit (Qiagen, 12162) as per the manufacturer's protocol. DNA was resuspended in RNase/DNase free H<sub>2</sub>O to a final concentration of ~1000 ng/µl (where possible).

#### **2.1.6 Production of Glycerol Stocks**

To prepare glycerol stocks 500 µl of overnight bacterial culture was taken and combined with 500 µl of 50% glycerol to give a final concentration of 25% glycerol in the freezing media. Glycerol stocks were then frozen immediately at -80°C.

### **2.1.7 Quantification of Plasmid DNA**

The concentration of plasmid DNA was quantified using a NanoDrop™ One Microvolume UV-Vis Spectrophotometer (ThermoFisher Scientific, ND-ONE-W).

## **2.2 Molecular cloning**

### **2.2.1 Plasmid DNA vectors and oligonucleotides**

A full list of oligonucleotides and plasmid vectors can be found in Appendix A.

### **2.2.2 PCR (Q5)**

Amplification of DNA target sequences was conducted using the Q5 high-fidelity DNA polymerase (NEB, M0491) in 50 µl reaction volumes. Each reaction contained 1x Q5 reaction buffer, 200 µM dNTPs, 1 unit of Q5 high-fidelity DNA polymerase, 500 nM of forward and reverse primers (Table A1) respectively and 0.1-50 ng of DNA template. All reactions were prepared on ice. Reactions were carried out using a T100 thermo cycler (BioRad, 1861096), according to the following protocol: an initial denaturation step at 98°C for 30 seconds, followed by a 98°C denaturation step for 10 seconds, then an annealing step of 20 seconds, followed by an elongation step at 72°C for 25 seconds per/kb. The annealing temperatures were determined for each primer set by performing a temperature gradient PCR reaction to establish the optimal temperature. The elongation time was adjusted according to the length of the target sequence. The amplification products were purified from the reaction via Monarch PCR and DNA cleanup kit (NEB, T1030L), as per the manufacturers protocol. DNA integrity was then confirmed by agarose gel electrophoresis (2.2.3).

### **2.2.3 Agarose Gel Electrophoresis**

PCR amplification products (Chapter 2.2.2), restriction digests (Chapter 2.2.4) and DNA laddering assays (Chapter 2.12.1) were separated by agarose gel electrophoresis. To do so 0.8-2% agarose gels were prepared (0.8-2% w/v agarose in Tris-acetate-EDTA buffer (TAE, 40 mM

Tris base, 20 mM Acetic acid and 1 mM ethylenediamine tetraacetic acid (EDTA))) with the addition of 1 x SYBR safe DNA gel stain (Invitrogen, S33102). Gel loading dye (NEB, B7025S) was added to samples to obtain a 1x concentration. Electrophoresis was carried out at 5V/cm for 2 hours in TAE buffer. The agarose gel was then imaged using a Syngene InGenius gel documentation system (Syngene Bioimaging).

#### **2.2.4 Restriction endonuclease digest**

Purified PCR products and plasmids were digested using restriction endonuclease enzymes (NEB), for a full list see Appendix A. Single and double digests were carried out. Reactions were carried out in a 50 µl reaction volume. Each reaction contained 1 µg of DNA, 1x CutSmart buffer and 10 units of the respective restriction enzymes. Reactions were incubated at 37°C for one hour. If the restriction product was a PCR product the DNA was then purified through use of the Monarch PCR and DNA cleanup kit, as per the manufacturers protocol. If the substrate was plasmid destined for shrimp alkaline phosphatase treatment (Chapter 2.2.5) the restriction enzymes were heat inactivated where possible. Temperature and times for heat inactivation varied between enzymes.

#### **2.2.5 Shrimp alkaline phosphatase treatment**

Linearised plasmid vectors were treated with 1 unit of recombinant shrimp alkaline phosphatase (NEB, M0371) at 37°C for 30 min, followed by heat inactivation at 65°C for 5 min.

#### **2.2.6 DNA ligation**

Ligations of PCR products into digested destination vectors was achieved through usage of T4 DNA ligase (NEB, M0202S). Reaction volumes of 10 µl were used. Each reaction contained 1x T4 DNA ligase buffer (NEB, B0202S), 0.02 pmol of vector DNA, 0.06 pmol of insert (PCR) DNA and 200 units of T4 DNA ligase. Reactions were incubated at 16°C overnight. 5 µl of ligation product was then transformed into competent DH5α cells (Chapter 2.1.3).

### **2.2.7 Gibson assembly reaction**

The Gibson assembly reaction was performed to assemble two DNA fragments. Single restriction enzyme digested DNA products were used, and these were resolved by agarose gel electrophoresis (Chapter 2.2.3) and purified through the usage of a Monarch DNA gel extraction kit (NEB, T1020L) as per the manufacturers protocol. 20 µl reaction volumes were used and prepared on ice, and a control reaction was prepared with the manufacturers positive control. Each reaction contained 1x of Gibson assembly master mix (NEB, E2611), 0.013 pmol of vector DNA and 0.041 pmol of insert DNA. Reactions were incubated in a T100 thermocycler at 50°C for 15 min. 5 µl of the Gibson assembly reaction was then transformed into competent DH5α cells (Chapter 2.1.3).

### **2.2.8 Screening of Clones**

Bacterial colonies from transformations (Chapter 2.1.3) were grown (Chapter 2.1.1) and purified (Chapter 2.1.4). Purified DNA was digested (Chapter 2.2.6) and the resulting samples were examined by agarose gel electrophoresis (Chapter 2.2.3). Those clones which produced restriction products indicative of containing the desired inserts were then confirmed by sanger sequencing.

### **2.2.9 Sequencing**

Sanger sequencing was performed by GATC-biotech (Eurofins genomics), using vector specific sequencing primers supplied alongside the DNA. The resulting DNA sequences were then analysed to confirm sequence integrity. Sequences were analysed using the Basic Local Alignment Search Tool (BLAST, National Centre for Biotechnology Information) to confirm the correct sequence was present. Sequences were confirmed to be correctly inserted through usage of the ExPASy translate tool (<https://web.expasy.org/translate/>, Swiss Institute of Bioinformatics) and manual examination.

### **2.2.10 Basic Bioinformatics**

The molecular weights of proteins were predicted through the usage of the ExpASy compute pI/Mw tool ([https://web.expasy.org/compute\\_pi/](https://web.expasy.org/compute_pi/), Swiss Institute of Bioinformatics).

Multiple sequence alignments of PRAF2 mutant sequences were aligned using the Clustal Omega tool (<https://www.ebi.ac.uk/Tools/msa/clustalo/>, EMBL-EBI).

String analysis was performed using the String tool (<https://string-db.org/>, ELIXIR Core Data resources).

## **2.3 Protein biochemistry**

### **2.3.1 Cell lysis**

Mammalian cells media was removed and then cells were washed twice with phosphate buffered saline (PBS), and RIPA buffer (150 mM NaCl, 1% Nonidet P-40 (v/v), 0.5% sodium deoxycholate (w/v), 0.1% sodium dodecyl sulphate (SDS) (w/v) and 25 mM Tris-HCl pH 7.4, plus 1x Protease inhibitor cocktail, EDTA-Free (Roche, Switzerland)) was applied to the cell monolayer (200/400/1,000  $\mu$ l for 6 well, 6 cm<sup>2</sup> and 10 cm<sup>2</sup> dishes respectively), and cells scraped and transferred to Eppendorfs. The resulting cell lysates were then incubated on ice for 20 min, then centrifuged at 17,000 xg at 4°C for 10 min to clarify lysates. Protein concentrations were then determined.

### **2.3.2 Protein bicinchoninic acid assay (BCA) for protein concentration**

Protein concentrations of cell lysates were determined with BCA protein assay kit (ThermoFisher Scientific, 23225). Standard dilutions 0  $\mu$ g/ml to 2  $\mu$ g/ml of bovine serum albumin (BSA) were prepared using matched lysis buffer to the samples. Cell lysates were diluted 1:40 in assay reagent. The BSA standards and the samples were run in duplicate in a 96 well plate. After 10 min incubation at 37°C, the absorbance at 562 nm was read on a PowerWave XS2 Microplate Spectrophotometer (BioTek, UK). Absorbance values were calculated by the software (Gen5

1.11, BioTek, UK) and a standard curve plotted in Excel to determine the samples' total protein concentration.

### **2.3.3 Extraction of protein from cytology samples**

800  $\mu$ l of biopsy sample in PreservCyt sample buffer was placed in an ice-cold Eppendorf and 1 ml of TRIzol reagent (Invitrogen, 15596026) added. The sample was then vortexed thoroughly and sample incubated for 5 min at room temperature (R.T.) 200  $\mu$ l of ice-cold chloroform was applied to the sample and then incubated for a further 3 min. The samples were then centrifuged at 12,000 xg for 4°C to separate the phases. The aqueous phase was removed, with care taken not to disturb the interphase and organic phase. 300  $\mu$ l of 100% ethanol was then applied to the sample, and the sample mixed by inversion, then incubated for 3 min at R.T. The sample was then centrifuged at 4,000 xg at 4°C for 5 min to precipitate the DNA. The phenol-ethanol supernatant was then transferred to a new tube. 1.5 ml of isopropanol was then applied to the phenol-ethanol supernatant, incubated for 10 min at R.T. then centrifuged at 12,000 xg at 4°C for 10 min to pellet the proteins and the supernatant was then discarded. 2 ml of wash solution (0.3 M guanidine hydrochloride in 95% ethanol) was then used to resuspend the protein pellet and the pellet incubated for 20 min at R.T. The sample was then centrifuged at 7,500 xg at 4°C for 5 min and the supernatant then discarded. This wash step was then repeated twice. The sample was then resuspended in 2 ml of 100% ethanol and briefly mixed by vortexing and incubated for 20 min at R.T. The sample was then centrifuged at 7,500 xg at 4°C for 5 min, the supernatant discarded and the protein pellet airdried for 10 min. The pellet was then resuspended in 200  $\mu$ l of 1% SDS (w/v) by pipetting, and incubated for 10 min at 50°C. The sample was then centrifuged at 10,000 xg at 4°C for 10 min to remove insoluble materials and then the supernatant transferred to a new tube. The protein concentration was then determined by BCA assay (Chapter 2.3.2)

### 2.3.4 SDS polyacrylamide gel electrophoresis (SDS-PAGE)

Proteins were separated according to molecular weight using a Mini-PROTEAN Tetra cell (Biorad). 8%, 10%, 12.5% and 15% SDS-polyacrylamide gels (v/v) were prepared according to required protein resolution (separating gel: 8%, 10%, 12.5% and 15% Acrylamide (v/v), 375 mM Tris/Cl, pH 8.8; 0.1% SDS (w/v), 0.1% APS (w/v), 0.01% TEMED (v/v); stacking gel: 6% Acrylamide (v/v), 125 mM Tris/Cl, pH 6.8; 0.1% SDS (w/v), 0.1% APS (w/v), 0.01% TEMED (v/v)). Protein samples, 30  $\mu$ l, with lithium dodecyl sulphate (LDS) sample buffer (Invitrogen, USA) and 0.1% 2-mercaptoethanol (v/v), or 1 x Laemmli Sample Buffer (32.9 mM Tris.HCl pH 6.8, 13.15% glycerol (v/v), 1.1% SDS (w/v), 0.01% bromophenol blue (w/v), 0.1%  $\beta$ -mercaptoethanol (v/v)), were loaded alongside 4  $\mu$ l BLUEye Pre-Stained Protein Ladder, 10-245 kDa (Geneflow, S6-0024) or Blue Pre-stained Protein Standard, Broad Range 11-190kDa (NEB, P7706). Electrophoresis was carried out at 100 - 150 V in 1 x SDS running buffer (34.7 mM SDS, 250 mM Tris Base, 1.92 M Glycine) until proteins were resolved.

### 2.3.5 Western Blotting

Separated proteins were transferred from the SDS-PAGE gels to Amersham Protran 0.2 $\mu$ m pore nitrocellulose, (Amersham BioSciences, 10600001) on a Trans-Blot Turbo Transfer System (BioRAD). Membranes were first equilibrated in transfer buffer (192 mM Glycine, 25 mM Tris Base, 20% methanol (v/v)) before conducting the transfer at 1.0 A, 25 V for 30 min. Membranes were then blocked by incubation in blocking solution (5% skimmed milk powder (Sigma, 70166) (w/v) in TBS-T (Tris Buffered Saline: 25 mM Tris/Cl, pH 7.5; 138 mM NaCl and 0.1% Tween-20 (v/v))) for 45 min at RT. Primary antibody (Appendix A) was diluted in blocking solution was added to the membrane and incubated overnight at 4°C on a rocker. Membranes were then washed for 5 min with TBS-T at RT, this wash was repeated four times.

Blots were visualised using secondary antibodies conjugated to horse radish peroxidase (Strattech JIR-115-035-174 and JIR-211-032-171) diluted in 5% milk TBS-T (1:5000) and incubated

for 2h at RT. Membranes were then washed for 5 min with TBS-T at RT, this wash was repeated four times. To detect the chemiluminescent signal, membranes were briefly incubated in equal amounts of enhanced chemiluminescent solution A (25 mM Luminol, 4 mM p-coumaric acid, 100 mM Tris.HCl, pH 8.5) and solution B (0.2% H<sub>2</sub>O<sub>2</sub> (v/v), 100 mM Tris.HCl, pH 8.5) or Amersham ECL Select Western Blotting Detection Reagent (GE Lifesciences, RPN2235). Membranes in a protective sleeve were exposed to CL-Xposure film (ThermoFisher Scientific, 34090). The film was developed using an Xograph developer. ReBlot Plus Strong Antibody Stripping Solution (Merck, 2504) was incubated with membranes for 10 min at RT to allow reprobing.

### **2.3.6 Densitometry**

Western blot film exposures (Chapter 2.3.5) were digitalised by scanning at 600 dpi and saved in tagged image file format (tif). Protein levels were quantified using ImageJ (National Institutes of Health). Image files were converted to 8-bit greyscale, and the bands of interest outlined using the select lane function, then plot lane function. The background was then subtracted from the resulting plots. The resulting data was input into Excel (Microsoft). Bands of the protein of interest were then adjusted for loading by comparison to the loading control.

## **2.4 Mammalian cell culture**

### **2.4.1 Cell Culture**

All transformed and cancer cell lines (Table A.6) were maintained in Dulbecco's Modified Eagle Medium (Sigma-Aldrich, D6429), supplemented with 10% fetal bovine serum (ThermoFisher Scientific, 10500-064), 50 U/ml penicillin and streptomycin (ThermoFisher Scientific, 15070063) in a 37°C incubator, humidified with 5% CO<sub>2</sub>. All cell culture work was carried out in a class II biological safety cabinet.

#### **2.4.2 Culture of transformed and cancer cell lines**

Cells were cultured until ~80-90% confluency was reached. To passage, the culture media was aspirated, and cells were washed once with sterile PBS. To detach cells from their culture flasks 0.05% trypsin, 0.2% EDTA in PBS (trypsin-EDTA solution) was applied and cells were incubated at 37°C, 5% CO<sub>2</sub> and periodically observed for rounding. Once detached trypsin was inactivated by application of complete DMEM. Cells were then seeded at a 1:3-1:10 ratio of cell suspension to complete DMEM, dependent upon cell line for further culture in appropriate cell culture flasks. Alternatively, cells were counted using a haemocytometer and seeded appropriately.

#### **2.4.3 Selection of the HEK293TT cell line**

HEK293TT cells were regularly selected with 250 µg/ml hygromycin B (InvivoGen, ant-hg-1) for one week to ensure maintenance of large T-antigen expression.

#### **2.4.4 Selection of the Phoenix A cell line**

Phoenix A cells were selected with 300 µg/ml hygromycin B and 1 µg/ml diphtheria toxin (Merk, 322326-1MG) every two months for one week to ensure maintenance of gag-pol and envelope protein expression.

#### **2.4.5 Freezing of cell lines**

Cells were grown until 80% confluent. Growth media was removed, and cells were then washed with PBS. Trypsin-EDTA solution was then applied and cells incubated at 37°C. Once dissociated growth media used to neutralise trypsin and the cell suspension was transferred to a 50 ml falcon tube, cells were then counted using a haemocytometer and the cell suspension then spun at 200 xg for 5 min at 4°C to pellet the cells. The supernatant was then removed, and cells were resuspended in freezing media (10% DMSO, 90% growth media) to give a suspension of 1x10<sup>6</sup> cells/ml. The resulting suspension was then aliquoted into cryotubes and placed in a

freezing chamber. The freezing chamber was then placed at  $-80^{\circ}\text{C}$  overnight, then cryotubes were transferred to liquid nitrogen.

#### **2.4.6 Thawing of cell lines**

Transformed cells were retrieved from liquid nitrogen and placed on ice. Cells were then transferred to a  $37^{\circ}\text{C}$  water bath and gently agitated with care taken to ensure that water did not come into contact with the cryovial seal. Cryovials were then surface sterilised with 70% ethanol and opened in a microbiological safety cabinet. Cells were gently resuspended by pipetting and then transferred into 9 ml of growth media and spun down at  $200\times g$  for 5 min. The resulting cell pellet was then resuspended into growth media and transferred to a fresh flask for cell culture.

#### **2.4.7 Transient transfection with polyethylenimine (PEI)**

For transfection of HEK293 and its derivative cell lines, cells were seeded into 6 well plates or  $10\text{ cm}^2$  dishes at a density of  $5\times 10^5$  per/well or  $2.5\times 10^6$  cells/plate and incubated overnight under standard culture conditions (Chapter 2.4.1).  $10\text{ }\mu\text{g}$  of plasmid DNA was combined with  $200\text{ }\mu\text{l}$  or  $500\text{ }\mu\text{l}$  of Opti-MEM I reduced serum medium (GIBCO, 31985070), mixed by vortexing and incubated at R.T for 5 min. The chemical transfection reagent PEI (PEI (Polyscience Inc., 23966),  $1\text{ mg/ml}$  in  $\text{H}_2\text{O}$ , pH 7.4) was then added at a ratio of 1:4 DNA to PEI, briefly mixed by vortexing and the incubated for a further 20 min at R.T. Culture medium on cells to be transfected was replaced with Opti-MEM I and the transfection complexes added in a dropwise manner. Cells were incubated overnight, then transfection media removed and replaced with complete DMEM. Cells were then incubated until their experimental endpoints.

#### **2.4.8 Transient transfection with Lipofectamine 2000**

For transfection of HeLa and C33A cells were seeded into 6 well plates or  $6\text{ cm}^2$  dishes at  $1.5\text{-}5\times 10^5$  cells/well (HeLa and C33A cells respectively) or  $4\times 10^5\text{-}1.5\times 10^6$  cells/plate (HeLa and C33A cells respectively) and incubated overnight under standard culture conditions (Chapter

2.4.1). The required amount of plasmid DNA was combined with 200  $\mu$ l Opti-MEM I reduced serum medium. In a separate Eppendorf the appropriate volume of Lipofectamine 2000 (Invitrogen, 11668019) added to 200  $\mu$ l of Opti-MEM I and mixed by gentle pipetting. The Lipofectamine 2000-Opti-MEM I solution was then added to the DNA-Opti-MEM solution and mixed by gentle pipetting and incubated at R.T. for 5 min. The culture media was removed from cells and replaced with Opti-MEM I media and the transfection complexes added in a dropwise manner. The cells were then incubated overnight, and media removed and replaced with complete DMEM. The cells were then incubated until their respective experimental endpoints.

#### **2.4.9 Transfection of siRNA with Lipofectamine 2000**

For siRNA transfection, HeLa cells were plated into 6 well dishes at  $1.5 \times 10^5$  cells/well and incubated overnight under standard culture conditions (Chapter 2.4.1). The required amount of siRNA was combined with 200  $\mu$ l Opti-MEM I reduced serum medium. In a separate Eppendorf the appropriate volume of Lipofectamine 2000 (Invitrogen, 11668019) added to 200  $\mu$ l of Opti-MEM I and mixed by gentle pipetting. The Lipofectamine 2000-Opti-MEM I solution was then added to the siRNA-Opti-MEM solution and mixed by gentle pipetting and incubated at R.T. for 5 min. The culture media was removed from cells and replaced with Opti-MEM I media and the transfection complexes added in a dropwise manner. The cells were then incubated overnight, and media removed and replaced with complete DMEM. The cells were then incubated until their respective experimental endpoints.

#### **2.4.10 Production of retrovirus**

Phoenix A cells were seeded at  $4.5 \times 10^5$  cells per well for a 6 well plate,  $1.5 \times 10^6$  cells for a 6 cm<sup>2</sup> dish or  $2.5 \times 10^6$  cells for a 10 cm<sup>2</sup> dish. 24 hours post seeding cells were transfected with 2.5 $\mu$ g/4 $\mu$ g/7.5 $\mu$ g of retroviral plasmid pBABE using Lipofectamine 2000 at a ratio of DNA to Lipofectamine 2000 of 1:2.5. Cells were left overnight to incubate with transfection complexes, then media was changed for cell culture media appropriate for the cell line to be transduced.

This media was supplemented with 20mM HEPES pH 7.4. 48 hours post transfection retroviral supernatant was harvested and fresh cell culture media plus 20mM HEPES added to the Phoenix A cells. The retroviral supernatant was then filtered through a 0.45  $\mu\text{m}$  regenerated cellulose filter (Sartorius, 16555-K) and 4 $\mu\text{g}/\mu\text{l}$  Polybrene (Santa Cruz, sc-134220) added and mixed by gentle pipetting.

#### **2.4.11 Production of 2<sup>nd</sup> generation lentivirus**

HEK293TT cells were seeded at  $4.5 \times 10^5$  cells per well for a 6 well plate. 24 hours post seeding cells were transfected with 0.8 $\mu\text{g}$  pZIP-hEF1 $\alpha$  (shNTC (short hairpin-non-targeting control) or shPRAF2 (short hairpin against the PRAF2 gene)), 0.8 $\mu\text{g}$  pCRV1-NLGP and 0.4 $\mu\text{g}$  pCMV-VSV-G using Lipofectamine 2000 at a ratio of DNA to Lipofectamine 2000 of 1:2.5. Cells were left overnight to incubate with transfection complexes, then media was changed for fresh cell culture media appropriate for the cell line to be transduced. This media was supplemented with 20mM HEPES pH 7.4. 48 hours post transfection retroviral supernatant was harvested and fresh cell culture media plus 20mM HEPES added to the HEK293TT cells. The retroviral supernatant was then filtered through a 0.45  $\mu\text{m}$  regenerated cellulose filter (Sartorius, 16555-K) and 4 $\mu\text{g}/\mu\text{l}$  Polybrene (Santa Cruz, sc-134220) added and mixed by gentle pipetting. A second media harvest also occurred at 72 hours post transfection.

#### **2.4.12 Production of 3<sup>rd</sup> generation lentivirus**

HEK293TT cells were seeded at  $4.5 \times 10^5$  cells per well for a 6 well plate. 24 hours post seeding cells were transfected with 1.96 $\mu\text{g}$  of pHIV-zsGreen, 0.65 $\mu\text{g}$  pMDLG-pRRE, 0.65 $\mu\text{g}$  RSV-Rev. 0.65 $\mu\text{g}$  pCMV-VSV-G using Lipofectamine 2000 at a ratio of DNA to Lipofectamine 2000 of 1:2.5. Cells were left overnight to incubate with transfection complexes, then media was changed for fresh cell culture media appropriate for the cell line to be transduced. This media was supplemented with 20mM HEPES pH 7.4. 48 hours post transfection retroviral supernatant was harvested and fresh growth media plus 20mM HEPES added to the HEK293TT cells. The

retroviral supernatant was then filtered through a 0.45  $\mu\text{m}$  regenerated cellulose filter (Sartorius, 16555-K) and 4 $\mu\text{g}/\mu\text{l}$  Polybrene (Santa Cruz, sc-134220) added and mixed by gentle pipetting. A second media harvest also occurred at 72 hours post transfection.

#### **2.4.13 Infection with virus**

Cells to be infected with virus were seeded 24 hours prior to transduction to be at approximately 40% confluent on day of transduction. Media was removed from cells to be transduced, and cell culture media from viral producer cell lines containing the viral vectors applied to the cells. The cells were incubated with virus at 37°C for 5 to 7 hours with occasional gentle swirling to mix the media in contact with the cells. Cells were then retrieved, viral supernatant removed, cells washed twice with PBS and growth media was then replaced.

#### **2.4.14 Production of polyclonal cell lines**

Stable cell lines in C33A and SiHa cells expressing either the pZIP-hEF1 $\alpha$ -shNTC or pZIP-hEF1 $\alpha$ -shPRAF2 were generated by transduction with 2<sup>nd</sup> generation lentivirus (Chapter 2.4.9, Chapter 2.4.11). 48 hours post transduction, the culture media was supplemented with 1  $\mu\text{g}/\text{ml}$  of Puromycin (InvivoGen, ant-pr-1) and cells were cultured under antibiotic selection for 14 days.

#### **2.4.15 Production of monoclonal cell lines**

Stable cell lines in C33A and HeLa cells expressing either the pHIV-zsGreen or pHIV-zsGreen-IRES-PRAF2 were generated by transduction with 3<sup>rd</sup> generation lentivirus (Chapter 2.4.10, Chapter 2.4.11). After transduction cells were passaged twice. On the day of sorting, 80% confluent flasks of T75 were washed twice with Ca<sup>2+</sup> and Mg<sup>2+</sup> free PBS, then treated with enzyme free, PBS based cell dissociation buffer (ThermoFisher Scientific, 13151014) until cells could be removed from the flasks by gentle tapping. Cells were then spun down at 100 xg at 4°C for 5 min, buffer discarded and resuspended in 1ml sort buffer (Ca<sup>2+</sup> and Mg<sup>2+</sup> free PBS, 1 mM EDTA pH7.0, 25 mM HEPES pH7.0, 2% FBS). Cells were then counted, and volumes were adjusted to provide 1x10<sup>6</sup> cells/ml. Un-transduced cells were resuspended to give 1x10<sup>6</sup> per/ml and acted

as a control. Cells were sorted on a FACS Melody (BD Biosciences) running FACS Chorus (BD Biosciences) software, gating for single cells expressing zsGreen. 1 cell was sorted per well of a 96 well plate. Cells were then expanded into monoclonal populations.

## **2.5 Culture of Primary Keratinocytes**

### **2.5.1 Culture of normal human keratinocytes**

Primary normal human keratinocytes (NHKs) isolated from neonate foreskin tissues (ethical approval no.06/Q1702/45) were obtained from Dr Sally Roberts, University of Birmingham, UK. NHKs were cultured in KBM gold keratinocyte growth medium (KGM) plus bullet kit supplements (Lonza, 00192060). Bullet kit contained the following supplements: Hydrocortisone, Transferrin, Epinephrine, BPE, hEGF, Insulin, Gentamycin and Amphotericin B. Before plating cell culture plates were treated with a collagen coating buffer containing 100 µg/ml bovine serum albumin (BSA, Sigma-Aldrich, A9418) , 20mM HEPES pH 6.5 (ThermoFisher Scientific, 15630106), 10 µg/ml rat tail Collagen Type I (Corning, 354236) in Hanks' Balanced Salt Solution (Gibco, 14180-046) made up to 1x from 10x in water (Sigma-Aldrich, W3500). 10 ml of coating buffer was added to plates and either incubated at 37°C for 3 hours or overnight at 4°C to treat culture plates. Coating buffer was then removed, leaving 1-2 ml behind before application of KGM.

Cells were cultured in KGM, with KGM changed every three days, until 80% confluent. Cell media was removed, and 10 ml of HEPES Buffered Saline Solution (HEPES-BSS) (4.0mM glucose, 3.0mM KCl, 122mM NaCl, 1.0mM Na<sub>2</sub>HPO<sub>4</sub>, 30mM HEPES NaOH (pH 7.6)) applied to wash. After washing, 2ml of Trypsin-EDTA (0.05%) (ThermoFisher Scientific, 25300054) was applied and cells were incubated at 37°C to dissociate cells. Cells were checked during incubation for rounding via microscope 5 min after trypsin addition. The plate was then held in one hand and gently tapped with a knuckle to release cells. Once in suspension 3.3 ml of defined trypsin inhibitor (DTI) (ThermoFisher Scientific, R007100) was added to neutralise trypsin. The

resulting suspension was then transferred into a falcon tube. The plate was then rinsed with 2ml of HEPES-BSS and then added to the cell suspension. Cells were then centrifuged at 200xg for 5 min and the supernatant gently aspirated. For passage, 1/5<sup>th</sup> of the cell suspension was reseeded.

### **2.5.2 Freezing of NHKs**

Freezing media was prepared with a composition of 80% KGM, 10% fetal bovine serum (Sigma-Aldrich, F2442) and 10% DMSO. Freezing media was ice-cold for cell freezing. NHKs were grown until 80% confluent and trypsinised as per growth protocol (2.5.1). NHKs were then resuspended into freezing media at  $1 \times 10^6$  cells/ml, then aliquoted into cryotubes and placed in a freezing chamber. The freezing chamber was then placed at -80°C overnight, then cryotubes were transferred to liquid nitrogen.

### **2.5.3 Thawing NHKs**

NHKs were retrieved from liquid nitrogen and thawed in a 37°C water bath. Cells were then gently pipetted up and down and then transferred into a collagen treated 10cm<sup>2</sup> dish containing 15 ml growth media, swirled gently to mix, placed at 37°C in an incubator and allowed to attach overnight. The media was then changed for fresh KGM in the morning.

### **2.5.4 Thawing of J2 3T3**

J2 3T3 cells were retrieved from liquid nitrogen and thawed in a 37°C water bath. Cells were then gently pipetted up and down and then transferred into a 10cm<sup>2</sup> dish containing 10 ml growth media, swirled gently to mix, placed at 37°C in an incubator and allowed to attach for 8 hours. The media was then changed for fresh DMEM with 10% bovine serum.

### **2.5.5 Culture of J2 3T3 mouse fibroblasts**

J2 3T3 cells were cultured in Dulbecco's Modified Eagle Medium (Sigma-Aldrich, D6429), supplemented with 10% bovine Serum (ThermoFisher Scientific, 16170078), 50 U/ml penicillin

and streptomycin (ThermoFisher Scientific, 15070063) in a 37°C incubator, humidified with 5% CO<sub>2</sub>. Cells were cultured until 80% confluent, then trypsinised and split at a ratio of 1:5 to 1:10. Cells were passaged no further than passage 20.

### 2.5.6 Mitomycin C treatment of J2 3T3 mouse fibroblasts

80% confluent plates of J2 3T3 cells growth media was removed, plates were washed with PBS and treated with 8 µg/ml Mitomycin C (Sigma-Aldrich, 10107409001) in DMEM with 10% bovine serum for 2 hours to induce cellular senescence. Mitomycin C treated J2 3T3 cells were then washed twice with PBS, before application of trypsin-EDTA. Once dissociated, cells were neutralised with complete E-media (Table 2.1) and cells were counted, then centrifuged at 200 xg at 4°C for 5 min to pellet cells. Cells were resuspended in complete E-media at 1x10<sup>6</sup> cells/ml and either used immediately or stored at 4°C for up to one week.

**Table 2.1** *List of components in complete E-media*

| Component                                       | Manufacture and product code       | Final concentration       | Volume in 500 ml media (ml) |
|---|------------------------------------|---------------------------|-----------------------------|
| DMEM  | Sigma-Aldrich, D6171               | N/A                       | 300                         |
| HAM's F12                                       | Thermofisher scientific, 21765-029 | N/A                       | 160                         |
| 0.018 M Adenine                                 | Sigma-Aldrich, A2786               | 180 µM                    | 5 of 100x cocktail          |
| 0.5 mg/ml Insulin                               | Sigma-Aldrich, I6634               | 5 µg/ml                   |                             |
| 0.5 mg/ml Transferrin                           | Sigma-Aldrich, T1147               | 5 µg/ml                   |                             |
| 2 nM Triiodo-L-thyronine                        | Sigma-Aldrich, T6397               | 0.02 nM                   |                             |
| 0.4 mg/ml Hydrocortisone                        | Sigma-Aldrich, H0888               | 0.4 µg/ml                 | 0.5                         |
| 100 nM Cholera toxin                            | Sigma-Aldrich, C8052               | 0.1 nM                    | 0.5                         |
| 5000 U/ml Penicillin<br>5000 µg/ml streptomycin | Lonza                              | 100 U/ml and<br>100 µg/ml | 10                          |
| Fetal bovine serum                              | (Sigma-Aldrich, F2442              | 5%                        | 25                          |
| 1 µg/ml mEGF in 0.1 mg/ml BSA/PBS               | Corning, 11573520                  | 5 ng/ml                   | 2.5                         |

### **2.5.7 Freezing of J2 3T3 mouse fibroblasts**

Freezing media was prepared with a composition 80% DMEM with 10% bovine serum, 10% DMSO, 10% bovine serum and filter sterilised using 0.2 µm regenerated cellulose membrane filter unit (Corning, 431222) and placed on ice. J2 3T3 cells were grown until 80% confluent, then trypsinised. Trypsin was inactivated with DMEM with 10% bovine serum. Cells were then counted and pelleted at 250xg. Cells were then resuspended in ice cold freezing media to give  $1 \times 10^6$  cells/ml, aliquoted into 1ml volumes in cryotubes and placed in a freezing chamber. The freezing chamber was then placed at -80°C overnight, then cryotubes were transferred to liquid nitrogen.

### **2.5.8 Production of HPV positive primary keratinocytes**

NHK were transfected with the WT HPV genome and the E5KO genome as previously described (Wasson et al., 2017). The plasmids containing the HPV-18 genome were digested with EcoRI to release the genome, which was then circularised via T4 DNA ligase ligation. The genomes were cotransfected with a plasmid encoding neomycin resistance into low passage NHKs. After 24 hours, the cells were harvested and seeded onto a feeder layer of γ-irradiated J2 3T3 mouse fibroblasts. The transfected NHKs were then selected with the antibiotic G418 in complete E-media. Cells were kept under selection for 8 days, then cell colonies were pooled and expanded on fibroblast feeder layers. After selection, stable expression of episomal WT and E5KO HPV-18 genomes was confirmed by Southern blotting.

### **2.5.9 Culture of HPV positive primary keratinocytes**

Once cultures of HPV positive primary keratinocytes reached ~80-90% confluent cells were dissociated by incubation with trypsin-EDTA 0.05% solution at 37°C. Once dissociated, trypsin was neutralised by the addition of complete E-media, cells were then seeded at a ratio of 1:10 onto fresh 10 cm<sup>2</sup> dishes which had been seeded with  $2 \times 10^6$  mitomycin C treated J2 3T3 mouse fibroblasts in complete E-media 24 hours prior, or adjusted to an appropriate cell

concentration for experiments and seeded onto appropriate plates/dishes of mitomycin C treated J2 3T3 cells. Media was changed on HPV positive primary keratinocytes every other day.

#### **2.5.10 Freezing of HPV positive primary keratinocytes**

Freezing media was prepared with a composition of 70% complete E-media, 10% FBS, 20 ml Glycerol (Sigma, G2025). Freezing media was ice-cold for cell freezing. ~80% confluent cultures of HPV positive primary keratinocytes were dissociated by incubation with Trypsin-EDTA 0.05% solution at 37°C. Once dissociated, trypsin was neutralised by the addition of complete E-media and cells counted. Cells were centrifuged at 200 xg at 4°C for 5 min to pellet cells. Cells were then resuspended in ice cold freezing media to give  $1 \times 10^6$  cells/ml, aliquoted into 1ml volumes in cryotubes and placed in a freezing chamber. The freezing chamber was then placed at -80°C overnight, then cryotubes were transferred to liquid nitrogen.

#### **2.5.11 Thawing of HPV positive primary keratinocytes**

NHKs were retrieved from liquid nitrogen and thawed in a 37°C water bath. Cells were then gently pipetted up and down and then transferred into a 10cm<sup>2</sup> dish pre-seeded with mitomycin C treated J2 3T3 mouse fibroblasts containing 15 ml growth media, swirled gently to mix, placed at 37°C in an incubator and allowed to attach overnight. The media was then changed for fresh complete E-media in the morning.

#### **2.5.12 Keratinocyte monolayer high-calcium differentiation**

Once NHKs and HPV positive keratinocytes reached ~90% confluent cells were induced to differentiate. KGM was removed, and cells washed twice with PBS to ensure that all KGM was removed. Media was then replaced with keratinocyte basal media, supplemented with 50 µg/ml gentamycin (Sigma, G1397) and 2.5 µg/ml amphotericin B (Sigma, A2942) and 1.4 mM CaCl<sub>2</sub> (Sigma, C7902). Cells were then differentiated for 0, 48, 72 and 96 hours. For the 72- and 96-hour differentiation timepoints, media was swapped for fresh high calcium media at 48 hours. Cells were then lysed as per (Chapter 2.5.13).

### **2.5.13 Lysis of HPV positive primary keratinocytes**

Prior to lysis of HPV positive primary keratinocytes, the mitomycin C treated J2 3T3 mouse fibroblasts must be removed. E-medium/high-calcium medium was aspirated, and plates washed once with PBS and 0.54 mM EDTA in PBS applied for 2 min to loosen fibroblasts, followed by vigorous rinsing of EDTA in PBS by pipetting, followed by a wash with PBS. Cell lysis was then carried out (Chapter 2.3.1).

## **2.6 Raft Cultures**

### **2.6.1 Production of PRAF2 overexpression primary cell lines**

NHK, HPV-18 WT and E5KO PRAF2 overexpression primary keratinocyte cell lines were produced through transduction with retrovirus generated from pBABE-hygro-3xFLAG-PRAF2 and control lines from pBABE-hygro in Phoenix A cells (Chapter 2.4.8, Chapter 2.4.11). Two rounds of retroviral infection were performed, and cells were expanded for 7 days before usage in raft cultures.

### **2.6.2 Production of PRAF2 knockdown primary cell lines**

NHK, HPV-18 WT and E5KO PRAF2 knockdown primary keratinocyte cell lines were produced through transduction with 2<sup>nd</sup> generation lentivirus generated from the pZIP-hEF1 $\alpha$ -shPRAF2 and control lines from pZIP-hEF1 $\alpha$ -shNTC in HEK293TT cells (Chapter 2.4.9, Chapter 2.4.11). Two rounds of lentiviral infection were performed. 48 hours after the last round of infection, cells were placed under 1  $\mu$ g/ml puromycin selection. Cells were kept under selection for 7 days, with media changed every two days. For HPV positive primary keratinocytes fresh mitomycin C treated J2 3T3 cells were provided every two days. Cells were removed from selection, washed well and then used for raft cultures.

### **2.6.3 Production of collagen plugs**

80% confluent 10 cm<sup>2</sup> plates of J2 3T3 fibroblasts sub passage 20 were trypsinised and neutralised in E-media. The volume of cells required for 1-2x10<sup>6</sup> cells was then spun down at 250xg for 5 min and the supernatant was removed. The resulting cell pellet was then resuspended in 0.3 ml 10x DMEM containing no NaHCO<sub>3</sub> (Biochrom, F0455), 0.3 ml 10x reconstitution buffer (262mM NaHCO<sub>3</sub> (Sigma-Aldrich, S5761), 200mM HEPES (Sigma-Aldrich, H3375) in 0.05M NaOH) and 2.4 ml Rat-tail collagen type I (Corning, 354236) on ice. The pH was adjusted by eye by addition of 1M NaOH until the collagen mixture was a red-orange colour. 3 ml of collagen mixture was then applied to a 35 mm<sup>2</sup> dish and incubated at 37°C for 30 min to allow solidification of the collagen plug. 2.5 ml of complete E-media was then applied to the collagen plug and the nascent collagen plug returned to 37°C to incubate. After 48 hours the collagen plug was seeded with primary foreskin keratinocytes.

### **2.6.4 Seeding of collagen plugs with primary keratinocytes and rafting**

Primary foreskin keratinocytes were trypsinised and then neutralised in complete E-media. Cells were counted and the cells spun down at 250xg. Cells were then resuspended in complete E-media to give between 4x10<sup>5</sup> to 8x10<sup>5</sup> cells/ml. Media was then removed from the collagen plug and 2.5 ml of primary cell suspension applied in its stead. Cells were then incubated at 37°C until confluent, for a maximum of 4 days. The nascent raft cultures were then removed from their 35 mm<sup>2</sup> dishes and placed onto stainless steel wire mesh support grids in 10cm<sup>2</sup> dishes, with care taken to avoid bubbles. E-media lacking mEGF was then applied until it touched the metal support, but not the collagen, with care taken to ensure no air pockets were visible under the rafts. Rafts were incubated at 37°C with media changed every other day. Rafts were harvested after 13 days and fixed in 4% paraformaldehyde (pH 6.9). Rafts were then sent for paraffin embedding, sectioning into 5 µm slices and H&E staining (Histology facility, University of Leeds).

## **2.7 Immunofluorescence**

### **2.7.1 Cell growth on coverslips**

Cells were seeded into wells containing 13 mm circular glass coverslips (VWR international, 631-0149), which had been pre-sterilised by incubation with 70% ethanol followed by washing with PBS. Cells were seeded at an assay and cell type dependent number. Where appropriate cells were transfected as per (Chapter 2.4.6). Cells were fixed at the appropriate experimental endpoint.

### **2.7.2 Fixation and permeabilisation of cells**

At the experimental endpoint media was aspirated, cells washed once with PBS and then fixed with 4% Paraformaldehyde in PBS (pH 7.6) for 15 min. Cells were then washed with PBS and permeabilised with 0.1% Triton X-100 in PBS for a further 10 min, then washed with PBS.

### **2.7.3 Immuno-labelling**

After permeabilisation cells were then blocked in immunofluorescence buffer (4% BSA in PBS) for 30 min at room temperature (R.T). Cells were then incubated with primary antibodies (Appendix A) diluted in immunofluorescence buffer at 4°C overnight or 1 hour at 37°C. Cells were then washed three times with PBS, and then secondary fluorescent conjugated antibodies (Appendix A) diluted in immunofluorescence buffer were applied and incubated for a further 2 hours at R.T. Cells were then washed three times in PBS and then mounted onto microscope slides using ProLong Gold Antifade Reagent with DAPI (Thermofisher scientific, P36931) and sealed with nail varnish and slides stored at 4°C until imaging.

### **2.7.4 Microscopy**

Images were taken with a Zeiss LSM 880 laser scanning confocal microscope under an oil-immersion 40 x objective lens. Representative images were processed using the Zen Blue 2.6 edition software (Zeiss).

### **2.7.5 Colocalisation analysis**

Colocalisation analysis was performed using the FIJI is just imageJ (FIJI) software using the Coloc 2 plugin. Colocalisation was determined based on the use of the Pearson's correlation coefficient.

## **2.8 Immunofluorescent immunohistochemistry**

### **2.8.1 ALTER (Agitated low temperature epitope retrieval) antigen retrieval**

1 L of ALTER buffer (0.1 mM EDTA-NaOH (pH 8.0), 0.1% Tween-20 (v/v)) was placed in a foil covered glass beaker and placed onto a magnetic hotplate stirrer (IKA, 12917246) and heated to a constant temperature of 65°C, stirring at 600 RPM. Raft sections for staining were placed into a rack and immersed in HistoClear (National Diagnostics, HS-200) for 10 min. Slides were removed from HistoClear and drained, then transferred into 100% ethanol (IMS) for 5 min, then drained well. Slides were then immersed in tap water, with water changed three times. Slides were then transferred into the stirring beaker of heated ALTER buffer and left overnight stirring. Hotplate stirrer was then switched off, ALTER buffer allowed to settle and slides removed and washed in tap water. Slides were then stained as required (Chapter 2.8.2)

### **2.8.2 Raft section staining for immunofluorescence**

Staining of ALTER treated raft sections was carried out as follows. The raft sections were blocked with 10% normal goat serum (NGS, Vector Labs, S-1000) (v/v) in PBS for 1 hour at R.T. in a humidity chamber. The blocking buffer was then drained off the sections and any excess remaining removed by wicking with tissue. The primary antibody was then applied in 1% NGS in PBS and left to incubate overnight in a humidity chamber at 4°C. Primary antibody was then drained off and raft section slides were then washed four times in PBS prior to incubation with AlexaFluor conjugated secondary antibodies in 1% NGS (v/v) in PBS. Incubation was carried out for 2 hours at R.T. in a humidity chamber protected from light. Secondary antibody was then drained off and raft section slides were then washed three times in PBS. A final fourth 5-minute

wash was carried out, with 0.5 µg/ml DAPI (Thermofisher Scientific, D1306) in PBS. Slides were then removed from the DAPI wash, drained and wicked dry and mounted with ProLong Gold antifade mountant (Thermofisher Scientific, P36930). Mountant was allowed to harden overnight at R.T. and slides were then imaged (Chapter 2.7.4).

## **2.9 Co-immunoprecipitation**

### **2.9.1 Cell lysis for co-immunoprecipitation**

HEK293TT cells were lysed in GFP trap lysis buffer (10 mM Tris-HCl (pH 7.5); 150 mM NaCl; 0.5 mM EDTA; 0.5% NP-40 (v/v), 1x Protease inhibitor cocktail, EDTA-Free). Cell lysates were incubated on ice for 20 min and then centrifuged at 17,000 xg at 4°C for 10 min to clarify lysates and the lysates transferred to a fresh tube. The total protein concentration was determined by BCA assay (Chapter 2.3.2).

### **2.9.2 GFP-trap co-immunoprecipitation**

Samples adjusted to those of the lowest concentration using dilution-wash buffer (10 mM Tris/Cl (pH 7.5); 150 mM NaCl; 0.5 mM EDTA). GFP-trap MA beads (Chromotek, gtma-10) were equilibrated with dilution/wash buffer, magnetically separated and washed a further two times. Adjusted cell lysates were then applied and incubated overnight at 4°C whilst being tumbled end-over-end. Beads were magnetically separated from lysates and then washed three times with dilution/wash buffer. Proteins were then dissociated from the beads by incubating the GFP-trap MA beads in 2x Laemmli Sample Buffer at 95°C for 10 min. Samples were then resolved by SDS-PAGE (Chapter 2.3.4) and analysed by western blotting (Chapter 2.3.5).

## **2.10 Flow cytometry**

### **2.10.1 Determination of cell cycle phase by propidium iodide staining**

Cells were fixed in 70% ethanol overnight. The ethanol was removed, and cells washed with incubation buffer (0.5% BSA (w/v) in PBS) cells were then pelleted and resuspended in

staining buffer (0.5% BSA (w/v), 16 µg/ml propidium iodide (Sigma-Aldrich) and 5 µg/ml RNase (Sigma-Aldrich) in PBS) and incubated in this solution for 30 min at R.T. Samples were processed on a Cytoflex S (Beckman coulter) and the PI histograms analysed on Cytexpert software (Beckman coulter).

### **2.10.2 Cell surface EGFR assay**

Cells were seeded at  $3.5 \times 10^5$  cells/well of a 6 well plate. After 48 hours, complete DMEM was removed, cells washed twice with PBS and replaced with serum free DMEM. Cells were serum starved for 4 hours. Cells were then washed with PBS and dissociated from the plate using cell dissociation buffer (ThermoFisher Scientific, 13151014) for 5 min. Cells were then spun at 200xg for 5 min to pellet, and the supernatant removed and replaced with 4% paraformaldehyde (pH 7.6). Cells were fixed for 20 min, then centrifuged at 200xg for 5 min to pellet, washed once with PBS and pelleted again and resuspended in 1% BSA (Sigma-Aldrich, A3912) in PBS and blocked at R.T for 1 hour. Samples were then pelleted and resuspended in rabbit anti-EGFR (Abcam, ab52894) at 1:100 in 1% BSA and incubated with rocking overnight at 4°C. Samples were then retrieved, centrifuged and supernatant discarded, samples were then washed twice with PBS by centrifugation. Samples were then stained with chicken anti-rabbit alexa-594 conjugated secondary antibody (ThermoFisher Scientific, A-21442) at 1:250 in 1% BSA for 1 hour at R.T, then centrifuged and washed in PBS three times by centrifugation. Samples were then resuspended in 100µl PBS. Data was sampled with a Cytoflex S (Beckman Coulter) using CytExpert software (Beckman Coulter). Samples were excited at 561 nm and a 561\_585-42A band pass filter used.

## **2.11 Cancer cell assays**

### **2.11.1 Colony formation assays**

To measure anchorage dependent cell proliferation, cells were trypsinised, and 500 cells were re-plated per well of a 6 well plate, with each experimental condition plated in triplicate. Cells were checked daily by microscopy until visible colonies could be observed (14 days). At this

point complete DMEM was removed and cells were washed with PBS and ice-cold methanol applied, and cells were incubated at  $-20^{\circ}\text{C}$  for 10 min to fix. Methanol was then removed, and crystal violet staining solution applied (1% crystal violet (CHE1680, Science Laboratory Support SLS, UK), 25% methanol) for 15 min. Plates were then washed with water and scanned. Colonies were counted on imagej software (NIH).

### **2.11.2 Soft agar assays**

To measure anchorage independent cell proliferation, cells were trypsinised and 1,000 cells/ml were added to 0.7% agarose (ThermoFisher Scientific, 16520050) in 2x DMEM (SigmaAldrich, SLM-202-B) supplemented with 20% FBS and overlaid onto 6 cm<sup>2</sup> dishes coated with 1% agarose. Once set, DMEM supplemented with 10% FBS and 50 U/ml pen/strep was added. The plates were then incubated for 38 days. Colonies were counted manually.

### **2.11.3 Growth curve assays**

Cells were seeded at a density of 25,000 cells/well for HeLa cells and 75,000 cells/well for C33A or SiHa cells per well of a 6 well plate. Cells were then harvested daily and counted using a haemocytometer.

### **2.11.4 Wound healing assays**

Cells were seeded at a density of  $1 \times 10^6$  cells/well of a 6 well plate. Cells were grown until confluent, then wounded with a P200 pipette tip. Wounds were gently washed with PBS, and complete DMEM replaced, wounds were then imaged. 18 hours later wounds were reimaged. All images were then analysed using ImageJ (NIH).

## **2.12 Apoptosis assays**

### **2.12.1 DNA laddering**

C33A and HeLa cells were seeded at  $1.5 \times 10^6$  and  $2.75 \times 10^5$  cells per 6cm<sup>2</sup> dish respectively. 24 hours post seeding cells were transfected with 4 $\mu\text{g}$  of DNA

(pcDNA3.1+/pcDNA3.1+ PRAF2-3xHA), using lipofectamine 2000 (ThermoFisher Scientific, 11668019) at a DNA to Lipofectamine 2000 ratio of 1:2.5. Transfection complexes were incubated overnight and complete DMEM changed the following morning. 5 hours prior to lysis Staurosporine (Fisher Scientific Ltd, BP2541-100) was added at a final concentration of 1 $\mu$ M. Cells were lysed by scraping into 500 $\mu$ l DNA laddering lysis buffer (50mM Tris-HCl (pH 7.5), 10 mM EDTA, 200 mM NaCl, 1% Nonidet P-40 substitute (v/v) and 50  $\mu$ g/ml Proteinase K (New England Biolabs, P8107S)) and cell lysates were incubated at 4°C overnight. DNA was then isolated by the addition of 1 volume of Phenol:Chloroform:Isoamyl alcohol (25:24:1, v/v) (ThermoFisher Scientific, 15593031). Samples were mixed by inversion for 30 seconds, then centrifuged at 17000xg for 5 min to separate the phases. The aqueous phase was then transferred to a fresh Eppendorf tube and 1 volume of Chloroform (Fisher Scientific Ltd, 15643700) added, and then mixed by inversion for 30 seconds. Samples were then spun at 17000xg for 5 min to separate the phases, and the aqueous phase transferred to a fresh Eppendorf tube. The DNA was then precipitated by the addition of 0.1 volumes of 3M sodium acetate (pH 5.2) and 2.5 volumes of 100% Ethanol. Samples were mixed thoroughly by inversion then placed at -20°C overnight to allow DNA precipitation. Samples were then centrifuged at 17000xg for 30 min at 4°C to pellet the DNA, the supernatant removed, and 70% ethanol added, and samples spun at 17000xg for 15 min to wash the pellet. The supernatant was then removed and the samples placed in a vacuum chamber to dry the DNA pellet. The pellet was redissolved in TE buffer (10 mM Tris-HCl pH 8.0, 1 mM EDTA) and RNase A added to a final concentration of 100 $\mu$ g/ml. Samples were then incubated at 37°C for 1 hour. DNA was then quantified by use of a Nanodrop and equal amounts loaded onto an 1.7% agarose gel with 2x SYBR safe (ThermoFisher Scientific, S33102). Agarose gel was run at 5 V/cm for 2 hours and imaged on a Syngene InGenius gel documentation system.

### 2.12.2 Active caspase-3 staining

C33A and HeLa cells were seeded onto coverslips in 6 well plates. 24 hours post seeding cells were transfected with 1.5 µg of DNA, after 8 hours media was removed and replaced with complete DMEM. 24 hours post transfection cells were retrieved, washed gently with PBS and fixed in 4% paraformaldehyde (pH 7.6) for 15 min, cells were then washed once with PBS and incubated with 0.1% Triton X-100 in PBS for 10 min and washed once with PBS. Cells were then blocked with 4% BSA in PBS for 30 min, before application of rabbit anti-cleaved caspase-3 (Asp175) (CST, 9661) at 1:400 in 4% BSA in PBS. Coverslips were incubated with primary antibody at 4°C overnight with gentle rocking, then washed three times with PBS before application of chicken anti-rabbit alexa-488 conjugated antibodies diluted in immunofluorescence buffer were applied and incubated for a further 2 hours at R.T. Cells were then washed three times in PBS and then mounted onto microscope slides using ProLong Gold Antifade Reagent with DAPI and sealed with nail varnish. Images were taken with a Zeiss LSM 880 scanning confocal microscope.

### 2.12.3 Annexin V staining assay

Cells were seeded at  $3.5 \times 10^5$  cells/well of a 6 well plate. 24 hours post seeding cells were transfected with pcDNA3 or PRAF2-3HA (Chapter 2.4.8). After 24 hours, complete DMEM was removed, cells were then washed with PBS and the PBS wash was saved. Cells were then dissociated from the plate using cell dissociation buffer for 5 min and added to the reserved PBS. Cells were then spun at 200xg at R.T. for 5 min to pellet. Cells were then resuspended in ice-cold PBS, cells counted and then centrifuged at 200 xg at R.T. for 5 min. Supernatant was removed and cells were resuspended at  $5 \times 10^5$  cells/100 µl in annexin V incubation reagent (1:100 TACS annexin V-FITC (RND Systems, 4830-01-1), 1:10 10x binding buffer (RND Systems, 4830-01-2) and 1:10 propidium iodide (RND Systems, 4830-01-3) in dH<sub>2</sub>O), and incubated on ice for 15 min. 400 µl of 1x binding buffer was then applied per 100 µl of cell suspension and immediately processed by flow cytometry. Data was sampled with a Cytoflex S (Beckman Coulter) using

CytExpert software (Beckman Coulter). Samples were excited at 488 nm and 561 nm and 488\_525-40A and 561\_585-42A band pass filters used.

## **2.13 BioID**

### **2.13.1 Generation of BioID cell lines**

Phoenix A cells were seeded at  $2.5 \times 10^6$  cells per  $10 \text{ cm}^2$  dish. 24 hours post seeding cells were transfected with 7.5  $\mu\text{g}$  of retroviral plasmid pBABE-puromycin-Myc-BioID2/pBABE-puromycin-Myc-BioID2-PRAF2 using Lipofectamine 2000 at a ratio of DNA to Lipofectamine 2000 of 1:2.5. Cells were left overnight to incubate with transfection complexes, then Opti-MEM was changed for complete DMEM supplemented with 20mM HEPES (pH7.4). 48 hours post transfection retroviral supernatant was harvested and fresh growth media plus 20mM HEPES added to the Phoenix A cells, to allow a second round of infection. The retroviral supernatant was then filtered through a 0.45  $\mu\text{m}$  regenerated cellulose filter and  $4 \mu\text{g}/\mu\text{l}$  Polybrene added and mixed by gentle pipetting.

24 hours prior to infection C33A cells were seeded at  $1 \times 10^6$  cells per  $10 \text{ cm}^2$  dish. To infect, complete DMEM was removed and replaced with retroviral supernatant, and incubated for 4 hours at  $37^\circ\text{C}$ , with regular agitation. Retroviral supernatant was then removed, cells were washed twice with PBS and complete DMEM was reapplied. 24 hours post initial infection a second round of infection was carried out. 24 hours after the final infection media was changed for media supplemented with  $1 \mu\text{g}/\text{ml}$  puromycin. Selection was carried out for 7 days. The surviving cells were then assayed for expression of the constructs. This generated the stable cell lines C33A Myc-BioID2 and C33A Myc-BioID2-PRAF2.

### **2.13.2 Induction of biotinylation**

A 5 mM biotin (Sigma-Aldrich, B4501) stock was prepared by dissolving Biotin in Opti-MEM I, then filter sterilised using a 0.2  $\mu\text{m}$  regenerated cellulose membrane filter unit. Cells

were seeded 24 hours prior to addition of biotin. Cell media was aspirated and replaced with complete DMEM supplemented with 50  $\mu$ M biotin and cultured for a further 18 hours prior to lysis or fixation.

### **2.13.3 Visualisation of biotinylated proteins by Streptavidin HRP**

Samples saved for analysis were processed via SDS-PAGE (Chapter 2.3.4) followed by western blot transfer (Chapter 2.3.5) membranes were incubated for 30 min in BSA blocking buffer (1% BSA (w/v) and 0.2% Triton X-100 (w/v) in PBS) with rocking. Membranes were then incubated with streptavidin-HRP (ThermoFisher Scientific, 21130) at 1:40,000 in BSA blocking buffer overnight at 4°C with rocking. The membrane was then washed quickly, three times with PBS and then incubated in ABS blocking buffer (10% bovine serum (v/v) and 1% Triton X-100 (v/v) in PBS) with rocking for 5 min. The membrane was then washed quickly in PBS a further three times, before a final 5-minute wash in PBS. The membrane was then developed (Chapter 2.3.5). After film exposure, the HRP was quenched by incubation with quenching solution (3% sodium azide (w/v) and 4.5% hydrogen peroxide (v/v) in PBS), for 20 min with rocking at R.T. The membrane was then washed three times with PBS to remove any residual quenching solution, before blocking with 5% milk (w/v) in TBS-T and standard western blotting (Chapter 2.3.5) for the Myc tag and loading control GAPDH.

### **2.13.4 Visualisation of biotinylated proteins by immunofluorescence**

Cells were grown on coverslips as per (Chapter 2.7.1), and biotinylation induced as per (Chapter 2.13.2). However, the fixation and permeabilisation differed from (Chapter 2.7.2). 18 hours post biotin addition complete DMEM supplemented with Biotin was aspirated, cells washed once with PBS and then fixed with 3% Paraformaldehyde in PBS (pH 7.6) for 10 min. Cells were then washed with PBS and permeabilised with 0.4% Triton X-100 in PBS for a further 15 min, then washed with PBS. Cells were then blocked with 3% BSA in PBS for 45 min, blocking buffer was removed and replaced with primary antibody in 3% BSA in PBS, and incubated

overnight at 4°C with gentle rocking. Primary antibody was then removed, and cells washed three times with PBS. The appropriate AlexaFluor conjugated secondary antibody was then added in 3% BSA (w/v) in PBS and incubated at R.T. for 2 hours, protected from light, before washing three times with PBS. Streptavidin-Alexa488 (ThermoFisher Scientific, S32354) was added at 1:1000 in 3% BSA in PBS and incubated at R.T. for 1 hour with rocking. Cells were then washed three times with PBS and then mounted onto microscope slides using ProLong Gold Antifade Reagent with DAPI and sealed with nail varnish and slides stored at 4°C until imaging.

### **2.13.5 BioID pulldown**

C33A, C33A Myc-BioID2 and C33A Myc-BioID2-PRAF2 cells were seeded at  $2.5 \times 10^6$  per 10 cm<sup>2</sup> dish. 4 plates were seeded for each cell line. Once the dishes reached 80% confluent, complete DMEM was changed for complete DMEM supplemented with 50 μM biotin. Cells were incubated with 50 μM biotin for 18 hours. Media was then removed via aspiration, and each plate washed twice with 5 ml of PBS. Cells were then lysed in 600 μl of BioID2 lysis buffer (50mM Tris.HCl (pH 7.4), 500mM NaCl, 0.4% SDS, 1mM dithiothreitol and 1x Protease inhibitors). Cells were gently scraped and lysates collected into 15ml falcons, and 240 μl of 20% Triton X-100 added per tube. Lysates were then gently mixed by pipetting and placed on ice. Cell lysates were then processed with two sessions of sonication on a Soniprep 150. Each session comprised of 30 cycles of 1 second 6 microns amplitude pulses, with 2 seconds off between pulses. 2.14 ml of 50mM Tris.HCl (pH 7.4) was then added and lysates were mixed by pipetting, followed by one further session of sonication. Lysates were then divided equally between 2ml protein lo-bind tubes and centrifuged at 16500xg for 10 min at 4°C.

Three 2ml tubes were set up on a magnetic rack and 0.75ml of BioID lysis buffer and 0.75ml of 50mM Tris.HCl, (pH7.4) was added to each tube and mixed. Dynabeads (MyOne Streptavidin C1) were resuspended gently by tapping and 200 μl of beads were added to each tube and allowed to separate magnetically for 3 min to allow equilibration of the beads.

Equilibration buffer was then removed and centrifuged lysate was applied to the beads. 75µl of lysate was reserved for later analysis. Samples were then placed on a rotator to incubate overnight at 4°C. Beads were then collected using a magnetic stand for 3 min, and 75 µl of bead supernatant reserved for later analysis. Supernatant was discarded and beads were resuspended in 1.5 ml of wash buffer 1 (2% SDS (w/v)), beads were then washed for 8 min on a rotator at R.T. Each subsequent wash step was carried out for 8 min and bead collection for 3 min. This wash step was repeated and then followed with washes in 1.5 ml wash buffer 2 (0.1% deoxycholate (w/v), 1% Triton X-100 (v/v), 500mM NaCl, 1mM EDTA and 50mM HEPES, pH7.5), then 1.5 ml wash buffer 3 (250mM LiCl, 0.5% Deoxycholate (w/v), 0.5% NP-40 (v/v), 1mM EDTA and 1mM Tris.HCl, pH7.4). Beads were then resuspended in 1.5 ml of Tris.HCl (pH7.5), and 10% removed for later analysis. Both 10% and 90% samples of beads were then pelleted by centrifugation at 2000xg for 5 min, supernatant discarded and with those destined for Mass spectroscopy resuspended in 50µl of 50mM Ammonium Bicarbonate. The sample for further analysis was resuspended in 100µl 1 x Laemmli Sample Buffer.

## **2.14 Mass spectroscopy (MS)**

This work was carried out by Dr. Stuart Armstrong at the University of Liverpool.

### **2.14.1 On bead digestion**

On bead trypsin digestion was performed essentially as described by (Branon et al., 2018). For each sample streptavidin beads (50 µl) were washed twice with 200 µl 50mM ammonium bicarbonate followed by two washes of 200 µl 50 mM ammonium bicarbonate with 2 M urea. Beads were then incubated in 80 µl 50 mM ammonium bicarbonate with 2 M urea, 1 mM DTT and 0.4 µg trypsin for 1 h at 25°C with shaking (1000rpm). The samples were centrifuged at 5000 xg for 1 min and the supernatant (eluate) was removed to a new tube. The beads were washed twice with 50 µl 50 mM ammonium bicarbonate with 2 M urea and pooled with the supernatant. The eluate was reduced with 10 µl of 60 mM DTT (final ~3 mM) for 30 min

at 25°C with shaking (1000 rpm) then alkylated with 10 µl of 180mM iodoacetamide (IA, final ~9 mM) 1h at 25°C with shaking (1000 rpm). Additional trypsin was added (0.5µg) and incubated overnight at 25°C with shaking (1000 rpm) (**Digest 1**).

The beads were then given an additional more extensive trypsin treatment. Beads were washed twice with 200 µl 50 mM ammonium bicarbonate, then re-suspended in 80 µl 50 mM ammonium bicarbonate, 3 mM DTT and incubated 37°C for 30 min with shaking (1000 rpm). The DTT solution was removed and 80µl 50 mM ammonium bicarbonate, 9 mM IA added and incubated 25°C for 1 h with shaking (1000rpm). The IA was removed and 80 µl 50mM ammonium bicarbonate with trypsin (0.6µg) was added. The beads were incubated overnight at 37°C with shaking (1000rpm) (**Digest 2**).

A small aliquot (5µl), was used to check that protein digestion was complete (by SDS PAGE). Another small aliquot from one sample (8, PRAF2) from each digest (1 and 2) was acidified with trifluoroacetic acid (TFA), desalted with Pierce C18 spin tips (ThermoFisher Scientific, 84850), evaporated to dryness with a centrifugal evaporator (Eppendorf) and reconstituted with 100mM tetraethylammonium bromide (TEAB). These test samples were analysed by on-line nanoflow LC using the Thermo EASY-nLC 1000 LC system (ThermoFisher Scientific) coupled with Q-Exactive mass spectrometer (ThermoFisher Scientific). Both digests were pooled (1 and 2) for future analysis.

The peptide digests for each sample were acidified with TFA, desalted using Pierce peptide desalting spin columns (ThermoFisher Scientific, 89851) and dried down as described above. Each sample was reconstituted in 100µl 100mM TEAB ready for tandem-mass-tag (TMT) labelling.

### 2.14.2 TMT labelling

Desalted peptides were labelled with TMT (10plex) reagents (ThermoFisher Scientific, 90110) according to the manufacturer's instructions (TMT sample labels, Table A.7). Each 0.8 mg vial of TMT reagent was reconstituted in 41  $\mu$ l of acetonitrile and added to the sample for 1 h at R.T. The labelling reaction was quenched with 8  $\mu$ l of 5% hydroxylamine for 15 min at R.T. An aliquot (5  $\mu$ l) of each sample was pooled for label QC checking. The remaining labelled samples were stored at -80°C until analysis.

The QC sample was acidified with TFA, desalted using Pierce peptide desalting spin columns and dried down before reconstitution in 0.1% TFA, 3% methanol. The sample was run on the Q-Exactive mass spectrometer to check label incorporation. Analysis was performed using PEAKs platform as described below but using TMT10plex as a variable modification. TMT label incorporation was 99%.

Samples were mixed and desalted as above, evaporated to dryness and reconstituted in 1% TFA. The sample was cleaned up using a SCX stage tip before analysis to remove PEG and the eluate dried down before reconstitution in 0.1% TFA, 3% methanol.

### 2.14.3 LC MS/MS analysis

Mass spectrometry analysis was essentially as described in (Dong, X. et al., 2017). Peptides were analysed by on-line nanoflow LC using the Thermo EASY-nLC 1000 LC system (ThermoFisher Scientific) coupled with Q-Exactive mass spectrometer (ThermoFisher Scientific). Samples were loaded on a 50 cm Easy-Spray column with an internal diameter of 75  $\mu$ m, packed with 2  $\mu$ m C<sub>18</sub> particles, fused to a silica nano-electrospray emitter (ThermoFisher Scientific). The column was operated at a constant temperature of 35°C. Chromatography was performed with a buffer system consisting of 0.1 % formic acid (buffer A) and 80 % acetonitrile in 0.1 % formic acid (buffer B). The peptides were separated by a linear gradient of 3.8–50 % buffer B over 90 min at a flow rate of 300 nl/min. The Q-Exactive was operated in data-dependent mode with

survey scans acquired at a resolution of 70,000. Up to the top 15 most abundant isotope patterns with charge states +2 to +5 from the survey scan were selected with an isolation window of 1.2 Th and fragmented by higher energy collisional dissociation with normalized collision energies of 32. MS2 resolution was set at 35,000. The maximum ion injection times for the survey scan and the MS/MS scans were 50 and 250ms, respectively, and the ion target value was set to 3E6 for survey scans and 1E5 for the MS/MS scans. Repetitive sequencing of peptides was minimized through dynamic exclusion of the sequenced peptides for 45s.

#### **2.14.4 Analysis of MS data**

Spectral data were analysed using the PEAKS studio 10 software (Bioinformatics Solutions Inc., Waterloo, ON, Canada). Tandem MS data were searched against the predicted protein set of the Human reference genome sequence (Uniprot, 2018) and an additional contaminants database (cRAP protein sequences, GPM, <https://www.thegpm.org/crap/>). Search parameters were as follows; precursor mass tolerance set to 20 ppm and fragment mass tolerance set to 0.01 Da. Two missed tryptic cleavages were permitted. Carbamidomethylation (cysteine) and TMT10plex (Lys, Nterm) were set as fixed modifications and oxidation (methionine) set as a variable modification. The false discovery rate was set at 1%. Quantification was performed using PEAKS Q. Results were filtered to include only proteins with greater than 2 unique peptides and a fold change of greater than two-fold (compared to cells group). Significant differences were tested by the PEAKSQ method (similar to Significance B method, (Cox and Mann, 2008)) with a 1% FDR filter (Benjamini–Hochberg adjusted p value). Data was auto normalized.

## Chapter 3 The interaction of PRAF2 with HPV

### 3.1 Introduction

#### 3.1.1 The E5 protein

The HPV E5 protein is the least well understood of the three oncoproteins of HPV. One of the challenges for the study of E5 is the lack of reagents. Whilst HPV E5 antibodies have previously been developed, they have mainly been directed to HPV-16. Antibodies have been generated to overexpressed E5, but are not available commercially (Sahab et al., 2012; Suprynowicz et al., 2010; Disbrow et al., 2003; Chang, J.L. et al., 2001; Chen, S.L. and Mounts, 1989). As a result, most studies on the E5 protein have been carried out with either epitope tagged overexpressed protein, or with overexpressed protein and mRNA detection as a read out.

Studies on the localisation of HPV E5 have observed this in the membranous compartments of the cell. HPV-16E5 has been consistently observed in the ER (Conrad et al., 1993; Disbrow et al., 2005; Disbrow et al., 2003; Lewis et al., 2008), reports of its localisation with the Golgi are conflicting, with some reporting co-localisation with the Golgi stain BODIPY TR ceramide (Ashrafi et al., 2006b) whilst others failed to see co-localisation with the cis-Golgi marker GM130 (Suprynowicz et al., 2010) or only minor co-localisation with the trans-Golgi marker TGN-38 (Disbrow et al., 2003). Others have reported localisation to the early endosomes and lysosomes (Lewis et al., 2008).

E5 is a non-enzymatic protein, and as such exerts its effects through binding with host proteins and modulating their functions. One of the best-defined roles for E5 is its ability to modulate trafficking within the host cell. HPV-16E5 has been shown by immunoprecipitation to bind with components of the secretory pathway such as Karyopherin  $\beta$ 3 (Krawczyk et al., 2008), as well as controlling the trafficking of MHC class I (Ashrafi et al., 2006b; Ashrafi et al., 2005) and

binding Bap31 a component of the trafficking machinery for MHC class I (Regan and Laimins, 2008). HPV16E5 has also been shown to be able to perturb the maturation of endosomes (Suprynowicz et al., 2010) through interference with endosome fusion, as well as acidification, through the tracking of EGF-pH sensitive dye conjugates and pH sensitive dyes. A possible mechanism for this could be the viroporin activity exhibited by HPV-18 and 16E5 (Wetherill et al., 2018; Wetherill et al., 2012).

Compared to the wealth of knowledge about the HPV oncoproteins E6 and E7, relatively little is known about the cellular interactome of the E5 oncoprotein. It was therefore of great interest when a large-scale proteomics screen was carried out on tumour virus oncoproteins that included several HPV E5 proteins. This proteomics screen identified several new putative HPV-18E5 interacting partners (Rozenblatt-Rosen et al., 2012). One of these was PRAF2, which was of interest as it was identified as an interactor for Bcl-X<sub>L</sub> and Bcl-2 (Vento et al., 2010), which had also been identified as interactor for HPV16E5 (Auvinen et al., 2004).

### **3.1.2 The PRAF2 protein**

PRAF2 is a member of the Prenylated Rab Acceptor Family of proteins, and was identified thirteen years ago (Fo et al., 2006). The family has 3 members, PRAF1, PRAF2 and PRAF3, of which PRAF2 was the last identified. The PRAF2 gene is located on the X chromosome (bases 49071161 and 49074002) at Xp11.23. The gene is comprised of 3 exons and 2 introns (Fo et al., 2006). However, nothing is known about its promoters or regulators. There are two forms of the PRAF2 protein the predominant form of 19257.90 Da (ENST00000376390.4) and a splice variant of 17188.23 Da (ENST00000376386.3) which has been observed expressed in U-87 malignant glioma cells (Borsics et al., 2010).

PRAF2 is modelled as a four transmembrane domain protein based on predictions by the TMHMM program (Schweneker et al., 2005) and with the HMMTOP program (Tusnády and Simon, 2001; Tusnády and Simon, 1998), with its N and C-termini directed towards the

cytoplasm (Fo et al., 2006). Phosphorylation prediction software NetPhos 2.0 predicts phosphorylation sites at Y43 and S97 (Fo et al., 2006), and NetPhosK predicts phosphorylation of the S97 site by Protein Kinase A (PKA) and Protein Kinase C (PKC (Blom et al., 1999)). Further putative sites S139 (PKA), T161 (p38 MAPK) and S70 (Cdc2) are also predicted by this software (Fo et al., 2006). Alignment of the PRAF members demonstrates two areas of high conservation NLLYYQTNY and HASLRLR (Fo et al., 2006), of which Y43 is located in.

PRAF2 is known to be expressed in 44 tissues from IHC data (Uhlén et al., 2015), in organs such as cerebellum, endometrium, testis, breast and cervix. It has also been observed expressed in rat brain (Doly et al., 2016) and mouse CNS (Cifuentes-Diaz et al., 2016) at the protein level, and was observed in 10 out of 11 tissues by western blot, such as brain, heart, lung and ovary (Fo et al., 2006). It has since been detected at the mRNA level in 41 different tumour types (Geerts et al., 2007) and in 91 tissues by RNA-seq (Bastian FB, 2008). And has been detected in tumours such as malignant gliomas (Borsics et al., 2010), hepatocellular carcinoma (Wang, C.H. et al., 2018) and oesophageal squamous cell carcinoma (Qian et al., 2019). PRAF2 has also been detected by western blotting diverse cell lines such as HEK293 (Fo et al., 2006), SK-N-SH, SH-SY5Y, LAN1 (Yco et al., 2013), LN229, U373 (Doly et al., 2016), U-87, U-251 (Borsics et al., 2010) and the TE-1 cell line (Qian et al., 2019). There are currently no data regarding the expression of PRAF2 in differentiating cells.

### **3.1.3 The localisation of PRAF2**

There are a range of subcellular localisations in which PRAF2 has been observed. In the neuroblastoma cell lines SK-N-SH and SH-SY5Y endogenous PRAF2 protein was observed in cytoplasmic puncta by immunofluorescence (Geerts et al., 2007). Endogenous PRAF2 protein was also detected in punctate cytoplasmic structures and partially colocalised with the ER in U-251 malignant glioma cells (Borsics et al., 2010). Overexpressed PRAF2 has been observed to colocalise with calnexin (ER) and M6PR (Trans-golgi and endosomes) in HeLa cells (Schweneker

et al., 2005) and to occupy the perinuclear region in the U2OS osteosarcoma cell line (Vento et al., 2010) and the ER with partial localisation to the cis-Golgi in HEK293 cells (Doly et al., 2016). Subcellular fractionation experiments have led to the observation of PRAF2 in the membranous fraction of Cf2Th cells (Schweneker et al., 2005) and HEK293 cells (Fo et al., 2006). However, PRAF2 has also been observed in the nuclear envelope fraction of U-87 cells (Borsics et al., 2010). PRAF2 has also been detected in endosomes of the neuroblastoma cell line LAN-1 (Geerts et al., 2007), synaptic vesicles (Koomoa et al., 2008) and most recently regulating exosomes (He et al., 2019).

Studies so far on PRAF2 can be broadly divided into apoptosis, migration and trafficking. PRAF2 has been implicated in cerulenin mediated cell death in neuroblastoma (Geerts et al., 2007) and as able to induce cell death through its overexpression (Vento et al., 2010). PRAF2 has also been identified as a promoting factor for cancer cell migration (He et al., 2019; Wang, C.H. et al., 2018; Yco et al., 2013; Borsics et al., 2010). Finally, PRAF2 has been identified as a protein involved in cellular trafficking. It has been shown by radio ligand binding assay to control the exit from the ER of the GABA<sub>B</sub> receptor (Doly et al., 2016), to be involved in the trafficking of CCR5 to the cell surface by flow cytometry (Schweneker et al., 2005), in retrograde Golgi-to-ER traffic by RNAi screening (Galea et al., 2015), to be associated with endosomes by immunofluorescence and fractionation (Borsics et al., 2010) and involved in exosome release (He et al., 2019).

The aim of this chapter is to explore the fundamental biology of PRAF2. Its interaction with the papillomavirus E5 protein is explored within this chapter as well as its relationship with other HPV18 proteins. Its subcellular localisation is investigated, with the aim of better understanding PRAF2.

## 3.2 Results

### 3.2.1 Confirming the interaction of PRAF2 and HPV18E5

To confirm the findings of the initial mass spectroscopy screen, a co-immunoprecipitation (Co-IP) experiment was performed. Owing to the lack of an antibody to HPV18E5 and poor reagents for PRAF2 epitope tagged constructs were used. Triple HA-tagged PRAF2, control GFP vector (GFP-c1) and GFP-18E5 were transfected into HEK293TT cells. Cells were lysed 24 hours post transfection and cell lysates were produced. These lysates were used to perform a GFP trap Co-IP and 10% of the resulting samples were resolved by SDS-PAGE and compared with the input. The resulting input westerns were probed with an antibody specific for HA, confirming the overexpression of PRAF2-3HA, with a clear band of approximately 24 kDa observed (lanes 1,2 and 4, Figure 3.1 A), and a higher molecular weight band of approximately 48 kDa corresponding to the dimeric form was also detected. Probing with an antibody specific for GFP detected a band of approximately 24 kDa corresponding to overexpressed monomeric GFP (lane 2), and also a band of approximately 37 kDa (lanes 3 and 4), as expected for overexpressed GFP-c1 tagged HPV18E5, there was also a corresponding multimeric form observed at greater than 58 kDa. The GFP co-immunoprecipitation successfully pulled down PRAF2-3HA (lane 4, IP:GFP, HA blot). It can be ruled out that the interaction between PRAF2 and GFP-18E5 is due to the GFP tag, as free GFP did not Co-IP PRAF2-3HA (lane 2, IP:GFP), nor did the PRAF2-3HA bind to the GFP trap beads in a non-specific manner, as no PRAF2-3HA could be detected when PRAF2-3HA was expressed alone (lane 3, IP:GFP). This corroborates the previous mass spectroscopy screen, confirming that PRAF2 interacts with HPV18E5 possibly directly or as part of a protein complex.

To then confirm that this interaction was occurring in cells, and not as an artefact of lysing the cells, PRAF2-3HA and GFP-18E5 and control GFP were overexpressed in HeLa cells. Cells were fixed, permeabilised and probed with an antibody specific for the HA-tag, and

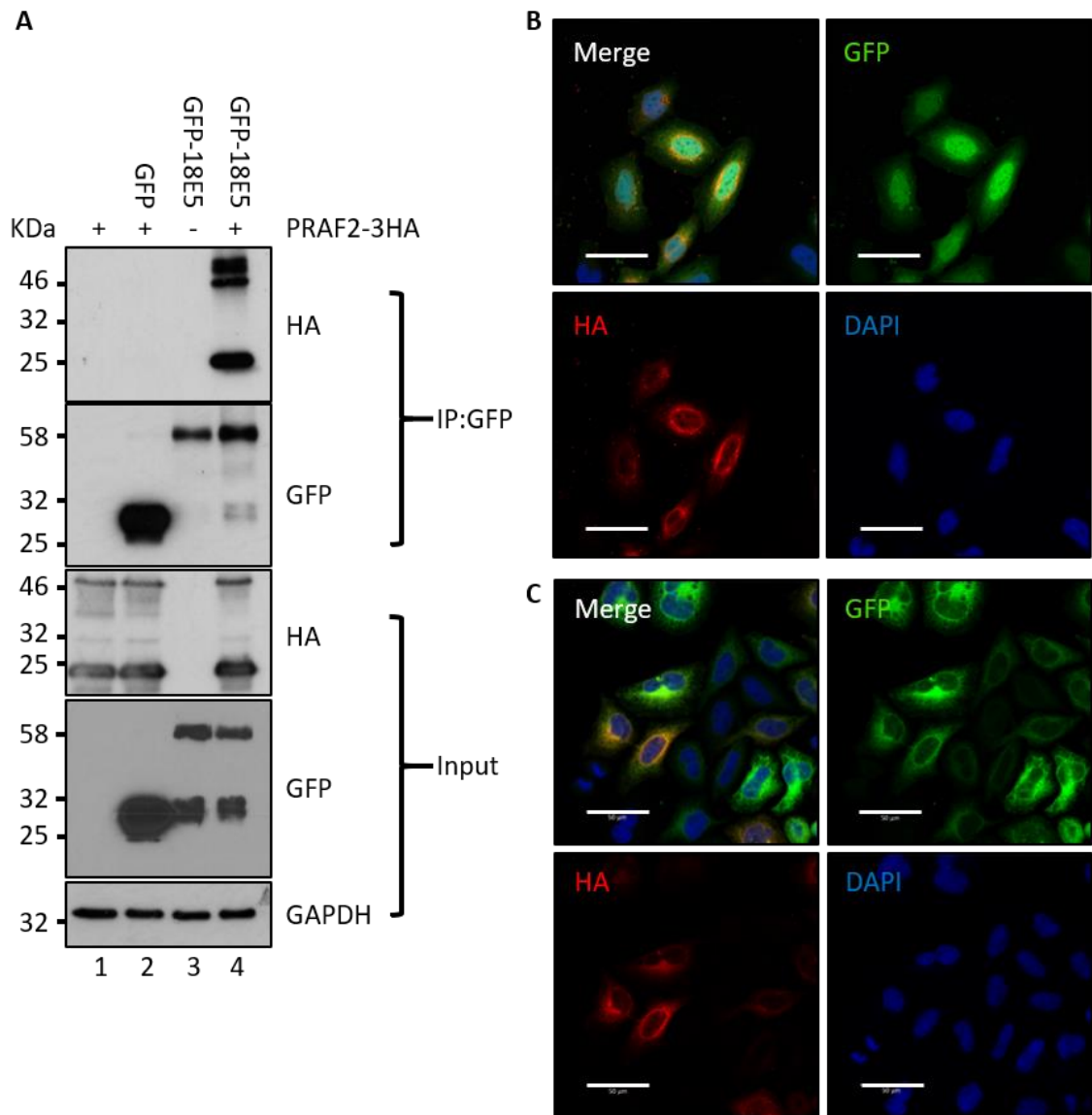


**Figure 3.1** Co-immunoprecipitation confirmed the interaction between PRAF2 and HPV18E5

**A.** PRAF2-3HA and GFP-18E5 as well as negative control GFP were overexpressed in HEK293TT cells. Co-immunoprecipitations were performed using GFP-trap magnetic agarose beads using equal amounts of protein. Representative blot is shown. N=3 **B.** PRAF2-3HA and GFP were overexpressed in HeLa cells. Co-immunofluorescence was performed using HA-antibody and secondary anti-mouse Alexa-594. Pearson's R value above threshold = 0.05. N=3 **C.** PRAF2-3HA and GFP-18E5 were overexpressed in HeLa cells. Co-immunofluorescence was performed using HA-antibody and secondary anti-mouse Alexa-594. Images representative. Scale bar 50 $\mu$ m. Pearson's R value above threshold = 0.9. N=3.

secondary anti-mouse Alexa-594 was used for co-immunofluorescence (Figure 3.1 B and C). When PRAF2-3HA was overexpressed in the presence of free GFP in HeLa cells, the GFP was localised throughout the cell, predominantly in the nucleus and cytoplasm, and PRAF2-3HA was detected in the ER (figure 3.1 B). No evidence of co-localisation could be observed, this was confirmed by colocalisation analysis using the Coloc2 software. Pearson's correlation coefficient was calculated, where a value of -1 is perfect anti correlation, 0 no correlation and 1 for perfect correlation (Bolte and Cordelières, 2006), the value for PRAF2 and GFP was 0.05, suggesting no correlation. When PRAF2-3HA was overexpressed with GFP-18E5, the two proteins co-localise (Pearsons R value=0.9). GFP-18E5 localises to the ER, as expected. This suggests that the interaction observed in the Co-IP is occurring in the cell as the proteins are in close proximity, due to occupying the same cellular compartments.

### **3.2.2 The amino acids 135-160 are essential for PRAF2 binding to HPV18E5**

So far, the interaction between PRAF2 and HPV18E5 has been confirmed by TAP-MS (Rozenblatt-Rosen et al., 2012) and by Co-IP (figure 3.1 A). The site responsible on PRAF2 was then identified by PRAF2 truncation mutants (Figure A.2). PRAF2 has been proposed to have 4 transmembrane domains (Fo et al., 2006), with its N and C-termini located in the cell cytoplasm (Figure 3.2 A). The truncation mutants were sequential deletion mutants from the N and C-termini (Figure 3.2 C and D). All N-terminal truncation mutants were designed with a C-terminal triple HA-tag and all C-terminal truncation mutants were designed with an N-terminal triple FLAG-tag (Figure 3.2 B). Each respective experiment was performed with a full-length sequence with the appropriate epitope tag to match the truncation mutants being assayed. Mutant (Figure 3.2 C) 19-178 is lacking the N-terminal region corresponding to the region of PRAF1 identified as being critical for its interaction with Rab GTPases (Martincic et al., 1997) and mutant 34-178 is truncated further, but leaves the N-terminal region of conservation intact (Fo et al., 2006). The 94-178 mutant entirely removes this region and also the first two predicted transmembrane domains (Figure 3.2 C), which includes the predicted amphiphysin SH3 domain (Fo et al., 2006).

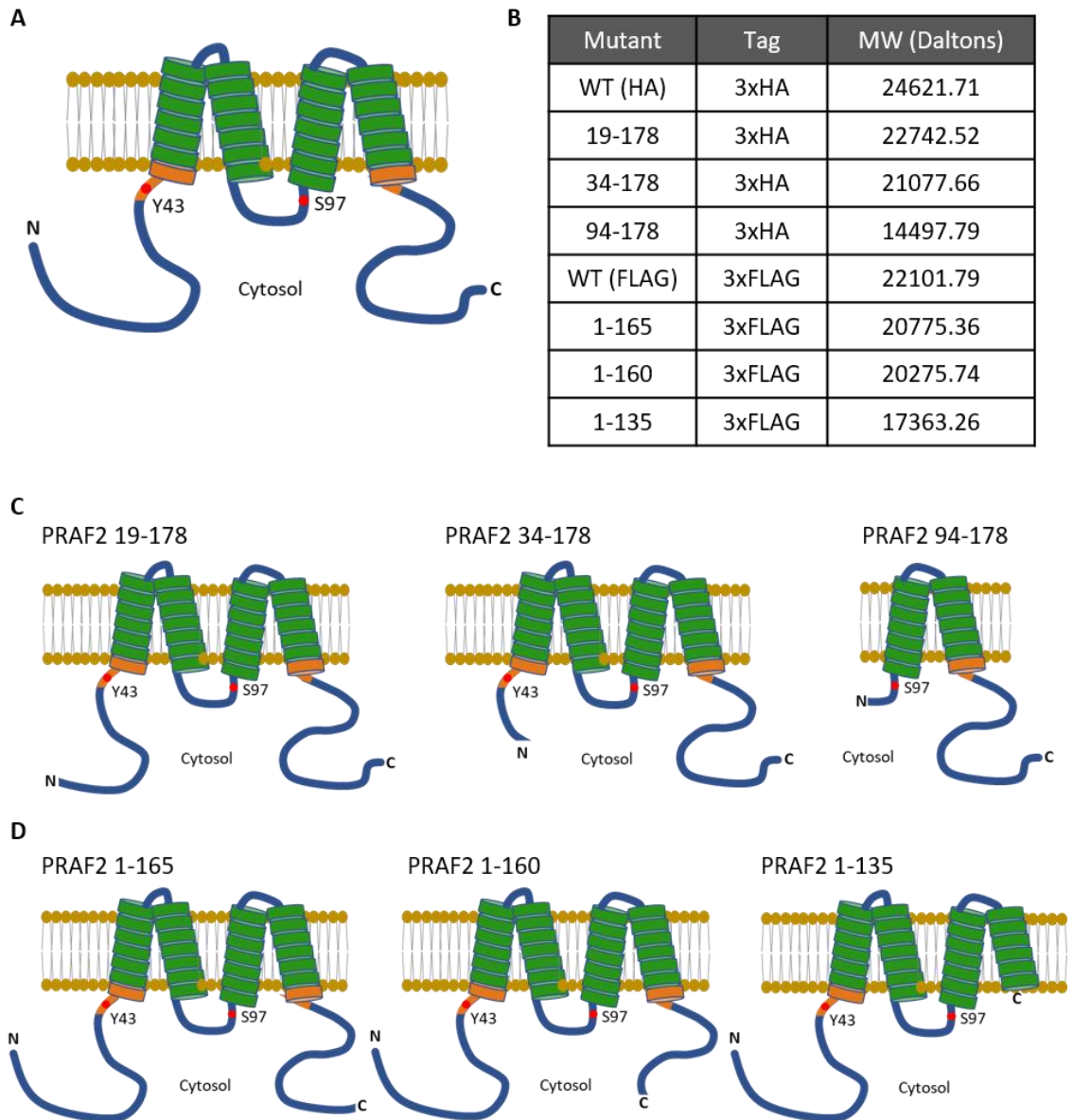


**Figure 3.2 Schematic of the PRAF2 truncation mutants**

A. A model of PRAF2 based upon membrane topology predictions and sequence analysis, transmembrane domains are shown in green, conserved domains in orange and free regions in blue. Putative phosphorylation sites shown with red. B. Table of the truncation mutants of PRAF2, listing mutation made, epitope tag and predicted size in daltons. C. N-terminal PRAF2-3HA truncation mutants, 19-178, 34-178 and 94-178. D. C-terminal 3xFLAG-PRAF2 mutants 1-165, 1-160 and 1-135. The sequences of the truncation mutants aligned against the WT protein can be found in the appendices (Figure A.2)

the C-terminal truncation mutants (Figure 3.2 D) were based on previous mutational studies performed on PRAF3 (Abdul-Ghani et al., 2001). Truncation 1-165 removes a run of acidic residues found at the C-terminus and the 1-160 truncation removes a tract of basic residues. The final truncation mutant 1-135 removes the C-terminal conserved region, which has been shown to be of importance in PRAF1 for its interaction with Rab GTPases and VAMP2 (Martincic et al., 1997). It is also possible that the truncations could alter the localisation of the PRAF2 protein, as PRAF3 localisation was altered by mutations to its C-terminus (Abdul-Ghani et al., 2001).

GFP-18E5, WT PRAF2 and PRAF2 truncation mutants were co-transfected into HEK293TT cells, along with control GFP and GFP18E5 and WT PRAF2 alone and GFP-trap IPs performed. The resulting Co-IPs (figure 3.3) were then probed for HA/FLAG and GFP, and inputs for HA/FLAG, GFP and GAPDH respectively. With the N-terminal truncation experiment (figure 3.3 A), expression of both wildtype and truncated PRAF2-3HA proteins could be clearly observed in the input, and GFP-18E5 was expressed well. Clear binding could be observed of the WT-PRAF2-3HA (lane 4) to GFP-18E5, and it should be noted that no binding was observed to GFP (lane 2). Binding was also observed for all the N-terminal truncation mutants of PRAF2 to GFP-18E5 (lanes 5,6 and 7), and there appeared to be no loss of binding for PRAF2 by GFP-18E5. Furthermore, all forms of PRAF2-3HA expressed showed the ability to dimerise, with both monomer and dimer successfully immunoprecipitated. The lower levels of PRAF2-3HA 94-178 observed in the IP relative to the other PRAF2 proteins (lane 7) could be attributed to the fact that this mutant appeared to yield lower levels of protein when overexpressed. This was consistently observed in all repeats.

With the C-terminal mutants, all were expressed in the input (figure 3.3 B), however, they expressed at lower levels than observed with the WT 3xFLAG-PRAF2 (lane 4). This in turn showed lower levels of expression relative to 3xFLAG-PRAF2 (lane 1) and GFP + 3xFLAG-PRAF2

(lane 2). It appeared that the 3xFLAG-PRAF2 constructs expressed at a lower level when co-transfected with GFP-18E5. The IP clearly pulled down the GFP and GFP-18E5, and interaction

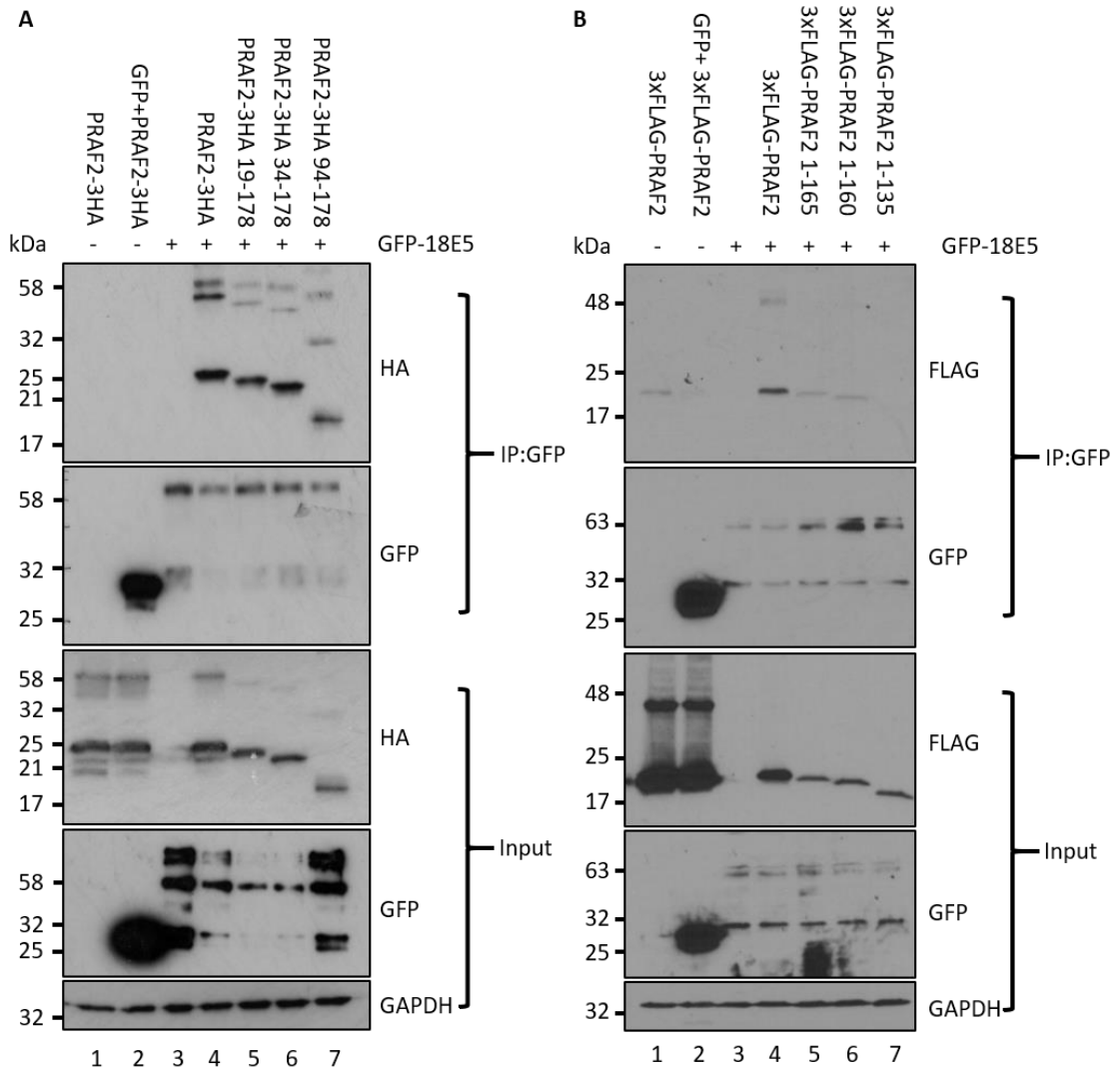


**Figure 3.3 PRAF2 requires amino acids 135-160 to bind to HPV18E5**

A. PRAF2-3HA and its corresponding N terminal truncation mutants (Figure 3.2 C) were co-transfected into HEK293TT cells with GFP-18E5 and negative control GFP. Co-immunoprecipitations were performed using GFP-trap magnetic agarose beads using equal amounts of protein. Representative blot is shown. N=4 B. 3xFLAG-PRAF2 and its corresponding C-terminal truncation mutants (Figure 3.2 D) were co-transfected into HEK293TT cells with GFP-18E5 and negative control GFP. Co-immunoprecipitations were performed using GFP-trap magnetic agarose beads using equal amounts of protein. Representative blot is shown. N=1.

of WT 3xFLAG-PRAF2 could be observed with GFP-18E5 (lane 4). Interestingly, the dimeric form of 3xFLAG-PRAF2 was immunoprecipitated. Truncation mutants 3xFLAG-PRAF2 1-165 and 3xFLAG-PRAF2 1-160 (lanes 5 and 6) were also bound by GFP-18E5, however, mutant 3xFLAG-PRAF2 1-135 was not successfully immunoprecipitated by GFP-18E5. This suggested that amino acids in the region of 135-160 of PRAF2 were important for its binding to HPV18E5. It should be noted that some 3xFLAG-PRAF2 appeared to have come down in a non-specific manner (lane 1) when expressed alone. However, this is not observed with GFP (lane 2) and the level of FLAG expression observed in the 3xFLAG-PRAF2 + GFP-18E5 sample (lane 4) was 0.23-fold lower than that of the 3xFLAG-PRAF2 (lane 1) sample. This coupled with the greater level of FLAG observed for the IP of GFP-18E5 + 3xFLAG-PRAF2 (lane 4), suggested that the interaction had occurred *in vivo*.

### 3.2.3 PRAF2 localises to primarily to the ER

In order to further understand the effects of truncation mutations on PRAF2 and its interaction with HPV18E5 it was first important to understand the normal cellular localisation of PRAF2. Previous studies had observed ER-Golgi localisation of PRAF2 when PRAF2 was overexpressed in HEK293 (Doly et al., 2016), and partial ER localisation in U-251 malignant

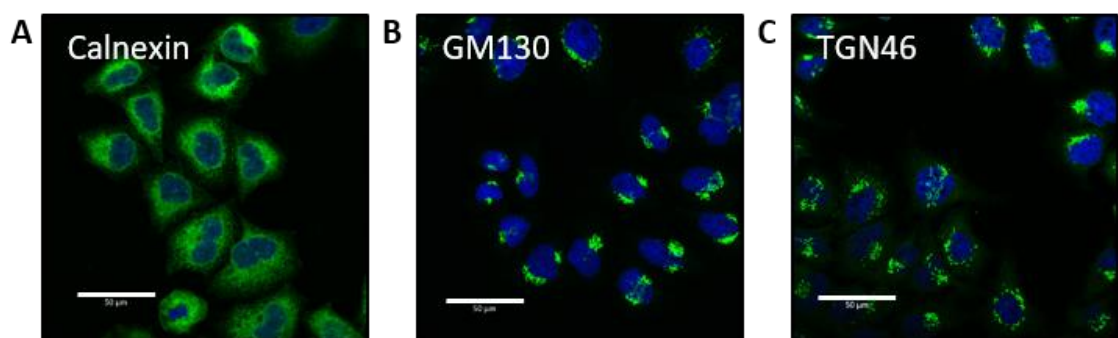


**Figure 3.4** Subcellular organelle marker localisation in untreated HeLa cells

A. Subcellular marker for the ER calnexin in green, nuclear counterstain DAPI blue. B. Subcellular marker for the cis-Golgi network GM130 in green, nuclear counterstain DAPI blue. C. Subcellular marker for the trans-Golgi network TGN46 in green, nuclear counterstain DAPI blue.

glioma cells (Borsics et al., 2010). However, other studies had observed endosomal localisation (Geerts et al., 2007) in SK-N-SH, SH-SY5Y and LAN-1 neuroblastoma cells. The variability could however be down to differences in cell lines. Owing to a lack of availability of a functionally validated PRAF2 antibody for immunocytochemistry (immunofluorescence), epitope tagging and overexpression of PRAF2 was required to study its subcellular localisation and a relevant keratinocyte cell line was chosen.

HeLa cells were transfected with PRAF2-3HA, and 24 hours post transfection were fixed, permeabilised and stained for the HA epitope, and either calnexin, GM130 or TGN46 (figure 3.4) to assess the subcellular localisation of PRAF2. In cells which overexpressed PRAF2, co-localisation could be observed between PRAF2-3HA (red) and the ER marker calnexin (green) (Figure 3.5 A), with a Pearson's R value of 0.7 indicating a strong correlation between PRAF2-3HA and calnexin. However, PRAF2-3HA was not wholly co-localised with calnexin and HA staining could be observed elsewhere in the cell. In cells co-stained with the cis-Golgi marker GM130 (Figure 3.5 B) PRAF2-3HA (red) was observed to partially co-localise with GM130 (green), however this was only weakly correlated (Pearson's R value 0.35). Finally, cells were also stained with the trans-Golgi network marker TGN46 (green). Cells (Figure 3.5 C) which expressed PRAF2-3HA (red) demonstrated a redistribution of TGN46, relative to when PRAF2-3HA was not expressed (Figure 3.4 C), whether this represents a large-scale change in the distribution of the trans-Golgi network, or was just limited to TGN46 remains to be seen. However, in cells stained for HA and TGN46 a high degree of co-localisation could be observed between PRAF2-3HA and TGN46, with a strong correlation between the two (Pearson's R value = 0.79). Its morphology was highly reminiscent of the staining observed for calnexin, so perhaps the overexpression of PRAF2-3HA had led to retention in the ER.

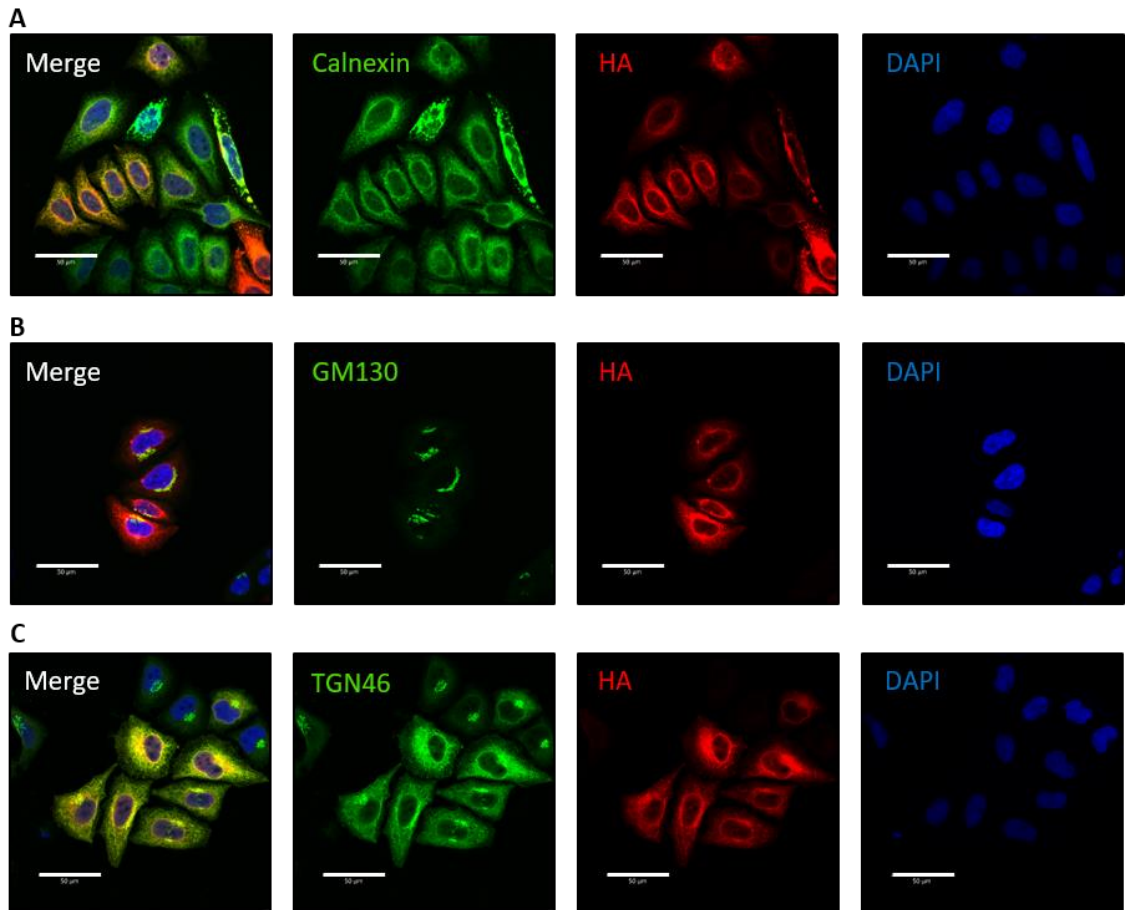


**Figure 3.5** Subcellular localisation of overexpressed PRAF2-3HA in HeLa cells

HeLa cells transfected with PRAF2-3HA and fixed and permeabilised 24 hours post transfection. Cells were stained for HA (Alexa 594, red) and then co-stained for subcellular organelle markers (Alexa 488, green). All cells mounted with a DAPI (blue) nuclear counterstain. A. Co-staining with the ER marker calnexin (green) Pearson's R value above threshold = 0.7. B. Co-staining with the cis-Golgi network marker GM130 (green), Pearson's R value above threshold = 0.35. C. Co-staining with the trans-Golgi network marker TGN46 (green), Pearson's R value above threshold = 0.79. Images are representative. Scale bar 50µm. N=3

### 3.2.4 Mutation of PRAF2 and its effect on subcellular localisation

The overexpression of PRAF2 showed that it primarily localised to the ER, with some localisation to the cis-Golgi in HeLa cells. With this in mind, the PRAF2 mutants could be examined for their subcellular localisation, to ascertain whether the mutations altered their localisation and to investigate if a change in their localisation could be responsible for the loss of interaction with HPV18E5. The PRAF2 constructs (Figure 3.2 B) were overexpressed in HeLa cells and cells were fixed and permeabilised 24 hours post transfection. Cells were then stained for either the HA or FLAG-tag and either calnexin or GM130.

In cells which overexpressed 3xFLAG-PRAF2 (red, Figure 3.6 A), PRAF2 could be observed to colocalise primarily with the ER marker calnexin (green), with a strong correlation between the two (Pearson's R value = 0.81). However, as before (Figure 3.5 A), not all the staining for 3xFLAG-PRAF2 localised with calnexin, which suggested that 3xFLAG-PRAF2 was not solely localised to the ER. 3xFLAG-PRAF2 (red, Figure 3.7 A) could also be observed to localise with GM130 (green), however colocalisation analysis only indicated a weak correlation (Pearson's R value = 0.24). Observing the morphology of 3xFLAG-PRAF2 expression in general (Figure 3.6 A and 3.7 A) it appeared that the FLAG staining was also quite strongly perinuclear. The localisation of the C-terminal PRAF2 mutant 3xFLAG-PRAF2 1-165 with calnexin (Figure 3.6 B) was similar to 3xFLAG-PRAF2 (Pearson's R value = 0.7), however the GM130 stain did not appear to co-localise (Figure 3.7 B), which agreed with the co-localisation analysis (Pearson's R value = -0.28). The FLAG staining of 3xFLAG-PRAF2 1-165 was however like that of the 3xFLAG-PRAF2. The mutant 3xFLAG-PRAF2 1-160 colocalised strongly (Pearson's R value = 0.76) with calnexin (Figure 3.6 C) and displayed weak (Pearson's R value = 0.17) co-localisation with GM130 (Figure 3.7 C), however the FLAG staining was more diffuse (Figure 3.6 C, Figure 3.7 C) than that of WT or 1-165. Mutant 1-135 had a more diffuse FLAG stain (Figure 3.6 D, Figure 3.7 D) than WT (Figure 3.6 A, Figure 3.7 A) and displayed a strong (Pearson's R value = 0.77) co-localisation with calnexin (Figure 3.6 D) and no colocalisation (Pearson's R value 0.01) with GM130 (Figure 3.7 D). Overall,

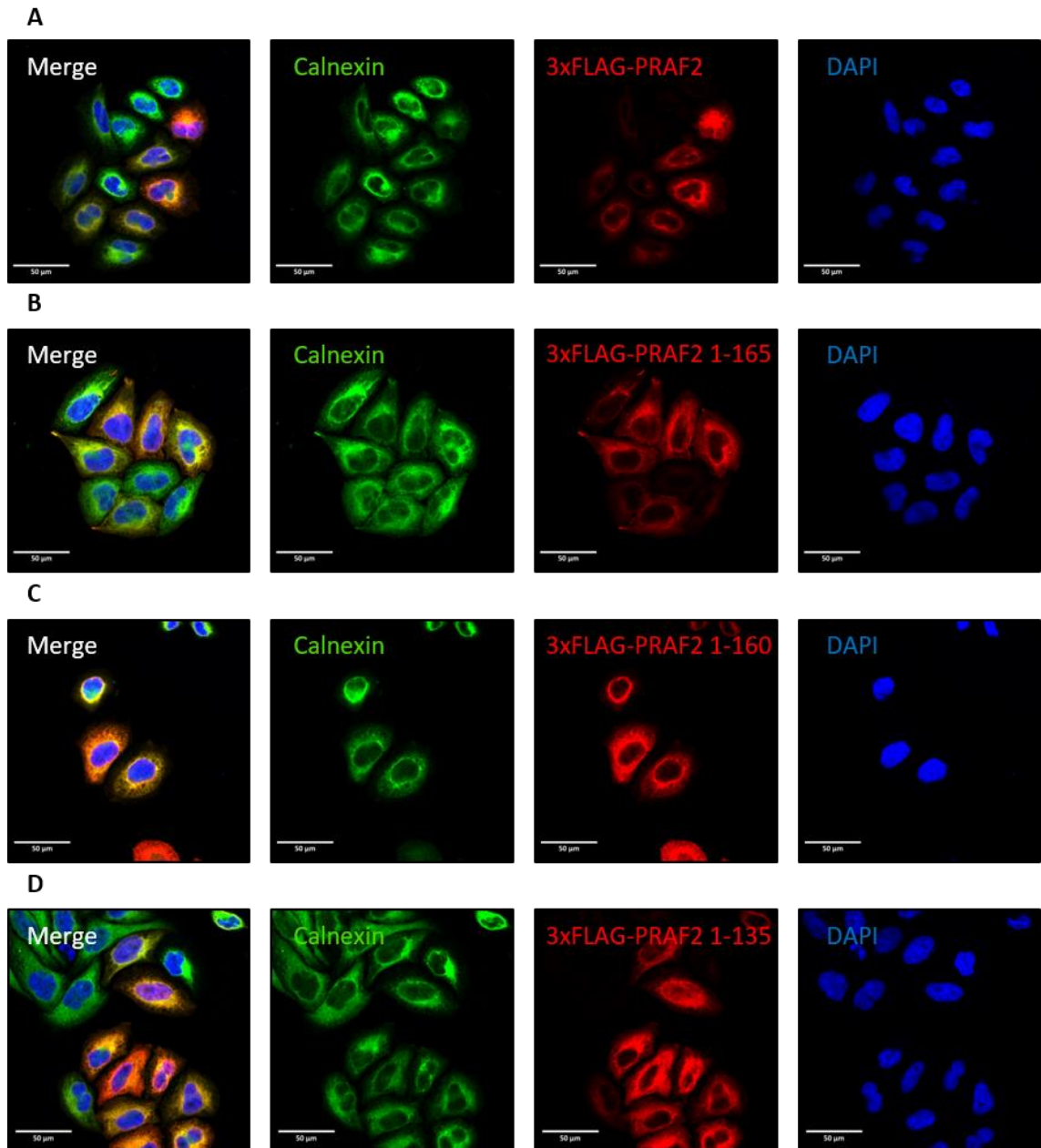


**Figure 3.6** Co-localisation of C-terminal PRAF2 mutants with calnexin

HeLa cells transfected with C-terminal PRAF2 mutants and fixed and permeabilised 24 hours post transfection. Cells were stained for FLAG (Alexa 594, red) and then co-stained for ER marker calnexin (Alexa 488, green). All cells mounted with a DAPI (blue) nuclear counterstain. A. WT 3xFLAG-PRAF2, Pearson's R value = 0.81. B. 3xFLAG-PRAF2 1-165, Pearson's R value = 0.7. C. 3xFLAG-PRAF2 1-160, Pearson's R value = 0.76. D. 3xFLAG-PRAF2 1-135, Pearson's R value = 0.78. Images are representative. Scale bar 50 μm. N=1.

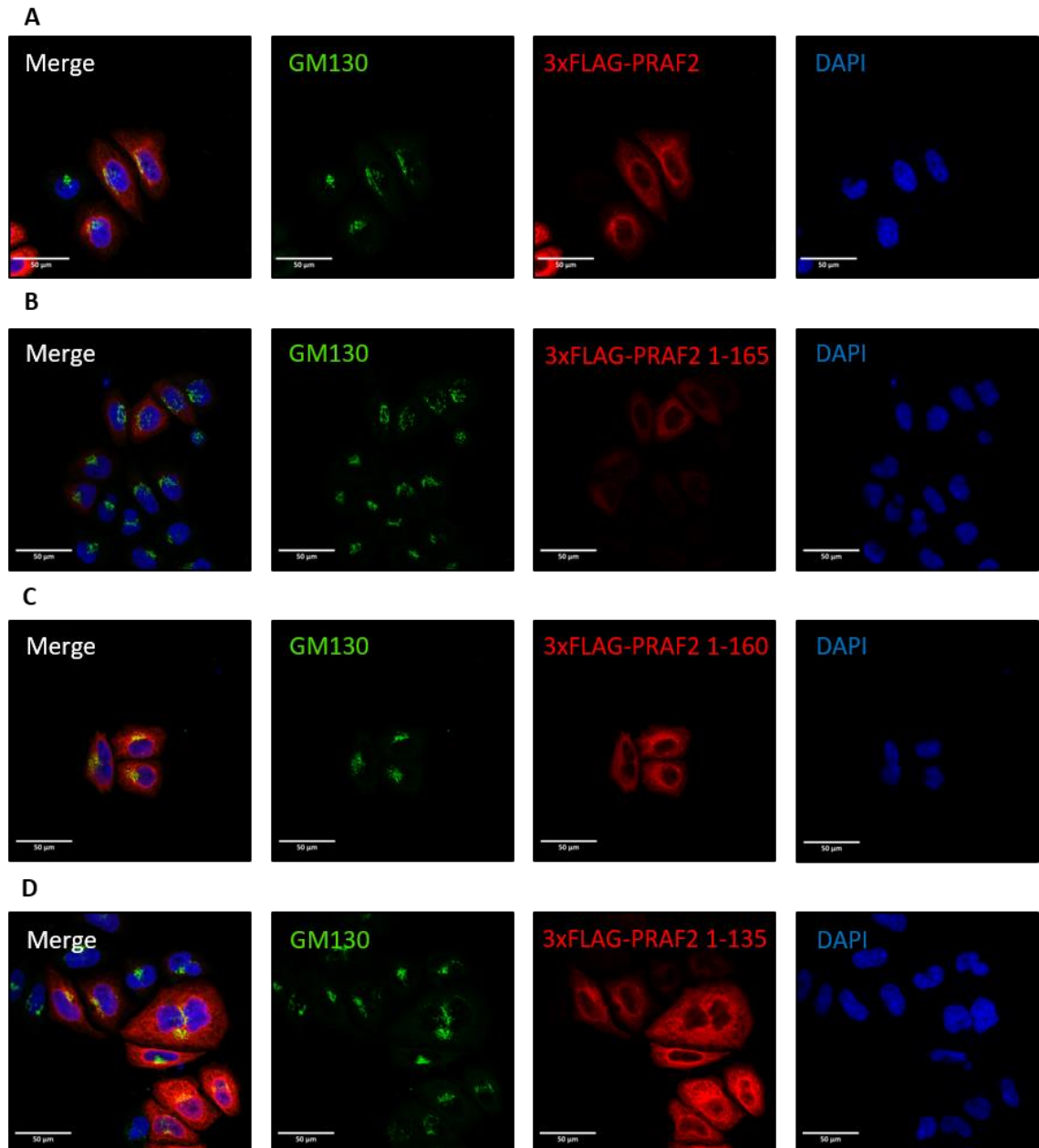


**Figure 3.7** Co-localisation of C-terminal PRAF2 mutants with GM130

*HeLa cells transfected with C-terminal PRAF2 mutants and fixed and permeabilised 24 hours post transfection. Cells were stained for FLAG (Alexa 594, red) and then co-stained for cis-Golgi marker GM130 (Alexa 488, green). All cells mounted with a DAPI (blue) nuclear counterstain. A. WT 3xFLAG-PRAF2, Pearson's R value = 0.235. B. 3xFLAG-PRAF2 1-165, Pearson's R value = -0.28. C. 3xFLAG-PRAF2 1-160, Pearson's R value = 0.17. D. 3xFLAG-PRAF2 1-135, Pearson's R value = 0.01. Images are representative. Scale bar 50 μm. N=1.*

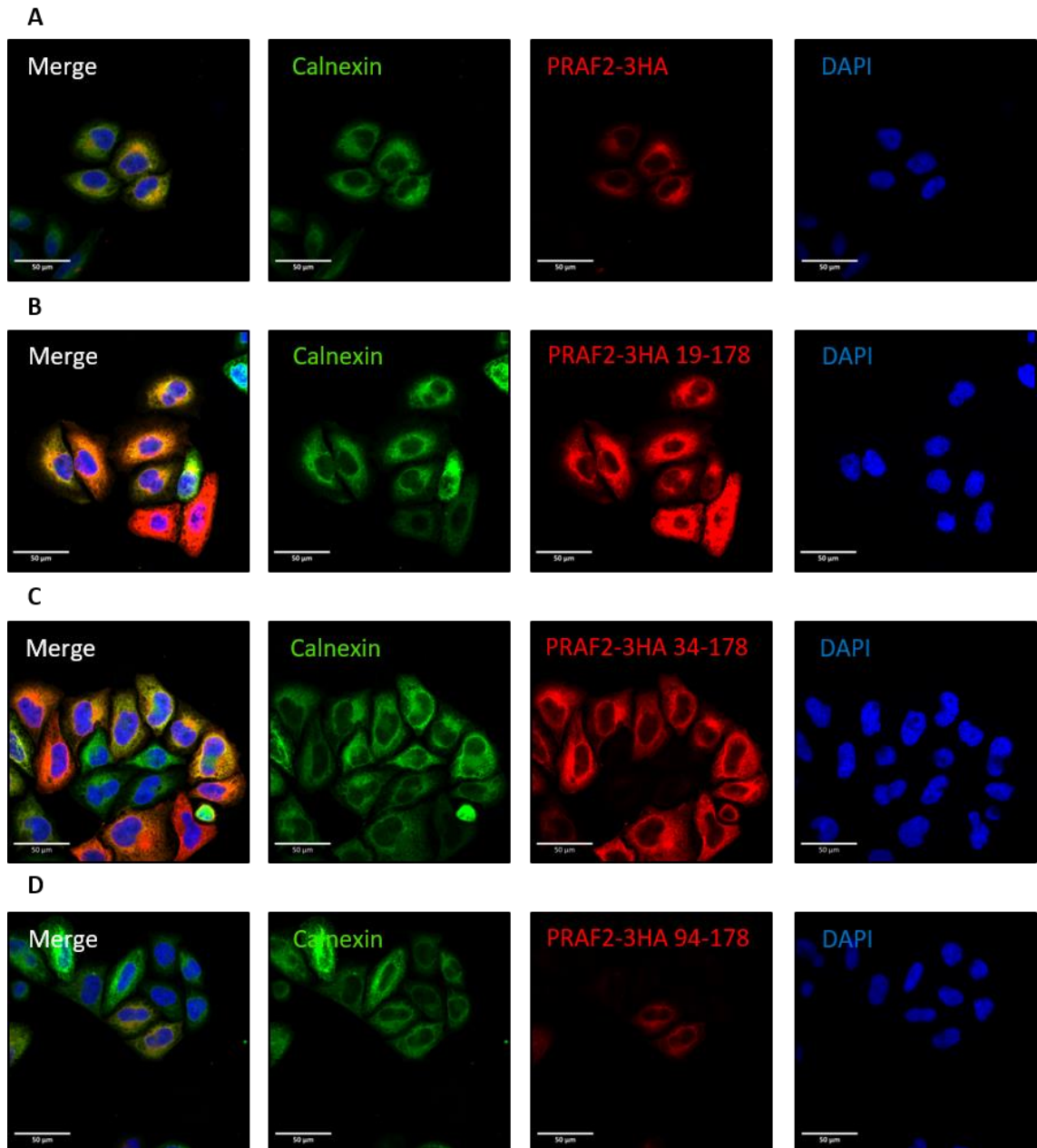


**Figure 3.8** Co-localisation of N-terminal PRAF2 mutants with calnexin

HeLa cells transfected with N-terminal PRAF2 mutants and fixed and permeabilised 24 hours post transfection. Cells were stained for HA (Alexa 594, red) and then co-stained for ER marker calnexin (Alexa 488, green). All cells mounted with a DAPI (blue) nuclear counterstain. A. WT PRAF2-3HA, Pearson's  $R$  value =0.74. B. PRAF2-3HA 19-178, Pearson's  $R$  value =0.78 C. PRAF2-3HA 34-178, Pearson's  $R$  value =0.73. D. PRAF2-3HA 94-178, Pearson's  $R$  value =0.62. Images are representative. Scale bar 50µm.  $N=1$ .

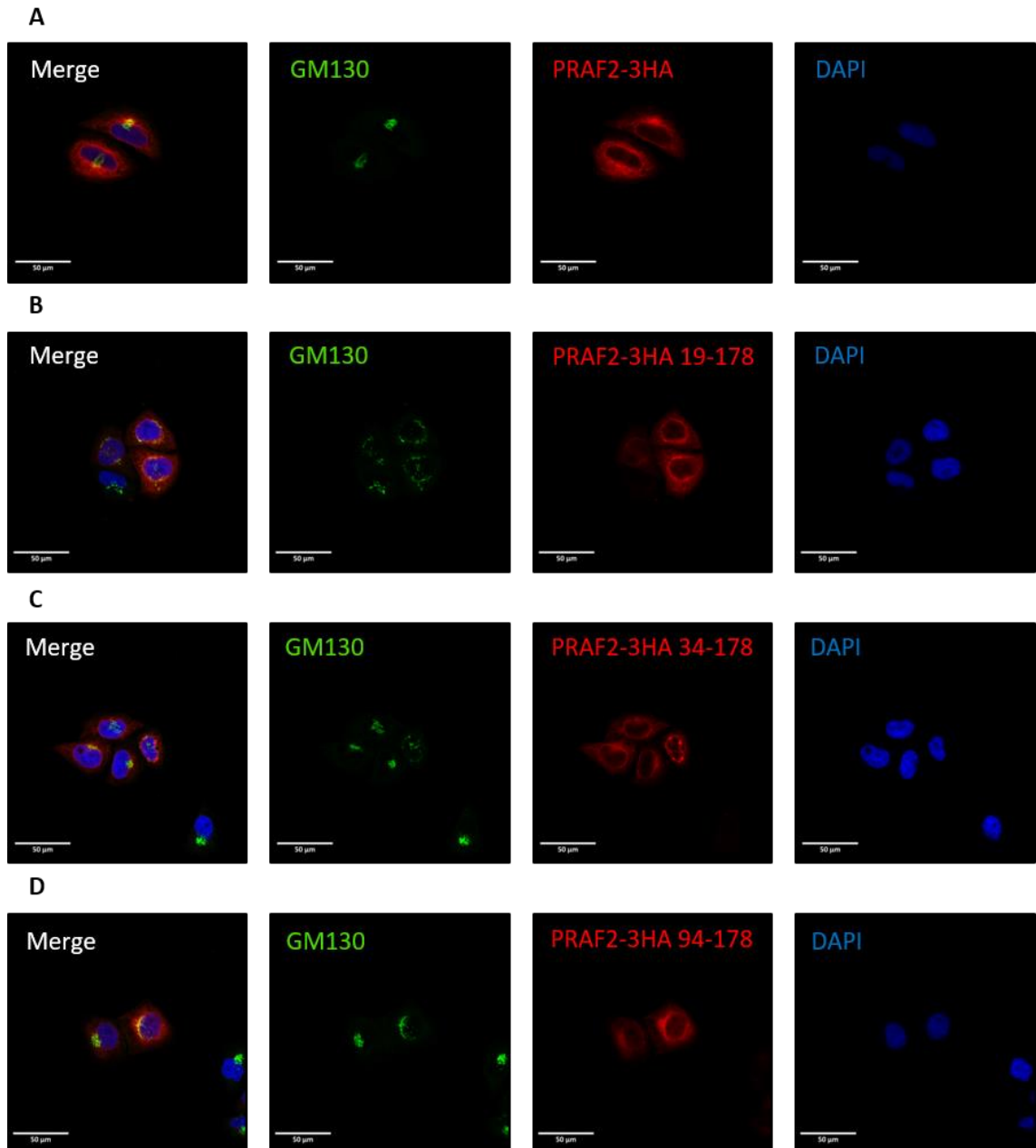


**Figure 3.9** Co-localisation of N-terminal PRAF2 mutants with GM130

HeLa cells transfected with N-terminal PRAF2 mutants and fixed and permeabilised 24 hours post transfection. Cells were stained for HA (Alexa 594, red) and then co-stained for cis-Golgi marker GM130 (Alexa 488, green). All cells mounted with a DAPI (blue) nuclear counterstain. A. WT PRAF2-3HA, Pearson's  $R$  value = 0.21. B. PRAF2-3HA 19-178, Pearson's  $R$  value = 0.33. C. PRAF2-3HA 34-178, Pearson's  $R$  value = -0.45. D. PRAF2-3HA 94-178, Pearson's  $R$  value = 0.33. Images are representative. Scale bar 50µm. N=1.

it appeared that the level of colocalisation with the ER marker calnexin remained the same and colocalisation with the cis-Golgi remained low.

In cells overexpressing PRAF2-3HA, as with 3xFLAG-PRAF2 (Figure 3.6 A) there was colocalisation (Pearson's R value = 0.74), Figure 3.8 A) between HA (red) and calnexin (green). However, as before the PRAF2-3HA was not totally co-localised with calnexin. PRAF2-3HA could also be observed to co-localise weakly (Pearson's R value = 0.21) with GM130 (green, Figure 3.9 A), however, the intensity of the co-localisation appeared to be lesser than its ER localisation. When the HA staining was examined, it appeared that the staining was strongly perinuclear. N-terminal mutant PRAF2-3HA 19-178 (Figure 3.8 B) co-localised strongly (Pearson's R value = 0.78) with calnexin, with less 'free' green visible. It also appeared to co-localise (Pearson's R value = 0.33) with GM130 (Figure 3.9 B) in a stronger manner than PRAF2-3HA. However, it still retained strong perinuclear HA staining. Mutant 34-178 (Figure 3.8 C) co-localised strongly (Pearson's R value = 0.73) with calnexin and but not with GM130 (Pearson's R value = -0.045, Figure 3.9 C). Its HA-staining appeared more diffuse than PRAF2-3HA. Finally, mutant 94-178 demonstrated weaker levels of expression than the WT and other mutants (Figure 3.8 D, Figure 3.9 D), it also co-localised with calnexin (Pearson's R value 0.62, Figure 3.8 D). This mutant also co-localised with GM130 (Pearson's R value = 0.33, Figure 3.9 D). Overall, the N-terminal mutants seemed to retain their perinuclear localisation and retained their ER localisation. Of the amino terminal mutants, all but 34-178 PRAF2-3HA were demonstrated to retain some cis-Golgi localisation. These data remain preliminary; however, they did not indicate an overall change of localisation from the ER, meaning that a loss of interaction with HPV-18E5 due to a change in localisation is unlikely.

### **3.2.5 Mutation of PRAF2 does not alter co-localisation with GFP-18E5**

PRAF2 localised with GFP18E5 (Figure 3.1 C), and the amino acids 135-160 appeared to be important for this interaction. However, the truncation mutants did not display radically

altered subcellular distribution when compared to WT (Figure 3.6, 3.7, 3.8 and 3.9), to confirm that the loss of binding between HPV18E5 and PRAF2 was due to amino acids 135-160 and not due a redistribution of one of the interaction partners the localisation of the mutants with GFP-18E5 was examined.

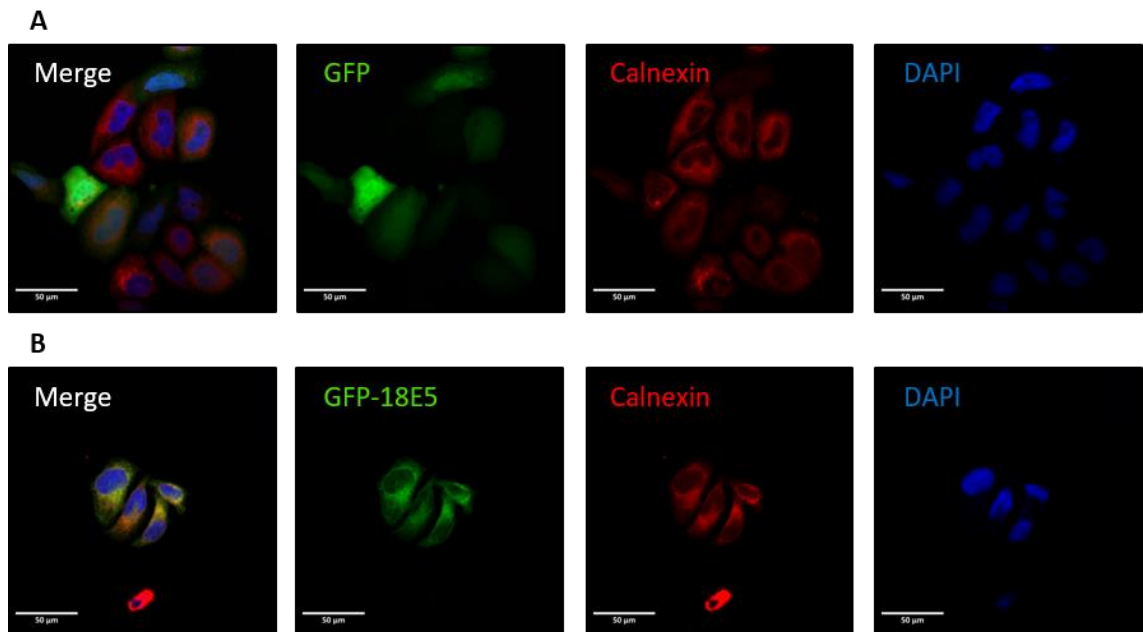


**Figure 3.10** *GFP-18E5 co-localises with the ER marker calnexin*

*HeLa cells transfected with GFP or GFP-18E5, fixed and permeabilised 24 hours post transfection. Cells were co-stained for ER marker calnexin (Alexa 594, red). All cells mounted with a DAPI (blue) nuclear counterstain. A. HeLa overexpressing GFP, Pearson's R value =0.07. B. HeLa overexpressing GFP-18E5, Pearson's R value = 0.8. Images are representative. Scale bar 50μm. N=3.*

The sub-cellular localisation of GFP-18E5 was determined by transfecting GFP-18E5 into HeLa cells. HeLa cells were transfected with GFP-18E5 or control GFP and 24 hours post transfection were fixed, permeabilised and stained for either calnexin or GM130. When compared to GFP (Figure 3.10 A) it was observed that GFP-18E5 (Figure 3.10 B) displayed a strong perinuclear GFP expression, with some bright puncta in the cytoplasm and some more diffuse staining towards the edges of the cells, whereas GFP is distributed throughout the

nucleus and cytoplasm. GFP-18E5 displays strong (Pearson's R value 0.8) co-localisation with calnexin (red, Figure 3.10 B). When co-stained for GM130 (Figure 3.11) no co-localisation (Pearson's R value = 0.04) could be observed between GM130 and GFP-18E5 (Figure 3.11 B). This suggested that GFP-18E5 was primarily localised to the ER, which was also the primary localisation of PRAF2.

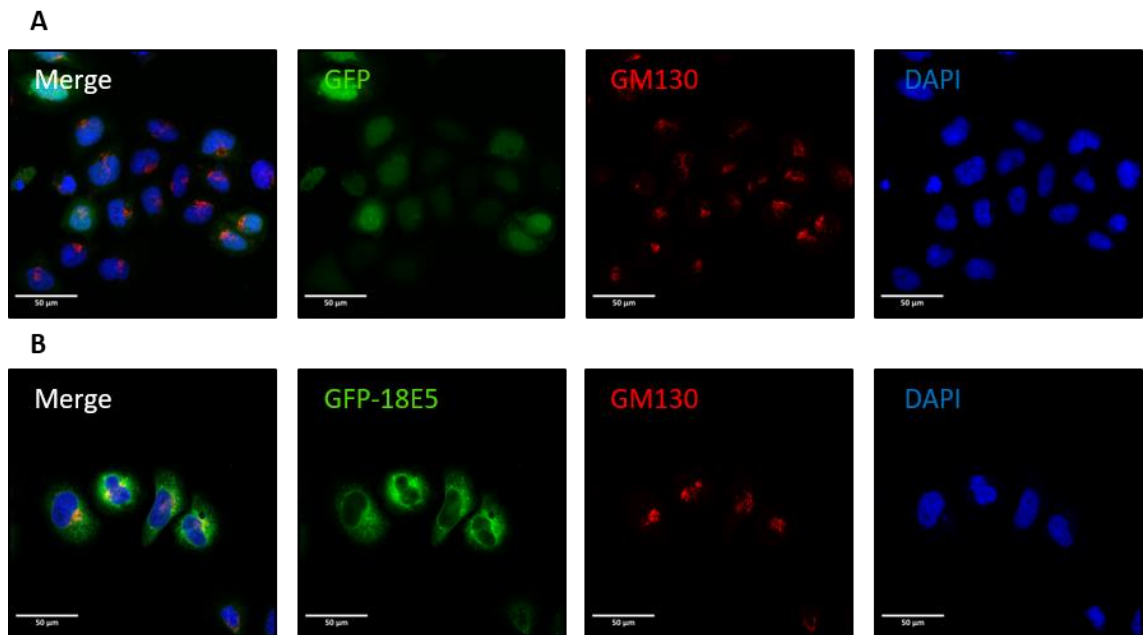


**Figure 3.11** *GFP-18E5 did not appear to co-localise with GM130*

*HeLa cells transfected with GFP or GFP-18E5, fixed and permeabilised 24 hours post transfection. Cells were co-stained for cis-Golgi marker GM130 (Alexa 594, red). All cells mounted with a DAPI (blue) nuclear counterstain. A. HeLa overexpressing GFP, Pearson's R value =-0.1. B. HeLa overexpressing GFP-18E5, Pearson's R value =0.04. Images are representative. Scale bar 50μm. N=3.*

As before HeLa cells were used for the co-transfections of GFP-18E5 and the PRAF2 truncation mutants. Cells were then fixed and permeabilised 24 hours post transfection and stained for either the FLAG or HA tag. As previously observed (Figure 3.1 C) strong co-localisation (Pearson's R value = 0.76) could be observed between PRAF2-3HA and GFP-18E5 (Figure 3.12 A). Co-localisation (Pearson's R value = 0.77) could also be observed between GFP-18E5 and PRAF2-

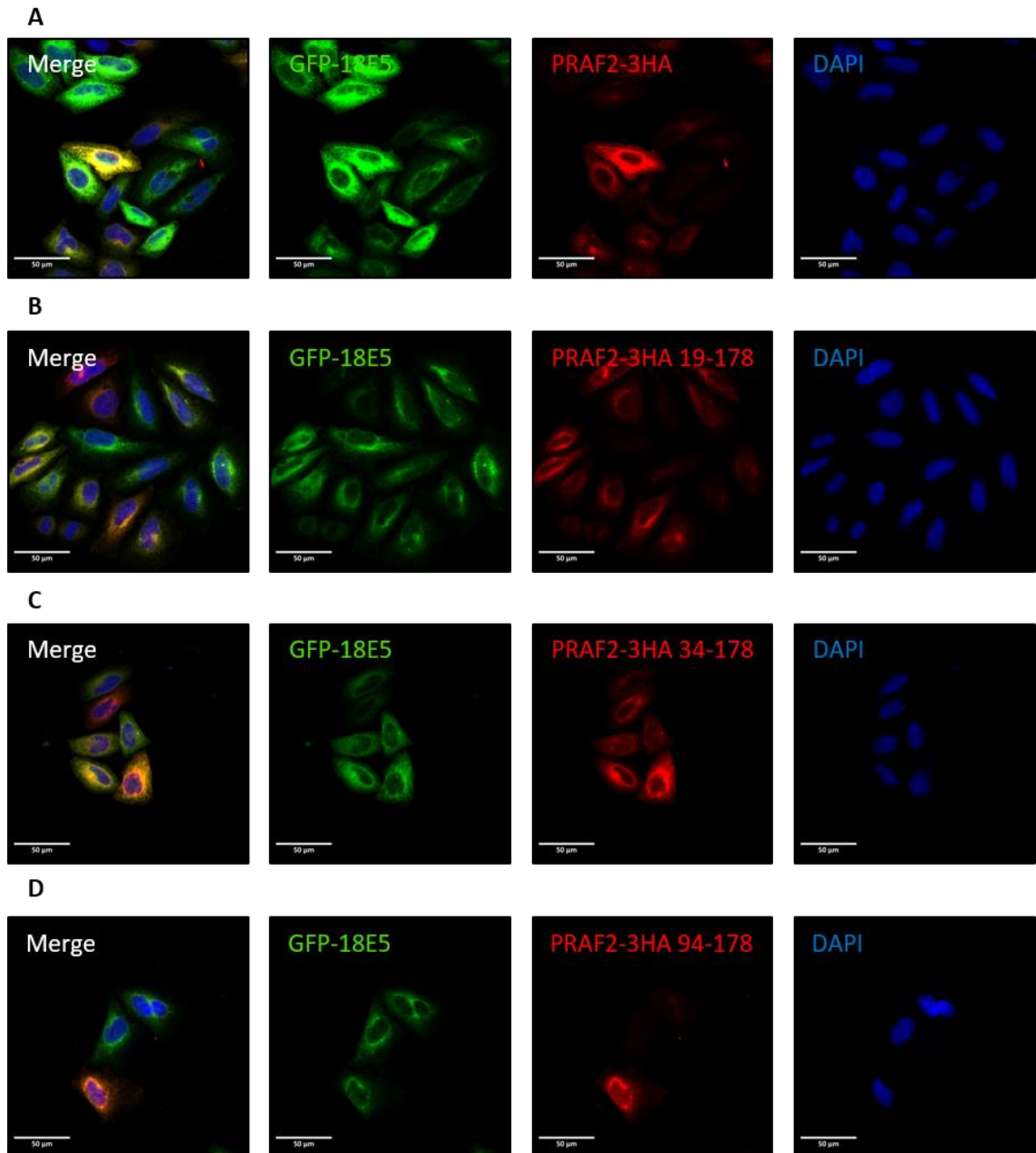


**Figure 3.12** Co-localisation of amino-terminal PRAF2 mutants with GFP-18E5

HeLa cells transfected with GFP-18E5 and amino-terminal PRAF2 mutants and fixed and permeabilised 24 hours post transfection. Cells were stained for HA (Alexa 594, red). All cells mounted with a DAPI (blue) nuclear counterstain. A. WT PRAF2-3HA and GFP-18E5, Pearson's  $R$  value = 0.76. B. PRAF2-3HA 19-178 and GFP-18E5, Pearson's  $R$  value = 0.77. C. PRAF2-3HA 34-178 and GFP-18E5, Pearson's  $R$  value = 0.79. D. PRAF2-3HA 94-178 and GFP-18E5, Pearson's  $R$  value = 0.79. Images are representative. Scale bar 50 $\mu$ m. N=3.

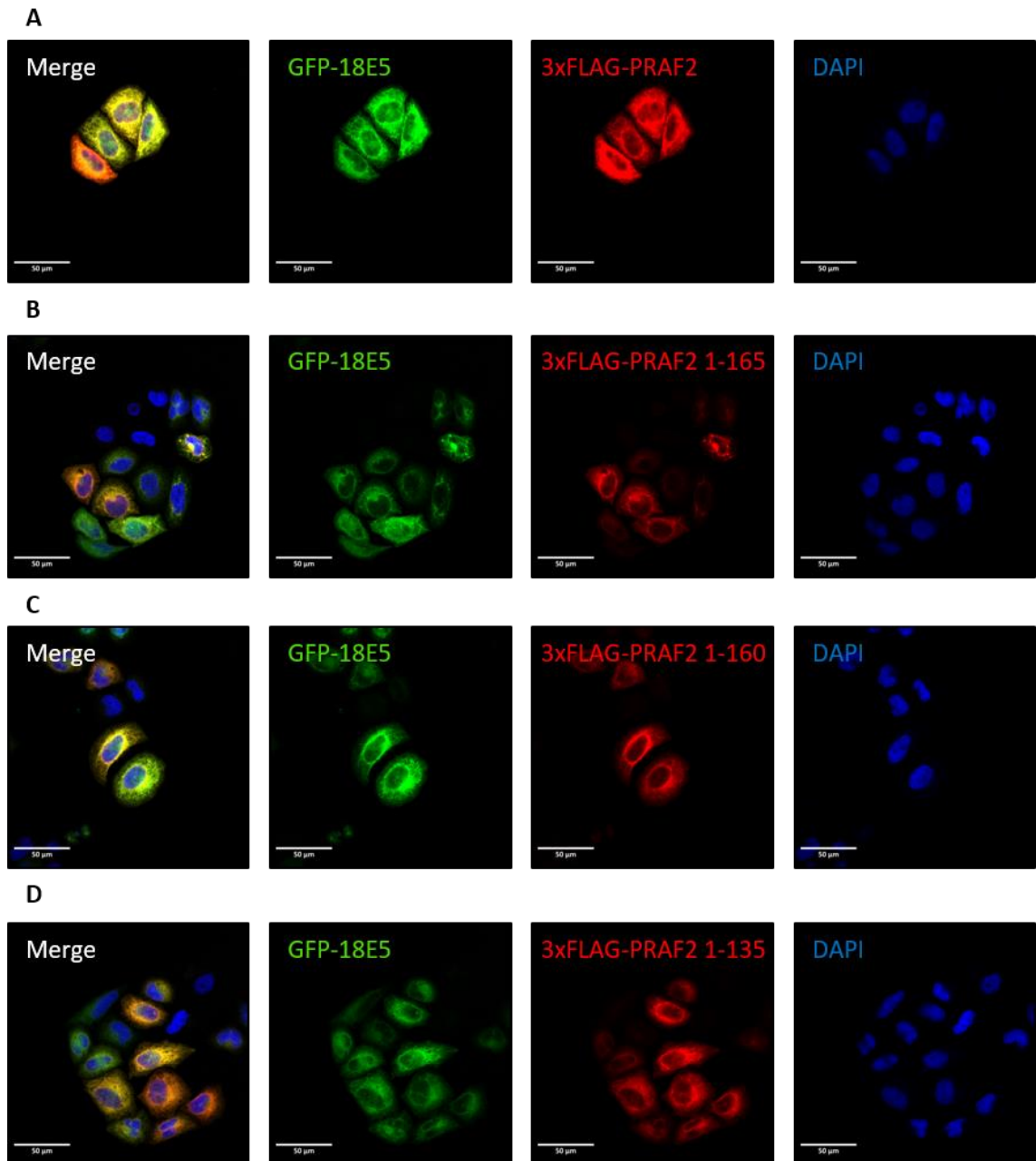


**Figure 3.13** Co-localisation of C-terminal PRAF2 mutants with GFP-18E5

HeLa cells transfected with GFP-18E5 and C-terminal PRAF2 mutants and fixed and permeabilised 24 hours post transfection. Cells were stained for FLAG (Alexa 594, red). All cells mounted with a DAPI (blue) nuclear counterstain. A. GFP-18E5 and WT 3xFLAG-PRAF2, Pearson's  $R$  value = 0.82. B. GFP-18E5 and 3xFLAG-PRAF2 1-165 C, Pearson's  $R$  value = 0.89. GFP-18E5 and 3xFLAG-PRAF2 1-160, Pearson's  $R$  value = 0.83). D. GFP-18E5 and 3xFLAG-PRAF2 1-135, Pearson's  $R$  value = 0.88. Images are representative. Scale bar 50µm. N=3.

3HA 19-178 (Figure 3.12 B), PRAF2-3HA 34-178 (Pearson's R value = 0.79, Figure 3.12 C) and PRAF2-3HA 94-178 (Pearson's R value = 0.79, Figure 3.12 D). As with the HA tagged PRAF2, strong co-localisation was observed for 3xFLAG-PRAF2 (Pearson's R value = 0.82, Figure 3.13 A). Co-localisation was also observed for 3xFLAG-PRAF2 1-165 (Pearson's R value = 0.89, Figure 3.13 B), 3xFLAG-PRAF2 1-160 (Pearson's R value = 0.83, Figure 3.13 C) and 3xFLAG-PRAF2 1-135 (Pearson's R value = 0.88, Figure 3.13 D). This suggested that the failure to IP 3xFLAG-PRAF2 1-135 by GFP-18E5 (Figure 3.3 B) is due to a loss of interaction due to deletion of required amino acids, and not due to a change in the localisation of the two proteins.

### **3.2.6 The subcellular localisation of PRAF1 and PRAF3**

The other PRAF family members, PRAF1 and PRAF3 (Abdul-Ghani et al., 2001), whilst not identified as interactors for HPV18E5 in the original screen, do possess the conserved HASLRLR motif located within the amino acids 135-160 that was required for the interaction of PRAF2 and GFP-18E5, so it was possible that they too could also interact with HPV18E5. Previous studies (Abdul-Ghani et al., 2001) in chinese hamster ovary cells (CHO) suggested a predominantly Golgi localisation for PRAF1 and ER for PRAF3, so there was the possibility that they could be in compartments with HPV18E5. Firstly, the subcellular localisation of PRAF1 and PRAF3 was examined in a relevant cell line.

PRAF1-3HA and PRAF3-3HA constructs were transfected into HeLa cells. 24 hours post transfection the cells were fixed, permeabilised and stained for HA and either calnexin, GM130 or TGN46. PRAF1-3HA appeared to co-localise with the ER marker calnexin (Figure 3.14 A), however, HA staining could also be observed elsewhere in the cell, in regions outside the ER, and Coloc2 analysis suggested that the PRAF1-3HA and calnexin were not in fact colocalised (Pearson's R value = -0.03). PRAF3-3HA co-localised with calnexin (Pearson's R Value = 0.74, Figure 3.14 B), and less HA staining was observed elsewhere in the cell than with PRAF1-3HA. When stained for the cis-Golgi marker GM130, PRAF1-3HA co-localised (Pearson's R value =

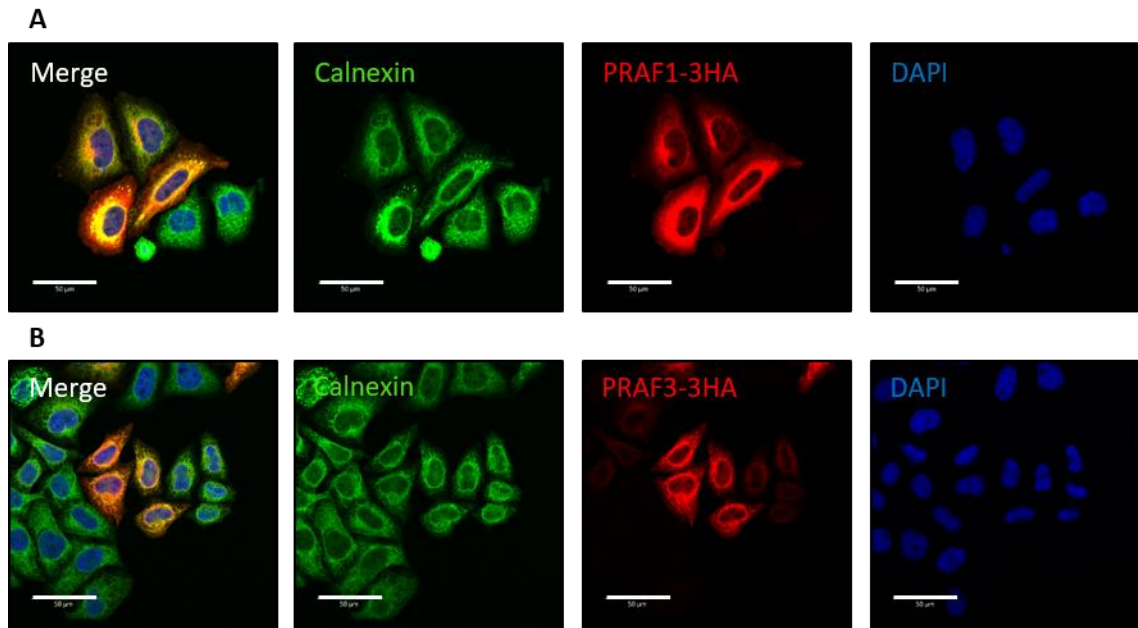


**Figure 3.14** *PRAF1 and PRAF3 localise with the ER marker calnexin*

*HeLa cells transfected with PRAF1-3HA or PRAF3-3HA and stained with HA (Alexa594, red) and co-stained for the ER marker calnexin (Alexa488, green) with DAPI nuclear counterstain (blue) A. PRAF1-3HA, Pearson's R value = -0.03. B. PRAF3-3HA, Pearson's R value = 0.75. All images are representative. Scale bar is 50 μm. N=1.*

0.61, Figure 3.15 A), and PRAF3-3HA was not co-localised with GM130 (Pearson's R value= 0.01, Figure 3.15 B). When stained for the trans-Golgi marker TGN46, PRAF1-3HA (Figure 3.16 A) co-localised (Pearson's R value = 0.49). Additionally, the distribution of TGN46 was not radically altered from that of control HeLa cells (Figure 3.4 C) as observed with PRAF2-3HA overexpressing HeLa cells (Figure 3.5 C). PRAF3-3HA did co-localise with TGN46 (Figure 3.16 B) however, the distribution of TGN46 was very different to control cells (Figure 3.4 C), except in cells expressing low levels of PRAF3-3HA. This was similar to the effect observed in PRAF2-3HA overexpressing cells (Figure 3.5 C). Perhaps similar to PRAF2, PRAF3 overexpression could result in TGN46 retention in the ER. The subcellular localisation observed for overexpressed PRAF1 and PRAF3 in HeLa cells seemed to be in line with previous observations.

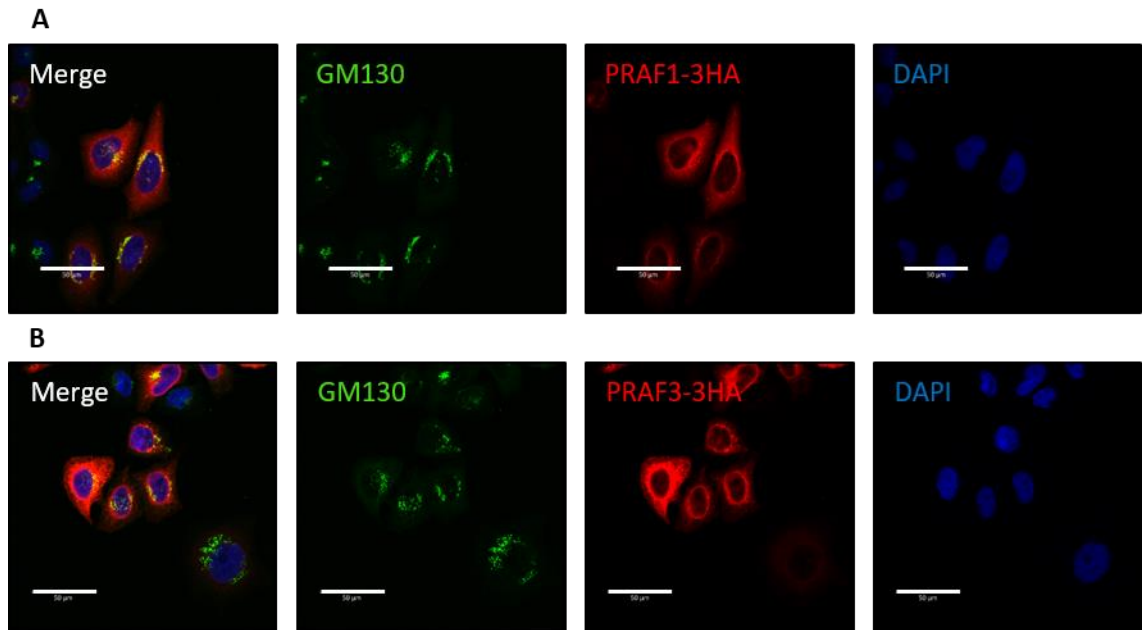


**Figure 3.15** *PRAF1 and PRAF3 co-localise with the cis-Golgi marker GM130*

HeLa cells transfected with PRAF1-3HA or PRAF3-3HA and stained with HA (Alexa594, red) and co-stained for the cis-Golgi marker GM130 (Alexa488, green) with DAPI nuclear counterstain (blue) A. PRAF1-3HA, Pearson's  $R$  value = 0.61. B. PRAF3-3HA, Pearson's  $R$  value = 0.01. All images are representative. Scale bar is 50  $\mu$ m.  $N=1$ .

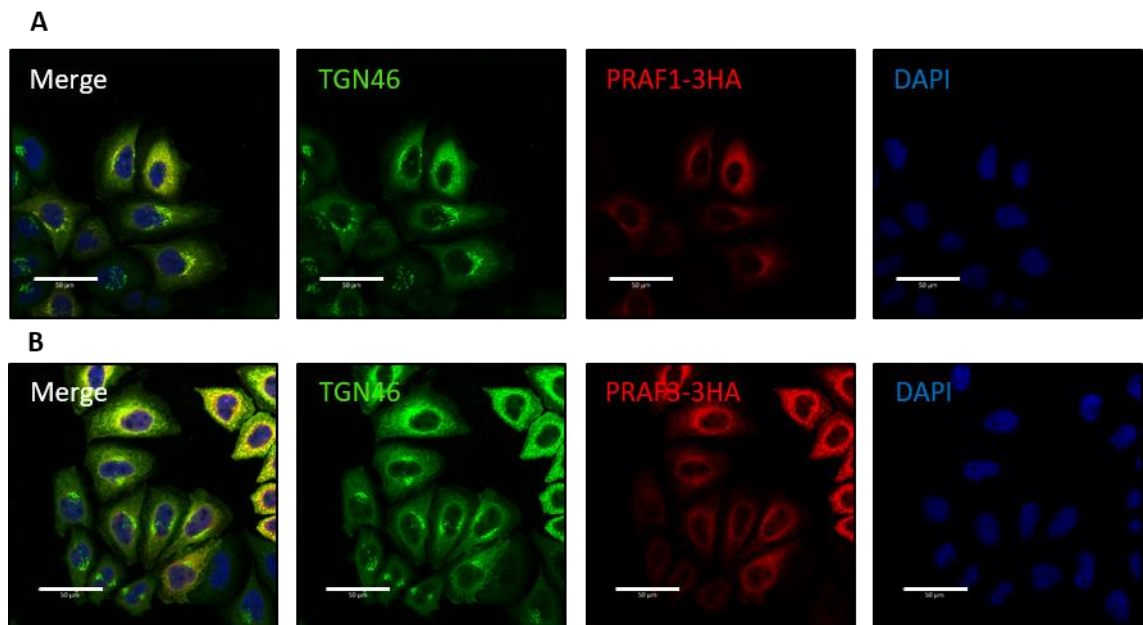


**Figure 3.16 Localisation of PRAF1 and PRAF3 with the trans-Golgi marker TGN46**

HeLa cells transfected with PRAF1-3HA or PRAF3-3HA and stained with HA (Alexa594, Red) and co-stained for the trans-Golgi marker TGN46 (Alexa488, Green) with DAPI nuclear counterstain (Blue) A. PRAF1-3HA, Pearson's  $R$  value =. B. PRAF3-3HA. All images are representative. Scale bar is 50 $\mu$ m. N=1.

**3.2.7 The interaction of HPV18E5 is conserved between PRAF family members**

As PRAF1 and PRAF3 both localised to the ER, where GFP-18E5 has also been observed to localise (Figure 3.10 B) it was therefore possible that they interacted. Cells were transfected with either PRAF1-3HA or PRAF3-3HA and GFP-18E5, and then 24 hours post transfection fixed and permeabilised and stained for HA. Co-localisation could be observed between GFP-18E5 and PRAF1-3HA (Red, Figure 3.17 A), and between GFP-18E5 and PRAF3-3HA (Red, Figure 3.17 B). As a result, the ability of GFP-18E5 to IP PRAF1 and PRAF3 was investigated.

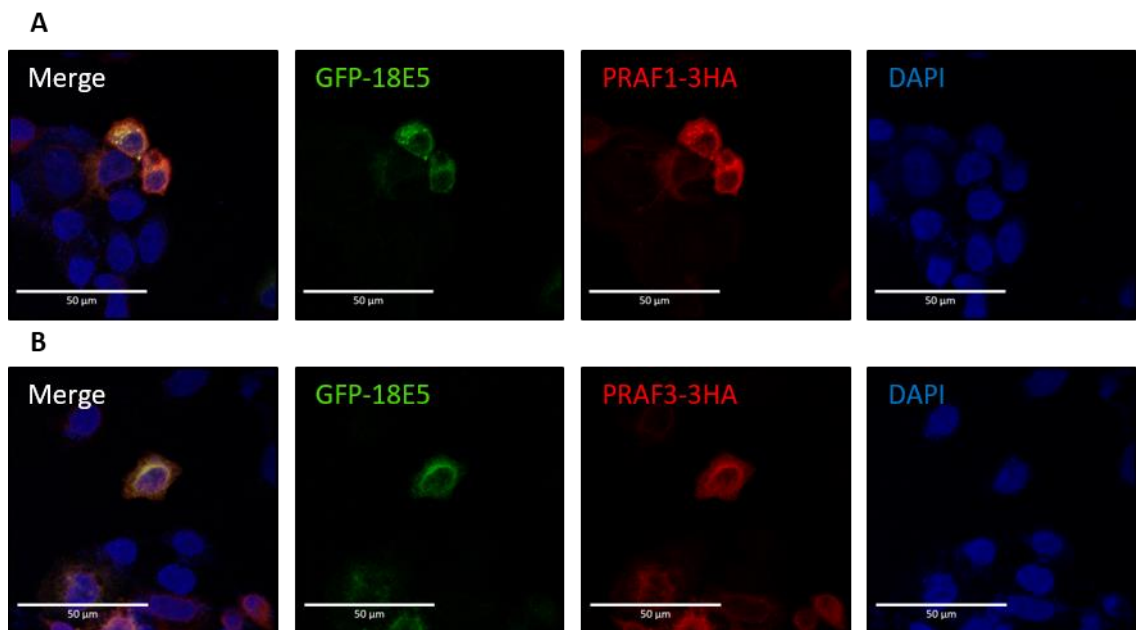


**Figure 3.17 PRAF1 and PRAF3 co-localise with GFP-18E5**

C33A cells transfected with GFP-18E5 and PRAF1-3HA or PRAF3-3HA and stained with HA (Alexa594, Red) with DAPI nuclear counterstain (Blue) A. GFP-18E5 and PRAF1-3HA. B. GFP-18E5 PRAF3-3HA. All images are representative. Scale bar is 50 $\mu$ m. N=1.

PRAF1-3HA or PRAF3-3HA, GFP-C1 and GFP-18E5 were transfected into HEK293TT cells. Cells were lysed 24 hours post transfection and cell lysates were produced. These lysates were used to perform a GFP trap CO-IP and 10% of the resulting samples were resolved by SDS-PAGE and compared with the input. The resulting input westerns were probed with an antibody specific for HA, which confirmed the overexpression of PRAF1-3HA and PRAF3-3HA. A clear band

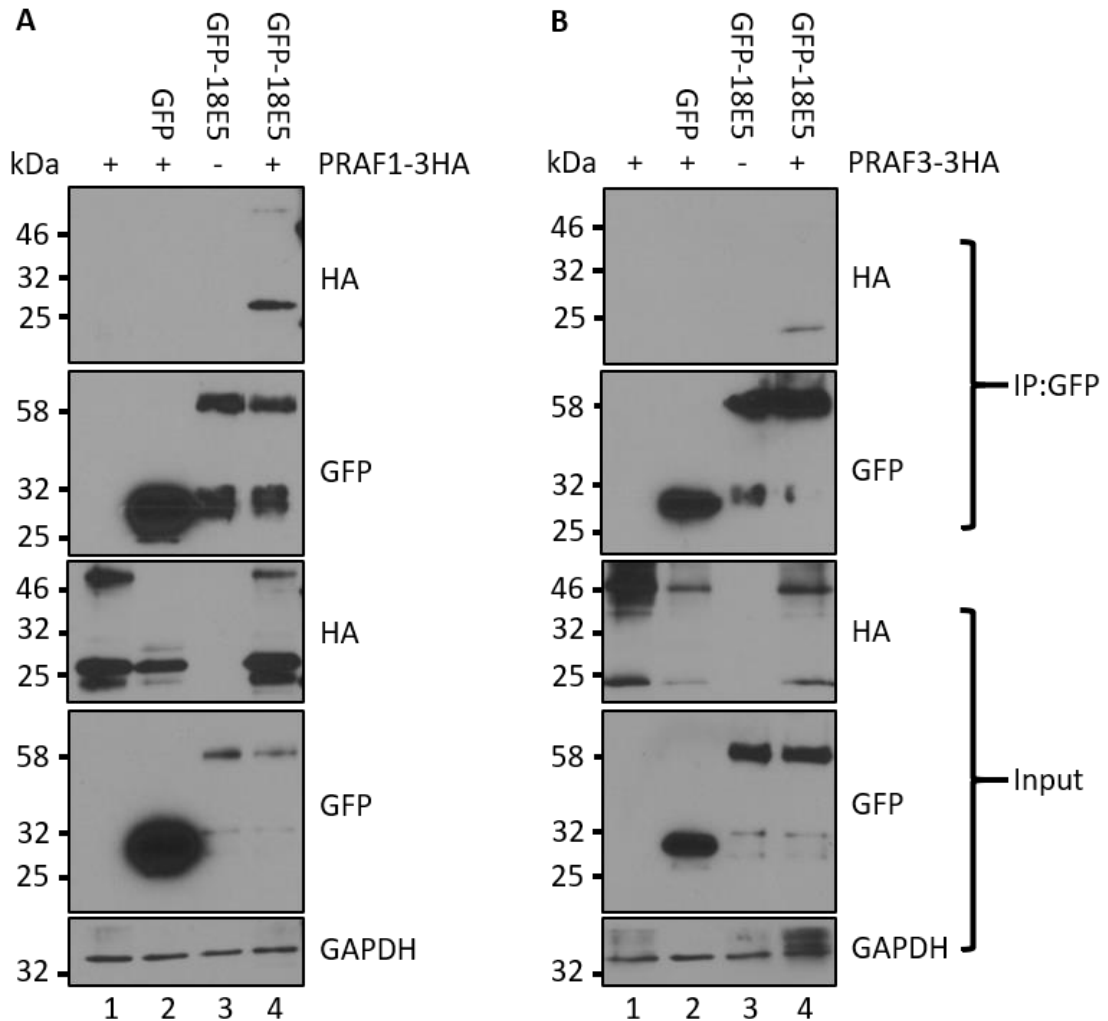


**Figure 3.18** *The interaction of HPV-18E5 with the PRA family is conserved*

*PRAF1-3HA and PRAF3-3HA were transfected into HEK293TT cells with GFP or GFP-18E5 and lysed. Co-immunoprecipitations were performed using GFP-trap magnetic agarose beads using equal amounts of protein. Representative blots are shown. A. PRAF1-3HA GFP-trap Co-IP B. PRAF3-3HA GFP-Trap Co-IP. N=3.*

of approximately 25 kDa was observed (lanes 1,2 and 4, Figure 3.18 A) corresponding to monomeric PRAF1 (expected MW 25277.96 Da), and a higher molecular weight band of approximately 50 kDa corresponding to the dimeric form was also detected. For PRAF3 a band was observed just below 25 kDa (Figure 3.18 B), which was a little smaller than the expected size (25920.34 Da), however this construct has been previously validated as PRAF3 (Vento et al., 2010).

The GFP co-immunoprecipitation successfully pulled down PRAF1-3HA and PRAF3-3HA (lane 4, IP:GFP, HA blot, Figure 3.18 A and B). As with PRAF2 (Figure 3.1 A) it could be ruled out that the interaction between PRAF1 or PRAF3 and GFP-18E5 was due to the GFP tag, as free GFP did not CO-IP PRAF1-3HA or PRAF3-3HA (lane 2, IP:GFP, Figure 3.18 A and B), nor did PRAF1-3HA and PRAF3-3HA bind to the GFP trap beads in a non-specific manner, as no PRAF1-3HA or PRAF3-3HA could be detected when they were expressed alone (lane 3, IP:GFP, Figure 3.18 A and B). This suggested that PRAF1 and PRAF3 did interact with HPV18E5.

### **3.2.8 The interaction of PRAF2 and E5 is conserved across Papillomavirus types**

The conservation of the interaction between HPV18E5 and the PRAF family suggests that the pathways that PRAF members are involved in are important for the HPV18 virus to modulate. It was therefore likely, as other papillomaviruses types often target similar host pathways, that the interaction could be shared with other papillomavirus types E5 proteins. As a result, CO-IPs were performed with other  $\alpha$ -genus E5 proteins: high risk mucosal HPV16, HPV18 and 31, low risk mucosal HPV6 and HPV11 and cutaneous HPV2a. In addition, bovine deltapapillomavirus BPV1 E5 was also used (see chapter 1). All PV E5 proteins were fused with GFP, and PRAF2-3HA was used.

All fusion proteins were expressed successfully, however, there were differences in the levels of expression, with HPV2aE5 and BPV1E5 expressing particularly well (lanes 8 and 9, Figure 3.19). All PV E5 proteins were successfully able to IP PRAF2-3HA. In addition to the previously

established interaction with GFP-18E5 (lane 4) GFP-16E5 was clearly able to bind PRAF2-3HA (lane 3, Figure 3.19), as was GFP-31E5 (lane 5, Figure 3.19), this suggested that the interaction with PRAF2 was conserved amongst high risk HPV. Low risk GFP-6E5 and GFP-11E5 (Lanes 6 and 7, Figure 3.19) were also able to IP PRAF2-3HA, as was cutaneous GFP-2aE5 (lane 8, Figure 3.19). This further suggested that the interaction with PRAF2 was conserved across alphapapillomaviruses. However, the interaction with GFP-11E5 appears to display the lowest binding. Finally, the deltapapillomavirus GFP-BPV1E5 was also able to IP PRAF2-3HA, suggesting that the interaction with PRAF2 is conserved amongst E5 proteins.

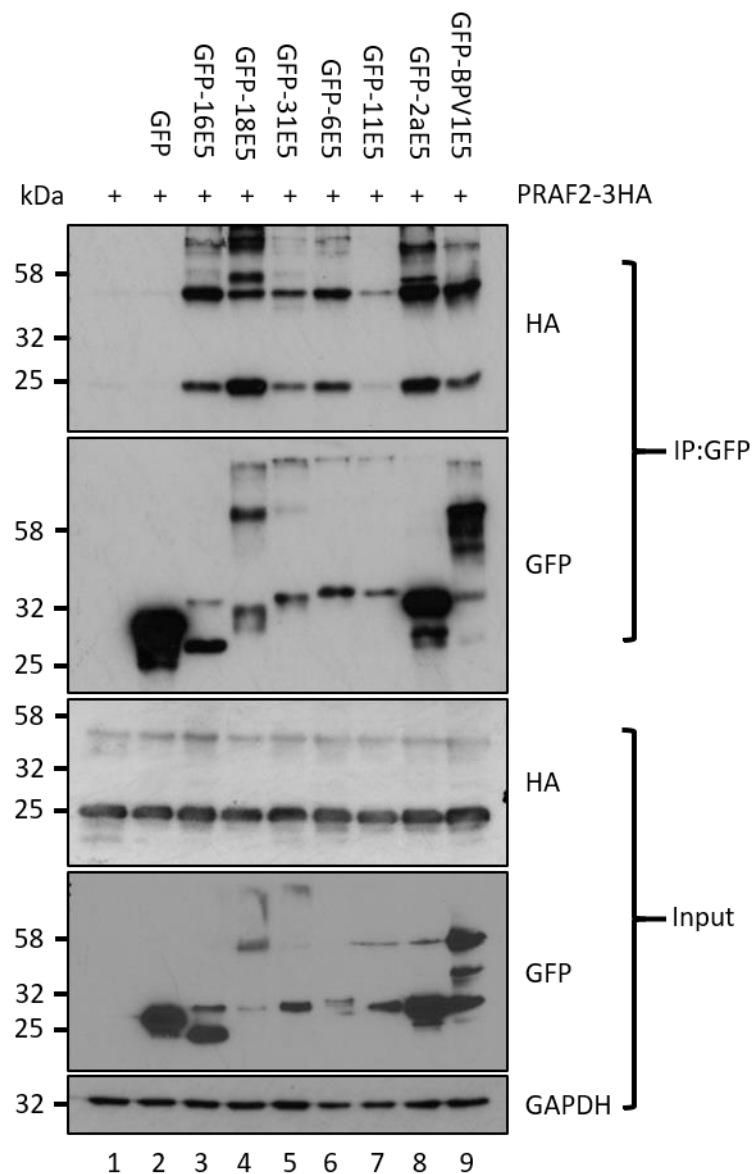


**Figure 3.19** *The interaction between PRAF2 and E5 is conserved amongst E5 types and genera*  
*PRAF2-3HA was co-transfected into HEK293TT cells with a GFP negative control or GFP-16E5, GFP-18E5, GFP-31E5, GFP-6E5, GFP-11E5, GFP-2aE5 or GFP-BPV1E5 and lysed. Co-immunoprecipitations were performed using GFP-trap magnetic agarose beads using equal amounts of protein. Representative blots are shown. N=3.*

### **3.2.9 PRAF2 did not interact with other HPV18 early proteins**

Often HPV proteins cooperate or share interacting partners, it was therefore possible that interactions with the other HPV oncoproteins could exist which were not picked up in the original screen (Rozenblatt-Rosen et al., 2012) and in addition there were other HPV early proteins that were not tested. HPV18 E1, E2 and E1<sup>E4</sup> were therefore cloned into the GFP-c1 vector and transfected into HEK293TT cells in addition to GFP-18E5, GFP-18E6 and GFP-18E7 and GFP Co-IPs performed.

However, there were issues with the expression of the HPV18 early proteins, E1 and E2. The full size GFP-18E1 fusion protein (expected size 102.6 kDa, lane 3, Figure 3.20) was only a small proportion of the protein expressed (\*red box, lane 3, Figure 3.20). It appeared that either expression was favouring smaller fragments or the GFP tag, or possibly that the fusion protein was being cleaved. HPV18E1 is known to contain the caspase-3 cleavage site DMVD (Moody et al., 2007), which would result in cleavage after amino acid 49. This fragment would result in a GFP 'fusion' of ~5 kDa greater in size than GFP, which could account for the low levels of full size GFP-18E1 detected. GFP-18E2 was only detectable at very low levels (expected size 70 kDa, lane 4, \*\*red box, Figure 3.20), perhaps due to the E2 proteins cellular toxicity (Parish et al., 2006b). GFP-18E1<sup>E4</sup> expressed well (expected size 38.8 kDa, lane 5, Figure 3.20), as did GFP-18E5 (expected size 37.2 kDa, lane 6, Figure 3.20. GFP-18E6 (expected size 47.8 kDa) had some issues with breakdown products (lane 7, Figure 3.20). GFP-18E7 (expected size 40.9 kDa) expressed well (lane 8, Figure 3.20). Of the Co-IPs, only GFP-18E5 (lane 6, Figure 3.20, HA, IP: GFP)

precipitated PRAF2-3HA. However, due to the issues with expression with GFP-18E1 and GFP-18E2 it was decided that further IPs would be done with the oncoproteins only.

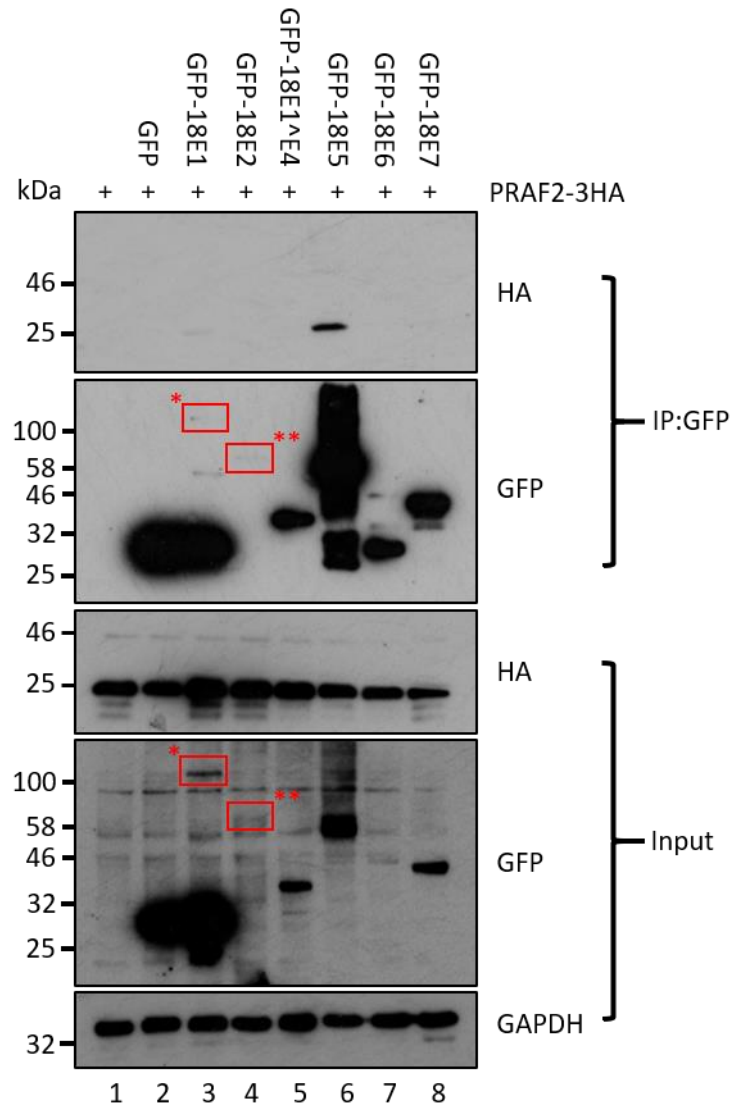


**Figure 3.20** *The interaction of PRAF2 is limited to only E5 of the E-proteins*

PRAF2-3HA was co-transfected into HEK293TT with either a GFP negative control or GFP-18E1, GFP-18E2, GFP-18E1<sup>ΔE4</sup>, GFP-18E5, GFP-18E6 or GFP-18E7. Co-immunoprecipitations were performed using GFP-trap magnetic agarose beads using equal amounts of protein. Representative blots are shown. \*red box= GFP-18E1, \*\*red box= GFP-18E2. N=2.

As before, GFP-18 oncoproteins and GFP control were expressed in HEK293TT and GFP trap Co-IPs were performed. All the constructs expressed well, however GFP-18E5 was faint in the input (lane 3, Figure 3.21). However, GFP-18E5 was enriched in the IP (lane 3, Figure 3.21, GFP, IP: GFP). Of the oncoproteins, only GFP-18E5 was precipitated PRAF2-3HA (lane 3, Figure 3.21, HA, IP: GFP). This suggested that possible protein interactions and complexes with HPV18 oncoproteins were limited to the E5 protein.

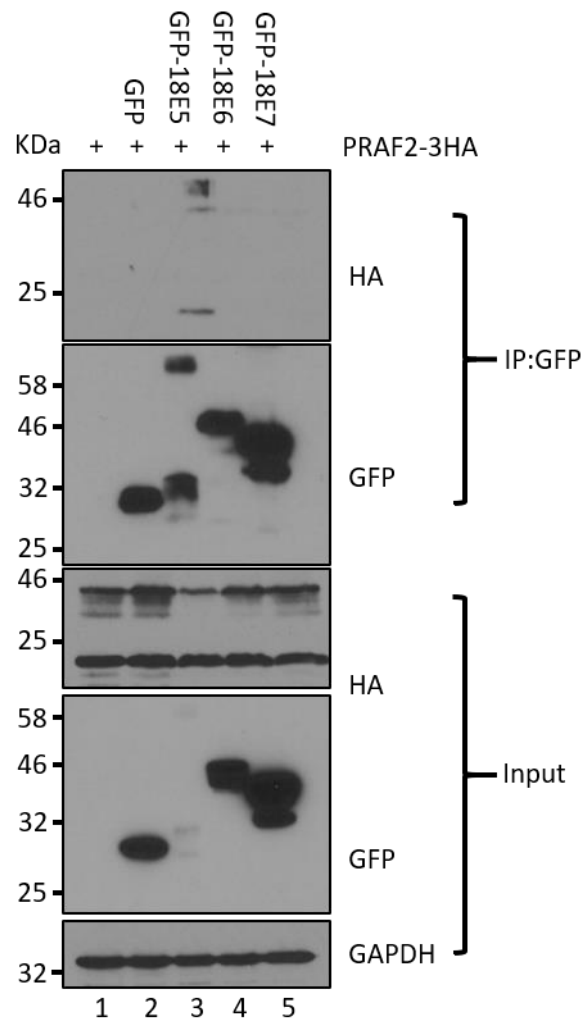


**Figure 3.21** *HPV-18E5 is the only HPV-18 oncoprotein interacting partner of PRAF2*

*PRAF2-3HA was co-transfected into HEK293TT with either a GFP negative control or GFP-18E5, GFP-18E6 or GFP-18E7. Co-immunoprecipitations were performed using GFP-trap magnetic agarose beads using equal amounts of protein. Representative blots are shown. N=3*

### 3.2.10 HPV18 oncoproteins do not affect PRAF2 protein expression levels

As PRAF2 has been identified as a conserved interactor for HPV18E5 it was decided to investigate whether the HPV18 oncoproteins were also able to alter the expression of the PRAF2 protein. GFP-18 oncoproteins were overexpressed in C33A cells, with GFP and non-transfected (N/T) controls. Cells were lysed 24 hours post transfection and equal amounts of protein were resolved by SDS-PAGE. The resulting western blots were probed with antibodies specific for GFP, PRAF2 and GAPDH (Figure 3.22). All GFP proteins were expressed successfully. No difference could be observed in the levels of the PRAF2 protein for GFP-18E5 (lane 2, Figure 3.22), GFP-18E6 (lane 3, Figure 3.22) or GFP-18E7 (lane 4, Figure 3.22) when compared to either the GFP (lane 1, Figure 3.22) or N/T (lane 5, Figure 3.22) controls. This suggested that the HPV18 oncoproteins did not mediate the levels of PRAF2 expression.

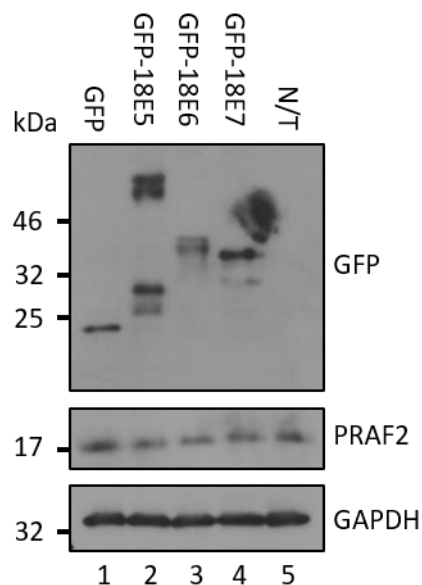


**Figure 3.22** *Overexpression of GFP-tagged HPV18 Oncoproteins and did not alter endogenous PRAF2 expression*

*GFP-tagged HPV18 oncoproteins were overexpressed in HPV negative C33A cells. Equal amounts of protein were loaded, and blots were probed for GFP, PRAF2 and GAPDH. Representative western blot shown. N=4*

### 3.2.11 HPV16 positive cancer cell lines maintain PRAF2 expression and it is lost in HPV18 positive cancer cell lines

Having ascertained that the interaction between PRAF2 and HPV E5 was conserved it was decided to examine PRAF2 protein expression in the context of HPV positive cervical cancer cell lines. Cervical cancer cell lines C33A (HPV negative), CaSki (HPV16 positive), SiHa (HPV16 positive), HeLa (HPV18 positive), SW756 (HPV18 positive) and a positive control of C33A overexpressing PRAF2 were lysed and equal amounts of protein resolved by SDS PAGE. The resulting western blots were probed for PRAF2 and GAPDH expression. In the positive control (lane 6, Figure 3.23 A) a band of approximately 19 kDa (expected 19257.90 Da) could be observed (single green arrow), and a higher MW band of approximately 36 kDa (expected 38515.8 Da) could be observed (double green arrow). These corresponded to the monomeric and dimeric forms of PRAF2. Monomeric PRAF2 could be observed in C33A, CaSki and SiHa (lanes

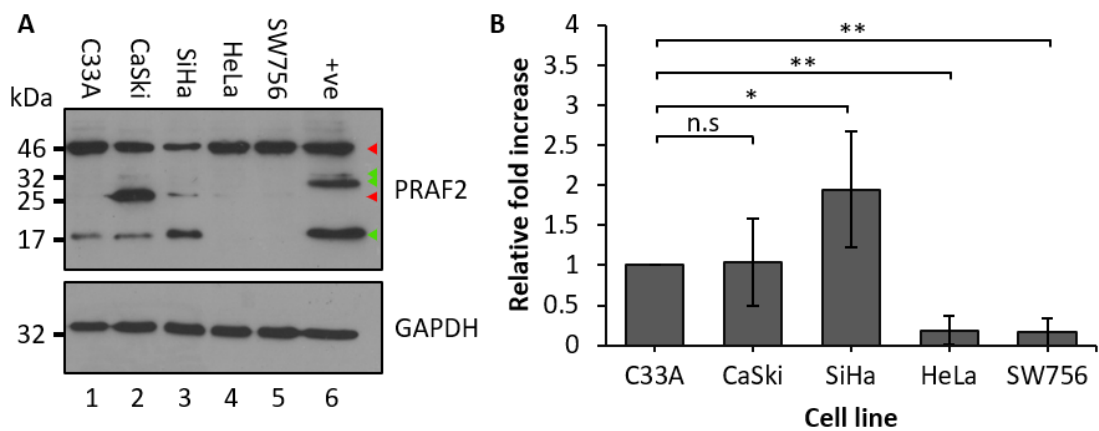


**Figure 3.23** PRAF2 is expressed by HPV negative and HPV-16 positive cervical cancer cell lines but not HPV-18 positive cervical cancer cell lines

Lysates from HPV negative C33A cells, HPV16 positive CaSki and SiHa cells, HPV18 positive HeLa and SW756 cells, equal amounts of protein were resolved by SDS PAGE and resulting blots probed for PRAF2 and GAPDH. A. Western blot of cervical cancer cell line PRAF2 expression, representative blot. Red arrows indicate nonspecific antibody activity, single green arrow

*indicates monomeric PRAF2, double arrow dimeric PRAF2 B. Densitometry of PRAF2 relative to the level of expression in C33A cells. \* p=0.039 \*\* p=0.0015 and 0.0011 respectively. N=4.*

1, 2 and 3, Figure 3.23 A), but not in HeLa or SW756 (lanes 4 and 5, Figure 3.23 A). Dimeric PRAF2 was faintly visible in CaSki cells (lane 2). Densitometry (Figure 3.23 B) showed that there was a statistically significant increase (\*p=0.039) in PRAF2 protein expression relative to C33A cells in SiHa cells and a statistically significant decrease (\*\*p=0.0015 and 0.0011 respectively) in PRAF2 protein expression in HeLa and SW756 cells. There are some non-specific bands visible on the blot (red arrows) at approximately 25 kDa and 46 kDa. It was interesting that PRAF2 expression was maintained in HPV16 positive cell lines but not in HPV18 positive cell lines.

### 3.3 Discussion

This study confirmed the previous observation by TAP-MS that PRAF2 was an interactor for HPV18E5 (Rozenblatt-Rosen et al., 2012). This was confirmed through GFP-Trap CO-IP and CO-IF for the first time. The interaction between PRAF2 and GFP-18E5 was mapped to PRAF2 through mutational studies, making use of PRAF2 truncation mutants and CO-IPs. The data suggested that amino acids 135-160 were crucial for the immunoprecipitation of PRAF2 by GFP-18E5, as this was the only truncation mutant that lost its ability to immunoprecipitated by PRAF2. However, there was the possibility that this truncation mutant was misfolding, and therefore prevented the interaction. Interestingly, the deletions at the amino-terminal, mutants 19-178, 34-178 and 94-178 had no effect on the ability of PRAF2 to bind GFP-18E5.

The rationale behind the N-terminal mutations was not known, as these mutants were a gift from Ingram Iaccorino (Vento et al., 2010). For mutants 19-178 and 34-178 the N-terminal cytosolic domain is removed and the two putative phosphorylation sites, S2 and S19. The 94-178 mutation removed the conserved NLLYYQTNY sequence, and the first two predicted transmembrane domains. This region includes the putative phosphorylation site Y43 and the predicted amphiphysin Src homology 3 group (SH3) domain. This could be a mutational region

of interest as amphiphysins are implicated in clathrin mediated endocytosis and interact with dynamin through their SH3 domains. Dynamin has been shown to be involved in the internalisation of GPCRs, of which an identified PRAF2 interactor CCR5 (Schweneker et al., 2005) is a member. This mutation could possibly interfere with one of the characterised roles for PRAF2, hence deleting this region. Furthermore, PRAF2 has been shown to be enriched in endosomes (Borsics et al., 2010) and synaptic vesicles (Koomoa et al., 2008), and PRAF family member PRAF1 has been shown to interact with VAMP2 (Martincic et al., 1997), which known to be enriched in synaptic vesicles and a known dynamin binding protein (Raimondi et al., 2011; Gorini et al., 2010). As a result, disruption of this region could impair an essential function of PRAF2. However, it should be noted that this deletion did not prevent its interaction with GFP-18E5. Additionally, it has yet be established whether the interaction between PRAF2 and HPV18E5 is direct or indirect, mediated by other proteins as part of a protein complex. Further studies will be required to elucidate this.

The C-terminal mutants were designed to disrupt a region that had been shown in PRAF1 and PRAF3 to be required for its localisation to membrane compartments (Abdul-Ghani et al., 2001) and also crucial in PRAF1 for its interaction with Rab GTPases (Gougeon et al., 2002; Hutt et al., 2000; Martincic et al., 1997). The first mutant 1-165 removed a run of acidic amino acids LLEALGQEQEAGS (amino acids 165 to 178) and the 1-160 mutant removed more residues (residues 160 to 178) to leave a C-terminus of a predominantly basic character, as the acidic character of the PRAF1 and PRAF3 C-terminus had been suggested to be important for their localisation (Abdul-Ghani et al., 2001). The 1-135 removed the conserved region (amino acids 135 to 178), which in PRAF1 had been demonstrated to be crucial for its interaction with Rab GTPases (Gougeon et al., 2002). Of all the mutants, only the 1-135 mutant had lost its ability to bind HPV18E5. This region could be potentially be required for PRAF2 to bind Rab proteins and hence its role in Golgi to ER traffic. Perhaps HPV18E5 binds to this region to modulate PRAF2s

effects on trafficking, possibly demonstrating why this region is important to its interaction with E5.

There are discrepancies with regards to where the PRAF2 protein localises within cells, with PRAF2 detected in the ER (Doly et al., 2016; Borsics et al., 2010), partial localisation to the Golgi (Doly et al., 2016), cytoplasmic puncta and endosomes (Borsics et al., 2010; Geerts et al., 2007). These differences could be down to endogenous protein versus overexpressed protein, or indeed cell line dependent. Our studies used overexpressed epitope tagged PRAF2 in HeLa cells, and we demonstrated that WT PRAF2 localised predominantly to the ER through co-localisation with calnexin, with some co-localised with the cis-Golgi marker GM130. Interestingly, PRAF2 was also observed to colocalise with the trans-Golgi marker TGN46, however, the distribution of TGN46 seemed to be disrupted, leading to a diffuse morphology relative to control cells.

This distribution of TGN46 was like that observed when cells have been treated with Brefeldin A (BFA) (Galea et al., 2015). BFA prevents retrograde traffic from the Golgi to the ER resulting in the collapse of the Golgi into the ER. Redistribution of the trans-Golgi marker TGN46 to the endosomal compartment is a side effect of BFA treatment. Interestingly, in this study, PRAF2 depletion was found to stabilise the Golgi in the presence of BFA, this suggested that PRAF2 acted to promote retrograde traffic. Perhaps the overexpression of PRAF2, which has been shown to localise to endosomes (Geerts et al., 2007) could be causing changes to the balance of retrograde traffic, resulting in a redistribution of TGN46. A similar phenotype was observed with PRAF3 and to a much lesser degree PRAF1.

An initial investigation suggested that truncating the N or C-terminal of PRAF2 did not alter its localisation to the ER or cis-Golgi. However, there was not time to repeat this experiment further, yet the initial indication is that no change in localisation to the ER or Golgi are observed. Another area PRAF2 has been demonstrated to be localised to are the Endosomes. However,

PRAF2 localisation to endosomes was not covered by this study but could be an interesting point of investigation, to determine if the mutations affect their localisation to endosomes.

Our study also investigated the localisation of HPV-18E5 for the first time, as most previous studies focus on HPV-6, 16 and BPV E5 (Disbrow et al., 2005; Disbrow et al., 2003; Ashrafi et al., 2005). GFP tagged HPV-18E5 co-localised with calnexin in the ER, which has previously been demonstrated as an interacting partner for HPV-16E5 (Gruener et al., 2007). HPV-18E5 appeared to also lack localisation to the Golgi, agree with what had previously been observed for HPV-16E5 (Suprynowicz et al., 2010). HPV-16E5 has also been demonstrated to localise to endosomes and lysosomes (Lewis et al., 2008), however this was not investigated, but could be of future interest, as there was suggestion that PRAF2 might also localise to these (Borsics et al., 2010). Additionally, these images are of a far higher resolution than those previously taken.

Further to this, the localisation of PRAF2 and its mutants with HPV18E5 was examined. Our studies showed that all PRAF2 mutants retained localisation with HPV18E5. This ruled out the possibility that the loss of interaction phenotype observed for 3xFLAG-PRAF2 1-135 was due to a change in the subcellular localisation of the mutant, resulting in localisation to a separate membrane compartment, as both localised to the ER. This was the same compartment as GFP-18E5 was localised to, and indeed the two still co-localised.

The subcellular localisation of PRAF1 and PRAF2 was also examined, with PRAF1 localised strongly to the cis-Golgi, whereas PRAF3 stained strongly in the ER and did not localise to the cis-Golgi. This was broadly in agreement with what had been observed previously (Abdul-Ghani et al., 2001). Interestingly PRAF1 appeared to be in the ER, however colocalisation analysis suggested this was not the case. The illusion of co-localisation could be due to the very high levels of PRAF1 expressed and strong intensity of calnexin staining giving the appearance of co-localisation.

We also investigated whether PRAF1 and PRAF3 would co-localise with GFP-18E5 and this was observed to be the case. PRAF1 and PRAF3 also were immunoprecipitated by GFP-18E5. That PRAF1 and PRAF3 are also interactors for HPV18E5 was interesting, but not surprising, as there was overlap between the reported functions of PRAF2 and its other family members (Vento et al., 2010), as both PRAF1 and PRAF3 have been reported to be involved with ER-golgi and vesicle trafficking and to associate with Rab proteins (Liu, H.P. et al., 2011; Lee, H.J. et al., 2011; Oshikane et al., 2018). In addition, PRAF2 was capable of immunoprecipitating PRAF3 (Schweneker et al., 2005), and a certain degree of functional redundancy exists (Vento et al., 2010). Clearly, regulation of protein trafficking is important to HPV18E5. However, PRAF2 can also hetero-oligomerise with PRAF1 and PRAF3, so it is possible that the immunoprecipitation of the other PRAF's is via PRAF2. To rule this out, immunoprecipitations could be carried out in cell lines with shPRAF2.

Our data also demonstrated that this interaction was evolutionarily conserved, as PRAF2 was successfully immunoprecipitated by a panel of E5s from a variety of high and low risk HPVs, as well as BPV. It has previously been demonstrated that PV E5s share cellular targets, such as EGFR pathway (Wasson et al., 2017; Fehrmann et al., 2003; Pim et al., 1992), so it should not be surprising that other targets are also conserved.

The direct targeting of PRAF2 by other HPV E proteins was ruled out. However, caution must be exercised regarding the interaction of PRAF2 and HPV18E1 and E2, as the proteins never expressed well enough to truly determine if they could affect each other. However, judging by the cellular localisation of PRAF2 and its known functions, it was unlikely that it would directly interact with E1 and E2, however there was the possibility that they could regulate the expression of PRAF2. The other HPV18 oncoproteins E6 and E7 showed no ability to bind PRAF2, so a direct interaction between them can be ruled out. However, they could exert effects on PRAF2 indirectly, through their wide-ranging effects on the host cell. Overexpression of GFP-

tagged HPV18 oncoproteins showed no effect on PRAF2 levels at the protein level. However, again this does not mean that they could not influence PRAF2, as they have large effects on the cellular landscape.

This study also investigated the expression of PRAF2 in several cervical cancer cell lines, including the HPV negative C33A, HPV16 positive CaSki and SiHa and the HPV18 Positive HeLa and SW756. Of these cell lines, only CaSki has been demonstrated to express E5 (Sahab et al., 2012). The PRAF2 protein was observed to be expressed in C33A, CaSki and SiHa cells, but not HeLa or SW756 cells. PRAF2 was observed to be statistically significantly increased in SiHa cells relative to C33A cells, and statistically significantly decreased in HeLa and SW756 cells relative to C33A. It was interesting that the HPV18 positive cell lines lost PRAF2 expression, but the negative and HPV16 positive cell lines maintained its expression. However, without knowing how the PRAF2 gene is regulated, it is difficult to ascertain as to why this is.

## Chapter 4 PRAF2, cancer and keratinocyte differentiation

### 4.1 Introduction

#### 4.1.1 PRAF2 and cancer

PRAF2 has been shown to be overexpressed in a variety of cancers, and indeed is a marker for poor prognosis in many, such as colorectal cancer, ESCC, hepatocellular carcinoma, malignant glioma and neuroblastoma (He et al., 2019; Qian et al., 2019; Wang, C.H. et al., 2018; Yco et al., 2013; Borsics et al., 2010; Geerts et al., 2007). PRAF2 has been seen expressed in a variety of cancer cell lines (Borsics et al., 2010). Previously we have demonstrated that PRAF2 is expressed in the HPV negative cervical cancer cell line C33A, and in the HPV-16 positive cervical cancer cell lines CaSki and SiHa, but not HPV-18 positive cancer cell lines HeLa and SW756 (Figure 3.23). Interestingly, PRAF2 is seen as a positive prognostic marker in cervical cancer (Uhlen et al., 2017), with a 20% increase in the survival rate of those with PRAF2 high cervical cancer.

The oncogenic potential of the PRAF2 protein in cancer has been previously investigated. In neuroblastoma cell lines such as SK-N-SH, knockdown of PRAF2 by shRNA resulted in decreased cellular proliferation as determined by BrdU proliferation assay, reduced cell viability and resulted in cell cycle arrest in G1 as assayed by flow cytometry (Yco et al., 2013). Furthermore, cell migration and attachment were also reduced by PRAF2 knockdown as determined by scratch assays and extra-cellular matrix adhesion assays respectively. Indeed, high PRAF2 expression in neuroblastoma is correlated with increased metastasis (Yco et al., 2013; Geerts et al., 2007). Similar results were seen in glioblastoma, with PRAF2 knockdown resulting in reduced cell viability, migration and invasive potential as determined by MTS assay and transwell migration and invasion assays respectively (Borsics et al., 2010). In ESCC, PRAF2 knockdown impeded cell proliferation, cell cycle progression and cell invasiveness as determined by absorbance, flow cytometry and transwell assays respectively (Qian et al., 2019).

Additionally, this also resulted in the induction of apoptosis in these cell lines, as determined by Annexin V staining and caspase-3 cleavage. Supporting the oncogenic potential of PRAF2 is its ability to drive increased cell viability, colony formation and cell migration when overexpressed in hepatocellular carcinoma cell lines, and to increase tumour growth and metastasis in xenografts (Wang, C.H. et al., 2018). Furthermore, PRAF2 has been shown to promote colorectal cancer metastasis through the promotion of paracrine signalling (He et al., 2019). This contrasts with the PRAF2 proteins previously reported proapoptotic roles (Geerts et al., 2007; Vento et al., 2010).

Other members of the PRAF family have also been investigated with regards to cancer. PRA family member PRAF1 is reported to inhibit TCF/beta-catenin signalling, a pathway known to be dysregulated in cancer (Kim, J.T. et al., 2006). PRAF1 knockdown has been shown to increase cell motility as demonstrated by wound healing assays (Liu, H.P. et al., 2011) and overexpression of PRAF1 has been shown to induce apoptosis, demonstrated by increased PARP and caspase-3 cleavage (Kim, J.T. et al., 2019). This would suggest that PRAF1 can function as a tumour suppressor. The other PRA family member PRAF3 has been studied in far more detail than either PRAF1 or PRAF2. Studies on PRAF3 suggest that PRAF3 acts as a tumour suppressor.

A reduction of PRAF3 expression is seen in various cancers, including bladder cancer, breast cancer, ESCC, gastric cancer, hepatocellular carcinoma and melanoma (Tang, W.Y. et al., 2007; Xu, L. et al., 2018; Lu et al., 2013; Zhou, J. et al., 2012; Xu, W. et al., 2014; Wu, X. et al., 2014). Indeed, in these cancers the loss of PRAF3 expression can be considered a negative prognostic marker. Knockdown of PRAF3 in various cancer cell lines has been carried out with similar results. Knockdown in breast cancer cells increased invasion and migration and decreased sensitivity to apoptosis as determined by transwell, scratch and MTT assays respectively (Xu, L. et al., 2018; Chen, X. et al., 2015). Similar results are seen with hepatocellular cancer, with a reduction in the levels of PRAF3 resulting in increased migration, adhesion and

invasion (Wu, X. et al., 2014). Similarly loss of PRAF3 in melanoma increased migration and invasion as determined by transwell assays and promoted metastasis in xenografts (Bai et al., 2010). These data suggest that PRAF3 acts as a tumour suppressor. This is further supported by PRAF3 overexpression data. When overexpressed, PRAF3 abrogated angiogenesis in melanoma, whereas knockdown was seen to promote angiogenesis as determined by Human umbilical vein endothelial cell (HUVEC) growth and tube formation assay (Chen, Y. et al., 2014; Lu et al., 2013). Additionally, PRAF3 overexpression in HeLa, B16 and HCCLM3 cancer cells inhibits migration in wound healing assays (Chen, H. et al., 2007). Finally, PRAF3 overexpression was also seen to decrease breast cancer cell lines migration and invasion potential (Xu, L. et al., 2018), with similar findings in gastric cancer (Kim, J.T. et al., 2019).

The literature for PRAF3 strongly supports its activity as a tumour suppressor, whereas the literature for PRAF2 suggests it has both oncogenic and tumour suppressor capabilities, however most literature suggests an oncogene function. This is interesting when considering the evolutionary history of the PRA family. The ancestral protein that gave rise to PRAF2 and PRAF3 diverged from PRAF1 first, before giving rise to PRAF2 and PRAF3. Both PRAF1 and PRAF3 have tumour suppressor activity, therefore it would be expected that PRAF2 would also, however, this does not appear to be the case. This could suggest that the processes that PRAF2 regulates might act in opposition to those that the other PRAF proteins regulate.

#### **4.1.2 The PRAF family- trafficking and signalling**

PRA family members have been reported to be able to alter signalling within cells. PRAF1 has been shown to be able to inhibit TCP/ $\beta$ -catenin signalling, through the sequestration of  $\beta$ -catenin in the cytosol through its direct binding. PRAF1 overexpression was also associated with dephosphorylation of ERK1/2 and decreased cyclin D1 levels (Kim, J.T. et al., 2006). Additionally, PRAF1 interacts with NDRG2 to dephosphorylate GSK3 $\beta$  and as a result decrease  $\beta$ -catenin signalling through preventing its nuclear translocation as assessed by western blotting,

fractionation and immunofluorescence (Kim, J.T. et al., 2012). PRAF1 has also been shown to modulate the trafficking of receptors, for example in tomatoes, PRAF1 was demonstrated to regulate trafficking and localisation of the PRR LeEIX2, in addition to its degradation (Pizarro et al., 2018). PRAF3 has also been demonstrated to regulate the G-protein coupled receptor (GPCR) CXCR4. Overexpression of PRAF3 resulted in a decrease in CXCR4 levels through proteasomal degradation, resulting in reduced cell surface CXCR4 expression and decreased Akt signalling in breast cancer cell lines (Xu, L. et al., 2018).

PRAF2 has also been demonstrated to regulate the levels of GPCRs. For example, PRAF2 controls the cell surface expression of the GPCR GABA<sub>b</sub>, preventing its exit from the ER and further progression along its biosynthetic pathway (Doly et al., 2016), and as a result influencing GABA signalling. Another GPCR identified as an interactor for PRAF2 is CCR5 (Schweneker et al., 2005), with PRAF2 overexpression resulting in a decrease in CCR5 levels within the cell as determined by western blotting, and reduced cell surface expression, as determined by flow cytometry. This could possibly be of interest in cancers, as CCR5 is known to increase the invasiveness and metastasis of glioblastoma (Zhao et al., 2015) and antagonists of CCR5 decrease invasiveness and metastasis of breast cancer, glioblastoma, melanoma and prostate cancer (Velasco-Velázquez et al., 2012; Sicoli et al., 2014; Zhao et al., 2015; Liu, J. et al., 2019). CCR5 levels are also elevated in cervical cancers, and its expression is regulated by EGFR (Sales et al., 2014)

#### **4.1.3 The PRAF proteins and differentiation**

Little is known regarding the PRAF proteins and differentiation. Currently, the only information available is for PRAF1 and PRAF3. PRAF1 expression has been followed in the development of mouse retinas, with PRAF1 possibly playing a role in vesicular trafficking during photoreceptor differentiation. Levels are seen to increase up until the photoreceptor is fully mature, at which point they decrease (Dickison et al., 2012). With regards to PRAF3, when

human myeloid leukaemia cells were differentiated via chemical stimulus, levels of PRAF3 were seen to increase in a time dependent manner, and when PRAF3 was knocked out the differentiation of myeloid leukaemia cells was impaired (Huang et al., 2006a; Huang et al., 2006b). In PRAF3 knockout mice bone morphogenesis is disrupted, with osteoblast proliferation and differentiation disrupted, in addition osteoblasts are under increased ER-stress, resulting in ER-stress mediated apoptosis (Wu, Y. et al., 2014). Furthermore, osteoclastogenesis is increased by PRAF3 knockdown through increased levels of RANKL. This results in a loss of bone density. Interestingly, when PRAF3 is overexpressed, levels of RANKL remain the same yet are retained in the ER, resulting in decreased osteoclastogenesis. This indicates that PRAF proteins control of cellular trafficking events can be important to cellular differentiation. Currently, nothing is known regarding PRAF2 and cellular differentiation.

The aim of this chapter is to explore the role of PRAF2 in cervical cancer and cellular differentiation. Cervical cancer cell lines are used as models, with overexpression and knockdown of PRAF2 used to determine its relationship with cervical cancer. The HPV primary keratinocyte system is used to inform the role of PRAF2 in keratinocyte differentiation.

## 4.2 Results

### 4.2.1 PRAF2 did not alter EGFR cell surface expression in cervical cancer cell lines

PRAF2 has previously been demonstrated to be involved in cell surface receptor trafficking. As a result, the receptor tyrosine kinase EGFR was investigated owing to its importance in HPV biology and as it is a pathway influenced by E5, a known PRAF2 interactor. To study this stable cell lines were generated from cervical cancer cell lines. The HPV negative cell line C33A, HPV16 positive cell line SiHa and the HPV18 positive cell line HeLa were used. Stable cell lines were generated using lentiviruses. Cell lines stably expressing control non-targeting short hairpin RNA (shNTC) and shRNA against PRAF2 (shPRAF2) were generated in the C33A and SiHa cell lines, as both have been demonstrated to express PRAF2 (Figure 3.23). Cell lines stably expressing either the green fluorescent protein zsGreen or PRAF2 were created in C33A and HeLa with HeLa cells selected owing to not expressing detectable levels of PRAF2 (Figure 3.23).

To confirm PRAF2 knockdown and overexpression cell pellets were taken from all stable cell lines in addition to control cells and lysed. Lysates were processed, and equal amounts of protein were loaded and resolved by SDS-PAGE. The resulting western blots were then probed with antibodies specific for PRAF2, EGFR and GAPDH. In C33A cells and C33A cells stably expressing shNTC (Lanes 1 and 2, Figure 4.1 A) a band of ~19 kDa could be observed corresponding to PRAF2. This band was absent in C33A cells expressing shPRAF2 (Lane 3, Figure 4.2 A), this indicated that PRAF2 had been successfully knocked down in C33A-shPRAF2. No difference was observed in EGFR expression between C33A, C33A shNTC and C33A shPRAF2. In SiHa cells and SiHa shNTC cells (Lanes 1 and 2, Figure 4.1 B) a band of approximately 19~ kDa was visible but was not present in SiHa shPRAF2 (Lane 3, Figure 4.1 B), this indicated the successful knockdown of PRAF2.

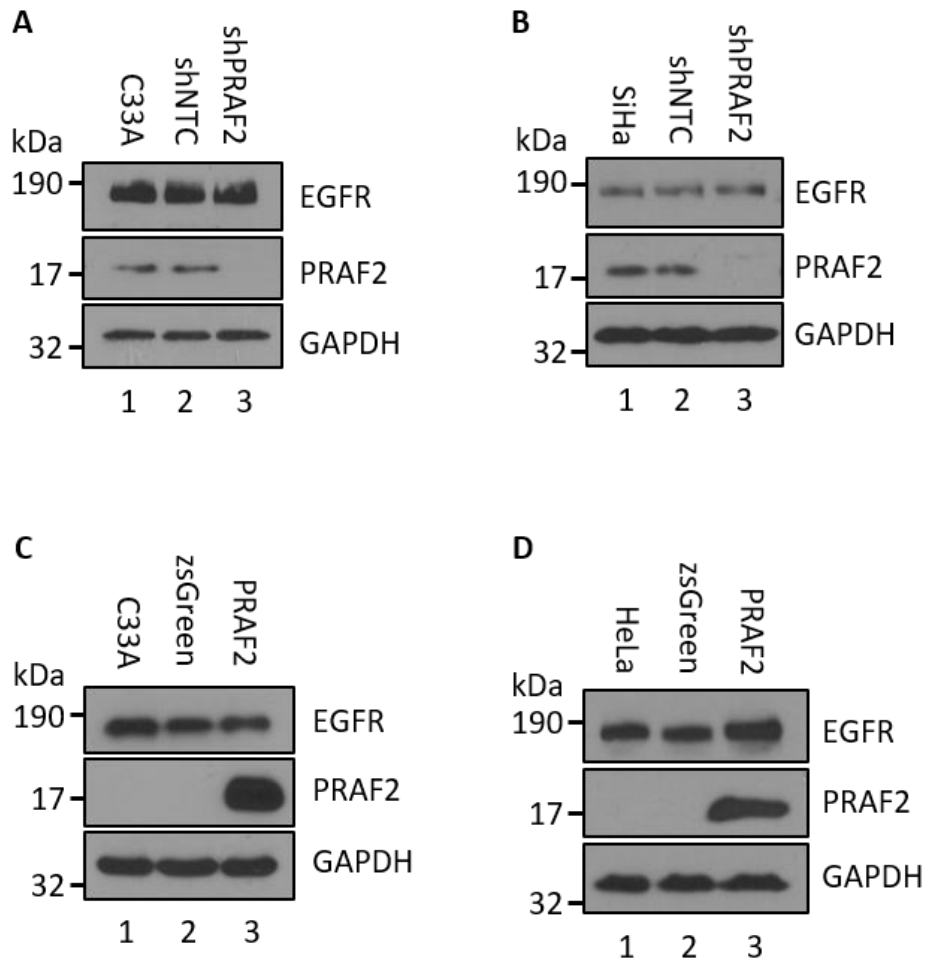


**Figure 4.1** *EGFR levels are unaffected by changes in PRAF2 in cervical cancer cell lines.*

Lysates from stable cell lines, equal amounts of protein were resolved by SDS PAGE and resulting blots probed for PRAF2, EGFR and GAPDH. Representative blots are shown A. C33A cells stably expressing either shNTC or shPRAF2 as well as control C33A cells. B. SiHa cells stably expressing either shNTC or shPRAF2 as well as control SiHa cells. C. C33A cells expressing either zsGreen or PRAF2 as well as control C33A cells D. HeLa cells expressing either zsGreen or PRAF2 as well as control HeLa cells. N=3.

No difference could be observed in the level of EGFR expression between SiHa, SiHa shNTC and SiHa shPRAF2. In C33A cells stably overexpressing PRAF2 (Lane 3, Figure 4.1 C) a strong band of ~19 kDa was observed, this indicated that PRAF2 had successfully been overexpressed. It should be noted that this exposure time was too short to detect the signal from endogenous PRAF2, at longer exposures overexpressed PRAF2 saturated the blot (see

Chapter 5, Figure 5.6 A). No difference was observed in the levels of EGFR between C33A, C33A zsGreen (Lanes 1 and 2, Figure 4.1 C) and C33A PRAF2. In HeLa cells overexpressing PRAF2 (Lane 3, Figure 4.1 D) a strong band of ~19 kDa was observed, this indicated that PRAF2 had successfully been overexpressed. No difference was observed in the levels of EGFR between HeLa, HeLa zsGreen (Lanes 1 and 2, Figure 4.1 D) and HeLa PRAF2. This indicated that PRAF2 overexpression did not affect the overall protein levels of EGFR in cervical cancer cell lines.

As no difference was observed in the total levels of EGFR protein in cells either expressing shPRAF2 or overexpressing PRAF2 it was decided to test whether PRAF2 was affecting

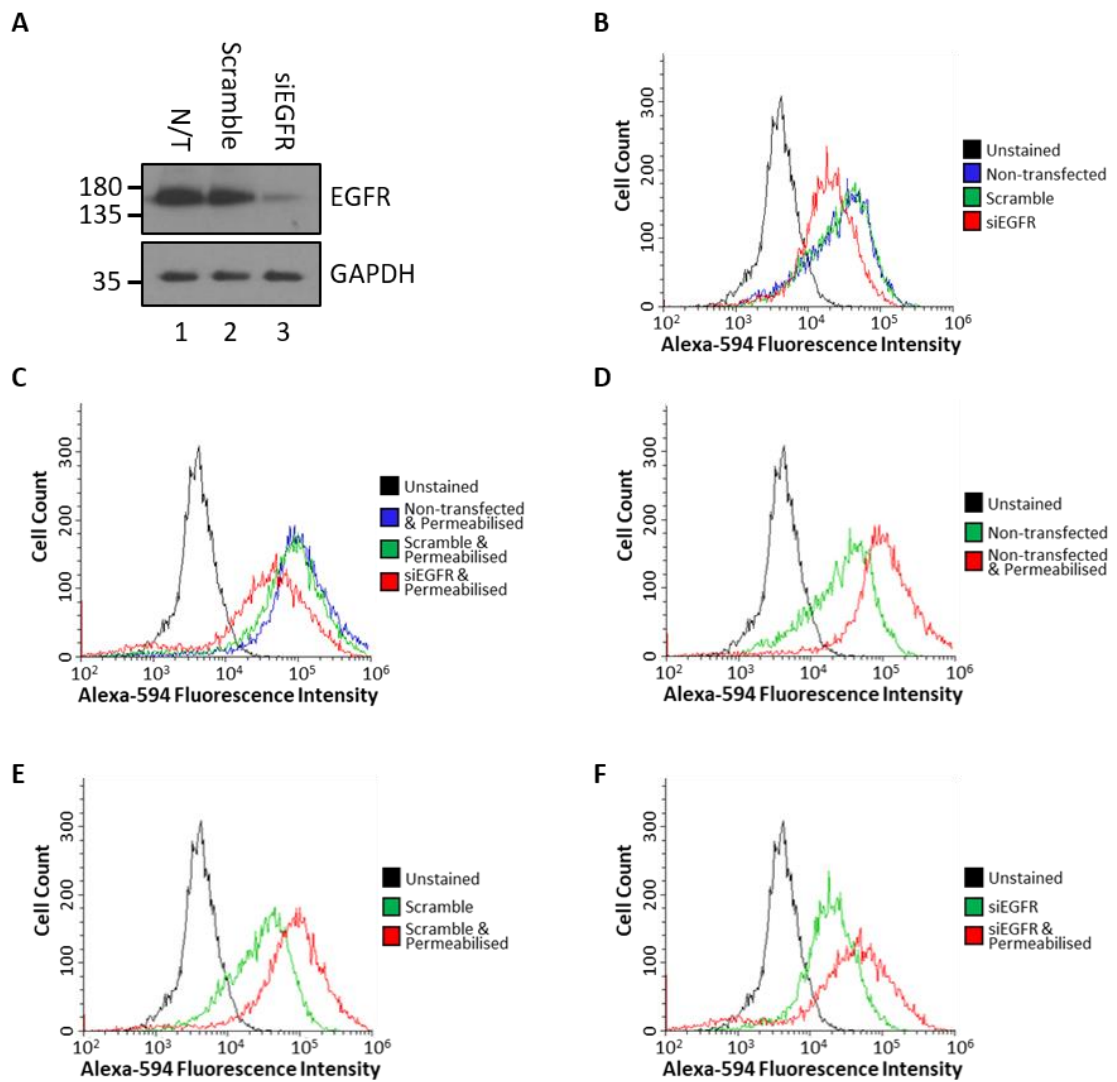


**Figure 4.2** *Flow cytometry detected cell surface EGFR in a specific manner*

*HeLa cells were transfected with scramble or siEGFR siRNA and harvested using cell dissociation buffer 72 hours post transfection and samples divided. A. Western blot of siEGFR samples. Equal amounts of protein were loaded, and samples probed for EGFR expression. N/T= non-transfected B-F Dissociated cells were fixed with 4% paraformaldehyde, blocked and probed with an antibody to EGFR, then stained with alexa-594 conjugated secondaries. Flow cytometry histograms of Alexa-594 stained EGFR. 561nm laser with a 585-42 BP filter. Histograms representative of 10000 cells. B. Comparison of non-permeabilised samples. C. Comparison of permeabilised samples. D. Comparison of non-transfected vs non-transfected permeabilised. E. Comparison of scramble vs scramble-non-transfected. F. Comparison of siEGFR vs siEGFR permeabilised. N=1.*

the trafficking of EGFR to the cell surface. To do so, cell surface EGFR was probed with a primary antibody and stained with a fluorescently conjugated secondary antibody. The samples were then assayed by flow cytometry. The intensity of fluorescence was then used as a read out for cells displaying cell surface EGFR. As a proof of concept, HeLa cells were transfected with small interfering (si) RNA against EGFR (siEGFR), and then harvested 72 hours post transfection. The population of cells were divided in two, with half fixed and processed for flow cytometry and the other half were lysed and processed for western blot. The resulting western blot (Figure 4.2 A) confirmed that the scramble siRNA (Lane 2, Figure 4.2 A) had comparable levels of EGFR to non-transfected control (Lane 1, Figure 4.2 A). When compared to non-transfected and scramble, siEGFR (Lane 3, Figure 4.2 A) resulted in a reduction in the level of that EGFR was observed. This confirmed the efficacy of the siRNA against EGFR.

The samples for flow cytometry were fixed in 4% paraformaldehyde and then divided into two separate samples, one of which was treated with 0.1% triton to permeabilise the cell membrane. These samples were then blocked and probed with the EGFR antibody, and then washed and stained with Alexa-594 conjugated secondary antibody. A sample of HeLa with the

secondary conjugate only was included as a control. The samples were then analysed by flow cytometry. Non-transfected, scramble and siEGFR (Figure 4.2 B) all fluoresced with greater intensity than unstained (black). A clear shift in the intensity of Alexa-594 could be observed in the siEGFR sample (Red, Figure 4.2 B) towards 'unstained' relative to scramble and control, this demonstrated that less EGFR had been detected. In the permeabilised samples (Figure 4.2 C) the intensity of EGFR staining was increased. However, the intensity of staining and the number of cell counts exhibiting EGFR staining in the siEGFR sample (red) was still decreased relative to the scramble and non-transfected samples. When permeabilised versus non-permeabilised samples (Figure 4.2, D-F) were compared, the intensity of Alexa-594 staining in the permeabilised samples (red) versus the non-permeabilised samples (green) was increased. This indicated that the assay was indeed staining surface EGFR and not total cellular EGFR, and the difference in intensity between scramble and siEGFR demonstrated that the assay can differentiate between different levels of EGFR expression in a specific manner.

This assay was then repeated with the stable cell lines generated previously to determine if PRAF2 expression was affecting cell surface levels of EGFR. C33A PRAF2 knockdown cell lines (Figure 4.3 A) all had histogram traces that overlaid, and no statistically significant difference could be detected in the total levels of cell surface EGFR (Figure 4.3 B). This suggested that PRAF2 knockdown did not affect levels of cell surface EGFR in C33As. Similar results were observed with PRAF2 knockdown in SiHa cells, the histogram traces overlaid (Figure 4.3 C) and no significant difference in cell surface EGFR was seen (Figure 4.3 D) compared to controls. In C33A cells that overexpressed PRAF2, the histograms overlaid (Figure 4.3 E) and no significant difference could be seen in cell surface EGFR (Figure 4.3 F) when compared to controls. The same was true of HeLa cells overexpressing PRAF2 (Figure 4.3 G and H), with no statistically significant difference observed. Taken together these data suggested that PRAF2 knockdown and overexpression did not influence levels of EGFR in the cell lines tested.

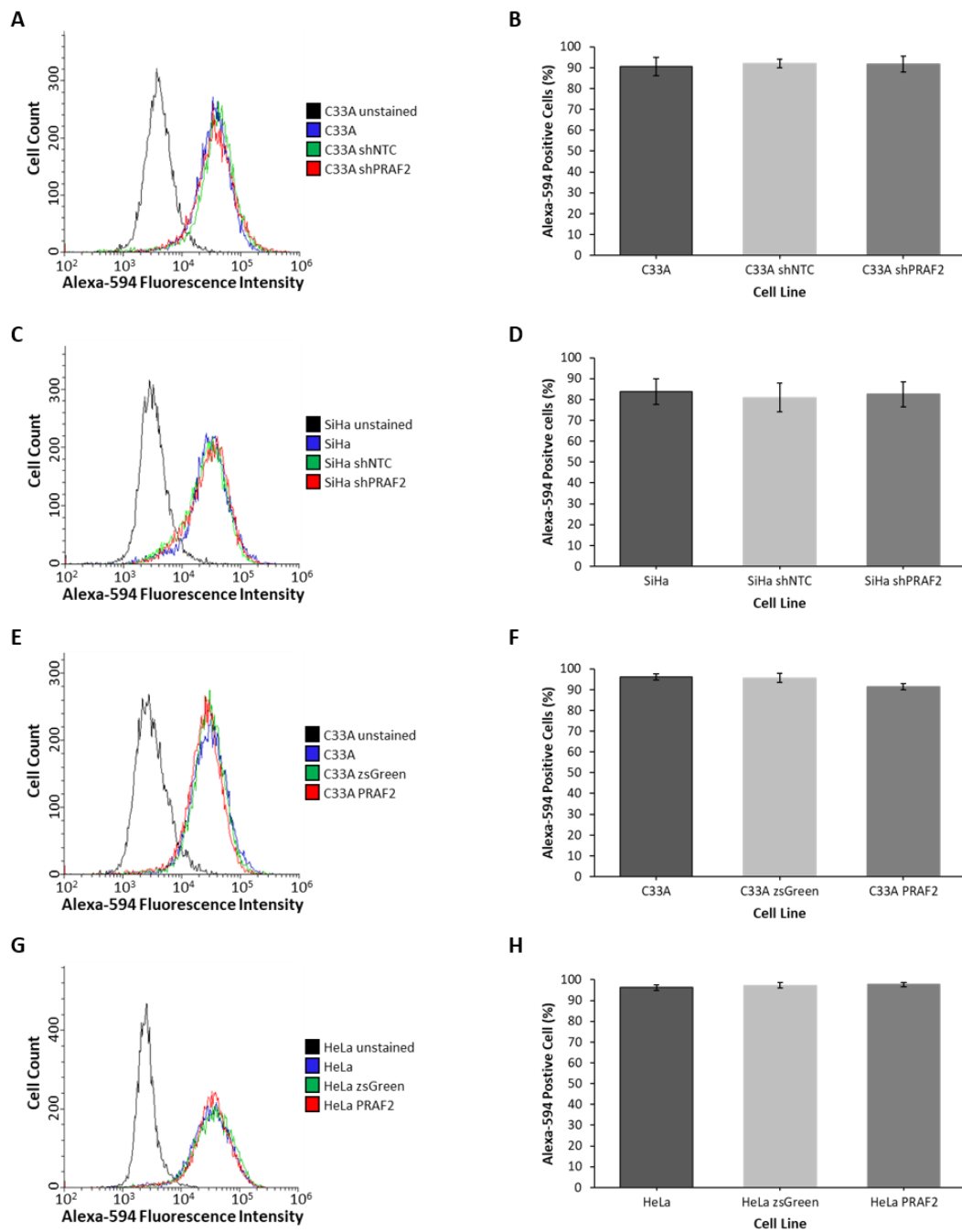


**Figure 4.3** Cell surface EGFR expression was not altered by changes in PRAF2 expression

Stable cell lines were harvested and probed for cell surface EGFR expression, then stained with Alexa-594 and analysed by flow cytometry with 561nm laser with a 585-42 BP filter. A, C, E and G. Flow cytometry histograms of Alexa-594 stained EGFR. Histograms representative of 10000 cells. N=3. B, D, F and H Average Alexa-594 positive cells (%) per cell line. N=3. Error bars show standard deviation. A, B. C33A, C33A shNTC and C33A shPRAF2. C, D. SiHa, SiHa shNTC and SiHa shPRAF2. E, F. C33A, C33A zsGreen and C33A PRAF2. G, H. HeLa, HeLa zsGreen and HeLa PRAF2.

#### 4.2.2 PRAF2 did not alter cell cycle progression in cervical cancer cell lines

Stable cell lines expressing shPRAF2 were assayed to determine if the cell cycle was altered due to loss of PRAF2 expression. Previous studies on PRAF2 knockdown in ESCC and neuroblastoma had demonstrated that loss of PRAF2 expression resulted in a G1 arrest (Qian et al., 2019; Yco et al., 2013). Cells were lysed and equal amounts of protein resolved by SDS-PAGE. The resulting blots were probed for Cyclin A1, Cyclin B1, Cyclin D1, Cyclin E1, PRAF2 and GAPDH. In the C33A shPRAF2 knockdown cell line (Lane 3, Figure 4.4 A) there was a clear knockdown of the PRAF2 protein. This did not result in any changes to the total levels of any of the cyclin proteins, relative to the control and shNTC control, which suggested no obvious change had occurred to the cell cycle. The same was true for the SiHa shPRAF2 cell line (Figure 4.4 B), which also demonstrated a loss of PRAF2 protein expression.

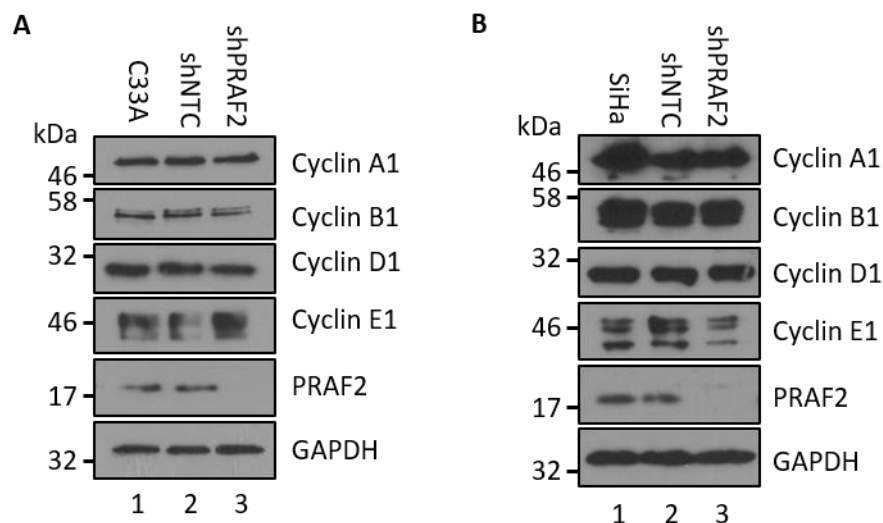


**Figure 4.4 PRAF2 knockdown in C33A and SiHa cells did not alter cyclin expression**

C33A and SiHa cell lines stably expressing shRNA against PRAF2 or control NTC were lysed and equal amounts of protein were resolved by SDS PAGE and resulting blots were probed for cyclin A1, cyclin B1, cyclin D1, cyclin E1, PRAF2 and GAPDH. A representative blot is shown. N=3. A. C33A, C33A shNTC and C33A shPRAF2 cell lines. B. SiHa, SiHa shNTC and SiHa shPRAF2.

We then asked if the same was true of PRAF2 overexpression. Both transiently transfected and stably expressing cell lines were investigated. Transient expression was chosen to test if the potentially higher temporary levels of expression would influence the cellular environment to a greater degree. C33A and HeLa cells were transfected with either pcDNA3.1+ or PRAF2-3HA using Lipofectamine 2000, then lysed 48 hours post transfection. Equal amounts of protein from the processed lysates were then resolved by SDS-PAGE. The resulting western blots were then probed for Cyclin A1, Cyclin B1, Cyclin D1, Cyclin E1, HA and GAPDH. No difference could be observed in the levels of cyclins expressed in cells overexpressing PRAF2-3HA (Figure 4.5 A and B) and pcDNA3.1+ in either C33A (Figure 4.5 A) or HeLa (Figure 4.5 B). Lysates from C33A and HeLa cells that stably overexpressed PRAF2 were also blotted for Cyclin A1, Cyclin B1, Cyclin D1, Cyclin E1, PRAF2 and GAPDH. In C33A cells overexpressing PRAF2 (Lane 3, Figure 4.5 C) no difference was observed between control C33A or C33A shNTC samples (Lanes 1 and 2, Figure 4.5 C). The same was also true for the HeLa stable cell lines (Figure 4.5 D), with no clear difference in cyclin expression observed between HeLa, HeLa shNTC and HeLa shPRAF2. From this we could determine that there was no clear difference in cyclin expression between the cell lines.

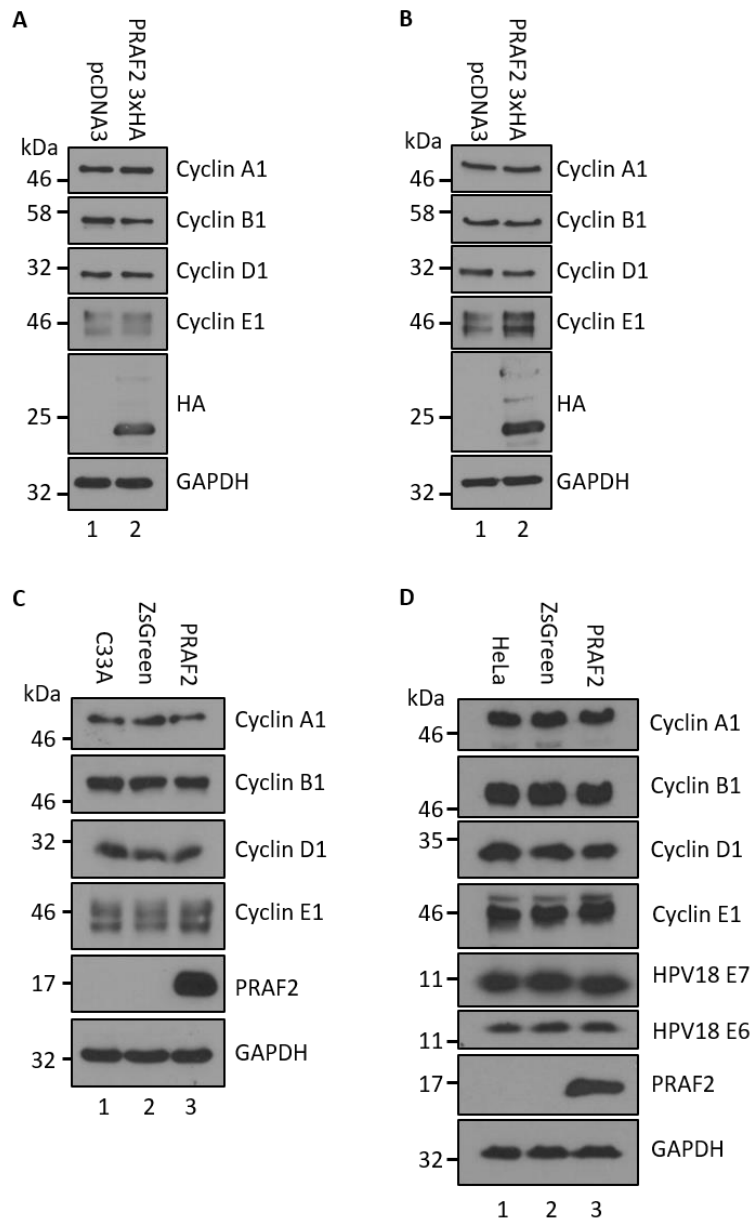


**Figure 4.5** *Transiently and stably expressed PRAF2 did not alter cyclin expression in C33A and HeLa cells*

C33A and HeLa cell lines transiently or stably overexpressing PRAF2 were lysed and equal amounts of protein were resolved by SDS PAGE and resulting blots were probed for cyclin A1, cyclin B1, cyclin D1, cyclin E1, HA-PRAF2 and GAPDH. A representative blot is shown. N=3 A. Transient overexpression of PRAF2-3HA in C33A cells. B. Transient overexpression of PRAF2-3HA in HeLa cells. C. Stable overexpression of either zsGreen or PRAF2 in C33A cells. D. Stable overexpression of either zsGreen or PRAF2 in HeLa cells.

To confirm that cell cycle progression was not impaired, cell cycle phase was determined by flow cytometry. Cells were harvested, fixed and permeabilised with ethanol and treated with RNase then treated with Propidium Iodide to stain DNA and analysed by flow cytometry. No significant difference was observed between C33A, C33A shNTC and C33A shPRAF2 (Figure 4.6 A) in their cell cycle profiles. No significant difference was observed between shPRAF2 SiHa cells and the

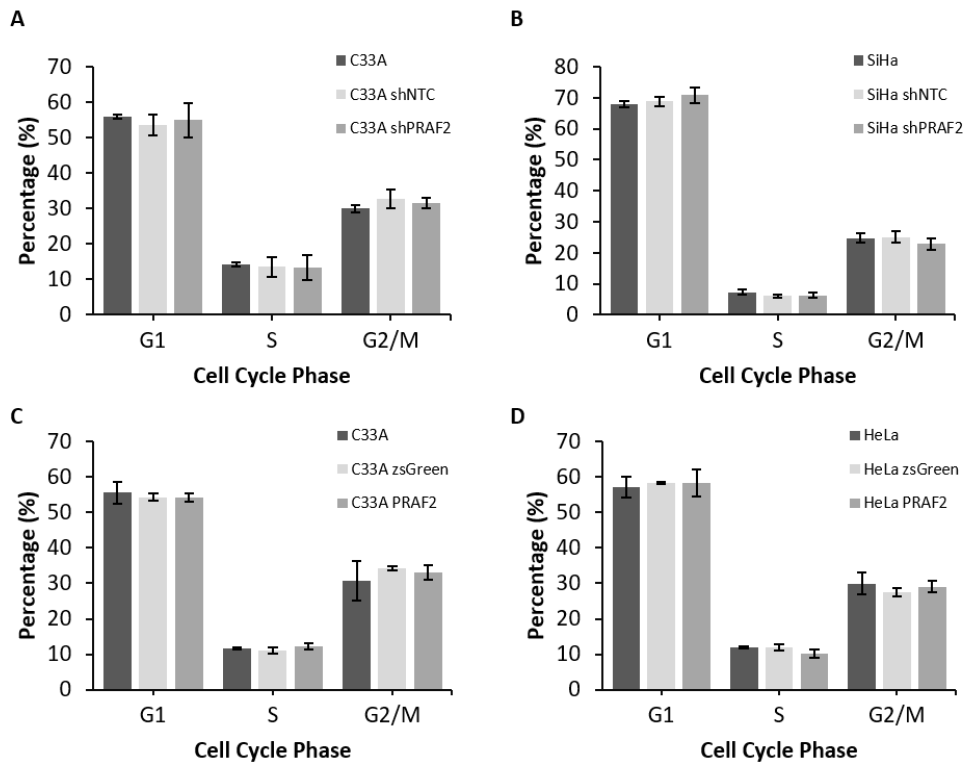


**Figure 4.6** Alterations in PRAF2 expression did not alter cell cycle progression in cervical cancer cell lines.

Stable cell lines were trypsinised, fixed in ethanol, blocked and then stained with propidium iodide and the DNA content of the cells determined by flow cytometry. PI excited at 561 nm, 585-42BP filter used. N=3. Each repeat 10000 events. A. Cell cycle profiles of C33A, C33A shNTC and C33A shPRAF2 cell lines. B. Cell cycle profiles of SiHa, SiHa shNTC and SiHa shPRAF2. C. Cell cycle profiles of C33A, C33A zsGreen and C33A PRAF2. D. Cell cycle profiles of HeLa, HeLa zsGreen and HeLa PRAF2.

SiHa or SiHa shNTC cell lines (Figure 4.6 B). Neither the C33A or HeLa PRAF2 overexpressing cell lines (Figure 4.6 C and D) showed any changes in their cell cycle profiles when compared to controls. These data agree with the western blot data (Figure 4.4 and Figure 4.5). In the cervical cancer cell lines tested PRAF2 overexpression or knockdown did not alter cell cycle progression.

#### **4.2.3 Loss of PRAF2 expression impaired the ability of SiHa to form colonies.**

Previous studies had reported that in ESCC that PRAF2 knockdown resulted in reduced colony formation (Qian et al., 2019), and PRAF2 overexpression in hepatocellular carcinoma enhanced the ability of cancer cells to form colonies (Wang, C.H. et al., 2018). The ability of the stable cervical cancer cell lines to proliferate and form colonies was therefore investigated by colony formation assay. 500 cells of each cell line were seeded per well of a 6 well plate and then the cells were cultured for 2 weeks and then fixed and stained with crystal violet to assess the level of colony formation.

C33A shRNA cell lines (Figure 4.7 A) were successfully able to form colonies. When quantified there was no statistically significant difference in the number of colonies formed by C33A shPRAF2 compared to either C33A or C33A shNTC. There was also no statistically significant difference in colonies formed by C33A shNTC when compared to C33A or C33A shPRAF2. Interestingly, the ability of the HPV16 positive cell line SiHa (Figure 4.7 B) to form colonies was impaired by the loss of PRAF2. SiHa shPRAF2 demonstrated a significantly impaired ability to form colonies compared to SiHa (\*\* $p \leq 0.0001$ ) and SiHa shNTC (\*\* $p \leq 0.0001$ ). There was no statistically significant difference observed in the ability of SiHa shNTC to form colonies relative to SiHa. This suggested that PRAF2 was important for SiHa colony formation. As a result, the SiHa shPRAF2 cell line was compared to SiHa shNTC in its ability to form colonies in an anchorage independent manner (Figure 4.7 E, assay performed by Dr Ethan L Morgan, University of Leeds). It was found that SiHa shPRAF2 cells showed a statistically significant reduction in colony formation (\* $p \leq 0.05$ )

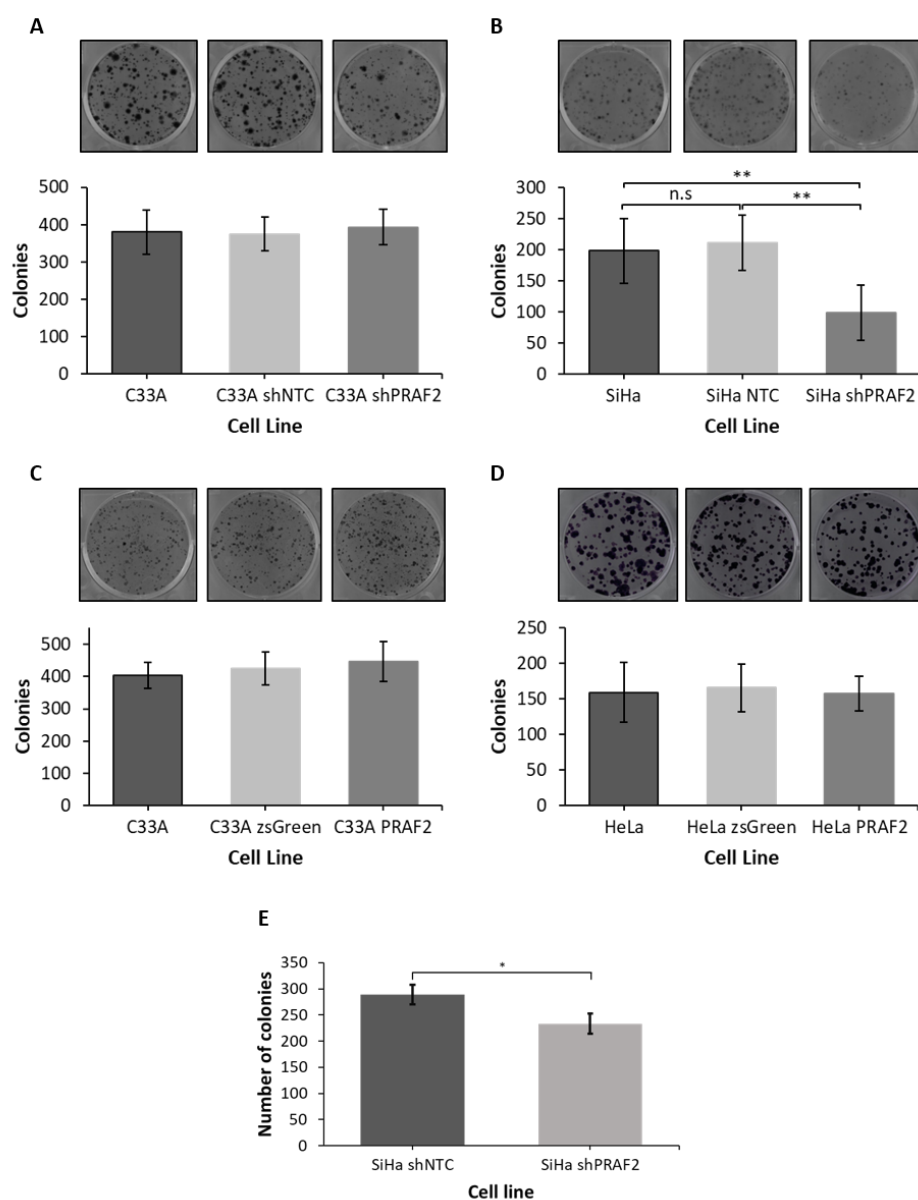


**Figure 4.7** Colony formation of SiHa but not C33A or HeLa cells was impaired by alterations to PRAF2 expression

A-D colony formation assays. 500 cells were seeded and stained after 2 weeks of growth. Representative images shown, assay performed in triplicate, N=3. Two-tailed paired students *t*.test performed, error bars standard deviation. A. C33A, C33A shNTC and C33A shPRAF2. B. SiHa, SiHa shNTC and SiHa shPRAF2 **\*\*** $p \leq 0.0001$ . C. C33A, C33A zsGreen and C33A PRAF2. D. HeLa, HeLa zsGreen and HeLa PRAF2. E. Soft Agar colony formation assay. Cells were grown for 38 days before fixation,  $p \leq 0.05$ . Assay performed by Dr Ethan L Morgan, University of Leeds.

relative to SiHa shNTC and were impaired in their ability to grow in an anchorage independent manner.

C33A PRAF2 cell lines were able to successfully form colonies (Figure 4.7 C), and no statistically significant difference in colony formation was observed between C33A PRAF2 and control C33A cells or C33A zsGreen cells, nor was there any statistically significant difference between C33A zsGreen cells and C33A or C33A PRAF2 cell lines. The same was also true for the HPV18 positive HeLa cell line (Figure 4.7 D) with no statistically significant difference observed between HeLa PRAF2 cells and HeLa or HeLa zsGreen in their ability to form colonies. Overall, only SiHa cells demonstrated a significant change in their ability to form colonies.

#### **4.2.4 PRAF2 overexpression enhanced proliferation in C33A cells**

PRAF2 knockdown had previously been observed to decrease the proliferative ability of cancer cell lines from cancers such as neuroblastoma and ESCC (Yco et al., 2013; Qian et al., 2019) and overexpression of PRAF2 was observed to enhance the proliferative potential of hepatocellular carcinoma cell lines (Wang, C.H. et al., 2018). To assess whether cell proliferation was affected by PRAF2 levels the PRAF2 stable cell lines were used to perform growth assays. 25000 (HeLa) or 75000 (C33A/SiHa) were seeded, and cells counted every 24 hours for 120 hours.

C33A shPRAF2 cells displayed no statistically significant change in growth rates when compared to C33A or C33A shNTC cells (Figure 4.8 A) across all time points. No difference was observed for C33A shNTC cells when compared to C33A and C33A shPRAF2 cells. SiHa shPRAF2 cells displayed no overall change in growth rates (Figure 4.8 B) relative to control SiHa and SiHa shNTC cells except at 96 hours when there was a statistically significant increase in SiHa shNTC growth rate relative to SiHa and SiHa shPRAF2 ( $p \leq 0.05$ ), however, this difference disappears by 120 hours. In C33A PRAF2 cells a statistically significant increase in growth rate relative to C33A and C33A zsGreen was observed ( $*p \leq 0.05$ ) at the 120-hour timepoint (Figure 4.8 C), however

this was only observed at the final timepoint so should be treated with caution. For HeLa cells, the data set for HeLa zsGreen was incomplete so was not included in the analysis. However, no statistically significant difference could be detected between HeLa and HeLa PRAF2 in growth rates (Figure 4.8 D).

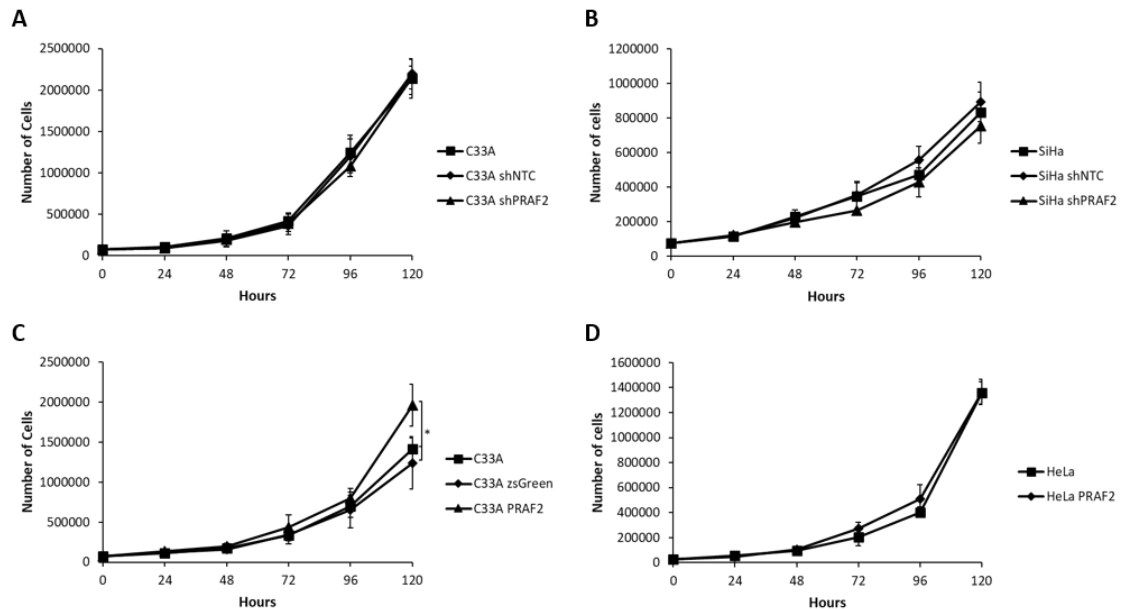


**Figure 4.8** PRAF2 knockdown did not affect C33A or SiHa cell growth rates, however overexpression increased growth in C33A but not HeLa cells.

HeLa (25,000) or C33A/SiHa (75,000) cells were seeded, and cells counted every 24 hours for 120 hours.  $N=3$ , statistical analysis Two-tailed paired students T-test, error bars are standard deviation. A. C33A, C33A shNTC and C33A shPRAF2. B. SiHa, SiHa shNTC and SiHa shPRAF2. C. C33A, C33A zsGreen and C33A PRAF2,  $*p \leq 0.05$ . D. HeLa and HeLa PRAF2.

#### 4.2.5 PRAF2 knockdown impairs wound closure by SiHa cells

It has previously been observed that knockdown of PRAF2 impairs migration as determined by wound healing assay in neuroblastoma (Yco et al., 2013), as well as migration in transwell assays in hepatocellular carcinoma and glioma (Qian et al., 2019; Borsics et al., 2010). To determine if the level of PRAF2 expression affected the migration ability of cervical cancer

cell lines, wound healing assays were performed. The stable cell lines generated previously were seeded out, and they were grown until a confluent monolayer had developed. The monolayer was then scratched with a pipette tip. The resulting scratch was cleaned with PBS, media applied and then the scratch was imaged. After 24 hours the scratch was reimaged, and the percentage wound closure was calculated.

C33A shPRAF2 cells demonstrated no significant difference in wound closure when compared to C33A shNTC cells (Figure 4.9 A). However, both C33A shPRAF2 and C33A shNTC demonstrated a statistically significant reduction in wound closure relative to the control C33A cells. SiHa shPRAF2 cells demonstrated a significantly reduced ability to close wounds relative to SiHa shNTC and SiHa cell lines (Figure 4.9 B,  $p \leq 0.001$  and  $p \leq 0.01$  respectively), this suggested that PRAF2 was enhancing SiHa cells migratory ability. C33A PRAF2 cells displayed no significant difference in wound healing compared to control C33A zsGreen and C33A cells (Figure 4.9 C), nor was there any observed difference between the controls. Finally, no significant difference was observed between HeLa PRAF2 (Figure 4.9 D) cells ability to close wounds relative to the control HeLa or HeLa zsGreen cells. It appeared that only in SiHa cells does the loss of PRAF2 impair wound healing.

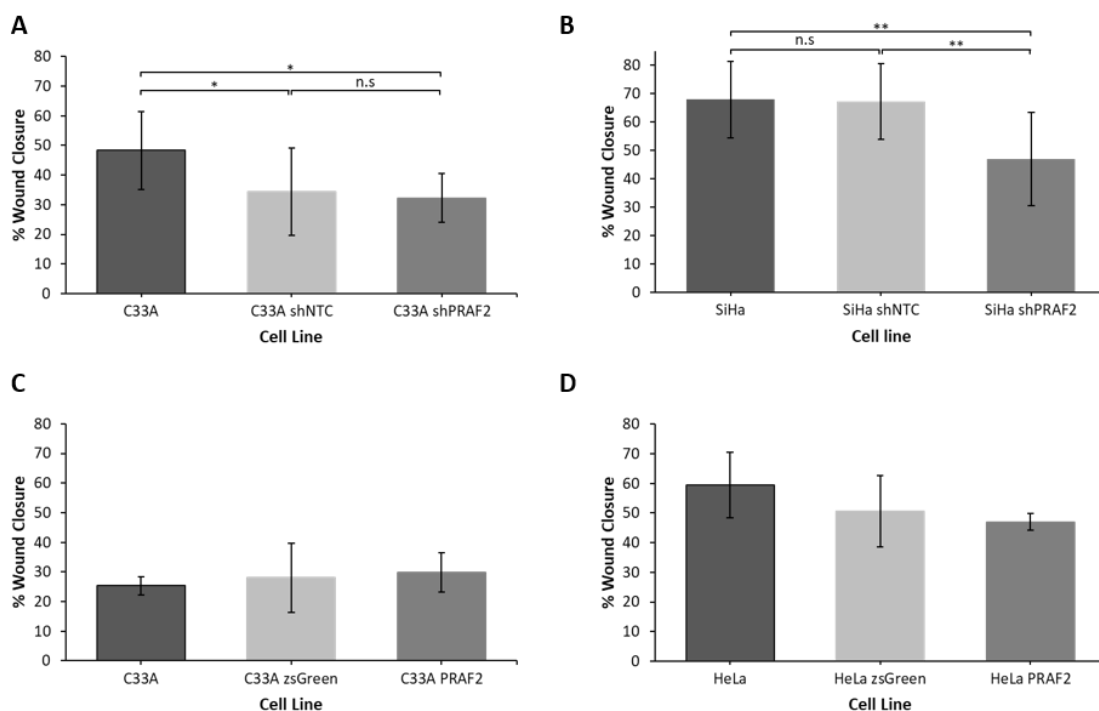


**Figure 4.9** Wound healing was impaired in SiHa cells but not C33A or HeLa cells by alterations to PRAF2 expression

Confluent monolayers were scratched with a pipette tip and imaged, 24 hours later the scratch was imaged, and the % wound closure was calculated. Error bars standard error, statistical test two-tailed paired t-test. A. C33A, C33A shNTC and C33A shPRAF2 cell line scratch assays  $*p \leq 0.01$  (C33A/C33A shNTC) and  $p \leq 0.05$  (C33A/C33A shPRAF2) B. SiHa, SiHa shNTC and SiHa shPRAF2  $**p \leq 0.01$  (SiHa/SiHa shPRAF2)  $**p \leq 0.001$  (SiHa shNTC/SiHa shPRAF2). C. C33A, C33A zsGreen, C33A PRAF2. D. HeLa, HeLa zsGreen and HeLa PRAF2.

#### 4.2.6 PRAF2 protein expression was increased in high grade HPV-16 positive cervical lesions

As PRAF2 expression has been observed to be increased in a variety of cancers it was decided to investigate PRAF2 expression in clinical samples of cervical cancer. Cytology samples from HPV-16 positive biopsies sourced from the Scottish HPV archive (*The Scottish HPV Archive*) covering the progression of disease (CIN1-CIN3) and normal cervical tissues were assayed for

PRAF2 expression by western blot. This work was performed by Dr Ethan L Morgan, University of Leeds.

In HPV negative 'normal' cervical tissue (Lanes 1 and 2, Figure 4.10 A) the levels of PRAF2 expression observed were low, with relatively little detected (Figure 4.10 B). In clinical samples graded as CIN1 (Lanes 3 and 4, Figure 4.10 A), again, low levels of PRAF2 were detected, with no statistically significant change in PRAF2 expression detected. In high grade lesions CIN2 and CIN3 (Lanes 5-8, Figure 4.10 A) PRAF2 is detected at higher levels, with a statistically significant increase in PRAF2 expression observed for CIN2 and CIN3 ( $p \leq 0.01$ ) clinical samples (Figure 4.10 B). These data suggested that PRAF2 expression is increased in cervical cancer, but not in the productive lifecycle of the virus.

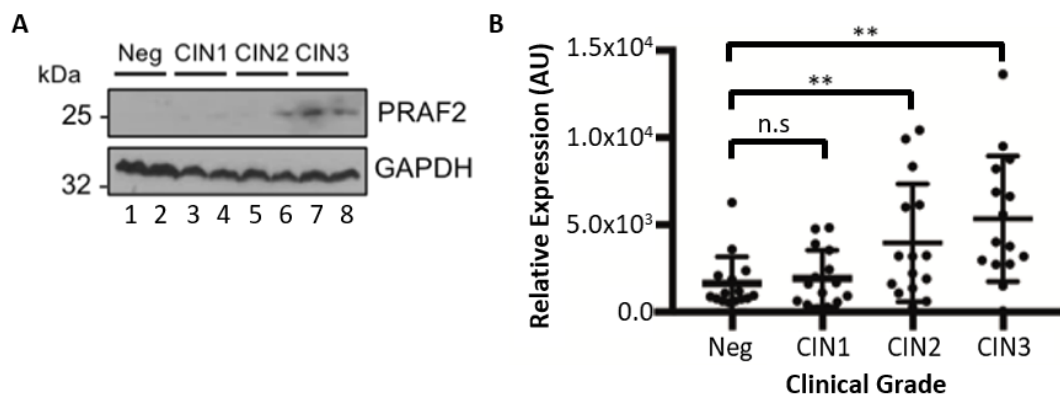


**Figure 4.10** PRAF2 protein expression is increased in high grade cervical lesions positive for HPV-16

HPV16 positive biopsies sourced from the Scottish HPV archive. Cytology samples processed and western blot probed for PRAF2 and GAPDH. Representative western blot. Experiment performed by Dr. Ethan L Morgan. A. Western blot of a representative panel of clinical samples. B. Densitometry analysis of western blots,  $n=15$  for each clinical grade.  $**p \leq 0.01$

#### **4.2.7 PRAF2 expression was increased upon differentiation in monolayer culture of HPV negative and positive keratinocytes**

Having examined the expression of PRAF2 in HPV positive and negative cervical cancer biopsies we decided to investigate PRAF2 and its relationship with keratinocytes. PRA family members have previously been studied in the context of differentiation, with PRAF1 examined in developing mouse retina (Dickison et al., 2012) and PRAF3 in the context of myeloid leukaemia differentiation (Huang et al., 2006a; Huang et al., 2006b) and bone morphogenesis (Wu, Y. et al., 2014; Wu, Y. et al., 2015). However, PRAF2 has not been studied previously in the context of differentiation. Using primary keratinocytes enables the study of PRAF2 biology in differentiation, as primary keratinocytes undergo differentiation when grown in monolayer when stimulated with high calcium.

Further to this, our primary keratinocyte cell system offered us the opportunity to examine PRAF2 biology not only in the presence and absence of HPV18, but also in the absence of its binding partner E5. Studies were carried out with normal human keratinocytes (NHKs), keratinocytes harbouring the wildtype HPV18 genome (WT18) and keratinocytes harbouring at HPV18 genome with a stop codon that knocks out expression of the E5 protein (E5KO) (Wasson et al., 2017).

Primary keratinocytes were grown in monolayer until 90% confluent, at which point the media was changed for basal media containing 1.4 mM CaCl<sub>2</sub> without growth supplements. Cells were then harvested at 0, 48, 72 and 96 hours post the onset of differentiation. The resulting lysates were processed, and equal volumes of protein resolved by SDS-PAGE followed by western blotting. The resulting western blots were probed with antibodies specific for CK10, Cyclin B1, HPV18E6, HPV18E7, PRAF2 and GAPDH. In both donors (Figure 4.11). A clear increase in the levels of the differentiation marker CK10 was observed at 48 hours in NHK (lane 2, Figure 4.11 A and B), relative to 0h (Lane 1, Figure 4.11 A and B) which intensified throughout the

timecourse, peaking at 96 hours post the induction of differentiation (Lane 4, Figure 4.11 A and B). This induction of Cytokeratin 10 was reduced in cells harbouring both WT and E5KO HPV18 genomes (Lanes 5-12, Figure 4.11 A and B) in both donors, relative to NHK. However, the reduction in CK10 expression was less pronounced in donor 2 relative to donor 1, with levels of CK10 closer to that of NHK.

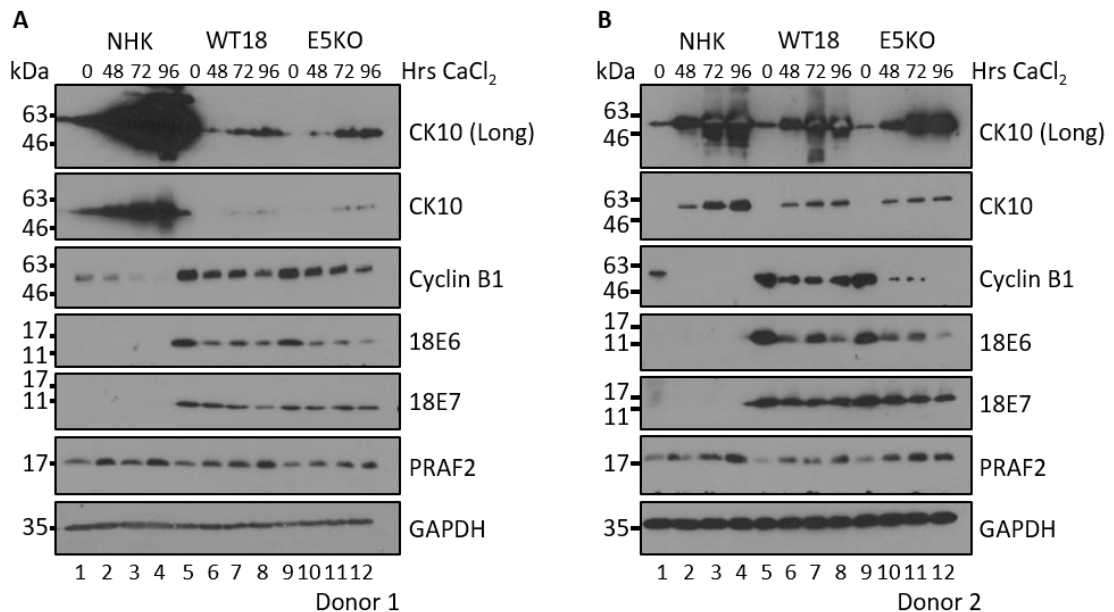


**Figure 4.11** *PRAF2 expression increases with high calcium mediated differentiation in NHKs, WT18 and E5KO keratinocyte cell lines.*

Monolayers of HPV negative (NHK), HPV18 positive (WT18) and HPV18 E5KO (E5KO) keratinocytes were stimulated with CaCl<sub>2</sub> and differentiation induced. Samples were harvested at 0, 48, 72 and 96 hours post the induction of differentiation. Equal amounts of protein were used to perform western blotting. The resulting western blots were probed for CK10, Cyclin B1, HPV-18E6, HPV-18E7, PRAF2 and GAPDH. Blots are representative. N=3. A. Calcium differentiation timecourse of donor 1. B. Calcium differentiation timecourse of donor 2.

Cyclin B1 expression was observed at 0 hours in both NHK donors (Lane 1), as would be expected in proliferating cells, as a Cyclin B1 is a proliferation marker. A clear reduction in levels of Cyclin B1 was seen upon onset of differentiation, with little or none detectable at 96 hours

(Lane 4) in both donors. This, taken with the CK10 data suggests that differentiation has been successfully induced in the keratinocytes. As would be expected for HPV positive keratinocytes Cyclin B1 expression was maintained even after the induction of differentiation. In donor 1 (Figure 4.11 A) Cyclin B1 levels decrease at a similar rate in both WT18 and E5KO, however in donor 2 E5KO undergoes a greater reduction in the level of Cyclin B1 compared to both donor 1 WT18 and E5KO and donor 2 E5KO.

The HPV18 oncoproteins were not detected in NHKs as expected (Figure 4.11 A and B). Interestingly, the levels of HPV-18E7 remained consistent throughout the differentiation timecourse in donor 1 in both WT18 and E5KO, with only a slight reduction observed at 96 hours in WT18 (Lane 8, Figure 4.11 A). In donor 2, levels of HPV-18E7 in WT18 and E5KO were highest at 0hrs, with a slight decrease observed at 48 hours, which remained constant until 96 hours (Figure 4.11 B). Overall, levels of HPV-18E7 remain high. With the oncoprotein HPV-18E6 a different pattern was observed, in WT18 and E5KO in both donors at 0 hours (Lanes 5 and 9, Figure 4.11) levels of E6 were high. However, when differentiation was induced, levels of E6 fall. At 96 hours (Lane 8) in WT18 in both donors' levels are markedly decreased. The same was observed for E5KO (Lane 12). When E5KO was compared to WT18, lower levels of E6 were observed in E5KO at 96 hours relative to WT18 at 96 hours. This effect was seen in both donors.

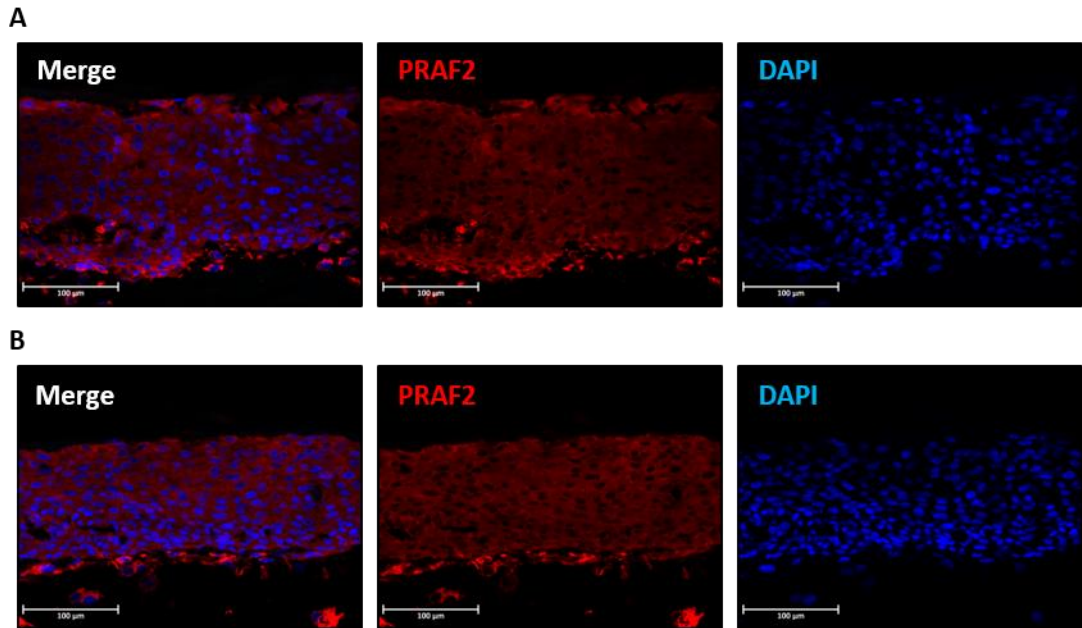
PRAF2 was observed at 0 hours in NHK, WT18 and E5KO (Lanes 1, 5 and 9) in both donors (Figure 4.11). In NHKs, when differentiation was induced the levels of PRAF2 protein were elevated at 48 hours (Lane 2), this increased level of expression persisted at 48 hours (Lane 3) and 96 hours (Lanes 4). This was observed in both donors. In WT18 cells, PRAF2 was detected at 0 hours (lane 5) with levels increased when differentiation was induced. In contrast to NHK, it appears that whilst expression was elevated at 48 hours (lane 5) the greatest levels of expression were observed by 96 hours (Lane 8). This was observed for both donors. Both E5KO donor cell lines expressed PRAF2 at 0 hours (Lane 9), and expression was observed to increase upon

differentiation (Lanes 8-12). The donors differ in the levels of expression observed when compared to the WT18. In donor 1 (Figure 4.11 A) the levels of PRAF2 were roughly equal to that of WT18, however in donor 2 (Figure 4.11 B) the levels of PRAF2 observed in the E5KO are greater than that of WT18. This study represented the first time PRAF2 had been studied in the context of differentiation.

#### **4.2.8 PRAF2 localisation and expression was not altered by the loss of HPV-18E5 in organotypic raft cultures**

To study PRAF2 in a more physiologically relevant manner in keratinocytes the organotypic raft culture system was used. Keratinocytes were seeded onto a collagen plug containing mouse J2 3T3 fibroblasts, grown to confluency and then grown on a grid at the air-liquid interface to promote differentiation, these rafts were then allowed to stratify for 14 days. This method recapitulates both the keratinocyte and HPV Lifecycle (Wasson et al., 2017). NHKs, WT18 and E5KO keratinocytes were cultured in this system. Rafts were then fixed and sectioned and stained with antibodies.

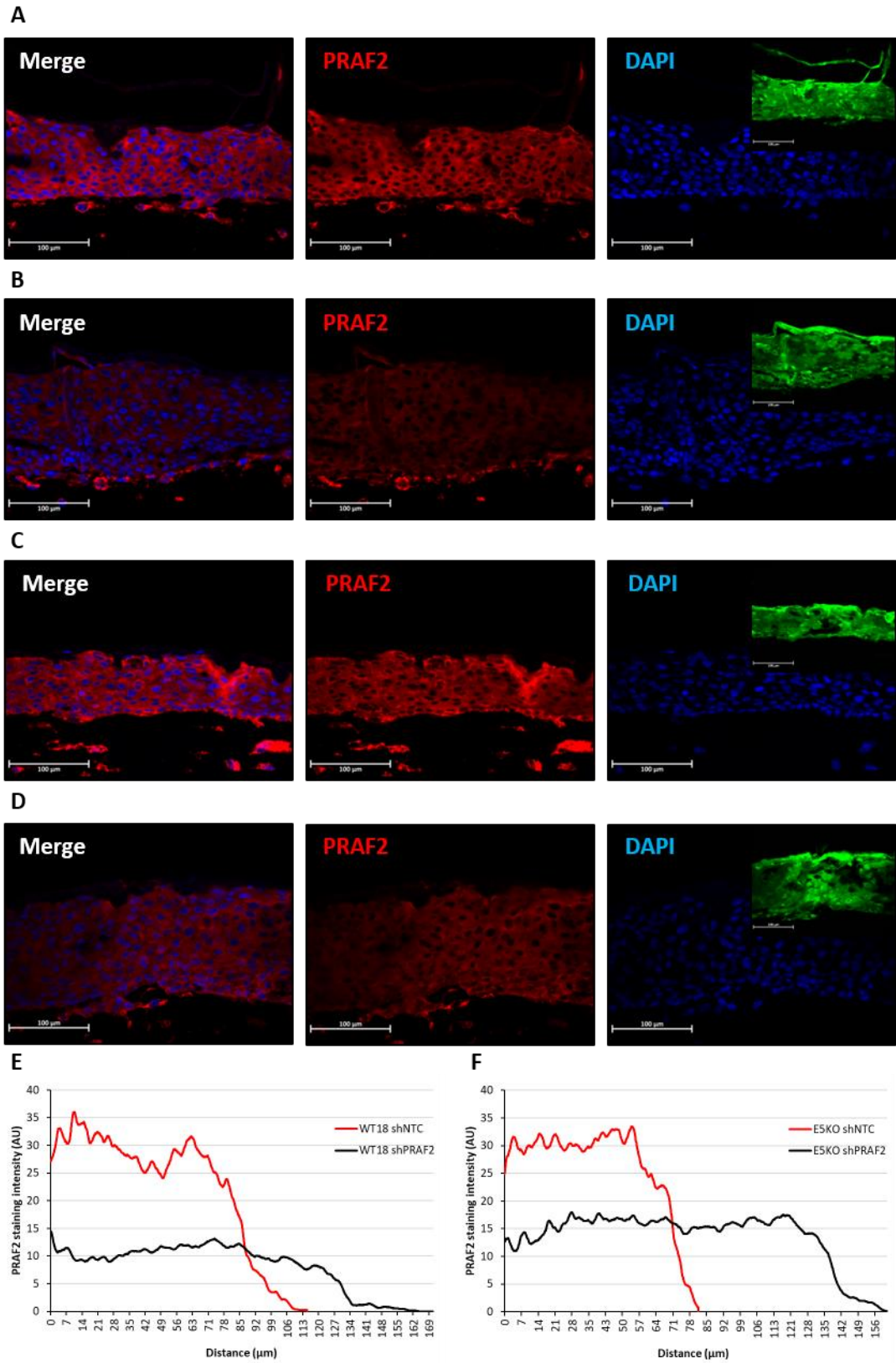
Unfortunately, the NHK raft failed to grow and stratify (Figure 4.17 A) as determined by H&E staining, however, WT18 and E5KO rafts underwent successful stratification, with basal and suprabasal layers evident and a cornified layer. These rafts were stained with an antibody specific for PRAF2. In both the WT18 (Figure 4.12 A) and E5KO (Figure 4.12 B) rafts the PRAF2 staining was localised to the cytoplasm, and no nuclear staining was observed as no PRAF2 staining co-localised with DAPI. When compared, the localisation and intensity of staining did not differ between WT18 and E5KO sections. The PRAF2 expression observed remained at the same level throughout the layers of stratified epithelium.



**Figure 4.12** *PRAF2 expression and distribution was not altered by the loss of HPV-18E5 in HPV18 positive raft cultures*

*Raft sections were probed with PRAF2 antibody and then stained with Alexa-594 secondary (red), and counterstained with DAPI (blue). Scale bar 100 µm. A. A representative image of a WT18 Raft section B. A representative image of E5KO sections. N=1*

NHK, WT18 and E5KO rafts were set up expressing either shNTC or shPRAF2 to further investigate the role of PRAF2 in the context of keratinocytes and HPV. To do so primary cells were transduced with lentivirus and then selected for 7 days with puromycin, and the expression of the constructs was validated by screening for the expression of the zsGreen protein expressed by these plasmids. These cells were then rafted. Unfortunately, the NHK shNTC and shPRAF2 rafts failed to stratify (Figure 4.17 B). However, WT18 and E5KO shRNA rafts were successfully produced. To confirm that the shRNA was working as intended these rafts were stained for PRAF2 expression.



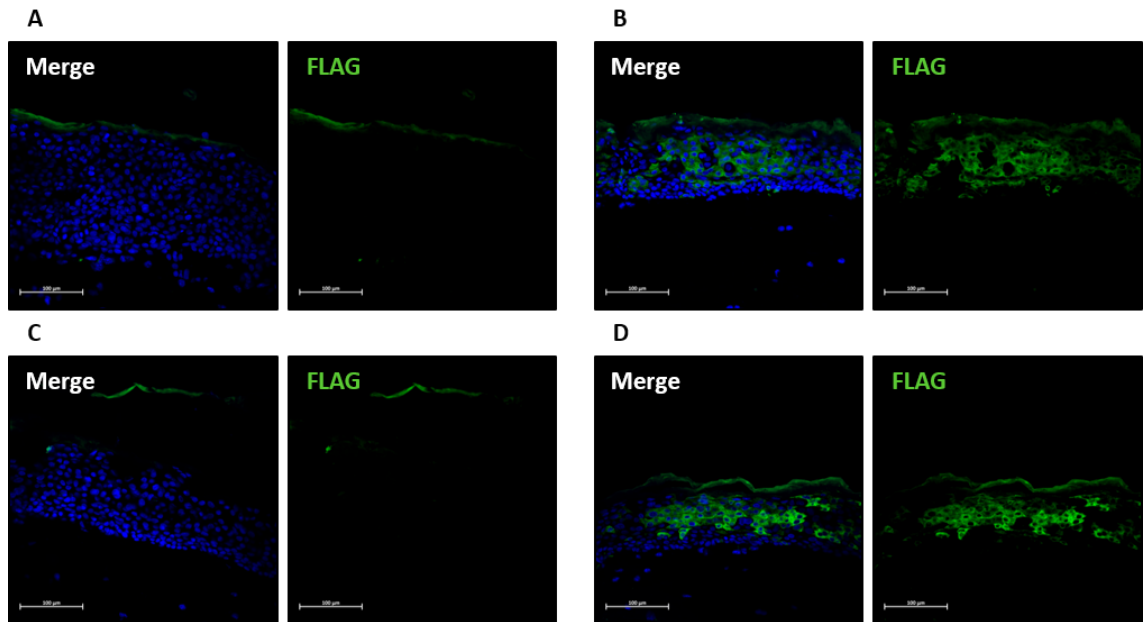
**Figure 4.13** *Reduced PRAF2 staining was detected in WT18 and E5KO shRNA raft sections*

Figure 4.13 cont. Raft sections probed with PRAF2 antibody then stained with Alexa-594 secondary (red), counterstained with DAPI (blue). Upper right-hand corner of DAPI tile displays *zsGreen* fluorescence for each section. Representative sections. Scale bar 100  $\mu$ m. A. WT18 shNTC. B. WT18 shPRAF2. C. E5KO shNTC. D. E5KO shPRAF2. E-F PRAF2 staining intensity across raft section average E. PRAF2 staining intensity plot of WT18 shNTC vs WT18 shPRAF2. F. PRAF2 staining intensity plot of E5KO shNTC vs E5KO shPRAF2.

When WT18 shNTC (Figure 4.13 A) and WT18 shPRAF2 (Figure 4.13 B) rafts stained for PRAF2 were compared there was a clear reduction in intensity of PRAF2 staining in the WT18 shPRAF2 raft compared to the WT18 shNTC raft. The average intensity of PRAF2 staining for each raft section was determined and plotted (Figure 4.13 E). A  $\sim$  63.5% average reduction in PRAF2 staining intensity across the section was observed in the WT18 shPRAF2 raft relative to WT18 shNTC. The knockdown in the E5KO rafts was also successful with a reduction in staining intensity observed in the E5KO shPRAF2 (Figure 4.13 D) relative to the E5KO shNTC (Figure 4.13 C), which equated to a  $\sim$ 46.4% reduction in staining intensity across the section (Figure 4.13 F).

In addition to PRAF2 knockdown rafts, PRAF2 overexpression rafts were also produced. To do so primary cells were infected with retrovirus either encoding empty plasmid (EV) or a plasmid expressing 3xFLAG-PRAF2. The resulting cells were then rafted. Both EV and 3xFLAG-PRAF2 rafted in WT18 and E5KO, however, the NHK rafts failed to grow (Figure 4.17 C and D). Successful overexpression of 3xFLAG-PRAF2 was confirmed in raft sections by probing with an antibody to the FLAG tag followed by staining with an Alexa-488 conjugated secondary. The FLAG antibody seemed to exhibit some non-specific staining in the cornified layer of the rafts, with some 488-staining observed in the WT18 and E5KO EV raft sections (Figure 4.14 A and C), however, no FLAG staining was observed in the basal or suprabasal layers. In both WT18 and E5KO 3xFLAG-PRAF2 sections (Figure 4.14 B and D respectively) there was clear FLAG staining

observed in the basal and suprabasal layers, with a non-nuclear localisation. Interestingly, there seemed to be relatively few cells in the basal layer that stained for 3xFLAG-PRAF2, and not all suprabasal cells stained for FLAG, however the majority did.



**Figure 4.14** *FLAG was successfully detected in the basal and suprabasal layers of 3xFLAG-PRAF2 rafts*

*Raft sections probed with FLAG antibody then stained with Alexa-488 secondary (green), counterstained with DAPI (blue), DAPI is shown in the merge. Representative sections. Scale bar 100  $\mu$ m. A. WT18 EV. B. WT18 3xFLAG-PRAF2. C. E5KO EV. D. E5KO 3xFLAG-PRAF2. N=1*

#### **4.2.9 PRAF2 overexpression reduced raft thickness in both WT18 and E5KO rafts**

The rafts produced in section 4.2.9 were sectioned and stained with haematoxylin and eosin (H&E, work carried out by Mr Tim Lee, Histology Facility, University of Leeds). Once stained, rafts were imaged on an Axio Scan.Z1 using automated tile scanning. For each raft condition three separate sections were scanned along their entire length. These sections were measured in qupath to obtain the average thickness of basal plus suprabasal layers. When

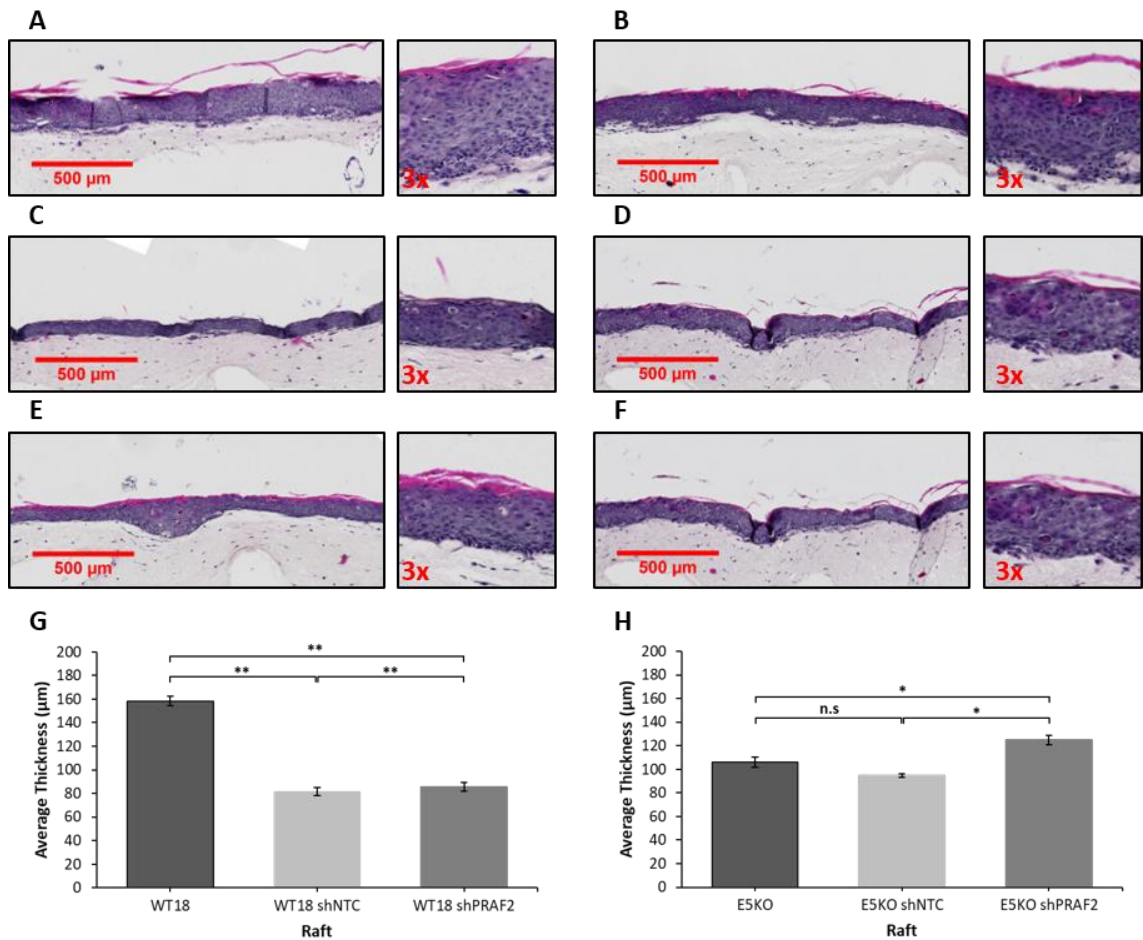


**Figure 4.15** A significant increase in the thickness of the stratified epithelium was observed in both WT18 and E5KO shPRAF2 raft sections.

Rafts were sectioned and stained with H&E by Mr Tim Lee, Histology Facility, University of Leeds.

Rafts were imaged with Axio Scan.Z1 at 20x by tile scanning in brightfield. Scale bar = 500 μm.

Representative image shown, in addition to 3x digital zoom. A. WT18. B. E5KO. C. WT18 shNTC.

D. E5KO shNTC. E. WT18 shPRAF2. F. E5KO shPRAF2. G-H. Thickness of 3x sections was measured

in Qupath and then averaged. Statistics Two-tailed paired students T-test, error bars standard

deviation. G. Average thickness plot of WT18, WT18 shNTC and shPRAF2, \*\*  $p \leq 0.0001$  (WT18 vs WT18 shNTC), \*\*  $p \leq 0.001$  (WT18 vs WT18 shPRAF2), \*\*  $p \leq 0.001$  (WT18 shNTC vs WT18 shPRAF2).

H. Average thickness plot of E5KO, E5KO shNTC and E5KO shPRAF2, \*  $p \leq 0.05$  (E5KO vs E5KO shPRAF2), \*  $p \leq 0.05$  (E5KO shNTC vs E5KO shPRAF2).

compared to the WT18 raft (Figure 4.15 A), both the WT18 shNTC (Figure 4.15 C) and WT18 shPRAF2 (Figure 4.15 E) exhibited a statistically significant decrease in the average thickness of the raft (Figure 4.15 G,  $p \leq 0.0001$  and  $p \leq 0.001$  respectively). When WT18 shNTC and shPRAF2 are compared there was a small but statistically significant increase in the rafts thickness observed ( $p \leq 0.001$ ). When the E5KO raft (Figure 4.16 B) was compared to the E5KO shNTC raft (Figure 4.15 D) there was no statistically significant change in the thickness of the raft. However, when E5KO and E5KO shPRAF2 (Figure 4.15 F) were compared there was a statistically significant increase ( $p \leq 0.05$ , Figure 4.15 H) in the thickness, this was also observed for E5KO shNTC compared to E5KO shPRAF2 ( $p \leq 0.05$ ).

The PRAF2 overexpression rafts were compared. When the WT18 raft (Figure 4.15 A) was compared to the WT18 EV raft (Figure 4.16 A) there was no statistically significant difference in the average thickness of the raft (Figure 4.16 E). When the WT18 3xFLAG-PRAF2 raft (Figure 4.16 B) was compared to the WT18 raft, there was a statistically significant reduction in the average thickness observed (Figure 4.16 E,  $p \leq 0.01$ ). This was also observed when the WT18 EV and WT18 3xFLAG-PRAF2 were compared (Figure 4.16 E,  $p \leq 0.01$ ). When the E5KO raft (Figure 4.15 B) was compared to the E5KO EV raft (Figure 4.16 C) there was no statistically significant change in average thickness observed (Figure 4.16 F). However, when the E5KO raft was compared to the E5KO 3xFLAG-PRAF2 raft (Figure 4.16 D), there was a statistically significant reduction in average thickness observed ( $p \leq 0.01$ ). This was also observed when E5KO EV and E5KO 3xFLAG-PRAF2 rafts were compared ( $p \leq 0.05$ ). This suggested that PRAF2 overexpression altered the stratification of WT18 and E5KO rafts.

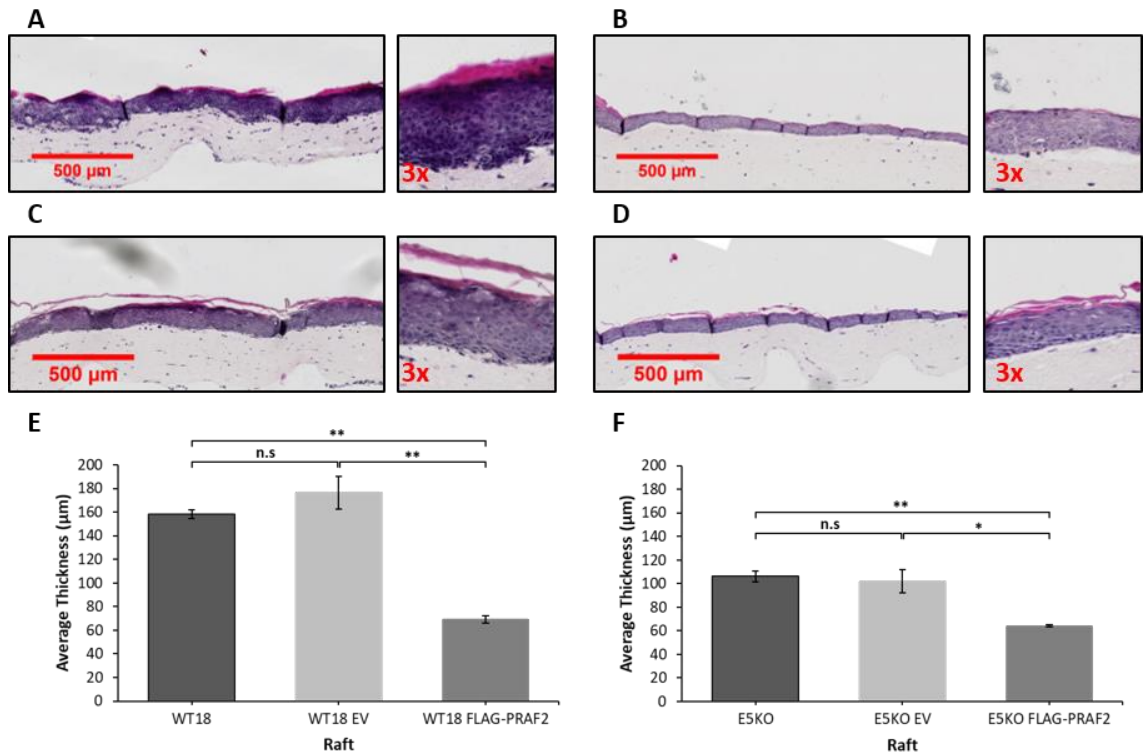


**Figure 4.16** A significant reduction in the thickness of the stratified epithelium was observed in both WT18 and E5KO 3xFLAG-PRAF2 raft sections.

Rafts were sectioned and stained with H&E by Mr Tim Lee, Histology Facility, University of Leeds. Rafts were imaged with Axio Scan.Z1 at 20x by tile scanning in brightfield. Scale bar = 500 μm. Representative image shown, in addition to a 3x digital zoom. A. WT18 EV. B. WT18 3xFLAG-PRAF2. C. E5KO EV. D. 3xFLAG-PRAF2. Thickness of 3x sections was measured in Qupath and then averaged. Statistics Two-tailed paired students T-test, error bars standard deviation. G. Average thickness plot of WT18, WT18 EV and WT18 3xFLAG-PRAF2. \*\* $p \leq 0.01$  (WT18 vs WT18 3xFLAG-PRAF2), \*\* $p \leq 0.01$  (WT18 EV vs WT18 3xFLAG-PRAF2). F. Average thickness plot of E5KO, E5KO EV and E5KO 3xFLAG-PRAF2. \*\* $p \leq 0.01$  (E5KO vs E5KO 3xFLAG-PRAF2), \* $p \leq 0.05$  (E5KO EV vs E5KO 3xFLAG-PRAF2).

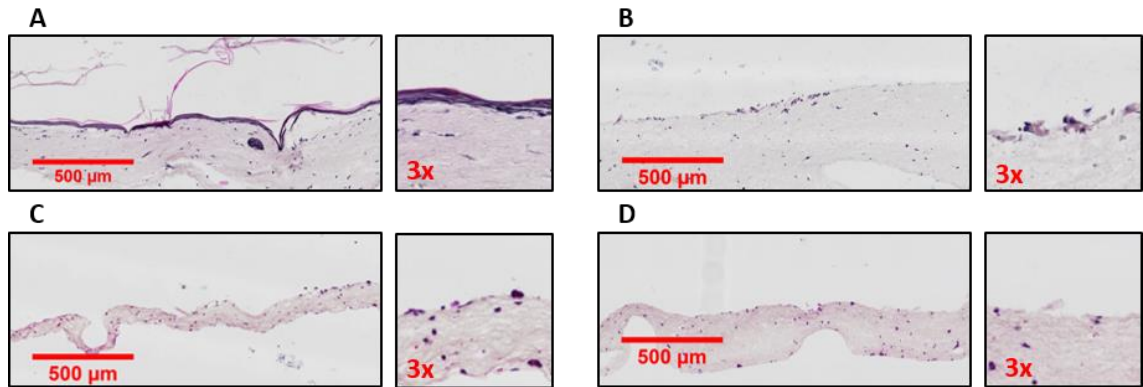


**Figure 4.17** *NHK rafts exhibited a failure to stratify as determined by H&E staining*

*Rafts were sectioned and stained with H&E by Mr Tim Lee, Histology Facility, University of Leeds.*

*Rafts were imaged with Axio Scan.Z1 at 20x by tile scanning in brightfield. Scale bar = 500  $\mu$ m.*

*Representative image shown, in addition to a 3x digital zoom. A. NHK. B. NHK shPRAF2. C. NHK EV. D. NHK 3xFLAG-PRAF2.*

#### **4.2.10 PRAF2 overexpression resulted in the loss of E1<sup>E4</sup> expression in E5KO organotypic rafts**

To assess whether the knockdown or overexpression of PRAF2 was affecting the lifecycle of HPV18, rafts were stained for HPV-18E1<sup>E4</sup>, which served as a marker for the successful completion of the viral lifecycle (Doorbar et al., 2015; Knight et al., 2011). HPV-18E1<sup>E4</sup> staining was detected in WT18, E5KO, WT18 shNTC, WT18 shPRAF2, E5KO shNTC, E5KO shPRAF2, WT18 EV, WT18 3xFLAG-PRAF2 and E5KO EV rafts (Figure 4.18, A-I). However, HPV-18E1<sup>E4</sup> staining was not detected in the E5KO 3xFLAG-PRAF2 raft sections (Figure 4.18 J), this suggested that the overexpression of PRAF2 impaired the ability of E5KO HPV-18 to complete its lifecycle.

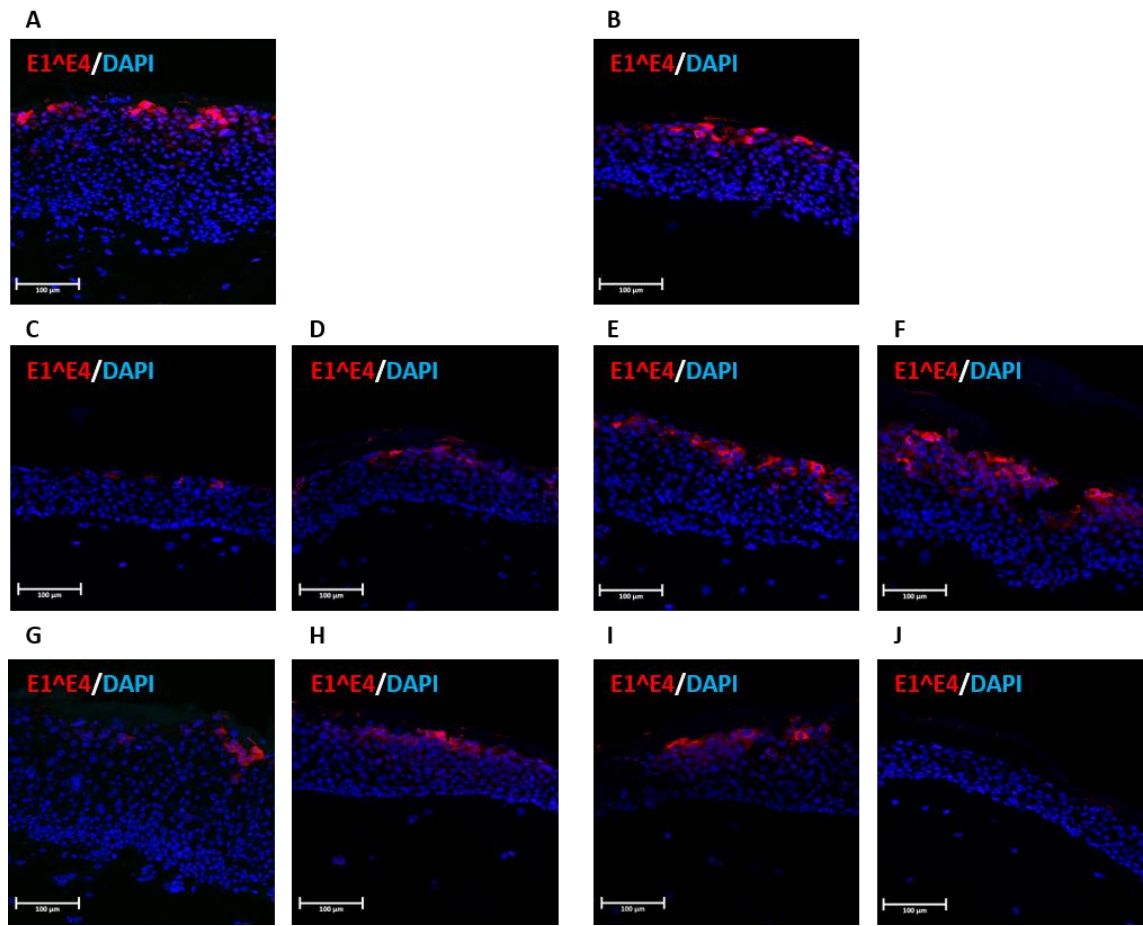


**Figure 4.18** HPV-18E1<sup>E4</sup> staining was lost in 3xFLAG-PRAF2 E5KO raft sections

Raft sections probed with HPV-18E1<sup>E4</sup> antibody then stained with Alexa-594 secondary (red), and counterstained with DAPI (blue), DAPI is shown in the merge. Representative sections. Scale bar 100 $\mu$ m. A. WT18. B. E5KO. C. WT18 shNTC. D. WT18 shPRAF2. E. E5KO shNTC. F. E5KO shPRAF2. G. WT18 EV. H WT18 3xFLAG-PRAF2. I. E5KO EV. J. E5KO 3xFLAG-PRAF2. N=1

#### 4.2.11 PRAF2 overexpression and knockdown did not alter the expression and distribution of CK10

To determine whether the reduction in raft thickness was due to an alteration of the state of differentiation the rafts were stained for the differentiation marker Cytokeratin 10 (CK10). In all rafts (Figure 4.19 A-E) cytokeatin could be detected in the cytoplasm upon exit from the basal layer. There did not appear to be a noticeable change in the levels of CK10 staining observed

between the different raft conditions, even in the WT18 3xFLAG-PRAF2 raft (Figure 4.19 E), which suggested that differentiation had not been perturbed.

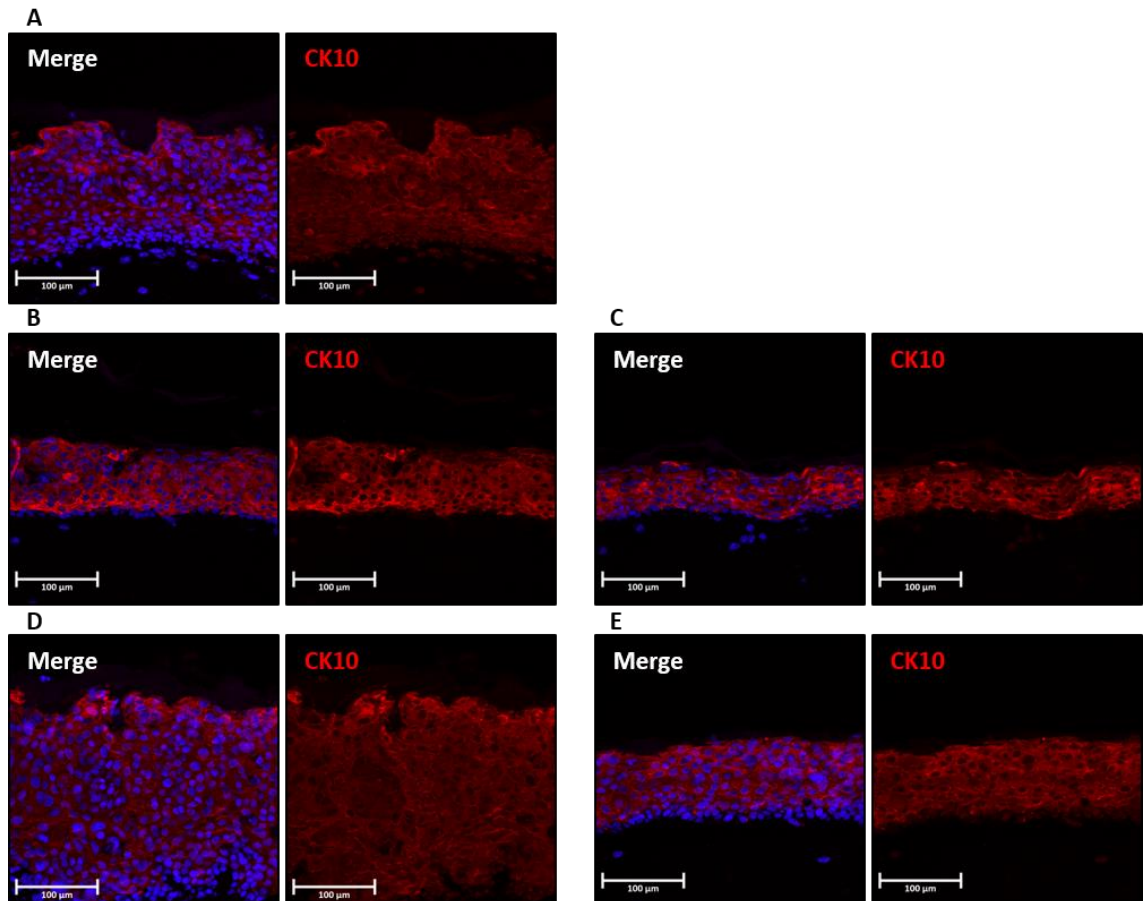


**Figure 4.19** *No changes in CK10 staining were observed between WT18 PRAF2 knockout and overexpression rafts when compared to controls.*

*Raft sections were probed with the CK10 antibody and then stained with Alexa-594 secondary (red), counterstained with DAPI (blue), DAPI is shown in the merge. Representative sections.*

*Scale bar 100 µm. A. WT18. B. WT18 shNTC. C. WT18 shPRAF2. D. WT18 EV. E. WT18 3xFLAG-PRAF2.*

In E5KO rafts a similar staining pattern for CK10 was observed (Figure 4.20). Interestingly, CK10 the staining of the E5KO shNTC and shPRAF2 sections (Figure 4.20 B and C) appeared to be more intense than that of the E5KO (Figure 4.20 A). The staining observed in the E5KO EV (Figure 4.20 D) was of similar intensity, however, the staining observed in the E5KO 3xFLAG-PRAF2 (Figure 4.20 E) appeared to be of a greater intensity than that of the E5KO or E5KO EV. This could indicate that this tissue differentiated to a greater degree.

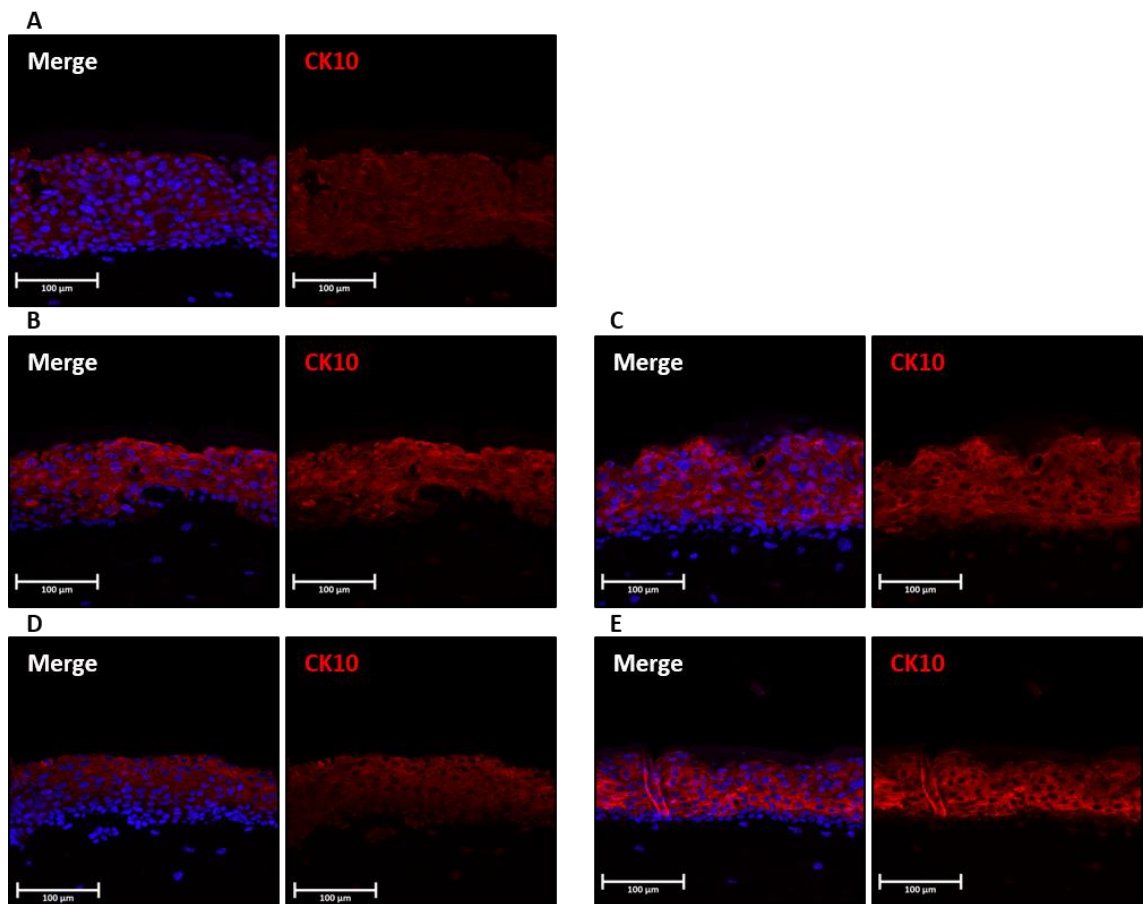


**Figure 4.20** *Increased CK10 staining was observed in PRAF2 overexpression but not knockdown in E5KO raft sections*

*Raft sections probed with Cytokeratin 10 antibody then stained with Alexa-594 secondary, counterstained with DAPI (Blue), DAPI is shown in the merge. Representative sections. Scale bar 100 µm. A. E5KO. B. E5KO shNTC. C. E5KO shPRAF2. D. E5KO EV. E. E5KO 3xFLAG-PRAF2.*

### 4.3 Discussion

Whilst PRAF2 had previously been shown to be important in the traffic of receptors to the cell surface, these receptors had all been GPCRs (Schweneker et al., 2005; Doly et al., 2016), this study was the first study investigating PRAF2 and receptor tyrosine kinases (RTK). We demonstrated that both the total levels of the RTK EGFR and EGFR cell surface expression were not altered by PRAF2 knockdown or overexpression in both HPV negative and HPV positive cancer cell lines, as would be the case if PRAF2 was acting on EGFR in a similar way to CCR5 (Schweneker et al., 2005) or GABA<sub>B</sub> (Doly et al., 2016). However, alterations to the internalisation and recycling of EGFR upon ligand stimulation were not investigated. This could not be ruled out as effected by alterations to PRAF2 levels, as PRAF2 has been demonstrated to be localised to endosomes (Borsics et al., 2010). This was also a cellular compartment that the EGFR interactor E5 (Hwang et al., 1995) has been shown to be localised to (Zhang, B. et al., 2005), which we have shown is also a binding partner of PRAF2. Possible future experiments could involve the use of fluorescently labelled EGF and immunofluorescence to see whether internalisation and recycling is altered.

Previous studies have demonstrated that PRAF2 knockdown results in G1 cell cycle arrest (Qian et al., 2019), however, PRAF2 has also been demonstrated to be a tumour suppressor (Vento et al., 2010). Here we observed no change in either cyclin levels or cell cycle profiles following knockdown or overexpression of PRAF2 levels in cervical cancer derived cell lines. This suggests PRAF2 expression does not affect cell cycle progression in cervical cancer.

SiHa cells demonstrated an impairment in their ability to form colonies when PRAF2 expression was altered, and their ability to grow in an anchorage independent manner was also impaired. This is in agreement with previous studies showing that the loss of PRAF2 impairs cancer cells ability to form colonies (Yco et al., 2013; Qian et al., 2019). It would be interesting to overexpress PRAF2 in SiHa cells to see if an enhancement in their ability to form colonies was

observed, as demonstrated in hepatocellular carcinoma (Wang, C.H. et al., 2018). However, this impairment was not observed in C33A cells, which are HPV negative, which could suggest that PRAF2 is important for HPV positive cervical cancer cells. However, PRAF2 overexpression in the HPV-18 positive HeLa cell line did not result in a change in colony formation, suggesting that this unlikely, or is an HPV-16 specific effect.

Unexpectedly the proliferative ability of SiHa shPRAF2 cells was not significantly impaired as assessed by growth curves, as might be expected for a cell line which formed fewer colonies, however there was a small but non statistically significant reduction in SiHa shPRAF2 cell growth rates. The only cell line where a significant difference in growth rates was observed was C33A PRAF2 with a significant increase in growth rate observed only at the 120-hour timepoint. This was surprising as C33A PRAF2 cells did not display greater colony formation, changes in cyclin expression or alterations to their cell cycle profiles.

SiHa cells demonstrated an impairment in their ability to close wounds when PRAF2 was knocked down. This is in agreement with previous observations in cancer cell lines, where impaired wound closure was observed in neuroblastoma (Yco et al., 2013), and impaired migration in ESCC (Qian et al., 2019) and malignant glioma (Borsics et al., 2010). However, PRAF2 overexpression did not alter wound closure in C33A or HeLa cells, which had been shown to be enhanced in hepatocellular carcinoma when PRAF2 was overexpressed (Wang, C.H. et al., 2018). Confusingly, in the C33A knockdown data, we observed a significant difference between control C33A cells and C33A shNTC and C33A shPRAF2, whose wound closure was impaired relative to C33A but not each other. This suggested that the shRNA construct was causing problems for the cells in a manner separate to PRAF2 knockdown. However, these differences are likely due to the stable C33A shNTC and shPRAF2 cell lines being at a higher passage number than the C33A control cells they were assayed against, resulting in slightly altered growth characteristics. Ideally, the cells would be passage matched, however this was not possible. It should be noted

that all the stable cell lines generated were stable for continuous passage, with no obvious adverse effects displayed.

It would appear that compared to PRAF3, which has a very clear tumour suppressor effect in a variety of cancer cell lines (Xu, L. et al., 2018; Chen, Y. et al., 2014; Bai et al., 2010), that PRAF2's role as a oncogene or tumour suppressor is less clear cut, as even within cervical cancer cell lines, different cell lines respond differently, with only the HPV-16 positive SiHa cells significantly affected. Others, such as C33A showed only a minor increase in proliferation in response to overexpression, or no affect at all, such as in the case of HeLa cells.

Following on from the cervical cancer cell line data, clinical samples were analysed from HPV16 positive cervical cancer biopsies. The expression pattern agrees with what was observed in the cancer cell line screen (Chapter 3), that HPV-16 positive cervical cancer overexpresses PRAF2, relative to normal tissue. This could suggest that PRAF2 acts as an oncogene in HPV-16 positive cervical cancer, however it was interesting to note that PRAF2 is a positive prognostic marker in cervical cancer (Uhlen et al., 2017). This contrasts with colorectal cancer, neuroblastoma, malignant glioma, hepatocellular carcinoma and ESCC in which it is a negative prognostic marker (Qian et al., 2019; He et al., 2019; Wang, C.H. et al., 2018; Yco et al., 2013; Borsics et al., 2010) and considering the less than clear cut data on the knockdown and overexpression in cervical cancer cell lines, whether PRAF2 is an oncogene in cervical cancer remains to be determined.

Interestingly, PRAF2 expression was comparable between HPV negative and HPV-16 positive CIN1 samples, these data were also in agreement with our investigations in NHK and HPV-18 positive keratinocytes, in which the level of PRAF2 expressed in primary monolayers is comparable between HPV negative and HPV positive samples at both 0 and 96 hours post differentiation. This was seen in both of our donor lines. Unfortunately, were unable to compare the expression of PRAF2 between NHK rafts and HPV18 positive rafts due to the failure of our

NHK rafts to stratify. Admittedly, this does not allow for the fact that HPV16 may regulate PRAF2 expression differently, however the comparison of negative and CIN1 biopsies and NHK and HPV18 monolayer data would suggest that in a productive lifecycle, that levels of PRAF2 are not altered by HPV.

We have previously shown that PRAF2 levels are not altered by the expression of the HPV18 oncoproteins in C33A cells. These findings were further supported by the comparison of NHK, WT18 and E5KO monolayer data. If the expression and action of the oncoproteins E6 and E7 were affecting PRAF2 levels, we would expect that when NHK samples were compared to WT18 to observe a difference in the levels of PRAF2, which was not the case. Furthermore, when the E5KO monolayer data were compared to the WT18 monolayer data we did not observe a change in the pattern of PRAF2 expression between the two. This was supported further by the comparison of WT18 and E5KO raft PRAF2 staining, if E5 was altering the expression of PRAF2 we would expect to see a difference in the staining pattern, which we did not. This suggested that the interaction between PRAF2 and the E5 protein was most likely one that alters its activity, rather than altering its levels to change the cellular environment.

We observed that PRAF2 knock-down by shRNA in both WT18 and E5KO rafts resulted in a small but significant increase in the thickness of the raft. Whilst there were some concerns relating to the control shPRAF2 WT18 rafts, these issues were not observed in the E5KO. The failure to produce NHK rafts is keenly felt here, as it removes an important point of comparison, that would allow us to possibly determine if the loss of PRAF2 expression is altering the lifecycle biology of the keratinocyte, or the lifecycle of HPV18.

If for example, we saw that a loss of PRAF2 expression in an NHK raft resulted in hyperplasia, we could reason that PRAF2 expression was the cause of the increased thickness. If, however, this was not seen it would suggest the change was due to the presence of HPV. The observation that the E5KO shPRAF2 raft displayed a similar change to that observed in the WT18

shPRAF2 suggested that this may be more due to keratinocyte biology than that of HPV, as in the E5KO raft the PRAF2 binding partner HPV18E5 is absent, yet the effect was still present. The effect of PRAF2 overexpression was more clear-cut, as in both WT18 and E5KO 3xFLAG-PRAF2 rafts there was a clear reduction in the thickness of the suprabasal layer relative to either control or empty vector rafts.

It was interesting to note that when we examined the expression of the 3xFLAG-PRAF2 in the raft sections that we detected relatively few basal cells that stained positive for FLAG. Logically, these are the most appealing reasons. The first option was that the transduction efficiency was low, resulting only a small percentage of the cell population expressing 3xFLAG-PRAF2. Yet, it gave these cells a competitive advantage and they out competed the 3xFLAG-PRAF2 negative cells and went on to compose the majority of the raft. This would fit the 'PRAF2 as an oncogene' story (Qian et al., 2019; He et al., 2019; Wang, C.H. et al., 2018; Yco et al., 2013). Alternatively, the second option was that the transduction was efficient, however, the overexpression of PRAF2 was disadvantageous to the proliferating cells of the basal layer. In this scenario, non 3xFLAG-PRAF2 basal cells would outcompete or outlive 3xFLAG-PRAF2 cells, hence their depletion in the basal compartment. This would fit with the idea of PRAF2 acting as a tumour suppressor.

To determine the effect of altering the levels of PRAF2 on HPV-18, we could examine markers of productive infection for the virus, for example E1<sup>E4</sup> (Knight et al., 2011). HPV-18E1<sup>E4</sup> was detected in all the WT18 and E5KO rafts, except for the E5KO 3xFLAG-PRAF2 raft. This suggested that the HPV lifecycle was unable to be completed. It was interesting that HPV18E1<sup>E4</sup> could not be detected in the E5KO 3xFLAG-PRAF2 raft as this raft did not express the PRAF2 proteins binding partner E5. It is therefore possible that PRAF2 was causing an alteration to the cellular milieu that created an environment that was not conducive to the virus. Under normal circumstances this would be prevented by E5, through a yet unknown mechanism.

However, before being certain that this was the case, further experiments need to be performed. Firstly, to re-stain sections for HPV-18E1<sup>E4</sup> to rule out possible experimental error, as this is only n=1. Additionally, to stain for other HPV late genes such as HPV-18L1. Further to this, performing HPV-18 genome Chromogenic In Situ Hybridisation (CISH) to see if genome amplification was occurring. Unfortunately, there was not time to do these experiments.

Once again, it was regrettable that there are no NHK rafts to compare to, as we could have asked if the change in thickness was due to an reversion to a more 'NHK' phenotype, which could also possibly have the effect of overcoming the delay to differentiation caused by HPV and restricting re-entry to the cell cycle in the suprabasal layers. Unfortunately, the proliferation status of the rafts could not be assessed, owing to a failure to obtain BrdU staining. The rafts were treated with BrdU prior to harvest, as per the literature (Wasson et al., 2017), however the staining was unsuccessful. This could have been due to not having time to optimise the antibody staining procedure. For future work, staining of the rafts for BrdU incorporation or cyclin B1 would be useful.

The rafts were stained for CK10 expression, with a view to determining whether the differentiation of the rafts was altered by changes to PRAF2 expression. In the WT18 and derivative rafts, there was no obvious change observed in the expression of CK10. In the E5KO rafts, again the intensities were very similar, except for the E5KO 3xFLAG-PRAF2, which appeared to have more intense CK10 staining. It is therefore possible that the loss of E1<sup>E4</sup> staining observed in E5KO 3xFLAG-PRAF2 raft is due to PRAF2 having prevented the delay in differentiation usually seen in HPV infection. However, CK10 staining is seen in all the other rafts and is a marker that comes on upon exiting the basal layer (Fuchs, 2008), so a later differentiation marker such as loricrin or filaggrin would help clarify the differentiation status of the raft section.

## Chapter 5 Investigation of the role of PRAF2 in apoptosis

### 5.1 Introduction

#### 5.1.1 The PRAF proteins and Apoptosis

Originally, PRAF2 was identified as an interactor for HPV18E5 (Rozenblatt-Rosen et al., 2012) by TAP-MS. We have since validated this interaction (see Chapter 3) and extended the interaction of HPV18E5 to the other PRA family members PRAF1 and PRAF3 (Chapter 3.2.7). In the previous chapter the role of the PRA family in cancer was discussed, with a focus on PRAF2. In this chapter the focus is on the PRA family in cell death.

Studies on PRAF1 have demonstrated that it can be found localised to the mitochondria by cell fractionation, and that it is able to bind the antiapoptotic protein Bcl2A1 by immunoprecipitation (Kim, J.T. et al., 2019). Overexpression of PRAF1 has been shown to induce cleavage of caspase-3 and PARP in a dose-dependent manner. Overexpression of PRAF1 has also been shown to sensitise cells to cytotoxic insult by cisplatin and mitomycin C, as assayed by an increased detection of cleaved caspase-3 and PARP, and to overcome the actions of antiapoptotic proteins such as Bcl2A1 and the viral Bcl-2 homologue BHRF1 (Li, L.Y. et al., 2001), demonstrating that PRAF1 can act as a tumour suppressor through enhancing cell death.

The PRA family member PRAF3 has a large body of literature attesting to its action as a tumour suppressor (Xu, L. et al., 2018; Chen, Y. et al., 2014; Wu, X. et al., 2014). One of the ways PRAF3 can act as a tumour suppressor is through induction of cell death. Studies on the CCAAT enhancer-binding protein (C/EBP), which has a role in proliferation and differentiation showed that the C/EBP isoform C/EBP $\alpha$  strongly inhibited proliferation and induced cell death (Wang, G.L. et al., 2008). It was found that the mechanism behind C/EBP $\alpha$  mediated cell death was through binding the PRAF3 promoter, which induced a 10-15-fold increase in PRAF3 expression.

siRNA mediated knockdown of PRAF3 confirmed that PRAF3 expression was required for this effect. Interestingly, this was highly cell line dependent, with C/EBP $\alpha$  overexpression increasing PRAF3 promoter activity in NIH3T3 cells but inhibiting it in Hep3G2 cells.

This was reinforced by treatment of HeLa cells with All-trans retinoic acid (ATRA). ATRA stimulates genes with a Retinoic Acid Response Element (RARE), one of which is C/EBP $\alpha$ . ATRA treatment led to an increase in PRAF3 levels. Interestingly, overexpression of PRAF3 and treatment with ATRA resulted in the induction of cell death, whilst knockdown prevented ATRA mediated cell death (Mao, W.G. et al., 2006).

It was later found that PRAF3 expression could be strongly induced through oxidative stress. When treated with H<sub>2</sub>O<sub>2</sub> (Wang, N.P. et al., 2003; Zhu, T. et al., 2005) or AsO<sub>3</sub> (Zhou, J. et al., 2008), PRAF3 levels were seen to increase in HeLa and MCF-7 cancer cells. Treatment also resulted in increased activation of the intrinsic cell death pathway and associated cleavage of caspases 8 and 9. This was found to be ameliorated by the knockdown of PRAF3, which reduced cell death and signalling via a reduction in phospho ERK1/2 and JNK. Overexpression of PRAF3 in ESCC has also been seen to induce cell death (Shi et al., 2012).

Fascinatingly, loss of PRAF3 expression has also been associated with cell death in differentiating tissues. In PRAF3 knockout mice, bone development and maintenance are impaired (Wu, Y. et al., 2015; Wu, Y. et al., 2014). When investigated it was found that various bone matrix proteins were accumulating in the ER. This would fit with the proposal of PRA family members as regulators of ER protein export (Oshikane et al., 2018; Doly et al., 2016). Indeed, this accumulation resulted in the induction of the unfolded protein response (UPR) and cell death via ER stress, with ER stress induced cell death proteins such as CHOP and Gadd34 elevated (Wu, Y. et al., 2014), resulting in increased levels of cleaved caspase-3 and 12. Interestingly, the addition of chemical chaperones ameliorated the effects of PRAF3 loss. This was not the case with PRAF3 overexpression.

Interestingly, this is not the only case of increased PRAF3 resulting in decreased cell death. PRAF3 has also been found to reduce extrinsically mediated cell death in gastric cancer, by downregulating the intracellular receptor of tumour necrosis factor-related apoptosis-inducing ligand (TRAIL), DR4, thereby preventing the potentiation of its apoptotic signalling (Wang, Q. et al., 2017). This is not the first instance of a PRA family member having both proapoptotic and pro-cancer functions. PRAF2 has been found to promote tumorigenesis in several cancer types (He et al., 2019; Qian et al., 2019; Wang, C.H. et al., 2018; Yco et al., 2013). However, PRAF2 has also been shown to be induced by cell death in the neuroblastoma cell line SH-SY5Y (Geerts et al., 2007). PRAF2 has also been demonstrated to bind to Bcl-xL and Bcl-2 and its overexpression has been shown to induce cell death in HeLa cells (Vento et al., 2010), as assayed by PI, PARP cleavage and Bax aggregation. Further to this, PRAF2 knockdown desensitised U2OS cells to etoposide mediated cell death. The aim of this chapter is to explore PRAF2 and cell death in the context of keratinocytes. Overexpression and knockdown of PRAF2 are used to try to understand this.

## 5.2 Results

### 5.2.1 PRAF2 titration into keratinocytes resulted in PARP cleavage in a dose-dependent manner

To ascertain whether we could replicate the findings that PRAF2 induced apoptosis (Vento et al., 2010), C33A and HeLa cells were transfected with increasing amounts of PRAF2-3HA plasmid. In order to ensure all cells received the same mass of DNA per transfection, the PRAF2 transfections with lower PRAF2 plasmid amounts were supplemented with the empty vector pcDNA3.1(+). Cells were transfected and then harvested 48 hours post transfection and assayed for the induction of PARP cleavage. Equal amounts of protein were loaded and resolved by SDS-PAGE. The resulting western blots were probed with antibodies specific for PARP, the HA tag and GAPDH, with PARP cleavage serving as a read out for the induction of apoptosis.

In both C33A and HeLa, PRAF2 induced PARP cleavage (Figure 5.1 A and B). However, it was noted that a large amount of uncleaved PARP remained at all concentrations (Lanes 2, 3 and 4). In C33A cells, the 2x and 3x concentrations of PRAF2 (Lanes 3 and 4, Figure 5.1 A) resulted in a significantly increased levels of PARP cleavage (Figure 5.1 C, \* $p \leq 0.05$ , \*\* $p \leq 0.01$ , respectively). In HeLa cells (Figure 5.1 B), a significant increase in PARP cleavage was observed at all PRAF2-3HA titration concentrations (Lanes, 2, 3 and 4, Figure 5.1 D, \* $p = 0.047$  (pcDNA3.1+/1xPRAF2), \*\* $p \leq 0.001$  (pcDNA3.1+/2xPRAF2), \* $p \leq 0.05$  (pcDNA3.1+/3xPRAF2) respectively). It should be noted that elevated levels of PARP cleavage were also observed in the pcDNA3 control relative to the non-transfected (Lane 5, Figure 5.1 B) sample. It was also noted that degradation of PRAF2-3HA was observed below the monomeric and dimeric forms of the protein in both C33A and HeLa cells. These were due to the triple HA tag sequence containing the caspase-3 cleavage sequence (Schembri et al., 2007), so upon the activation of caspase-3 the tag was cleaved.

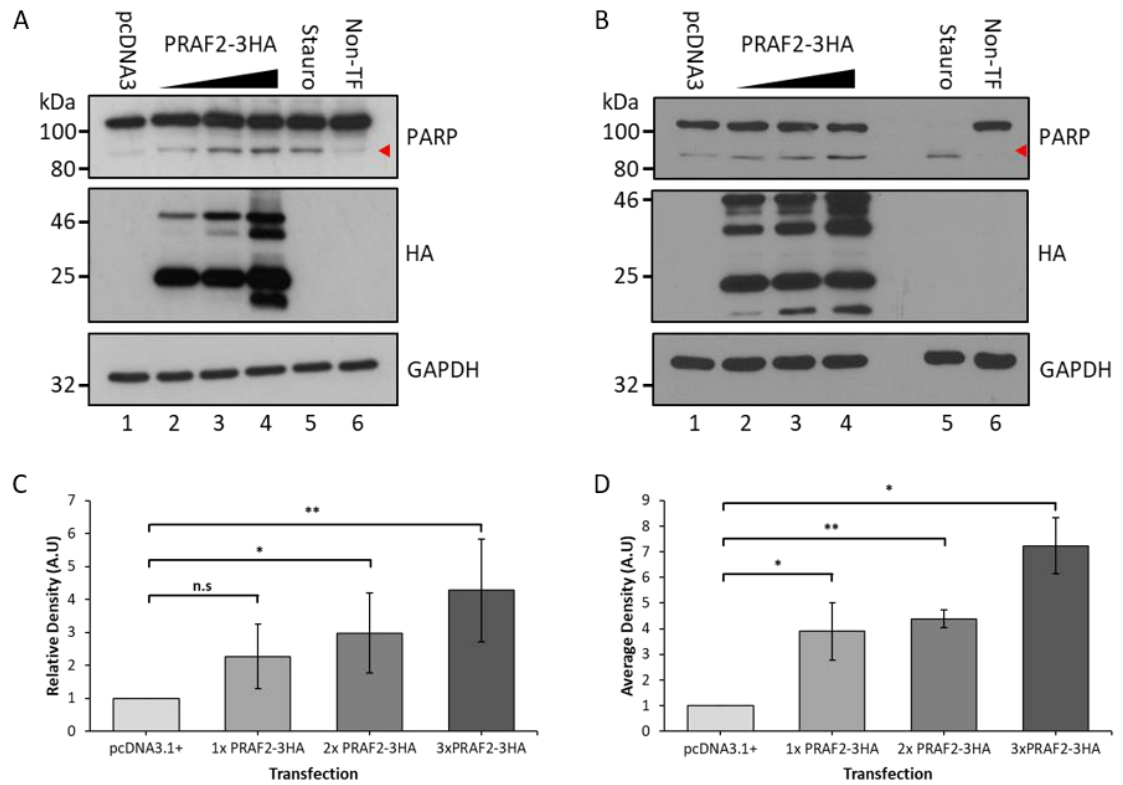


**Figure 5.1** PRAF2-3HA expression induces PARP cleavage in a dosage dependent manner

C33A or HeLa cells were transfected with increasing amounts (25%, 50% and 100% DNA mass of pcDNA3.1(+)) of the pcDNA3-PRAF2-3HA plasmid. pcDNA3.1(+) as control, Stauro (staurosporine), Non-TF (non-transfected). Representative western blots. Probed for PARP (red arrow, cleaved PARP), HA and GAPDH A. Western blot of C33A PRAF2 titration. B. Western blot of HeLa PRAF2 titration. C. Densitometry analysis of C33A PRAF2 titration \* $p \leq 0.05$ , \*\* $p \leq 0.01$ . D. Densitometry analysis of HeLa PRAF2 titration, \* $p \leq 0.05$  (pcDNA3.1+/1xPRAF2), \*\* $p \leq 0.001$  (pcDNA3.1+/2xPRAF2), \* $p \leq 0.05$  (pcDNA3.1+/3xPRAF2) respectively.

### 5.2.2 Induction of apoptosis could not be demonstrated by other methods

It is generally considered good practice to confirm the induction of apoptosis by two or more different methods (Elmore, 2007). To do so additional assays were performed in each cell line. To assay for the onset of cell death the cells were seeded onto coverslips, and 24 hours post seeding transfected with the highest dose of PRAF2-3HA titrated previously (3x, Figure 5.1), 24 hours post transfection the cells were fixed, permeabilised and probed for active caspase-3 and stained using Alexa-488 conjugated secondary antibodies. Negative controls non-transfected, DMSO and pcDNA3 were included. As a positive control, staurosporine was also included.

In both C33A (Figure 5.2 A) and HeLa cells (Figure 5.2 C) no active caspase-3 staining could be detected in pcDNA3 or PRAF2-3HA transfected cells, or in non-transfected or DMSO control cells. A significant increase in active caspase-3 staining was only detected in staurosporine treated C33A cells (Figure 5.2 B). Induction of cell death could be observed in the staurosporine treated HeLa cells (Figure 5.3 C), however it could not be quantified in the manner of the C33A cells, as unlike C33A, HeLa nuclei were stained with the active caspase-3 antibody in a non-specific manner (Figure 5.3), even in cells not currently undergoing cell death. The antibody did stain active caspase-3 in a noticeable fashion that was distinguishable from the nuclear staining.

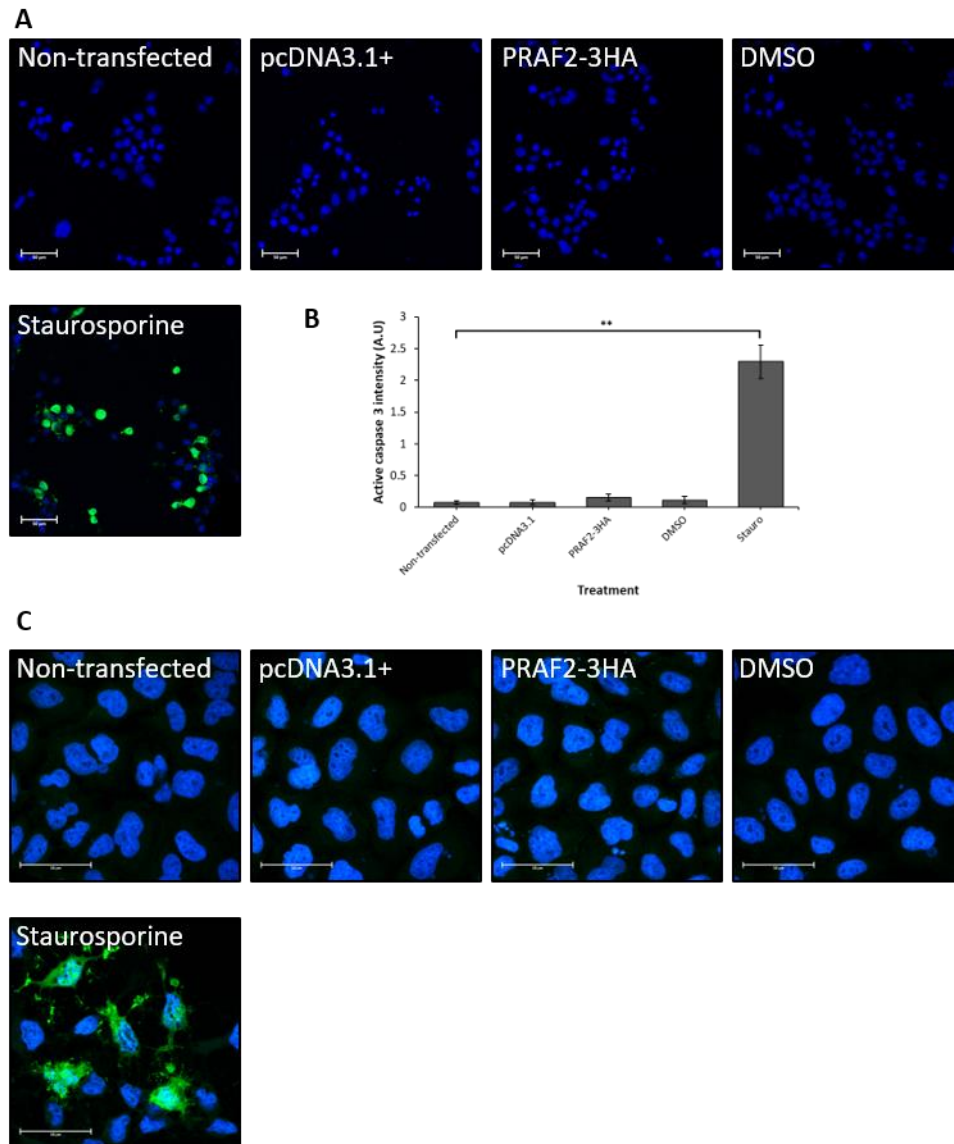


**Figure 5.2** *PRAF2-3HA overexpression failed to induce detectable caspase-3 cleavage*

*C33A and HeLa cells were transfected with PRAF2-3HA or pcDNA3.1, with non-transfected, DMSO and staurosporine controls included. 1  $\mu$ M staurosporine treatment for 3 hours served as a positive control for caspase-3 cleavage. Cells were fixed and permeabilised 24 hours post transfection. Cells were probed with an antibody against active caspase-3 and then were stained with a Alexa-488 conjugated secondary antibody (green). Representative Images. Nuclei counterstained with DAPI Scale bars 50  $\mu$ m. A. C33A cells stained for active Caspase-3. B. Active caspase-3 intensity. C. HeLa cells stained for active caspase-3.*

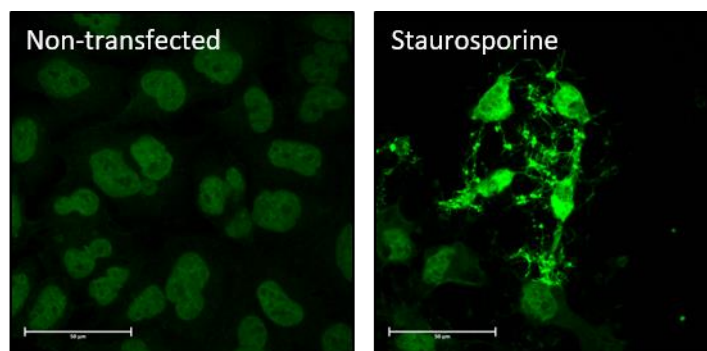


**Figure 5.3** *Active caspase-3 antibody stained the nuclei of non-apoptotic HeLa cells.*

*HeLa cells were fixed, permeabilised and probed with an antibody to active-caspase-3 and then stained with an alexa-488 conjugated secondary. In non-transfected cells fluorescence is observed in the 488-channel in the nucleus but not the cytoplasm, however in staurosporine treated cells there is an increased level of fluorescence detected and it is localised to the cytoplasm.*

It was attempted to ascertain whether cell death was occurring by DNA laddering assay. DNA laddering detects DNA fragmentation because of caspase activated DNase (CAD) activation, which results in a distinct ladder of DNA fragments with ~200bp staggering. Cells were transfected with either pcDNA3.1+ or PRAF2-3HA, with non-transfected DMSO treated cells as a negative control and staurosporine treated cells as a positive control. 48 hours post transfection the cells were harvested, with the cell media also harvested and spun down to ensure that any detached apoptotic cells were retained. The DNA was then extracted and run out on agarose gels and the resulting DNA ladders imaged.

In C33A cells, DNA laddering was only observed in the staurosporine treated cells (Lanes 3, 7 and 11, Figure 5.4 A) in each repeat. The pcDNA3 (Lanes 1, 5 and 9, figure 5.4 A) and PRAF2-3HA (Lanes 2, 6 and 10, figure 5.4 A) transfected samples were comparable to non-transfected control cells in the absence of laddering observed. The same was true of HeLa cells, however, the laddering in the staurosporine treated cells (Lanes 3, 7 and 11, figure 5.4 B) was not as

defined as in C33A cells. There was no discernible difference observed between pcDNA3, PRAF2-3HA and non-transfected HeLa cells in the DNA laddering assay.

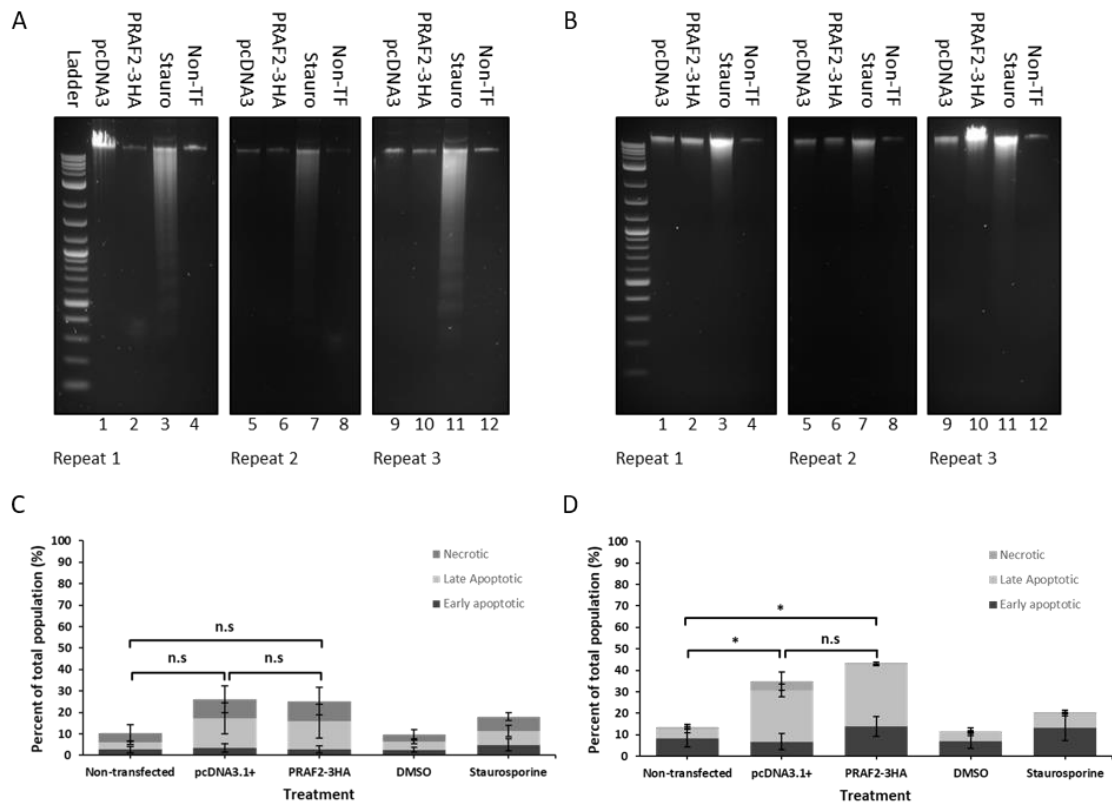


**Figure 5.4** DNA laddering and Annexin V assays did not detect a significant increase in cell death between pcDNA3 and PRAF2 transfected cells

A-B. C33A and HeLa cells were transfected with PRAF2-3HA or pcDNA3.1, DMSO, non-transfected (Non-TF) and staurosporine (Stauro) controls were included. Cells were harvested 48 hours post transfection. 1  $\mu$ M staurosporine treatment for 6 hours. A. Three repeats of C33A DNA laddering assay. B. Three repeats of HeLa DNA laddering assay. C-D. C33A and HeLa cells were transfected with PRAF2-3HA or pcDNA3.1, with non-transfected, DMSO and staurosporine controls included. Cells harvested 24 hours post transfection. 1  $\mu$ M staurosporine treatment for 3 hours. N=3 C. Annexin V assay of C33A cells. D. Annexin V assay of HeLa cells. \* $p \leq 0.05$  and 0.01 respectively.

As a further assay, the cell lines were assayed for apoptosis by annexin V/propidium iodide assay. As before cells were transfected and appropriate controls were included. Cells were then carefully harvested 24 hours post transfection and assayed by flow cytometry. In C33A cells (Figure 5.4 C) there was a noticeable increase in the % of the total population of cells in late apoptosis and necrosis for those transfected with pcDNA3 and PRAF2-3HA, however, the populations of early apoptotic, late apoptotic and necrotic cells were not significantly different when taken individually and compared to the non-transfected control, nor were they significantly different from each other.

When HeLa cells were assayed by annexin V/propidium iodide assay, there was a significant increase in late apoptotic cells in pcDNA3 transfected cells ( $p \leq 0.05$ ) and in PRAF2-3HA transfected cells ( $p \leq 0.01$ ) relative to non-transfected cells. However, when the late apoptotic populations of pcDNA3 and PRAF2-3HA transfected HeLa cells were compared there was no statistically significant difference. There was a statistically significant increase in the population of early apoptotic cells in PRAF2-3HA transfected cells relative to non-transfected cells ( $p = 0.0083$ ), however, there was not between the pcDNA3 and PRAF2-3HA transfected cells. Overall, this suggested that for both C33A and HeLa cells transfection mediated toxicity was a large problem, as no difference can be distinguished between the two transfected controls, this prevented meaningful interpretation.

### **5.2.3 GFP-18E5 co-expression abrogates PRAF2 mediated PARP cleavage**

We decided to investigate what effect the co-expression of the PRAF2 binding partner GFP-18E5 would have on the ability of PRAF2-3HA to induce PARP cleavage. To do so, HEK-293 cells were transfected with either GFP, GFP-18E5, PRAF2-3HA or GFP-18E5 and PRAF2-3HA. To ensure all cells received the same amount of DNA, pcDNA3.1(+) was supplemented in to ensure equal DNA mass in 'single' transfectants. Cells were lysed 48 hours post transfection. Equal

volumes of protein were resolved by SDS-PAGE and the resulting western blots probed for PARP, HA, GFP and GAPDH.

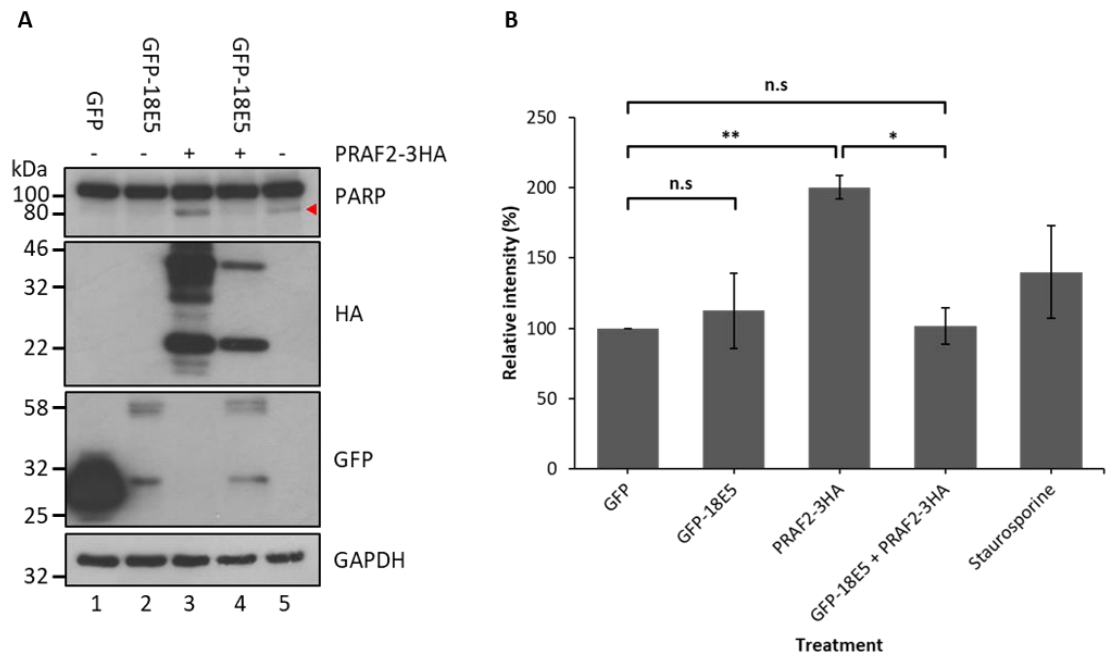


**Figure 5.5** **Coexpression of GFP-18E5 with PRAF2-3HA prevented PARP cleavage**

HEK-293 cells were transfected with either GFP, GFP-18E5, PRAF2-3HA or GFP-18E5 and PRAF2-3HA and lysed after 48 hours, equal amounts of protein resolved by SDS-PAGE and resulting westerns probed for PARP, HA, GFP and GAPDH. PARP cleavage indicated by red arrow. Representative western blot shown. A. Western blot of PARP cleavage experiment. B. Densitometry analysis of PARP cleavage. Two-tailed paired t-test. Error bars standard deviation. \*\* $p \leq 0.01$ , \* $p \leq 0.05$ .

In cells transfected with GFP or GFP-18E5 alone, no PARP cleavage was observed (Lanes 1 and 2, Figure 5.5 A). Moderate PARP cleavage was detected in cells expressing PRAF2-3HA only and in those treated with staurosporine (Lanes 3 and 5, Figure 5.5 A). Indeed, PRAF2-3HA overexpression resulted in a statistically significant increase (\*\* $p=0.0034$ , Figure 5.5 B) in PARP cleavage. When PRAF2-3HA and GFP-18E5 were coexpressed (Lane 4, Figure 5.5 A) a statistically significant decrease (\* $p=0.0198$ ) in PARP cleavage (Figure 5.5 B) relative to PRAF2-3HA alone

was observed. It was noted that the levels of PRAF2-3HA observed in the coexpression (Lane 4) were lower than that of PRAF2-3HA expressed alone (Lane 3) despite having the same amount of PRAF2-3HA plasmid transfected.

#### **5.2.4 PRAF2 knockdown and overexpression is tolerated by stable cell lines**

We have previously made stable cell lines overexpressing PRAF2 in C33A and HeLa (Chapter 4, Figure 4.1) and those with PRAF2 knockdown by shRNA (Chapter 4, Figure 4.1). These cell lines were stable across multiple passages. In C33A cells stably expressing PRAF2, we did not observe an elevated level of basal PARP cleavage relative to control zsGreen or normal C33A cells (Lane 3, Figure 5.6 A), and PRAF2 expression was detected at levels far above endogenous levels in C33A cells. Indeed, by the time endogenous PRAF2 was detectable in the control cells (Lanes 1 and 2, PRAF2 (long), Figure 5.6 A), the signal from the PRAF2 overexpressing cells had overwhelmed the signal from the C33A zsGreen (lane 2).

It had also previously been demonstrated that the knockdown of PRAF2 increased the survival of cells when treated with a cytotoxic agent such as etoposide (Vento et al., 2010). We therefore tested this with our C33A shPRAF2 cell line. The C33A cell lines were treated with the cytotoxic agent staurosporine at a final concentration of 1 $\mu$ m 48 hours post seeding. Cells were incubated with staurosporine for 3 hours, then lysed. Equal amounts of protein were then resolved by SDS-PAGE and the resulting western blots probed for PRAF2, PARP and GAPDH (Figure 5.6 B). PRAF2 was still detectable with a long exposure in C33A shPRAF2 cells (Lanes 5-10), however levels were decreased relative to the C33A and C33A shNTC cells (Lanes 1-4). When treated with staurosporine (even lanes), levels of PRAF2 were not altered (odd lanes). staurosporine successfully caused PARP cleavage in all the samples treated (even lanes). There was also no difference detected in the levels of PARP cleavage seen between control and shPRAF2 cells. This suggested that PRAF2 knockdown was not protective against cytotoxic insult.

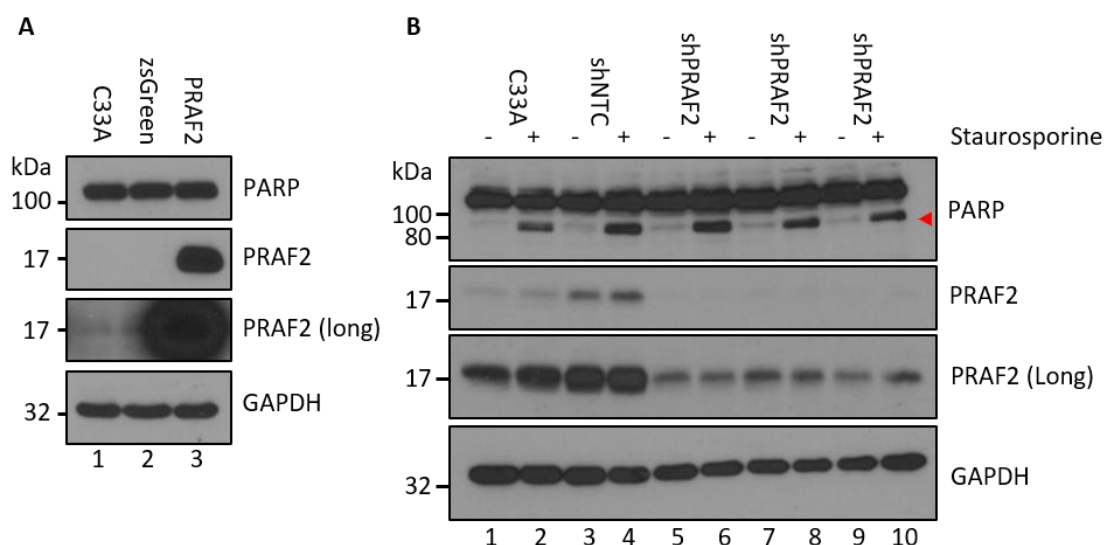


**Figure 5.6** *Stable overexpression of PRAF2 in C33A cells did not increase levels of PARP cleavage and PRAF2 knockdown did not desensitise C33A cells to staurosporine*

Western blots of C33A stable cell lines, equal amounts of protein were loaded, resolved by SDS PAGE and the resulting western blots probed for PARP, PRAF2 and GAPDH expression, representative blots. PARP cleavage indicated by red arrow. A. Western blot of C33A, C33A zsGreen and C33A PRAF2 stable cell lines. N=3 B. Western blot of C33A, C33A shNTC and C33A shPRAF2 cells treated with 1 $\mu$ M staurosporine or DMSO for 3 hours. N=3.

### 5.2.5 The localisation of PRAF2 and changes to cellular morphology

It was noted when testing the expression and localisation of a GFP-PRAF2 plasmid that there were instances where the cell had disturbed cellular morphology. In these cells, small amounts of a GFP-PRAF2 plasmid had been transfected into HeLa cells, and then the cells fixed, permeabilised and probed for the ER marker calnexin and stained with an alexa-594 conjugated secondary antibody. It was found that the distribution of the ER cellular marker Calnexin was greatly disturbed when the expression of the GFP-PRAF2 plasmid was particularly high, as judged by the intensity of the GFP observed. In these cells, the ER was no longer in the typical pattern

one would expect (Chapter 3, Figure 3.4 A), but had taken on a granular, droplet like morphology (Figure 5.7). This suggested the possibility that high levels of PRAF2 expression could disrupt ER morphology, which would likely lead to cell death.

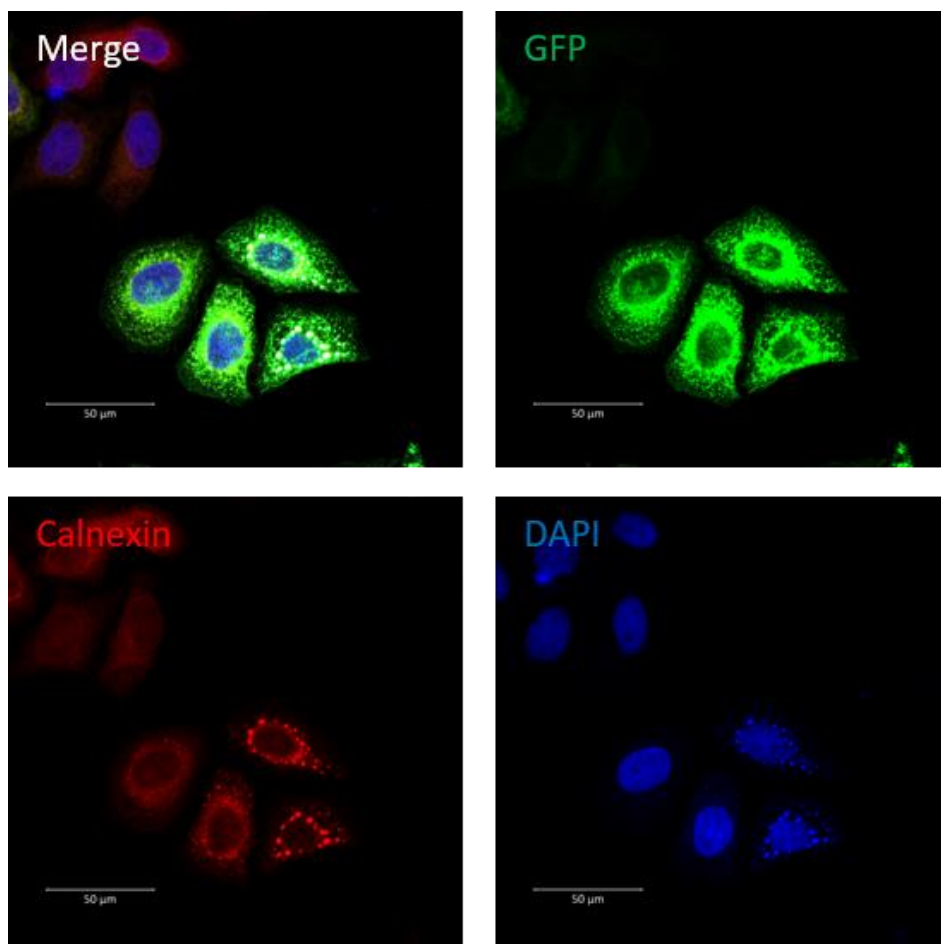


**Figure 5.7** *High levels of GFP-PRAF2 expression result in the redistribution of calnexin to puncta*

*HeLa cells were transfected with GFP-PRAF2, 24 hours post transfection cells were fixed, permeabilised and probed with an antibody to the ER marker Calnexin. Calnexin was stained with an alexa-594 conjugated secondary antibody (red). Nuclei were counterstained with DAPI (blue). Scale bar 50μm.*

In previous work on apoptosis and PRAF2, we attempted to see if the induction of apoptosis would result in a redistribution of the PRAF2 protein within the cell. One of the places

considered was the Mitochondria, as PRAF2 had been demonstrated to interact with Bcl-xL (Vento et al., 2010) an antiapoptotic protein which localises to mitochondria. However, despite trying a variety of cell lines (C33A, SiHA and HPV positive primary keratinocytes) the PRAF2 antibody was not able to stain endogenous PRAF2 in a specific manner (Appendix C.3).

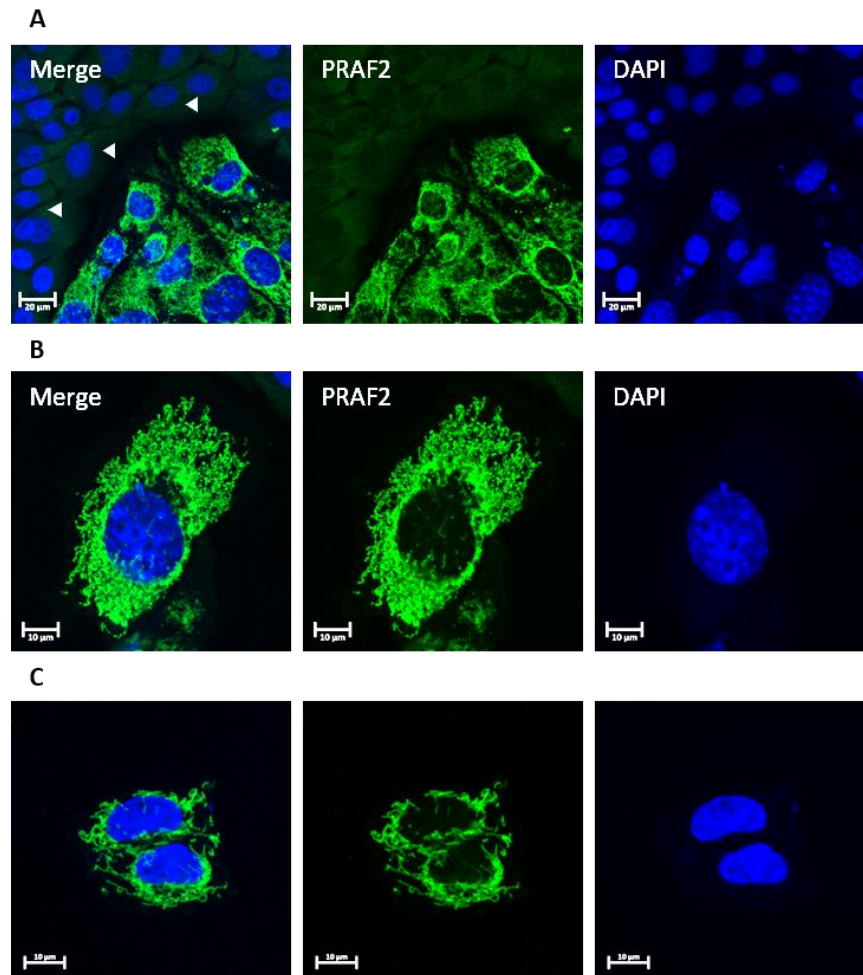


**Figure 5.8** PRAF2 staining in mitomycin C treated 3T3 cells resembles mitochondrial staining in C33A cells

A-B, Primary keratinocytes and mitomycin C treated 3T3 cells stained for PRAF2 (Green) and DAPI (Blue). A. Primary keratinocytes and mitomycin C treated 3T3 cells, scale bar 20 µm, stained for PRAF2. B. Mitomycin C treated 3T3 cell stained for PRAF2. 2x Digital zoom. Scale bar 10 µm. C. C33A cell with mitochondria stained with the dye Mitotracker CMXRos (Appendix B.1). Mitotracker false coloured to green. 2x Digital zoom. Scale Bar 10 µm

However, it was noticed when attempting to optimise the antibody in HPV positive primary keratinocytes that it stained J2 3T3 cells. HPV primary keratinocytes are cultured on a replication incompetent J2 3T3 mouse fibroblast feeder layer. These 3T3 cells are rendered quiescent through treatment with 8 µg/ml of the DNA damaging agent mitomycin C for 2 hours. These mitomycin C treated J2 3T3 cells were seeded onto coverslips with HPV positive keratinocytes, these keratinocytes were then grown for a further 48 hours prior to treatment with either staurosporine or DMSO for 1, 2 or 3 hours. These cells were then fixed, permeabilised and probed with an antibody to PRAF2 and stained with an alexa-488 conjugated secondary antibody and then imaged by confocal microscopy.

The HPV primaries (White arrows, Figure 5.8 A) did not stain for PRAF2 in a specific manner, however, the mitomycin C treated J2 3T3 cells stained strongly with the PRAF2 antibody (Figure 5.8 A and B). The staining pattern exhibited was strongly reminiscent of the staining one would expect for mitochondria (Figure 5.8 C). It was interesting that the mitomycin C treated J2 3T3 cells exhibited a mitochondrial staining pattern for PRAF2, and that the keratinocytes failed to stain.

## 5.3 Discussion

This study returned conflicting data about the PRAF2 protein and cell death. Of the previous papers which studied PRAF2 in the context of cell death, the first paper only suggested that the levels of PRAF2 increased upon treatment with the cytotoxic agent cerulenin (Geerts et al., 2007). The second paper however demonstrated that the overexpression of PRAF2 was sufficient to induce apoptosis (Vento et al., 2010). We have shown that it was possible to induce moderate PARP cleavage via transfection of PRAF2 in both HeLa and C33A cells, as, and that this was a dose dependent effect. A similar dose dependent effect has been observed for PRAF1 (Kim, J.T. et al., 2019) and PRAF3 (Shi et al., 2012).

However, whilst the initial data seemed clear cut, we encountered issues with attempting to demonstrate cell death via other methods. The original publication demonstrating the proapoptotic nature of PRAF2 demonstrated apoptosis via propidium iodide staining, PARP cleavage and GFP-Bax aggregation. Attempts at demonstrating caspase-3 activity were unsuccessful, with no significant difference observed between non-transfected and pcDNA3/PRAF2 transfected C33A cells, the staurosporine control did however demonstrate that the assay would work if PRAF2 had been inducing caspase-3 cleavage. This was particularly odd as the amount of PRAF2 DNA transfected was equivalent to the maximum dose previously used. The HeLa data showed that there was no observable difference in caspase-3 activity between the non-transfected cells and pcDNA/PRAF2. It was notable that the active caspase-3 antibody stained the cell nuclei in HeLa cells in the absence of caspase-3 activation, which prevented analysis in the manner of the C33A samples.

Similar observations regarding the lack of apoptosis were observed in attempts at a DNA laddering assay. Whilst all repeats were successfully able to detect DNA laddering when apoptosis was occurring i.e. staurosporine treated cells. There was no difference observed

between non-transfected and transfected cells, with no DNA ladder observed, this was true for both C33A and HeLa cells. Taken with the lack of Caspase-3 activation, this suggested that PRAF2 was not acting in a proapoptotic manner.

There was no significant difference between PRAF2 transfected cells and pcDNA3 transfected cells in C33As in the Annexin V-Propidium Iodide assay in any cell population (Early/Late Apoptotic, Necrotic), nor was there a significant difference from the non-transfected controls. Notably, the staurosporine failed to induce cell death. In HeLa cells, there was a significant increase in late apoptotic cells relative to the non-transfected cells in both pcDNA3 and PRAF2 transfected cells. However, there was no significant difference between pcDNA3 and PRAF2 cells in late apoptotic cells. A small significant change was observed in the population of early apoptotic cells. However, with the overall picture considered, it appeared that transfection mediated cytotoxicity was highly problematic, as both transfected samples show an increase in apoptosis relative to the non-transfected control. This makes it impossible to tell if PRAF2 was having an effect. This was also a problem with attempts to replicate the GFP-Bax aggregation assay, as the act of transfection caused GFP-Bax aggregation in a manner unrelated to the action of PRAF2.

These data paint a contradictory picture, as in only one out of four assays suggested the induction of significant cell death, and in this only moderate PARP cleavage was detected, however in the other three this failed. An additional point of frustration was that in the original paper (Vento et al., 2010) HeLa cells were the cell line used for both the Propidium Iodide and PARP assays. In addition to these cell death assays, we were able to produce monoclonal C33A and HeLa cell lines that overexpressed PRAF2 in a stable manner, with no decrease in PRAF2 expression seen over many passages. If the PRAF2 protein was inducing cell death- and no evidence of PARP cleavage is detected, we would not have expected these cell lines to persistently passage. Further to this, when these cells were tested for their ability to form

colonies and to proliferate, no negative effects were detected. These data also need to be considered with regards to what is known about PRAF2 in the literature, that is that in most reports PRAF2 acts in a pro-cancer function, such as increasing proliferation and colony formation (Qian et al., 2019; He et al., 2019; Yco et al., 2013; Borsics et al., 2010; Geerts et al., 2007), which is contradictory to its role in cell death. This can often be a cancer tissue specific difference, but here we use HeLa cells, as in the original paper.

We did observe that when PRAF2-3HA and GFP-18E5 were coexpressed that the PARP cleavage detected with PRAF2-3HA expression alone was abrogated which would suggest that PRAF2s ability to induce moderate PARP cleavage was being disrupted. It should be noted however, that this was a different cell line to those used previously (HEK293 versus C33A and HeLa), and that in the GFP-18E5, PRAF2-3HA cotransfection the levels of PRAF2-3HA detected are reduced compared to PRAF2-3HA alone. It has been previously observed with PRAF1, that when coexpressed with another membrane protein, levels of PRAF1 expression are reduced (Jacobs and Pirson, 2003), this effect was not seen when PRAF1 was expressed with cytosolic proteins. It could therefore mean that the loss of PARP cleavage is due to PRAF2 expression being reduced to below the threshold of toxicity.

It should be noted that this assay was carried out prior to any of the other research in this chapter and the chapter previous. When this assay was performed there were issues with producing detectable and physiologically relevant levels of E5 expression that have since been overcome by the codon optimisation of the gene. HEK293 cells were used at the time as they expressed the GFP-18E5 protein at useable levels. With the codon optimised HPV-18 E5 it may be possible now to repeat this assay in a more physiologically relevant cell line such as SiHa or HeLa to see if the same effects are observed.

Our data also failed to show a protective effect for PRAF2 knockdown on cell survival on treatment with cytotoxic agents. Previously, it had been demonstrated that siPRAF2 treated

U2OS cells treated with Etoposide exhibited reduced Caspase 3 and 7 activation relative to controls (Vento et al., 2010), and post treatment displayed a greater ability to form colonies relative to control cells. However, there are two key differences in our experimental data, firstly, C33A cells not U2OS cells were used, and secondly staurosporine was used instead of Etoposide. The mechanism of action of staurosporine differs to that of Etoposide. Staurosporine is a non-selective inhibitor of PKC and cyclin-dependent kinase (CDKs) (Antonsson and Persson, 2009), whereas Etoposide is a Topoisomerase II inhibitor. Etoposide treatment results in double stranded DNA (dsDNA) breaks (Montecucco et al., 2015), single strand breaks (Muslimović et al., 2009) and reactive oxygen species (ROS) (Shin, H.J. et al., 2016), and hence apoptosis by DNA damage. To speculate, it is therefore possible that the differences observed could be due to their different modes of action.

The PRA family member PRAF3 has been demonstrated to be induced by stimulation with producers of ROS, such as H<sub>2</sub>O<sub>2</sub>, AsO<sub>3</sub> and cisplatin (Wang, N.P. et al., 2003; Zhu, T. et al., 2005; Chen, R. et al., 2007; Zhou, J. et al., 2008; Wang, S. et al., 2009; Xu, W. et al., 2014). In studies on PRAF3, knockdown resulted increased sensitivity to H<sub>2</sub>O<sub>2</sub> induced ROS (Chen, R. et al., 2007). It was also found that increased PRAF3 resulted in an increase in the base excision repair (BER) protein XRCC1. It was later found that PRAF3 was a member of the BER complex, with H<sub>2</sub>O<sub>2</sub> inducing translocation to the nucleus and association with XRCC1, PARP1 and DNA ligase III (Wang, S. et al., 2009), protecting against DNA damage. Further to this, PRAF3 was found to be required for dsDNA break repair in cisplatin treated gastric cancer cells, and enhanced cisplatin-induced cell death via regulating DNA damage induced apoptosis (Xu, W. et al., 2014). It was found that overexpression of PRAF3 resulted in increased PARP cleavage and  $\gamma$ H2AX in response to cisplatin and hence cell death, and that PRAF3 knockdown reduced PARP1 cleavage and cell death on cisplatin treatment. It is therefore possible that the increased survival in response to the DNA damaging agent Etoposide in siPRAF2 U2OS cells is due to PRAF2

mediating DNA damage induced apoptosis in a manner like PRAF3 in response to cisplatin. As a result, this effect would not be seen with staurosporine, due to a different mechanism of action.

Further to this, there is the interesting observation regarding the mitomycin C treated J2 3T3 cells. Mitomycin C is also a DNA damaging agent, with a mechanism similar to that of cisplatin (Palom et al., 2002) and also targets the enzyme thioredoxin reductase (TrxR) (Paz et al., 2012), which is a target of the PRAF3 inducing agent AsO<sub>3</sub> (Lu et al., 2007; Chen, H. et al., 2007) inducing ROS production and oxidative stress (Alili et al., 2014). Could it therefore be possible that the localisation of PRAF2 to bodies with a mitochondrial morphology is in response to the production of ROS owing to Mitomycin C induced senescence?

Regarding the disruption to the localisation of the Endoplasmic reticulum seen in HeLa cells expressing high levels of GFP-PRAF2, I have been unable to find many examples of disruption to the localisation of Calnexin due to protein overexpression. However, the closest looking article in the literature was the example of the overexpression of the protein Starch-binding domain-containing protein 1 (Stbd1). At low levels of Stbd1 expression, an ER staining pattern was observed. However at high levels of Stbd1, Stbd1 was localised to rounded structures, which stained positive for the ER markers Calnexin and Sec61β (Demetriadou et al., 2017). It was found that these structures also contained mitochondria, and that Stbd1 was localising to mitochondrially associated ER membranes (MAMs) and playing a role in the association of mitochondria with the ER. Whilst highly speculative, the redistribution of Calnexin in GFP-PRAF2 high HeLa cells is reminiscent of the staining observed in Stbd1 high cells, so perhaps PRAF2 is also playing a role in mitochondrial-ER tethering. We have also observed the possible localisation of PRAF2 to mitochondria in 3T3 cells. In addition to this, the PRAF2 interacting protein HPV-16E5 has been demonstrated to interact with other ER-Mitochondria bridging proteins such as BAP31 (Regan and Laimins, 2008; Iwasawa et al., 2011) and FATE1

(Doghman-Bouguerra et al., 2016; Rozenblatt-Rosen et al., 2012), therefore it is possible that PRAF2 is also involved in this function.

## Chapter 6 Investigating the PRAF2 interactome by BioID

### 6.1 Introduction

#### 6.1.1 The PRAF2 interactome

Little is known about the PRAF2 interactome. Currently, PRAF2 has a small number of confirmed host cell interactors, in addition to the interaction with HPV E5 proteins (explored in chapter 3), PRAF2 is known to interact with the antiapoptotic proteins Bcl-2 and Bcl-xL (Vento et al., 2010), as well as being able to homodimerize and heterodimerise with its family member PRAF3 (Schweneker et al., 2005). In addition to this PRAF2 has been immunoprecipitated with VAPA (Gougeon and Ngsee, 2005), CCR5 (Schweneker et al., 2005) and GABAB1 (Doly et al., 2016) receptor subunit. Yeast two-hybrid assays also identify the Glycerophosphodiester Phosphodiesterase 1 (GDE1) as a PRAF2 interactor. Further to these direct interactors, a possible interaction with the Rab proteins Rab1b, Rab11a and Rab21 can be inferred from RNAi experiments (Galea et al., 2015). To gain greater understanding of the PRAF2 protein it would therefore be helpful to understand more about its protein interactome. This in turn could help explain some of the phenotypes observed in PRAF2 overexpression and knockdown studies.

PRAF2 has been previously demonstrated to reside in the ER (Chapter 3), Golgi and Endosomes (Geerts et al., 2007), and is predicted to be a transmembrane protein, with both amino and carboxyl termini residing in the cytoplasm. Membrane protein interactions can be difficult to study, owing to their dynamic nature and the complex environment in which they reside (Avila et al., 2015). Retrieval of proteins from membranes involves the use of detergents, however these are often deleterious for maintaining protein-protein interactions (Vento et al., 2010), so the resulting co-immunoprecipitation mass spectroscopy analysis may not paint the full picture of a proteins interactions.

Recently, a new method for investigating protein-protein interactions has been developed called BioID. BioID is a method that enables the identification of other proteins in the proximity of your protein of interest. It was inspired by the concept of DamID, whereby a DAM methylase was fused to a DNA binding protein, which would then bind DNA and methylate the region in its proximity, so you could see where your DNA binding protein bound (van Steensel and Henikoff, 2000). With BioID, a biotin ligase (BirA) is fused to your protein of interest. This BirA has been humanised and mutated to promiscuously biotinylate proteins (Roux et al., 2012). The result is the biotinylation of proteins near the BirA-protein of interest fusion. These samples can then be processed and isolated using very harsh methods to ensure maximal biotinylated protein recovery, and then screened by mass-spectroscopy to ID possible interactors. Since its initial publication, there have been ~183 publications using this method (at the time of writing), and has been used to study weak, transient interactions as well as traditionally insoluble proteins, for example in the nuclear envelope (Kim, D.I. et al., 2014), cell-cell junctions (Van Itallie et al., 2014) and has even been used to produce recombinant viruses to identify virus host interactions (V'kovski et al., 2019). It is important to note however, that the BioID method cannot distinguish between direct interactions and indirect interactions e.g. as part of a protein complex, nor can it distinguish between interactors and proteins in proximity to the protein of interest.

Since its initial inception, the BioID method has been refined, and new biotin ligases have come available, such as TurboID (Branon et al., 2018) and BioID2 (Kim, D.I. et al., 2016). The BioID2 BirA is derived from *A. aeolicus* rather than *E. coli*, and it is both smaller and lacks the DNA binding domain of the *E. coli* BirA. The BioID2 BirA has been humanised and mutated to also promiscuously biotinylate, and is more efficient than the BioID BirA, requiring less biotin.

The aim of this chapter is to use the BioID method to explore the interactome of PRAF2 in keratinocytes. The validation of the BioID2-PRAF2 construct is explored here, as well as the PRAF2 BioID interactome.

## 6.2 Results

### 6.2.1 Fusion of PRAF2 to GFP does not alter subcellular localisation

It was important when making the BioID2 fusion protein to ensure that the function and localisation of the fusion was as physiologically relevant as possible. Fusing the protein of interest to GFP was a good way to determine if an N or C-terminal fusion was going to disrupt the cellular localisation of the protein (Roux et al., 2013). To this end GFP N and C terminal fusions of PRAF2 were created (Figure 6.1 A). These fusions were transfected into HeLa cells, and 24 hours post transfection the cells were fixed, permeabilised and probed for the ER marker

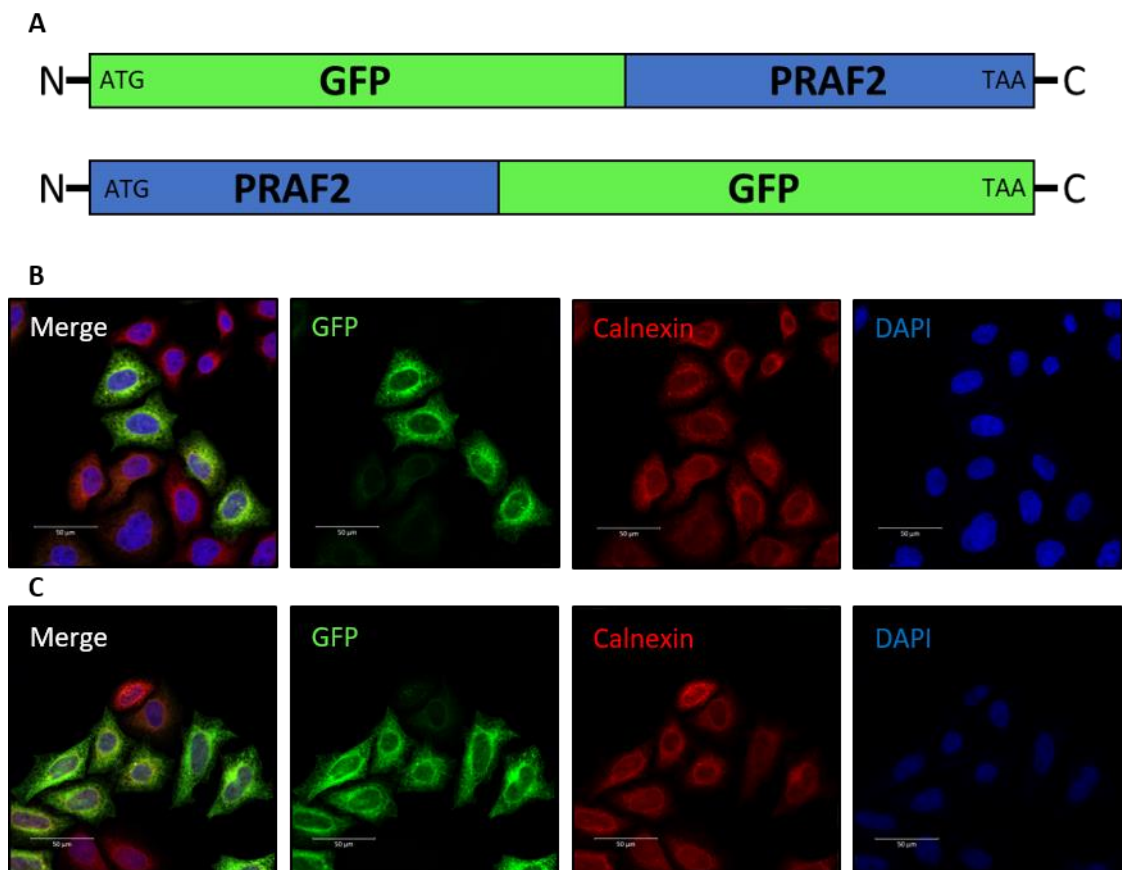


**Figure 6.1** GFP fusion of PRAF2 did not alter its subcellular localisation

A. Schematic representation of N and C terminal GFP-PRAF2 fusions. B-C. GFP-PRAF2 fusions were transfected into HeLas, 24 hours post transfection was fixed and permeabilised and probed for calnexin, then stained with an Alexa-594 conjugated secondary (red). Nuclei counterstained with DAPI (blue). Scale bars 50 µm. B. N-terminal GFP-PRAF2. C. C-terminal GFP-PRAF2. N=3

calnexin. Previously, we had established that PRAF2 primarily localised to the ER in HeLa cells (Chapter 3), and as with HA and FLAG tagged PRAF2, GFP tagged PRAF2 colocalised with calnexin (Figure 6.1 B and C). There was no difference observed in localisation between GFP-PRAF2 (Figure 6.1 B) and PRAF2-GFP (Figure 6.1 C), suggesting that either GFP fusion was permissible. This was fortunate, as it enabled the use of a retroviral BioID2 vector, which only existed as an N-terminal BioID2 fusion option.

### 6.2.2 Myc-BioID2-PRAF2 does not display altered localisation relative to GFP fusions

After the initial cloning and production of the retroviral pBABE-Myc-BioID2-PRAF2 vector, this construct was used to create a stable C33A cell line. To make the cell line, the retroviral plasmid was transfected into the retroviral helper cell line Phoenix A, to produce infectious virus. This retrovirus (Figure 6.2) was then used to infect C33A cells, which were then selected with Puromycin to produce a stable cell line. Once produced, this cell line was validated for its expression of the Myc-BioID2-PRAF2 fusion protein. Initial validation was performed by immunofluorescence.

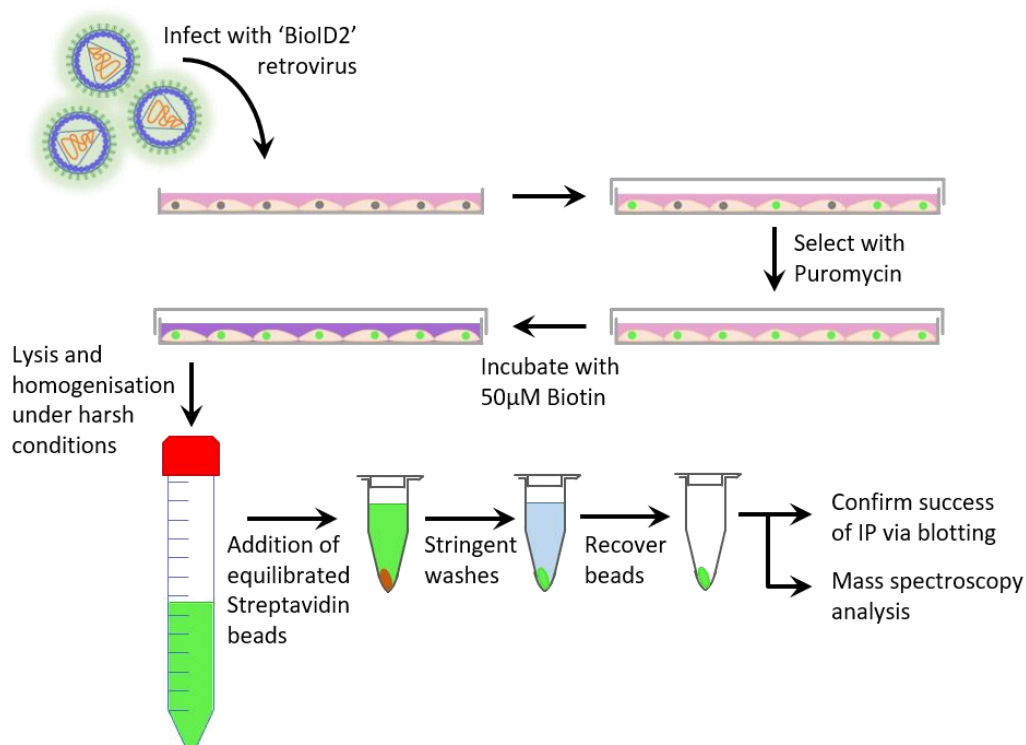


**Figure 6.2** *Schematic of the BioID workflow*

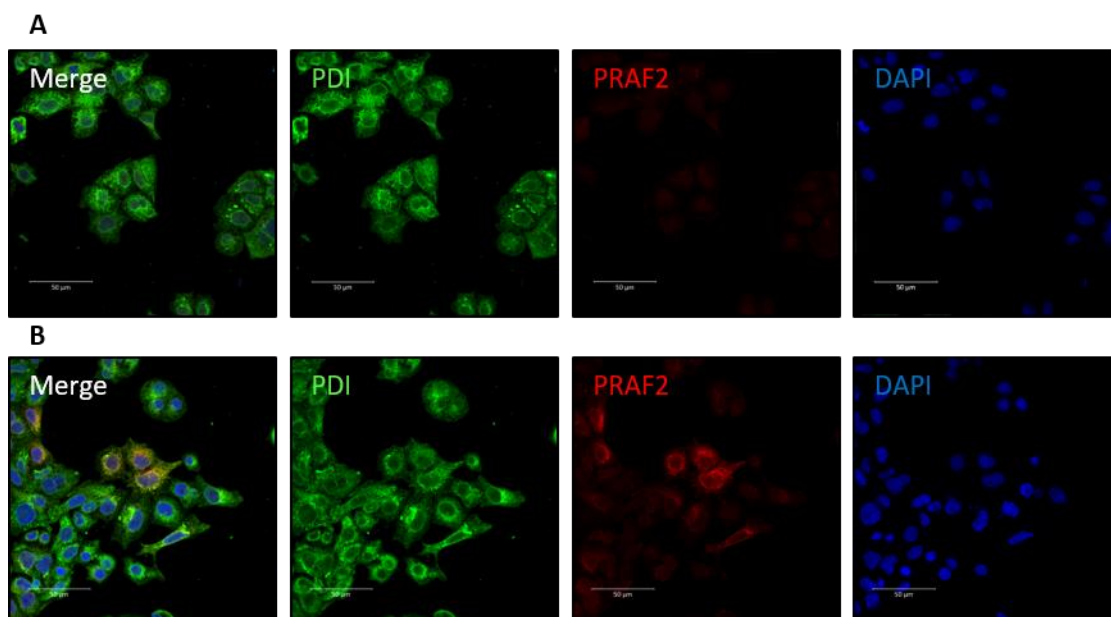


**Figure 6.3** *Myc-BioID2-PRAF2 colocalised with the ER marker PDI*

*C33A Myc-BioID2 and Myc-BioID2-PRAF2 cell lines were fixed and permeabilised and probed with antibodies to PRAF2 and PDI, then stained with Alexa-488 and 594 conjugated secondary antibodies. PDI (green), PRAF2 (red). Nuclei counterstained with DAPI (blue), Scale bars 50 µm, images representative. A. C33A-Myc-BioID2. B. C33A-Myc-BioID2-PRAF2 n=1*

C33A Myc-BioID2 and Myc-BioID2-PRAF2 cell lines were fixed and permeabilised and probed for the expression of PRAF2 and the ER marker protein disulphide isomerase (PDI) and imaged. PRAF2 staining could be observed in the Myc-BioID2-PRAF2 (Red, Figure 6.3 B), and it colocalised with the PDI staining (green). No staining with the PRAF2 antibody was observed in the C33A-Myc-BioID2 control cells (Figure 6.2 A). To confirm that the Myc-BioID2-PRAF2 was localised correctly, cells were also probed with the Myc-tag antibody and an antibody to calnexin. No Myc staining was detected in C33A cells (Figure 6.4 A), Myc-staining was detected in the Myc-BioID2 cell line, but it did not colocalise with calnexin (Figure 6.4 B). As previously demonstrated, Myc-BioID2-PRAF2 colocalised with the ER marker calnexin (Figure 6.4 C). This together with the PDI data (Figure 6.3) suggests that Myc-BioID2-PRAF2 localises as expected.

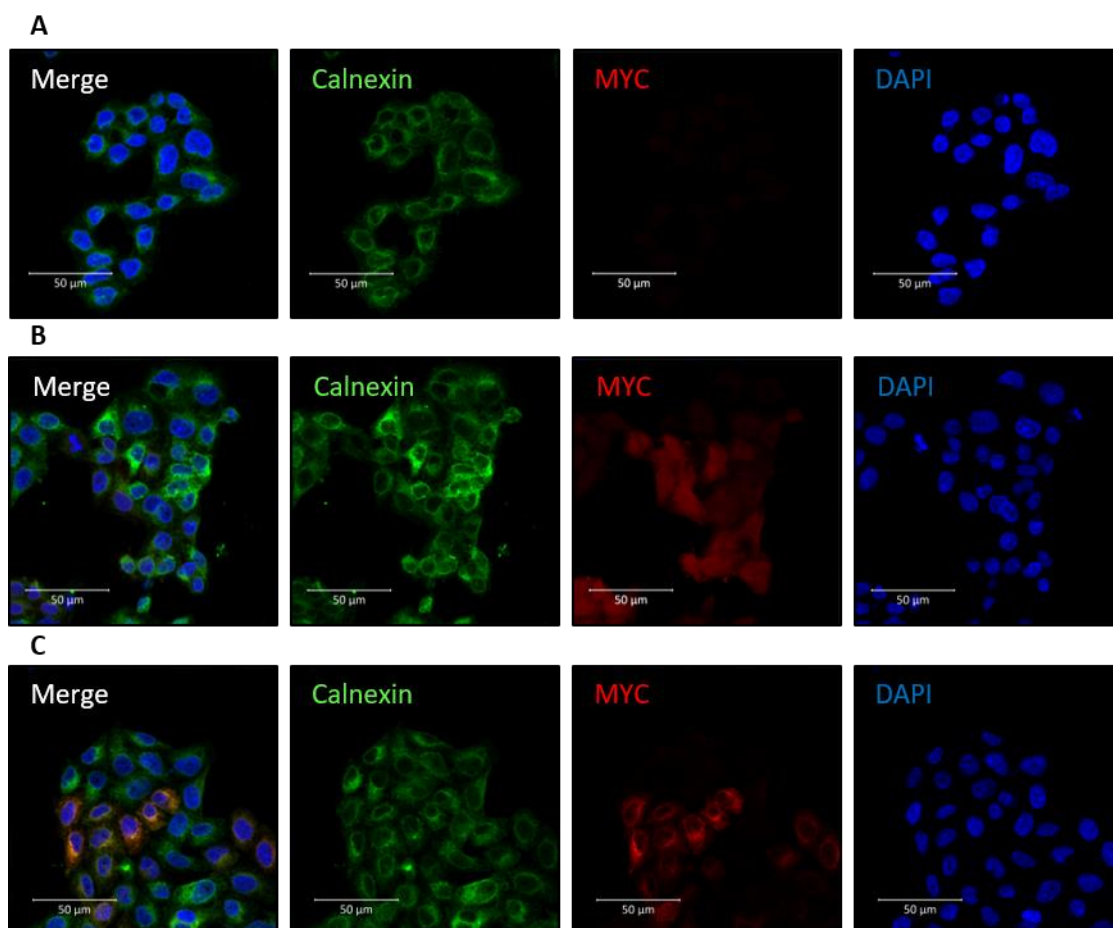


**Figure 6.4** *Myc-BioID2-PRAF2 colocalised with the ER marker calnexin*

*C33A, C33A Myc-BioID2 and C33A Myc-BioID2-PRAF2 cell lines were fixed and permeabilised and probed with antibodies to the Myc-tag and Calnexin, then stained with Alexa-488 and 594 conjugated secondary antibodies. Calnexin (green), Myc (red). Nuclei counterstained with DAPI (blue), Scale bars 50 µm, images representative. A. C33A-Myc-BioID2. B. C33A-Myc-BioID2. C. C33A-Myc-BioID2-PRAF2. N=3*

### **6.2.3 The Myc-BioID2-PRAF2 fusion is functional and displays the ability to biotinylate**

Once the localisation of the fusion protein was validated, western blotting was performed to confirm that the fusion protein was of the expected size. C33A, C33A Myc-BioID2 and C33A-Myc-BioID2-PRAF2 were lysed, and equal amounts of protein resolved by SDS-PAGE. The resulting western blots were then probed for GAPDH and the Myc-tag (Figure 6.5 A), the

Myc antibody detected the BioID2 protein (lane 2, Figure 6.5 A), and it was the correct size of ~28 kDa, a band of ~47 kDa was detected in the C33A Myc-BioID2-PRAF2 cell line lysate (Lane 3, Figure 6.5 A) which was the expected size, the expression of the two constructs was also roughly equal.

Next, we assayed whether the BioID2 fusion protein was acting as expected by performing a Co-IP with the known PRAF2 interacting partner HPV-18E5 (Chapter 3). The C33A Myc-BioID2 and C33A Myc-BioID2-PRAF2 cell lines were transfected with either GFP or GFP-18E5, with C33A and non-transfected controls also included, then after 48 hours the cells were lysed, and a GFP-trap IPs performed. The resulting Co-IPs (Figure 6.5 B) were then probed for Myc and GFP, and inputs for Myc, GFP and GAPDH respectively. As before (Chapter 3, Figure 3.1), we observed that GFP-18E5 successfully immunoprecipitated PRAF2, with Myc-BioID2-PRAF2 specifically precipitated (Lane 7, Figure 6.5 B). Interestingly, the dimeric form of Myc-BioID2-PRAF2 could be detected in the GFP:IP, but it was not visible in the input. This confirmed that the BioID2 PRAF2 fusion had maintained its functionality.

Finally, the ability of the BioID2 constructs to biotinylate cellular proteins was assayed. The BioID2 cell lines plus C33A control cells were treated with 50  $\mu$ M biotin for 18 hours, then lysed. Equal amounts of protein were resolved by SDS-PAGE and the resulting western blots probed with Streptavidin HRP to detect biotinylated proteins, as well as antibodies against Myc and GAPDH. In the control C33A cells (Lane 1, Figure 6.5 C), some biotinylated proteins were detected, these correspond to endogenous carboxylases (Roux et al., 2012), when compared to the BioID2 cell lines, the difference was stark, with the levels of biotinylated proteins clearly increased in comparison. Additionally, the pattern of biotinylated proteins observed in C33A Myc-BioID2 (Lane 2, Figure 6.5 C) was different from that of the C33A Myc-BioID2-PRAF2 (Lane 3, Figure 6.5 C). This indicated that the Myc-BioID2- PRAF2 fusion protein could biotinylate proximal proteins.



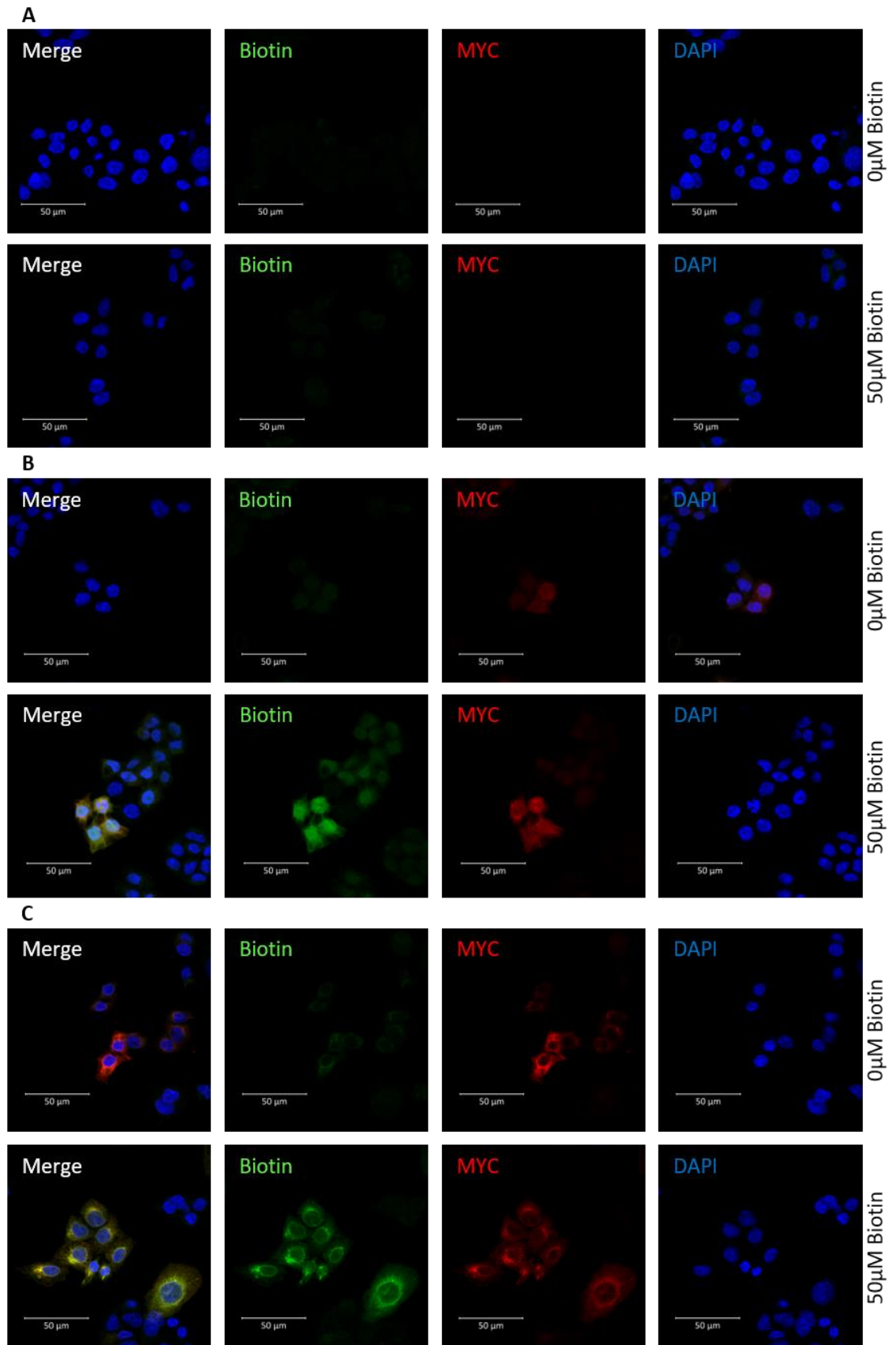


**Figure 6.6**      ***The addition of 50  $\mu$ M biotin resulted in biotinylation of proteins and the biotinylated proteins co-localised with their respective BioID2 constructs***

*C33A cell lines were treated incubated with 50  $\mu$ M biotin or control carrier for 18 hours, then fixed, permeabilised and probed with an antibody against the Myc-tag, then stained with Alexa-594 secondary and Alexa-488 conjugated Streptavidin. biotin (green), Myc (red) and nuclei counterstained with DAPI (blue). Representative images shown, scale bars 50  $\mu$ m. A. C33A cells. B. C33A Myc-BioID2. C. C33A Myc-BioID2-PRAF2 cells. N=3*

In addition to assaying the biotinylation ability of the constructs by western blotting, immunofluorescence for biotinylated proteins was also performed. C33A cell lines were seeded onto coverslips, then 24 hours post seeding were treated with 50  $\mu$ M biotin or control carrier, the cells were incubated with biotin for 18 hours, then fixed and permeabilised. The cells were then probed with anti-Myc-tag antibody, then stained with an Alexa-594 conjugated secondary. The cells were costained with 488-conjugated Streptavidin, and then imaged. In C33A cells (Figure 6.6 A and 6.7 A) no Myc staining was observed and no biotinylation was detected (Streptavidin-488). In C33A Myc-BioID2 cells (Figure 6.6 B and 6.7 B) Myc staining was detected throughout the cell nucleus and cytoplasm. At 0  $\mu$ M biotin, some biotinylated proteins are detectable. This was due to the growth media containing biotin, enabling the biotinylation of proteins. There was a marked increase in the detection of biotinylated proteins once the cells had been incubated with 50  $\mu$ M of biotin and staining of biotinylated proteins could be observed (green), located throughout the nucleus and cytoplasm. The Myc (red) and biotinylated proteins were also colocalised (Figure 6.7 B). In the C33A Myc-BioID2-PRAF2 cells we observed basal levels of biotinylation in the absence of additional biotin, with the greatest degree detected in those expressing the most Myc-BioID2-PRAF2 (Myc, 0 $\mu$ M, Figure 6.6 C). Upon the addition of 50  $\mu$ M there was a clear increase in the amount of biotinylated proteins detected (biotin, 50 $\mu$ M, Figure 6.6 C), and they displayed an ER like distribution, with some diffuse, possibly vesicular staining towards the edges of the cell. This staining largely colocalises with the Myc staining and

was particularly intense in the ER (Figure 6.7 C), this suggested that most of the proteins biotinylated were ER resident.

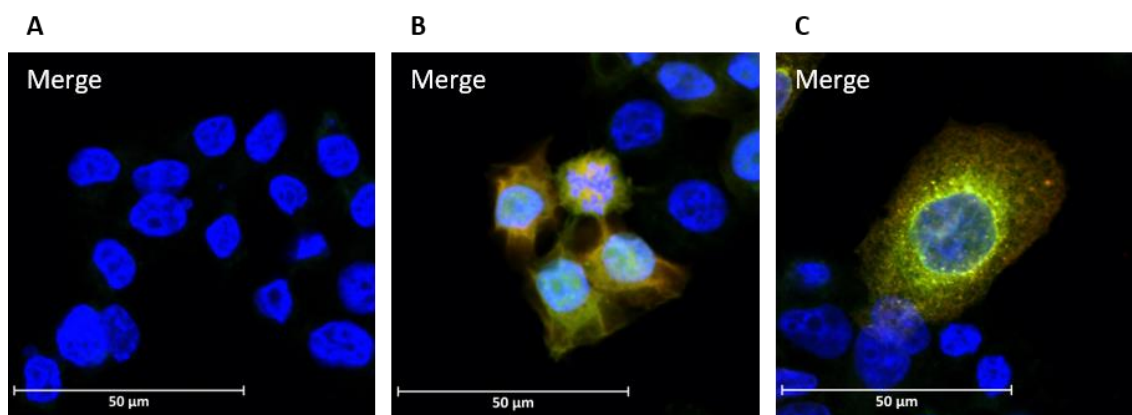


**Figure 6.7** *Biotinylated proteins colocalised with the BioID2 constructs*

*Close up of merged images from figure 6.6. All images are of cells plus 50 µM biotin 2xDigital Zoom, Scale bar 50 µm. biotin (green), Myc (red) and nuclei counterstained with DAPI (blue) A. C33A. B. C33A Myc-BioID2. C. C33A Myc-BioID2-PRAF2*

To determine if we observed the same levels of biotinylation as previously observed in the literature for the BioID2 construct a biotin titration into the C33A cell lines was performed. C33A, C33A Myc-BioID2 and C33A Myc-BioID2-PRAF2 were seeded, and grown for 24 hours, then growth media supplemented with additional biotin was added. 0.001, 0.01, 0.1, 1 and 50 µM of biotin was added and cells were incubated for 18 hours to allow biotin labelling to occur. Basal levels of biotinylation were observed in both C33A Myc-BioID2 and C33A Myc-BioID2-PRAF2 with no added biotin, this was expected as growth media contains biotin (Lanes 7 and 13, Figure 6.8). A slight increase in biotinylation could be observed at 0.01 µM additional biotin (Lanes 9 and 15), however, levels of biotinylation were noticeably increased at 0.1 µM (Lanes 10 and 16) in C33A Myc-BioID2 and C33A Myc-BioID2-PRAF2 cells, with no noticeable increase in biotinylation observed past this point. This matched with what was reported in the original

BioID2 paper, in which 0.1  $\mu\text{M}$  of biotin was sufficient to achieve biotin saturation (Kim, D.I. et al., 2016).

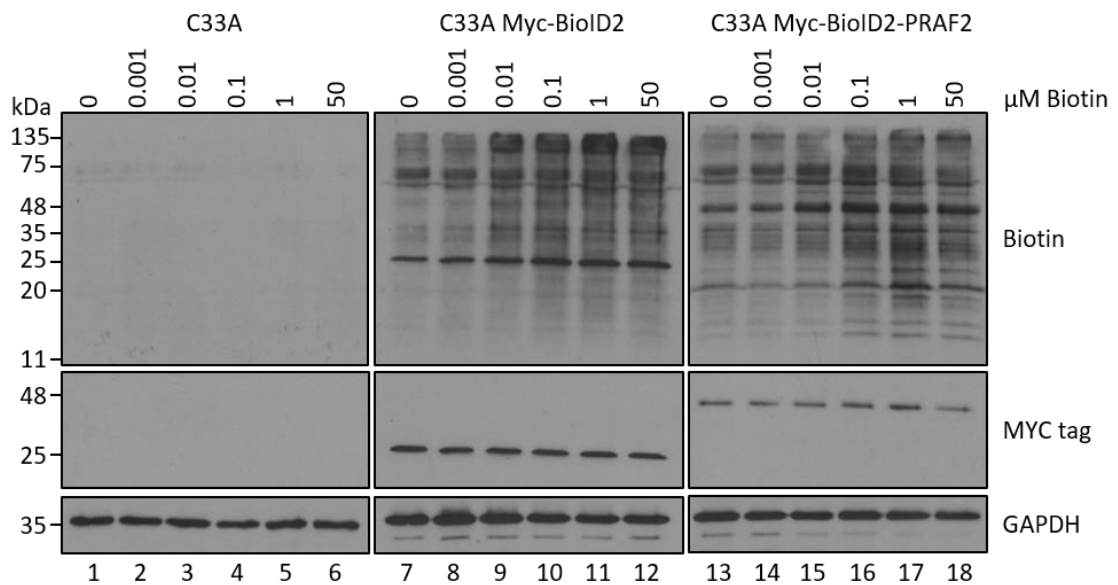


**Figure 6.8** *Biotin titration into C33A BioID cell lines resulted in increased biotinylation until saturation at 0.1  $\mu\text{M}$  biotin*

*C33A, C33A Myc-BioID2 and C33A Myc-BioID2-PRAF2 cell lines were titrated with additional biotin, up to 50  $\mu\text{M}$  additional biotin. Cells were lysed and equal amounts of protein resolved by SDS-PAGE. Resulting western blots were probed for biotin, Myc and GAPDH expression. N=1*

#### **6.2.4 Streptavidin Immunoprecipitation successfully precipitated biotinylated proteins**

Having successfully validated the C33A Myc-BioID2-PRAF2 cell line, the BioID experiment was carried out. To do so, four 10 cm dishes of C33A, C33A Myc-BioID2 and C33A Myc-BioID2-PRAF2 were grown to 80% confluency, then treated with 50  $\mu\text{M}$  of biotin for 18 hours. Cells were then lysed, and a streptavidin pulldown was carried out (Figure 6.2). The input, bead supernatant and streptavidin immunoprecipitation eluates were then analysed by western blotting to determine if the samples were of sufficient quality, before proceeding to mass spectroscopy analysis.

Successful biotinylation of proteins could be observed in the input samples (Figure 6.9 A), with a clear increase observed in the Myc-BioID2 and Myc-BioID2-PRAF2 samples. Additionally, there was a clear difference between the two samples (Lanes 2 and 3, Figure 6.9 A). The Streptavidin IP was also successful, with biotinylated proteins clearly pulled down for both Myc-BioID2 and Myc-BioID2-PRAF2 (Lanes 2 and 3, Figure 6.9 C). There was also a much clearer difference between the two BioID2 constructs in the bead eluates from the immunoprecipitation. Interestingly, there appeared to be a considerable amount of biotinylated protein detected in the bead supernatant (Figure 6.9 B) for all samples, and there seems to be a pattern common to both BioID2 and BioID2-PRAF2 samples, and to a lesser extent the control C33As, for example, just below 75kDa and at ~30kDa and ~11kDa. Additionally, the Myc tagged proteins were detectable in the supernatant but not the IP. The samples were then sent for mass spectroscopy.

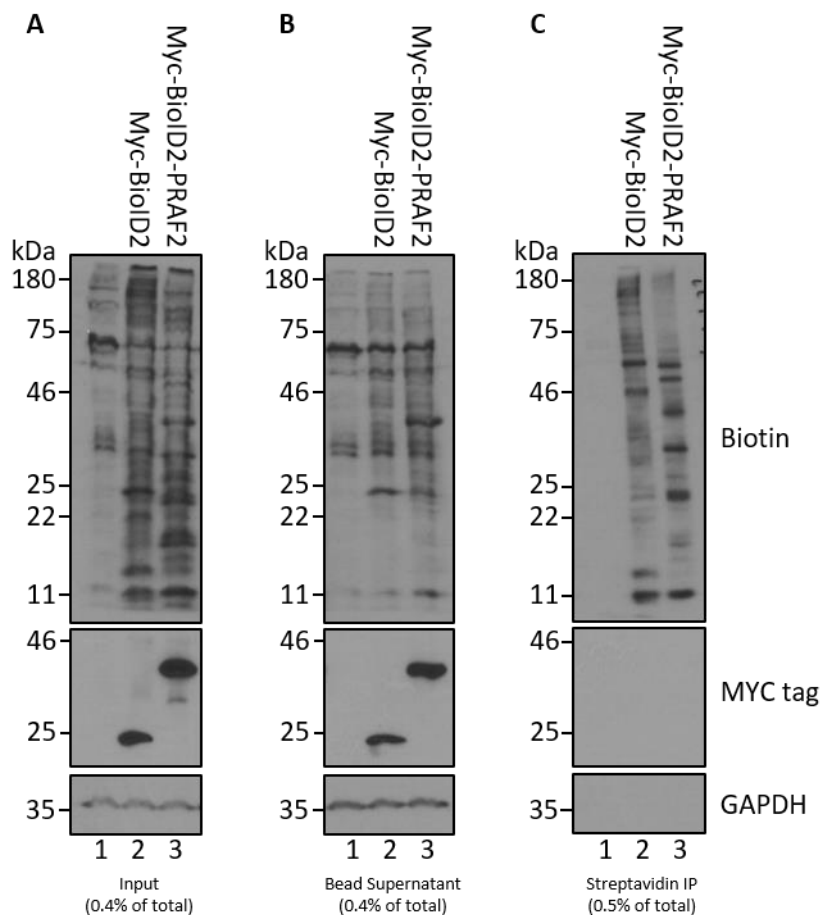


**Figure 6.9**      ***Biotinylated proteins were successfully immunoprecipitated by streptavidin pulldowns***

*Western blots of samples C33A, C33A Myc-BioID2 and C33A Myc-BioID2-PRAF2, with equal amounts of protein loaded, and % of total sample indicated below each blot. The blots were probed with streptavidin-HRP, GAPDH and Myc tag antibodies. A representative repeat is shown. N=3 A. Input samples for streptavidin IP. B. Supernatant of Input samples post bead incubation. C. Streptavidin bead eluate samples.*

**6.2.5 Mass spectroscopy successfully identifies putative proximal partners for PRAF2**

The streptavidin beads with bound biotinylated proteins were sent for mass spectroscopy. The sample preparation, mass spectroscopy and data analysis were performed at the University of Liverpool by Dr. Stuart Armstrong. The biotinylated proteins bound to the streptavidin beads were digested with trypsin on the bead. The resulting peptide digests were then processed and labelled with Tandem Mass Tags (TMT), enabling all three repeats of samples to be run at the same time. Peptides were analysed by nano-LC ESI-MS/MS, and spectral data was analysed using the PEAKS studio 10 software. Potential proximal partners for PRAF2 were then identified relative to control C33A and C33A Myc-BioID2 interacting proteins.

The TMT MS data was then searched against the predicted proteins of the human reference genome and an additional contaminants database, this resulted in a list of 838 identified proteins for all samples (data not shown). To narrow down the identified proteins and to increase confidence in those identified, only proteins which satisfied the following criteria were displayed: two missed tryptic cleavages permitted, fixed modifications of Carbamidomethylation and TMTplex. Results were then filtered to only include proteins with greater than 2 unique peptides and a 2-fold or greater change in enrichment relative to the C33A sample. Proteins also enriched in the C33A Myc-BioID2 sample were also excluded.

59 proteins were deemed to be significant from groups C33A, C33A Myc-BioID2, C33A Myc-BioID2-PRAF2, (Figure 6.10). It was notable that there was variability between the replicates, with the intensity of TMT10-128C (C33A Myc-BioID2) and TMT10-129C (C33A Myc-BioID2-PRAF2) being particularly different. The proteins deemed to be significantly enriched and unique to the C33A Myc-BioID2-PRAF2 were then investigated further (Table 6.1). Of the proteins identified as putative proximal interactors, two were possibly false positives (Table 6.1). Keratin 16 could be a contaminant from preparation of the samples, and the albumin could possibly be from the cell culture media. 11 out of 18 of the proteins identified are known to localise to the ER, and 7 out of 18 are known to localise to the nucleus.

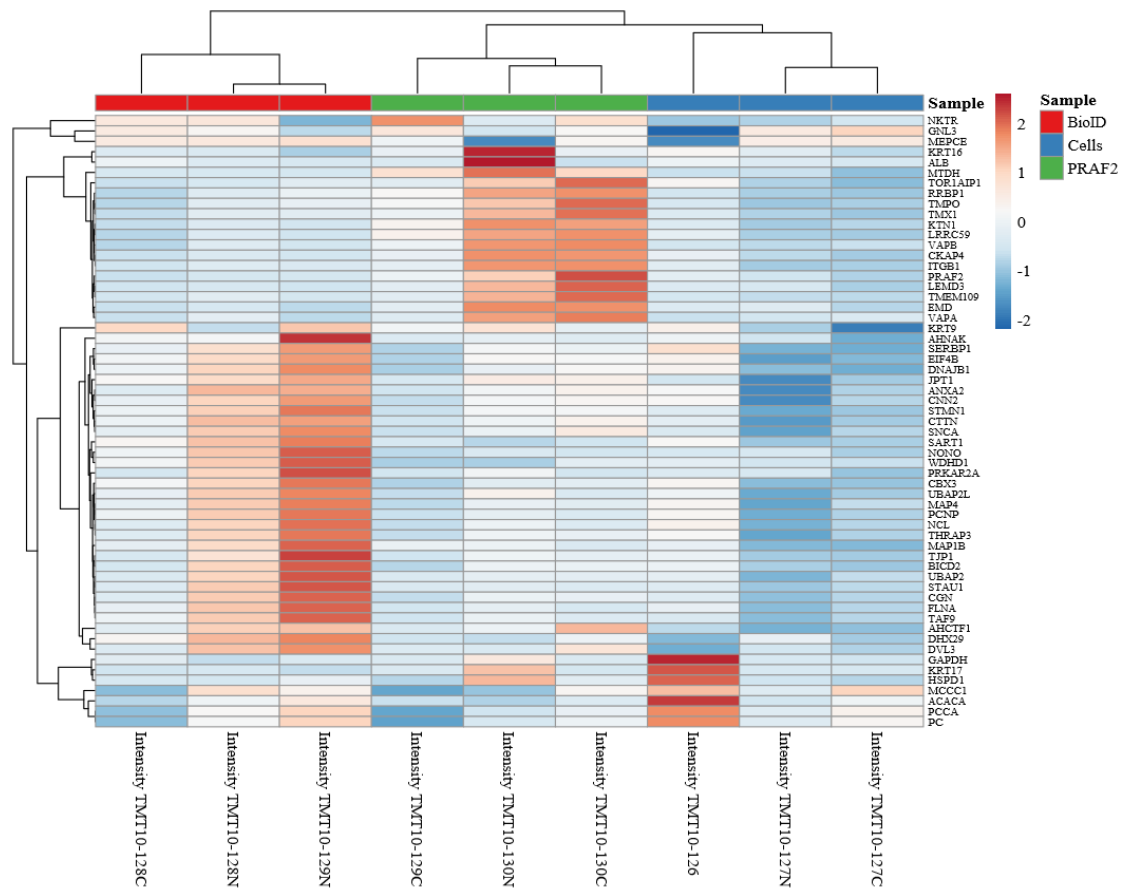


**Figure 6.10 Protein intensity clustering of BioID2 samples**

Figure produced by Dr. Stuart Armstrong. Proteins (PEAKS Q False discovery ratio 1%,  $\geq 2$  peptides,  $\geq$  fold change) were clustered using ClustVis (<https://biit.cs.ut.ee/clustvis/>, (Metsalu and Vilo, 2015)). Rows are centred, unit variance scaling is applied to rows. Both rows and columns are clustered using correlation distance and average linkage. Shows 59 rows, 9 columns (each column represents a repeat). Samples C33A (blue), C33A Myc-BioID2 (red) and C33A Myc-BioID2-PRAF2 (green)

**Table 6.1** Potential PRAF2 proximal interaction partners determined by TMT MS.

Proteins were annotated with the PANTHER (protein annotation through evolutionary relationship) classification system, information of cellular localisation was derived from the uniprot database and the human protein atlas. n/n= not named

| Accession          | Gene ID | Gene Name                                   | Enrichment Factor | PANTHER Protein Class           | Cellular localisation              |
|--------------------|---------|---|-------------------|---------------------------------|------------------------------------|
| P05556 ITB1_HUMAN  | ITGB1   | Integrin subunit beta 1                     | 21.77             | Cell adhesion molecule receptor | Endosome and Plasma Membrane       |
| Q9H3N1 TMX1_HUMAN  | TMX1    | Thioredoxin-related transmembrane protein 1 | 15.53             | n/n                             | Endoplasmic Reticulum              |
| P42167 LAP2B_HUMAN | TMPO    | Thymopoietin                                | 14.08             | n/n                             | Nuclear                            |
| Q9BVC6 TM109_HUMAN | TMEM109 | Transmembrane protein 109                   | 11.98             | n/n                             | Endoplasmic Reticulum and Nuclear  |
| Q9P2E9 RRBP1_HUMAN | RRBP1   | Ribosome binding protein 1                  | 11.15             | n/n                             | Endoplasmic Reticulum              |
| Q96AG4 LRC59_HUMAN | LRRC59  | Leucine rich repeat containing 59           | 9.74              | n/n                             | Endoplasmic Reticulum and Nuclear  |
| O60831 PRAF2_HUMAN | PRAF2   | PRA1 domain family member 2                 | 9.51              | Amino acid transporter          | Endosome and Endoplasmic Reticulum |
| Q86UP2 KTN1_HUMAN  | KTN1    | Kinectin 1                                  | 6.98              | n/n                             | Endoplasmic Reticulum              |
| P50402 EMD_HUMAN   | EMD     | Emerin                                      | 6.83              | n/n                             | Nuclear Membrane                   |

|                    |          |   |      |   |  |
|--------------------|----------|---|------|---|--|
| Q07065 CKAP4_HUMAN | CKAP4    | Cytoskeleton associated protein 4       | 6.49 | n/n                                     | Cytosol, Endoplasmic Reticulum and Plasma Membrane |
| Q86UE4 LYRIC_HUMAN | MTDH     | Metadherin                              | 5.28 | n/n                                     | Endoplasmic Reticulum                              |
| O95292 VAPB_HUMAN  | VAPB     | VAMP associated protein B and C         | 4.4  | Membrane trafficking regulatory protein | Endoplasmic Reticulum                              |
| Q9Y2U8 MAN1_HUMAN  | LEMD3    | LEM domain containing 3                 | 4.07 | n/n                                     | Nuclear Membrane                                   |
| Q5JTV8 TOIP1_HUMAN | TOR1AIP1 | Torsin 1A interacting protein 1         | 3.96 | n/n                                     | Nuclear Membrane                                   |
| P08779 K1C16_HUMAN | KRT16    | Keratin 16                              | 3.28 | n/n                                     | Intermediate Filaments                             |
| P02768 ALBU_HUMAN  | ALB      | Albumin                                 | 3.09 | Transfer/carrier protein                | Endoplasmic Reticulum and Golgi Apparatus          |
| Q9P0L0 VAPA_HUMAN  | VAPA     | VAMP associated protein A               | 2.54 | Membrane trafficking regulatory protein | Endoplasmic Reticulum                              |
| P30414 NKTR_HUMAN  | NKTR     | Natural killer cell triggering receptor | 2.36 | n/n                                     | Cytosol, Plasma Membrane and Nucleoplasm           |

## 6.3 Discussion

### 6.3.1 The proximal protein interactors of PRAF2

This was the first study to investigate the cellular binding partners of PRAF2 by mass spectroscopy and the first study of a PRA family member using the BioID technique. An initial observation of the data was that there were fewer protein candidates identified that one might have expected from a BioID screen (18 vs 80) (Kim, D.I. et al., 2016). However, this could in part be due to the controls run with the experiment, as most BioID pulldowns use just cells without the BioID2 construct as a control, rather than no construct and BioID2 alone as controls. This had the effect of excluding possible protein hits.

It is important to note that biotinylation in the BioID experiment and subsequent precipitation does not mean that the protein is an interactor of PRAF2. Whilst it could be a direct interactor, it could also interact with the protein as part of a complex, or indeed have just been in the vicinity. However, due to the short linker between the BirA ligase and PRAF2, proteins biotinylated would have to have been within 10 nm (Kim, D.I. et al., 2016). Interestingly, only two known PRAF2 interactors were detected by the BioID2 screen (Table 6.1), these were PRAF2 and VAPA. VAPA had previously been validated by yeast two hybrid and GST-immunoprecipitations (Gougeon and Ngsee, 2005), and PRAF2 is known to homodimerise (Schweneker et al., 2005), however it is possible that the biotinylation of PRAF2 could be due to auto-biotinylation of the fusion protein.

The lack of detection of known interactors such as PRAF3, CCR5 (Schweneker et al., 2005) and Bcl-xL (Vento et al., 2010) could be due to differences in the cell lines these interactions were observed in e.g. HEK-293 and HeLa cells versus C33A cells. However, C33A cells are known to express CCR5 (Che et al., 2016) and Bcl-xL (Dho et al., 2013), so this may not be the reason. Another reason could be due to the orientation of the BioID2-PRAF2 fusion. With the fusion, the

BioID2 was on the cytosolic side of the ER, owing to PRAF2 N-terminus being cytosolic (Figure 6.11). To biotinylate a protein, the protein must come within 10 nm of the BioID2 (1 and 2, Figure 6.11), however, if it was localised to the luminal side of the ER (4, Figure 6.11), possibly interacting with the loops of PRAF2, it could not come into contact with the BioID2 protein owing to the physical barrier of the ER membrane, therefore a potential interaction could be missed.

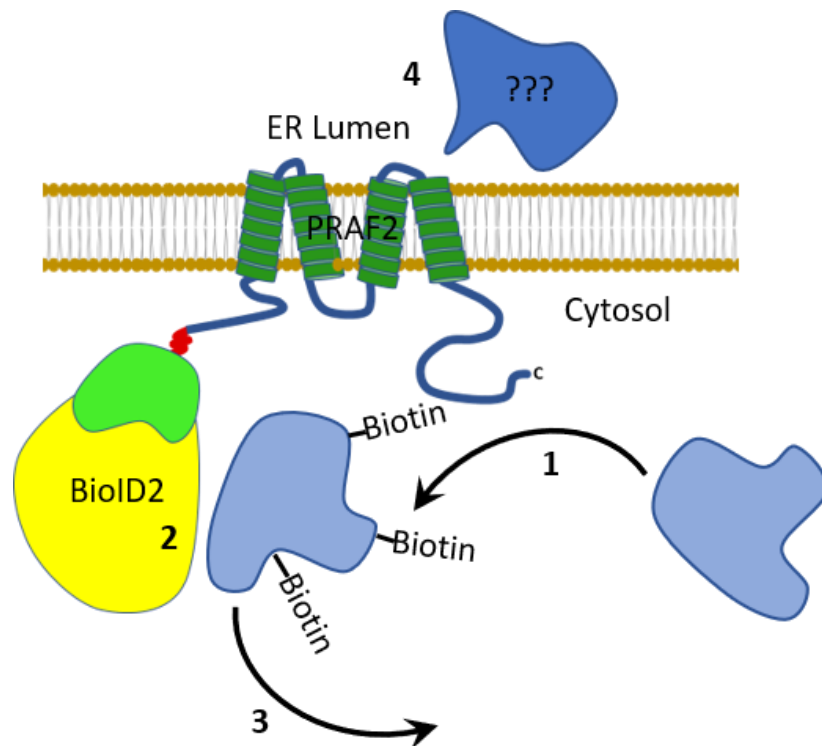


**Figure 6.11** Schematic of the BioID2-PRAF2 protein fusion biotinylating proximal proteins

The N and C-termini of PRAF2 are localised to the cytosol of the cell, whilst PRAF2 is embedded in the ER membrane, the BioID2 protein is fused by a short linker to PRAF2 and is cytosol facing.

1. A protein comes within 10nm of the BioID2-PRAF2 protein fusion. 2. Due to proximity, the BioID2 protein can biotinylate this protein. 3. The protein is no longer interacting with PRAF2 or in its immediate neighbourhood, and is trafficked or moves elsewhere, however it is marked by biotinylation. 4. A protein that interacts with PRAF2 inside the ER lumen is not biotinylated as the BioID2 protein is physically separated from it by the membrane.

The proteins identified as exclusive to the PRAF2 construct can be divided into two groups, ER and NE, the majority of the proximal proteins identified localise to the ER. There appear to be two potential hubs of proteins. The first was composed of the ER proteins VAPA, VAPB, CKAP4 and KTN1 (Figure 6.12 A). This collection of proteins was promising as VAPA has already been identified as a PRAF2 interactor (Gougeon and Ngsee, 2005) and are already known to interact with each other. The second hub was composed of EMD, LEMD3, TMPO and TOR1AIP1 (Figure 6.12 B), these were NE proteins. Whilst PRAF2 is not known to localise to the NE, it has been observed in a perinuclear localisation. Additionally, these proteins were known interactors of the SUN domain-containing protein 2 (SUN2), which in a BioID screen identified PRAF2 as a proximally biotinylated protein (Kim, D.I. et al., 2014), increasing confidence in these BioID hits.

The protein with the highest enrichment factor (21.77) relative to the controls was integrin subunit beta 1 (ITGB1). ITGB1 is the predominant subunit of the integrin heterodimer (Moreno-Layseca et al., 2019) which is composed of an  $\alpha$  and  $\beta$  subunit. There are 18 $\alpha$  and 8 $\beta$ -subunits which associate non-covalently to make 24 distinct integrin heterodimers. ITGB1 interacts with  $\alpha$ -subunits 1-13 (Figure 6.12 D). Variation of these subunits dictates what extracellular matrix (ECM) component they interact with. Integrins possess active and inactive states, which are governed by inside-out signals, in which an intracellular signal promotes the binding of proteins such as talin or kindlin to the intracellular tail of the  $\beta$ -subunit (Ye et al., 2014) which activate the integrin enabling it to bind ECM ligands. This triggers signals leading to the recruitment of protein complexes composed of kinases and phosphatases to the intracellular tail of the integrin (mostly the  $\beta$ -subunit) (Horton et al., 2015) enabling intracellular signal transduction via kinases such as focal adhesion kinase (FAK), integrin linked kinases (ILK) or Rho GTPases (Hehlhans et al., 2007).

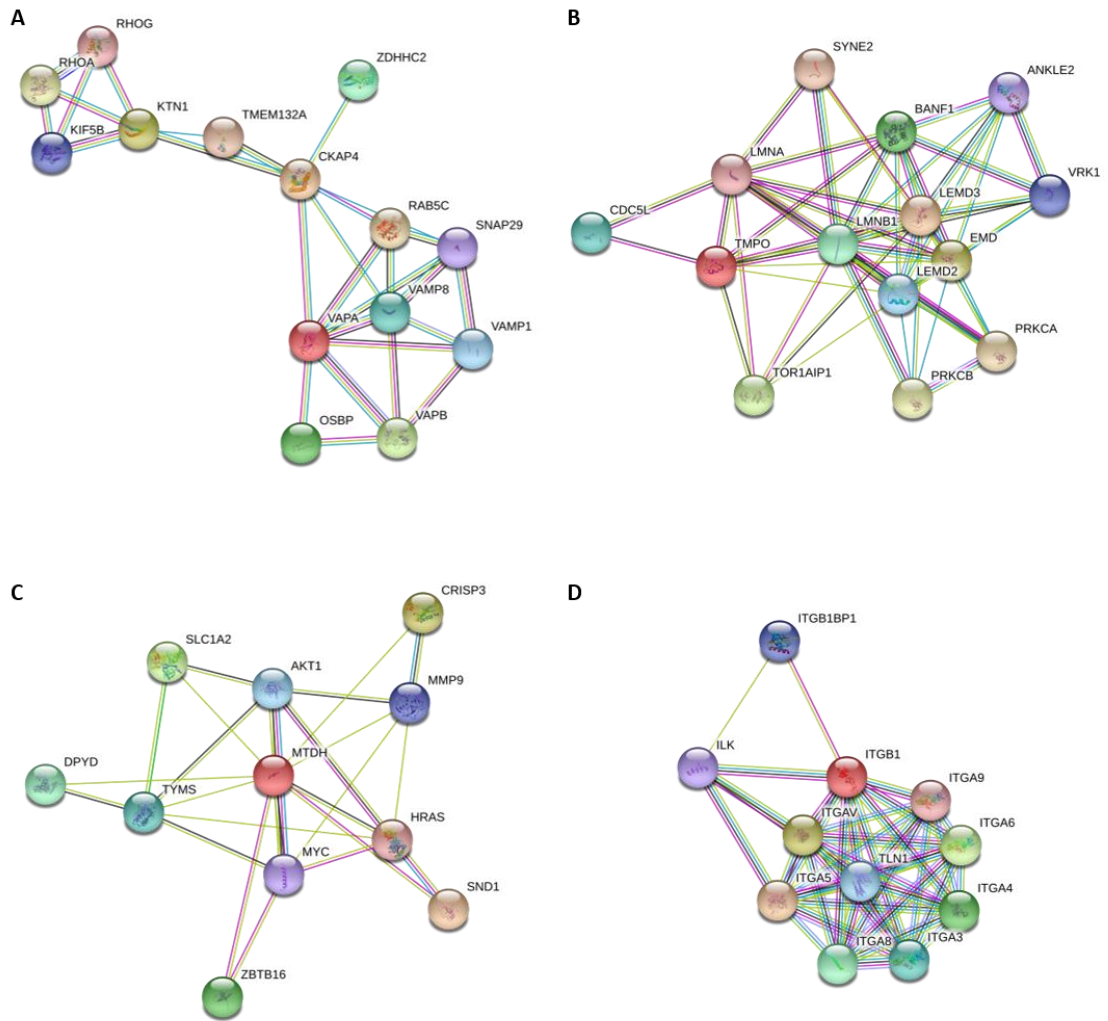


**Figure 6.12** *STRING analysis of proximal interactors of PRAF2 identified by Bioid2*

*STRING network of interactions of KTN1, CKAP4, VAPA and VAPB. B. STRING network of interactions of LEMD3, TMPO, TOR1AIP1 and EMD. C. STRING network of interactions for MTDH. D. STRING network of interactions for ITGB1.*

These integrin-ECM adhesions are known as focal adhesions (FAs) (Partridge and Marcantonio, 2006) and are highly dynamic in nature undergoing rounds of assembly and reassembly, directed by endocytosis and exocytosis of integrins and their degradation and recycling (Valdembri and Serini, 2012). These FAs are anchorage points to the ECM, and are hubs for signalling, directing processes such as protein recruitment, cell spreading, cell migration and

ECM remodelling (Hamidi and Ivaska, 2018). Integrins initially heterodimerise in the ER (Tiwari et al., 2011), and are trafficked to the Golgi where they undergo post translational modifications (PTMs) before export to the cell surface in an inactive state (De Franceschi et al., 2015). It could therefore be possible that the possible interaction between ITGB1 and PRAF2 is occurring in the ER, and that PRAF2 is acting as a gatekeeper for its traffic, like with the GABA receptor (Doly et al., 2016). Owing to integrins importance in cellular behaviour, if PRAF2 can influence their expression or transport this would be highly interesting.

The thioredoxin-related transmembrane protein 1 (TMX1) was the next highest enriched protein (15.53). It is a member of the PDI family that forms disulphide bonds in new proteins in the ER (Pisoni et al., 2015; Matsuo et al., 2001), interacting with calnexin and in maturation of cysteine containing membrane associated proteins. Interestingly, this protein has been demonstrated to act in the maturation of ITGB1 and LRRC59 (Pisoni et al., 2015), both of which were identified as enriched in our PRAF2-BioID pulldown. That proteins known to interact are labelled by the BioID2-PRAF2 increases the confidence in the relevance of the hits identified.

Leucine rich repeat (LRR) containing protein 59 (LRRC59) is a type II transmembrane domain protein, which is membrane anchored at its C-terminus, localising to the ER and NE (Blenski and Kehlenbach, 2019). It has previously been demonstrated to promote nuclear import of fibroblast growth factor 1 (FGF1) and cancerous inhibitor of PP2A (CIP2A) (Skjerpen et al., 2002). LRRs are often found in proteins involved in innate immunity, such as TLRs. LRRC59 is important for nucleic acid sensing TLRs 3, 8 and 9s exit from the ER post synthesis via COPII coated vesicles to endosomes through its association with Uncoordinated 93 homolog B1 (UNC93B1) (Tatematsu et al., 2015). LRRC59 has also been demonstrated to associate with the pattern recognition receptor (PRR) DexD/H-Box helicase 58 (DDX58, also known as RIG-I) upon viral infection, promoting type I interferon (IFN) signalling through preventing its degradation via autophagy (Xian et al., 2019). Whilst PRAF2 may not be involved with TLR or PRR trafficking

due to its proximity labelling of LRRC59, a PRA protein in the tomato (*Solanum lycopersicum*) SLPRA1A modulates the trafficking and degradation of the PRR LeEIX2 (Pizarro et al., 2018). It is therefore exciting to speculate that PRAF2 could have a role in the transport and regulation of PRRs. It is also interesting that LRRC59 and ITGB1 were identified as HPV-E5 interactors by TAP-MS in the same screen that identified PRAF2 as a HPV-E5 interactor (Table 6.2) (Rozenblatt-Rosen et al., 2012).

Metadherin (MTDH, also known as AEG-1 and LYRIC) was enriched 5.28-fold in the BioID2-PRAF2 samples relative to controls. MTDH is of interest as it is a tumour associated antigen (Dhiman et al., 2019). MTDH is a type 2 transmembrane protein which localises to the ER and perinuclear region. However, its localisation is known to be altered to the cytoplasm in cancers (Thirkettle et al., 2009). MTDH has been shown to be regulated by a variety of microRNAs (miRNAs) such as miR-630, miR-145, miR-342-3p, miR-22 and miR-433 (Zhou, C.X. et al., 2016; Dong, R. et al., 2014; Zhang, S. et al., 2017; Tang, Y. et al., 2015; Liang, C. et al., 2017). MTDH has also been shown to be regulated by TNF $\alpha$ , and is a positive regulator of NF- $\kappa$ B, increasing levels of the active p50/p65 complex and increasing expression of NF- $\kappa$ B downstream genes (Emdad et al., 2006), enhancing anchorage independent growth and invasion. In malignant glioma, a cancer which PRAF2 levels are elevated (Borsics et al., 2010), MTDH complexes with the cAMP-responsive element binding protein (CREB)-binding protein (CBP) and NF- $\kappa$ B to enhance NF- $\kappa$ B driven transcriptional activity (Sarkar et al., 2008), enhancing migration and invasion. MTDH is also elevated in colorectal cancer (Song et al., 2014), ESCC (Dhiman et al., 2019) and HCC (Zhu, K. et al., 2011; Yoo et al., 2009), enhancing invasion and metastasis. These cancers are also cancers in which PRAF2 is elevated (Qian et al., 2019; He et al., 2019; Wang, C.H. et al., 2018). MTDH also activates many other signalling pathways that are important in cancer, such as Wnt, PI3K/Akt and MAPK signalling. Interestingly, MTDH signalling through PI3K/Akt has been shown to be driven by H-Ras (Figure 6.12 C) (Lee, S.G. et al., 2008), which I have demonstrated to be a PRAF2 interactor (Figure A.4), raising the possibility that PRAF2 might

not only modulate MTDH through a direct interaction, but also through interactions with upstream signalling factors. The possible interaction with MTDH could possibly provide a mechanism for the increased invasiveness of cancer cells overexpressing PRAF2, perhaps PRAF2 overexpression helps drive MTDH mediated effects. MTDH is a possible binding partner that warrants further investigation.

As mentioned earlier, there seem to be hubs of biotinylated proximal proteins, for example the ER proteins CKAP4, KTN1, VAPA, and VAPB (enriched 6.49, 6.98, 2.54 and 4.4 times relative to controls respectively). STRING analysis (Figure 6.12 A) shows that these proteins are known to interact with each other in the literature. CKAP4 is a type II transmembrane protein that anchors the ER to microtubules (Schweizer et al., 1993) and possesses receptor activity for Dickkopf WNT signalling pathway inhibitor 1 (DKK1). Binding DKK1 results in CKAP4 mediated activation of the PI3K/Akt pathway (Shinno et al., 2018), promoting proliferation in ESCC cells. Interestingly in HCC, CKAP is associated with reduced invasion and proliferation (Li, S.X. et al., 2014b), through its ability to suppress EGFR signalling via associating with EGFR in its basal status (Li, S.X. et al., 2014a). CKAP4 is also known to interact with another putative PRAF2 binding partner KTN1. KTN1 is an integral membrane protein that acts to extend the ER along microtubules, through its interaction with the molecular motor kinesin (Machleidt et al., 1998; Zhang, X. et al., 2010). It is also a key regulator of RhoG microtubule dependent activity (Vignal et al., 2001), and it has been demonstrated that KTN1 transports the ER to focal complexes, in order to transform these into FA (Ng et al., 2016) and is important in chemotaxis. It is intriguing to speculate that the increased invasion and proliferation observed in PRAF2 overexpressing cancers (Qian et al., 2019; Wang, C.H. et al., 2018; Yco et al., 2013) could be due to its interaction with CKAP4 and KTN1.

VAPA and VAPB are type II transmembrane proteins, and belong to the VAMP-associated protein family (Mao, D. et al., 2019). VAPA has previously been demonstrated to be

a PRAF2 interactor (Gougeon and Ngsee, 2005), and PRAF1 interacts with a family member, the VAMP2 protein (Martincic et al., 1997). VAP proteins are important in direct lipid transport between the ER and other membranes, and possess an N-terminal major sperm protein (MSP) domain, responsible for binding the FFAT motif (Dong, R. et al., 2016). The MSP motif enables VAPA binding to Oxysterol-binding protein-related protein 3 (ORP3). ORP3 is an R-Ras interactor that regulates cell adhesion through complexing with VAPA and stimulating R-Ras (Weber-Boyvot et al., 2015; Lehto et al., 2008) resulting in reduced ITGB1 cell surface activation. We have also shown that PRAF2 binds R-Ras, so it is interesting that it may also bind another R-Ras interactor.

Mutations in VAPB that disrupt its FFAT binding are responsible for a form of amyotrophic lateral sclerosis (ALS) (Nishimura et al., 2004). VAPs also regulate the degradation of  $\Delta F508$  CFTR, through complexing with RMA1, BAP31 and Derlin-1 (Ernst et al., 2016). Interestingly the PRAF2 interacting partner HPV-16E5 also interacts with a member of this complex, BAP31 (Regan and Laimins, 2008). VAPA has been demonstrated to be important for Norovirus replication, through its interaction with NS1/2 (McCune et al., 2017), and VAPA and VAPB are important for the assembly of the Hepatitis C virus replication complex, through their association with NS5A (Xu, G. et al., 2013). VAP proteins are also important in vesicle traffic, with VAPA binding vSNARE and tSNARES (Weir et al., 2001). Perhaps the interaction between PRAF2 and VAP proteins influences vesicle and lipid transport, or even serves a role in the regulation of R-Ras, as both are known PRAF2 interactors. VAP proteins also appear to play a role in vesicular transport to the ER. VAP proteins are found in complexes at membrane contact sites between the ER and other organelles, such as endosomes, where they enable tethering. This tethering effect is thought to be achieved through its ability to bind SNARE proteins, and also lipid transfer proteins, that bind VAP through the FFAT motif, which can also bind other membranes in trans.

The next hub of proteins (Figure 6.12 B) proteins EMD, LEMD3, TMPO and TOR1AIP1 (enriched 6.83, 4.07, 14.08 and 3.96 relative to controls respectively), is centred around the NE. It is likely that these proteins were biotinylated and identified as part of a complex, as LEMD3 and TOR1AIP1 directly interact with EMD (Mansharamani and Wilson, 2005; Shin, J.Y. et al., 2013) and TMPO indirectly through binding EMD binding partners (Berk et al., 2014; Berk et al., 2013). LEMD3, Emerin and TMPO are all LEM (LAPB2/Emerin/MAN1) domain proteins, which enables lamin binding (Berk et al., 2014; Bourgeois et al., 2013; Qi et al., 2015). EMD interacts with SUN2 (Haque et al., 2010), in the inner nuclear membrane, forming a bridge across the NE to the cytoplasm known as the LINC complex, which influences actin dynamics. That PRAF2 was observed to be biotinylated and enriched by a BioID-SUN2 construct previously (Kim, D.I. et al., 2014) increases confidence in the identification of these proteins as true hits.

EMD is also involved in the nuclear entry of  $\beta$ -catenin, by preventing its accumulation in the nucleus (Markiewicz et al., 2006) by binding it with its adenomatous polyposis coli (APC) domain. Interestingly, PRAF1 has previously shown to prevent  $\beta$ -catenin translocation to the nucleus by binding and retaining it in a seemingly ER localisation (Kim, J.T. et al., 2012; Kim, J.T. et al., 2006). It would be interesting if PRAF2 also possessed the ability to bind  $\beta$ -catenin and prevent its nuclear translocation, and if this might be involved in the EMD mechanism of  $\beta$ -catenin nuclear exclusion. EMD has also been demonstrated to prevent notch signalling, by retention of the Notch intracellular domain (NICD) at the NE (Lee, B. et al., 2017). Notch stimulation promotes JAG2 expression, which can be secreted by exosomes to act in a paracrine manner (He et al., 2019). Interestingly, JAG2 overexpression increased the level of PRAF2 expression and PRAF2 knockdown was shown to decrease the level of JAG2 expression. Therefore, could PRAF2 possibly be acting on EMD to inhibit its NICD binding function, thereby enabling entry of the NICD into the nucleus. This would then enable NICD target gene expression and therefore the increased JAG2 expression seen in cancers overexpressing PRAF2.

EMD is not the only putative PRAF2 interactor from the NE with signalling protein binding ability. LEMD3 possesses the ability to bind SMAD proteins through binding their MH2 (MAD Homology 2) domains via its c-terminal region (Lin et al., 2005). LEMD3 competes with transcription factors such as Forkhead Box H1 (FOXH1, also known as FAST1) for binding of activated phosphorylated SMAD2/3, thereby decreasing TGF- $\beta$  signalling (Bourgeois et al., 2013). LEMD3 also acts as a scaffold protein, recruiting and binding PPM1A (protein phosphatase, Mg<sup>2+</sup>/Mn<sup>2+</sup> dependent 1A). PPM1A is a phosphatase that catalyses the dephosphorylation of SMAD2/3, this provides a mechanism for further repression of SMAD mediated transcription. TGF- $\beta$  signalling can both act as a tumour suppressor and as a tumour promoter (Bachman and Park, 2005), often switching to a tumour promoter in later stages of cancers. TGF- $\beta$  has been seen to be overexpressed in malignant glioma, where it promotes proliferation, invasion and migration (Han, J. et al., 2015) and promotes migration and aids in EMT in neuroblastoma (Shao et al., 2017). These are cancers in which PRAF2 is also highly expressed (Yco et al., 2013; Borsics et al., 2010), and perhaps PRAF2 plays a role in the modulation of TGF- $\beta$  signalling through its interaction with LEMD3, perhaps preventing its association with the SMAD proteins, to potentiate TGF- $\beta$  signalling. The validation of PRAF2 and its interaction with these NE proteins is one that merits further investigation, to find out whether they are true interactions and whether they are individual interactions or as part of a complex. It would also be a previously unexplored area of interaction for PRAF2, as it is not currently known to interact with nuclear proteins.

We decided to compare the PRAF2 BioID2 hits against the TAP-MS data that originally indicated that there was an interaction between PRAF2 and the HPV E5 proteins (Rozenblatt-Rosen et al., 2012). When compared (Table 6.2), it became evident that many of the hits also interacted with the HPV E5 proteins. For example, ITGB1 was identified as an interactor of HPV-16E5, HPV-18E5, HPV-6BE5A, HPV-6BE5B, HPV-11E5B proteins. Proteins, TMPO, TMEM109, RRBP1, LRRC59, EMD, VAPB and VAPA also were identified by TAP-MS as putative HPV E5

interactors. Firstly, this increases confidence in the BioID2 hits, and secondly, it suggests that HPV E5 proteins could be acting via PRAF2 to modulate these proteins, or that PRAF2 is part of protein complexes including these proteins, which HPV E5 also modulates. Interestingly, no other HPV oncoproteins were found to interact with these proteins. These data also open up the possibility of new pathways that are modulated by HPV E5.

**Table**

| Gene ID  | HPV oncoprotein                                     |
|----------|---|
| ITGB1    | HPV-16E5, HPV-18E5, HPV-6BE5A, HPV-6BE5B, HPV-11E5B |
| TMX1     | N/D   |
| TMPO     | HPV-16E5, HPV-18E5, HPV-6BE5A, HPV-6BE5B, HPV-11E5B |
| TMEM109  | HPV-16E5, HPV-18E5, HPV-6BE5A, HPV-6BE5B, HPV-11E5B |
| RRBP1    | HPV-6BE5B, HPV-11E5B                                |
| LRRC59   | HPV-6BE5B   |
| PRAF2    | HPV-16E5, HPV-18E5, HPV-6BE5A, HPV-6BE5B, HPV-11E5B |
| KTN1     | N/D   |
| EMD      | HPV-16E5, HPV-18E5, HPV-6BE5A, HPV-6BE5B, HPV-11E5B |
| CKAP4    | N/D   |
| MTDH     | N/D   |
| VAPB     | HPV-6BE5A   |
| LEMD3    | N/D   |
| TOR1AIP1 | N/D   |
| KRT16    | N/D   |
| ALB      | N/D   |
| VAPA     | HPV-16E5, HPV-18E5, HPV-6BE5A, HPV-11E5B            |
| NKTR     | N/D   |

**6.2**

***Comparison of BioID2-PRAF2 hits to DNA tumour virus oncoprotein TAP-MS data***

*BioID2 hits were compared against the TAP-MS data that originally identified PRAF2 as a HPV E5 interactor. HPV oncoproteins that were hits are listed. N/D= none detected.*

Further work is needed to confirm these BioID hits (Table 6.1) as interactors of PRAF2, however a good starting point would be to perform a GFP trap pulldown with GFP-PRAF2, followed by mass spectroscopy analysis to attempt to confirm these preliminary interactors. It would also be interesting to perform the BioID experiment in cells overexpressing the HPV E5 protein, for example HPV-18E5 to see if it altered the interactome of PRAF2.

## Chapter 7 Final discussion and summary

The work presented in this thesis was initiated by an observation made in a TAP-MS screen of DNA tumour virus oncoproteins (Rozenblatt-Rosen et al., 2012), which suggested the PRAF2 protein was an interactor for a diverse panel of HPV E5 proteins. The PRAF2 protein was then investigated further to confirm this as a binding partner for the E5 proteins.

This study not only confirmed PRAF2 as a binding partner for high-risk HPV-16, 18 and 31E5 and low risk HPV-6 and 11E5s, but also for mucosal HPV-2aE5 and BPV1-E5, suggesting that the interaction with PRAF2 is likely to be a conserved phenotype for all E5 encoding PV. This study also expanded the known binding partners of HPV-18E5 to PRAF1 and PRAF3. This study also confirmed PRAF2 localised primarily to the ER in keratinocytes, and that the interaction with HPV-18E5 occurred in the ER. In addition, the region of PRAF2 responsible for E5 binding was putatively mapped to amino acids 135-160 of the C-terminus (Chapter 3).

This study was the first to examine whether the regulation of receptor cell surface expression by PRAF2 could be expanded from GPCRs to RTKs, as PRAF2 had been shown to regulate the cell surface export of GABA<sub>B</sub>, CCR5, CXCR4 and CD4 (Doly et al., 2016; Schweneker et al., 2005), through studying EGFR in both HPV negative and positive cell lines. However, it was found that PRAF2 did not alter cell surface expression of EGFR.

This is the first investigation into keratinocyte PRAF2 expression, in both HPV negative and positive cancer cell lines. It was determined that there appears to be HPV type-specific differences in PRAF2 cancer cell line expression, with HPV-16 favouring PRAF2 expression and HPV-18 resulting in a loss of PRAF2 expression. This could be contrasted with findings in the HPV lifecycle, in which in HPV-16 positive CIN1 samples and HPV-18 positive keratinocytes displayed no change in PRAF2 expression relative to normal tissue. However, in HPV-16 positive CIN2 and CIN3 samples PRAF2 protein expression increased, which agrees with the findings in the HPV-16-positive cancer cell lines. The expression of PRAF2 was also found to be independent of E5

expression. It was also determined for the first time that PRAF2 expression in skin increases upon differentiation.

The most striking finding was with regards to PRAF2 overexpression in the lifecycle of HPV-18. In both WT and E5KO HPV-18 organotypic rafts, a significant decrease in the thickness of rafts was observed, suggesting that PRAF2 was affecting hyperplasia. Whilst E1<sup>E4</sup> expression was observed in the WT18 PRAF2 overexpression rafts, it was not detected in the E5KO PRAF2 overexpression rafts, suggesting the possibility that E5 is required to modulate the actions of PRAF2 to ensure the cellular environment is conducive to the later lifecycle stages of HPV-18. However, it is unknown what changes PRAF2 overexpression was having on HPV-18 positive rafts, due to the lack of data on the proliferative status of basal and suprabasal cells, late differentiation markers and viral genome amplification. Future work is needed to investigate this to determine the effects of PRAF2 here. This could be guided by the PRAF2 interactome data supplied by the BioID experiment. Perhaps PRAF2 is influencing these potential interacting partners in such a way as to disadvantage HPV. One crucial point that needs to be addressed is the expression of PRAF2 in an NHK raft, and also the effects of PRAF2 knockdown and overexpression in NHKs, which would enable us to distinguish whether the effects seen in our HPV-18 rafts upon overexpression and knockdown were HPV or keratinocyte related.

One of the aims of this thesis was to determine whether in keratinocytes the PRAF2 protein was exerting tumour suppressor or oncogene functions. Assays for effects on markers related to cell proliferation, invasion and apoptosis suggested that the PRAF2 protein was able to exert a mild pro-migration and pro-colony formation effect in HPV-16 positive cancer cell line SiHa (Chapter 4), however this phenotype did not extend to HPV negative or HPV-18 positive cervical cancer cells. It would be interesting to see if overexpression of PRAF2 in HPV-16 positive cervical cancer cell lines promoted migration and invasion, as only knockdown studies were carried out. Studies in other cancers such as colorectal, ESCC and HCC would suggest that this

could be the case (He et al., 2019; Qian et al., 2019; Wang, C.H. et al., 2018). Assays for effects on markers related to cell proliferation, invasion and apoptosis did not suggest that PRAF2 was acting as a tumour suppressor in cervical cancer. Attempts to determine whether the PRAF2 protein was proapoptotic in cervical cancer were largely unsuccessful, with conflicting results. Most of the apoptosis assays here suggested that PRAF2 overexpression was tolerated by cervical cancer cell lines, with only PARP cleavage suggesting the PRAF2 could act in a proapoptotic fashion.

Unfortunately, the research in this thesis was not able to determine what the benefits to the virus of the interaction between PRAF2 and E5 were. Experimental data from the HEK293 cell line suggested that PRAF2 induced cell death could be blocked by HPV-18E5 overexpression, however, this assay has yet to be carried out in keratinocytes.

The work in this thesis also describes the first proteomic study of PRAF2, and the first time the BioID method has been applied to the PRAF family. One of the surprises of the putative PRAF2 interactome study was the lack of identification of Rab proteins, however, known vesicular trafficking proteins such as VAPA were identified (Gougeon and Ngsee, 2005). The lack of Rabs could be due to the limitations of the BioID technique and not due to a lack of interaction. It is possible that PRAF2 interaction with Rab proteins requires a stimulus, and our interactome represents the basal interactors of PRAF2. It is established in the literature that PRAF2 can act as an endoplasmic reticulum gatekeeper, so the putative interaction with the integrin  $\beta$ -1 subunit which is known to be trafficked from the ER is an interesting target for further study. The putative interactor metadherin would be an excellent target for further study, due to its role as an oncoprotein.

In conclusion, the conserved interaction between E5 proteins and the PRAF proteins is likely to be of importance to the virus as it is highly conserved. The interaction of E5 with PRAF2 could allow HPV to govern exit of proteins from the ER, and to regulate vesicular trafficking.

Further research is needed to determine what the phenotype of the PRAF2 and E5 interaction is and increasing knowledge of what the cellular function of PRAF2 is will facilitate this. Future characterisation of the PRAF2 interactome will serve to elucidate this.

## Appendices

### Appendix A Supplementary reagent tables

**Table A. 1** *Cloning of constructs used in this study.*

*Final construct names are listed, and the template DNA used to provide the sequence. Forward and reverse primer sequences are provided, and restriction enzymes required for insertion into the destination vector listed. The annealing temperatures and elongation times listed are for PCR using NEB Q5 high fidelity DNA polymerase.*

| Construct                  | Forward primer 5'-3'          | Reverse primer 5'-3'    | Restriction enzyme(s) | Annealing Tm (°C) | Elongation (s) |
|----------------------------|-------------------------------|-------------------------|-----------------------|-------------------|----------------|
| pcDNA3-PRAF1-3HA           | GACTGGGAA<br>TTCGCCGCC        | CCAGTCGCG<br>GCCGCGCCA  | EcoRI-HF,<br>NotI-HF  | 70                | 15             |
| U2OS cDNA                  | AGGATGGCA<br>GCGCAGAAG<br>GAC | CGGGTTCCA<br>TCTGCAGCTC |                       |                   |                |
| GFPc1-18E1 <sup>Δ</sup> E4 | GACTGGGTC<br>GACATGGCT        | ACTTCGGAT<br>CCTTATAGG  | Sall-HF,<br>BamHI-HF  | 66.1              | 20             |
| WT18 cDNA                  | GATCCAGAA<br>GTACCAGTG        | CGTAGTGTT<br>ACCACTACA  |                       |                   |                |
| GFPc1-18E1                 | GACTGGGTC<br>GACATGGCT        | ACTTCGGAT<br>CCTCATAGT  | Sall-HF,<br>BamHI-HF  | 65.3              | 80             |
| HPV-18 gDNA                | GATCCAGAA<br>GGTACAGAC        | GGTCTATGA<br>TTTTGTCCT  |                       |                   |                |
| GFPc1-18E2                 | GACTGGGTC<br>GACATGCAG        | ACTTCGGAT<br>CCTTACATTG | Sall-HF,<br>BamHI-HF  | 66                | 30             |
| HPV-18 gDNA                | ACACCGAAG<br>GAAACCCTT        | TCATGTATCC<br>CACCAAT   |                       |                   |                |
| GFPc1-18E5                 | GACTGGGTC<br>GACATGCTG        | CCAGTCGGA<br>TCCCTACTGC | Sall-HF,<br>BamHI-HF  | 66                | 10             |
| Codon optimised HPV-18E5   | AGCCTGATT<br>TCCTG            | AGGCTCAGG<br>ATAGCGTG   |                       |                   |                |

|                             |  |  |                      |    |    |
|-----------------------------|--|--|----------------------|----|----|
| pHIV-zsGreen-IRES-PRAF2     | TATATAGAA<br>TTCGCCGCC                                     | ATATATCCCG<br>GGCTAGGAT                                    | EcoRI-HF,<br>XmaI    | 56 | 15 |
| pcDNA3-PRAF2-3HA            | ACCATGTCG<br>GAGGTGCGG<br>CTGCCA                           | CCAGCCTCCT<br>GCTC   |                      |    |    |
| pcDNA3-3xFLAG-PRAF2 1-165   | TATAGGAAT<br>TCGCCGCCA                                     | TATAGCGGC<br>CGCCTACAG                                     | EcoRI-HF,<br>NotI-HF | 70 | 15 |
| pcDNA3-3xFLAG-PRAF2         | GGATGGACT<br>ATAAGGATC<br>ACG                              | GCCATTGG<br>CGTCCGC  |                      |    |    |
| pcDNA3-3xFLAG-PRAF2 1-160   | TATAGGAAT<br>TCGCCGCCA                                     | TATAGCGGC<br>CGCCTACCG                                     | EcoRI-HF,<br>NotI-HF | 64 | 15 |
| pcDNA3-3xFLAG-PRAF2         | GGATGGACT<br>ATAAGGATC<br>ACG                              | CTTGAGACC<br>AATGCTC                                       |                      |    |    |
| pcDNA3-3xFLAG-PRAF2 1-135   | TATAGGAAT<br>TCGCCGCCA                                     | TATAGCGGC<br>CGCCTACAG                                     | EcoRI-HF,<br>NotI-HF | 60 | 15 |
| pcDNA3-3xFLAG-PRAF2         | GGATGGACT<br>ATAAGGATC<br>ACG                              | GATCAGAAG<br>CACCGGC                                       |                      |    |    |
| pBABE-hygro-3xFLAG-PRAF2    | ATATGAATTC<br>GCCGCCAGG                                    | ATATGTCGA<br>CCTAGGATC                                     | EcoRI-HF,<br>Sall-HF | 56 | 15 |
| pcDNA-3xFLAG-PRAF2          | AT   | CAGCCTCCT<br>G   |                      |    |    |
| pBABE-puro-Myc-BioID2-PRAF2 | GGCGAGTTC<br>AGCCTGAGA                                     | GGGTCGACT<br>CAGCGGTTT                                     | XhoI                 | 58 | 15 |
| pHIV-zsGreen-IRES-PRAF2     | AGAAGCCTC<br>GAGATGTCG<br>GAGGTGCGG<br>CTGCCACCG<br>CTACGC | AAACTTAAG<br>TCACTAGGA<br>TCCAGCCTCC<br>TGCTCTTGTC<br>CCAG |                      |    |    |

**Table A. 2 Primers for triple FLAG tagging**

To produce a triple FLAG tagged PRAF2 at the N-terminus the triple FLAG-tag was built by sequential rounds of PCR (2.2.2). Round 1 of PCR amplified the PRAF2 gene from pHIV-zsGreen-IRES-PRAF2. This PCR product was purified and used as the template for round 2 of PCR, purification was then purified, and this was used for round 3 of PCR. The final round of PCR (4) was used to add the kozak sequence and restriction site to the N-terminus of the 3xFLAG-PRAF2 construct. This product was then amplified and cloned into pcDNA3.1(+) as per 2.2.2, 2.2.4-2.2.6.

| PCR round       | Forward primer 5'-3'  | Reverse primer 5'-3'                          | Restriction enzyme(s) | Annealing Tm (°C) | Elongation (s) |
|-----------------|---|---|-----------------------|-------------------|----------------|
| Round 1         | TTACAAAGA<br>TGATGACGA<br>CAAATGTC<br>GGAGGTGCG<br>GCTGCC     | CTAGGATCC<br>AGCCTCCTG<br>CTCTTGTC            | N/A                   | 62                | 15             |
| Round 2         | ATTACAAGG<br>ATCATGACA<br>TCGATTACA<br>AAGATGATG<br>ACGAC     |   | N/A                   | 62                | 15             |
| Round 3         | ATGGACTAT<br>AAGGATCAC<br>GATGGAGAT<br>TACAAGGAT<br>CATGACATC |   | N/A                   | 62                | 15             |
| Round 4 (final) | TATAGGAAT<br>TCGCCGCCA<br>GGATGGACT<br>ATAAGGATC<br>ACG       | TATAGCGGC<br>CGCCTAGGA<br>TCCAGCCTCC<br>TGCTC | EcoRI-HF,<br>NotI-HF  | 62                | 15             |

**Table A. 3** *Plasmids used in this study.*

*Plasmid name, backbone and expression type listed. The bacterial resistance gene is also listed.*

*The sources for the plasmids are listed, with addgene codes where appropriate.*

| <b>Plasmid name</b> | <b>Plasmid backbone</b> | <b>Expression type</b> | <b>Resistance</b> | <b>Source</b>                  |
|---------------------|-------------------------|------------------------|-------------------|--------------------------------|
| pcDNA3.1(+)         | pcDNA3.1(+)             | Transient              | Ampicillin        | Invitrogen                     |
| PRAF1-3HA           | pcDNA3.1(+)-3HA         | Transient              | Ampicillin        | Cloned by D.Kealy              |
| PRAF3-3HA           | pcDNA3.1(+)-3HA         | Transient              | Ampicillin        | Gift from Dr. Ingram laccarino |
| PRAF2-3HA           | pcDNA3.1(+)-3HA         | Transient              | Ampicillin        | Gift from Dr. Ingram laccarino |
| PRAF2-3HA 19-178    | pcDNA3.1(+)-3HA         | Transient              | Ampicillin        | Gift from Dr. Ingram laccarino |
| PRAF2-3HA 34-178    | pcDNA3.1(+)-3HA         | Transient              | Ampicillin        | Gift from Dr. Ingram laccarino |
| PRAF2-3HA 94-178    | pcDNA3.1(+)-3HA         | Transient              | Ampicillin        | Gift from Dr. Ingram laccarino |
| 3xFLAG-PRAF2        | pcDNA3.1(+)             | Transient              | Ampicillin        | Cloned by D.Kealy              |
| 3xFLAG-PRAF2 1-165  | pcDNA3.1(+)             | Transient              | Ampicillin        | Cloned by D.Kealy              |
| 3xFLAG-PRAF2 1-160  | pcDNA3.1(+)             | Transient              | Ampicillin        | Cloned by D.Kealy              |
| 3xFLAG-PRAF2 1-135  | pcDNA3.1(+)             | Transient              | Ampicillin        | Cloned by D.Kealy              |
| peGFPC1             | peGFPC1                 | Transient              | Kanamycin         | Clontech                       |
| peGFPC1-18E5        | peGFPC1                 | Transient              | Kanamycin         | Cloned by D.Kealy              |
| peGFPC2-6E5         | peGFPC2                 | Transient              | Kanamycin         | Cloned by Dr. Marietta Müller  |
| peGFPC2-11E5        | peGFPC2                 | Transient              | Kanamycin         | Cloned by Dr. Marietta Müller  |

|                          |                   |                                   |            |   |
|--------------------------|-------------------|-----------------------------------|------------|---|
| peGFPC2-16E5             | peGFPC2           | Transient                         | Kanamycin  | Cloned by Dr. Marietta Müller             |
| peGFPC1-31E5             | peGFPC1           | Transient                         | Kanamycin  | Cloned by Dr. Marietta Müller             |
| peGFPC2-2aE5             | peGFPC2           | Transient                         | Kanamycin  | Cloned by Dr. Marietta Müller             |
| peGFPC1-BPV-1E5          | peGFPC1           | Transient                         | Kanamycin  | Cloned by Dr. Marietta Müller             |
| peGFPC1-E1^E4            | peGFPC1           | Transient                         | Kanamycin  | Cloned by D.Kealy                         |
| peGFPC1-E1               | peGFPC1           | Transient                         | Kanamycin  | Cloned by D.Kealy                         |
| peGFPC1-E2               | peGFPC1           | Transient                         | Kanamycin  | Cloned by D.Kealy                         |
| GFP-H-Ras                | peGFPC1           | Transient                         | Kanamycin  | Gift from Dr. Darren Tomlinson            |
| GFP-K-Ras                | peGFPC1           | Transient                         | Kanamycin  | Gift from Dr. Darren Tomlinson            |
| GFP-N-Ras                | peGFPC1           | Transient                         | Kanamycin  | Gift from Dr. Darren Tomlinson            |
| pcDNA3.1(+)-GFP-PRAF2    | pcDNA3.1(+)-N-GFP | Transient                         | Ampicillin | Genscript                                 |
| pcDNA3.1(+)-PRAF2-GFP    | pcDNA3.1(+)-C-GFP | Transient                         | Ampicillin | Genscript                                 |
| pcDNA3.1(+)-GFP-18E6     | pcDNA3.1(+)-N-GFP | Transient                         | Ampicillin | Genscript                                 |
| pcDNA3.1(+)-GFP-18E7     | pcDNA3.1(+)-N-GFP | Transient                         | Ampicillin | Genscript                                 |
| pBABE-hygro              | pBABE-hygro       | Retroviral                        | Ampicillin | Addgene #1765, gift from Dr. Bob Weinberg |
| pBABE-hygro-3xFLAG-PRAF2 | pBABE-hygro       | Retroviral                        | Ampicillin | Cloned by D.Kealy                         |
| pHIV-zsGreen-IRES        | pHIV-zsGreen-IRES | 3 <sup>rd</sup> gen<br>Lentiviral | Ampicillin | Addgene #18121, gift from Dr. Bryan Welm  |
| pHIV-zsGreen-IRES-PRAF2  | pHIV-zsGreen-IRES | 3 <sup>rd</sup> gen<br>Lentiviral | Ampicillin | Cloned by D.Kealy                         |

|  |                                      |  |            |   |
|--|--------------------------------------|--|------------|---|
| pRSV-Rev   | pRSV-Rev                             | 3 <sup>rd</sup> gen<br>lentiviral<br>packaging | Ampicillin | Addgene #12253, gift<br>from Dr. Didier Trono |
| pMDLg/pRRE                                       | pMD                                  | 3 <sup>rd</sup> gen<br>lentiviral<br>packaging | Ampicillin | Addgene #12251, gift<br>from Dr. Didier Trono |
| pCMV-VSV-G                                       | pCMV                                 | Lentiviral/<br>retroviral                      | Ampicillin | Addgene #8454, gift from<br>Dr. Bob Weinberg  |
| pZIP-hEF1 $\alpha$ -<br>zsGreen-Puro-<br>shNTC   | pZIP-hEF1 $\alpha$ -<br>zsGreen-Puro | 2 <sup>nd</sup> gen<br>lentiviral              | Ampicillin | Transomic technologies                        |
| pZIP-hEF1 $\alpha$ -<br>zsGreen-Puro-<br>shPRAF2 | pZIP-hEF1 $\alpha$ -<br>zsGreen-Puro | 2 <sup>nd</sup> gen<br>lentiviral              | Ampicillin | Transomic technologies                        |
| pCRV1-NLGP                                       | pCRV1                                | 2 <sup>nd</sup> gen<br>lentiviral<br>packaging | Ampicillin | Gift from Dr. Sam Wilson                      |
| pBABE-puro-<br>Myc-BioID2                        | mycBioID2-<br>pBABE-puro             | Retroviral                                     | Ampicillin | Addgene #80900, Gift<br>from Dr. Kyle Roux    |
| pBABE-puro-<br>Myc-BioID2-<br>PRAF2              | mycBioID2-<br>pBABE-puro             | Retroviral                                     | Ampicillin | Cloned by D.Kealy                             |

**Table A. 4** Antibody reagents used in this study.

Manufacturer/source, product code, antibody type and applications are listed. The dilutions listed are in the order the applications are listed in e.g WB, IF|1:5000, 1:500, means the WB dilution is 1:5000 and the IF dilution is 1:500 etc.

| Antibody          | Manufacturer  | Product code | Antibody type | Application | Dilution             |
|-------------------|---------------|--------------|---------------|-------------|----------------------|
| Calnexin          | CST           | 2679         | Rabbit mAb    | IF          | 1:100                |
| Cleaved caspase-3 | CST           | 9664         | Rabbit mAb    | IF          | 1:400                |
| Cyclin A1         | SCBT          | sc-198       | Rabbit pAb    | WB          | 1:1000               |
| Cyclin B1         | CST           | 12231        | Rabbit mAb    | WB          | 1:1000               |
| Cyclin D1         | Abcam         | ab134175     | Rabbit mAb    | WB          | 1:2000               |
| Cyclin E1         | Abcam         | ab211342     | Mouse mAb     | WB          | 1:2000               |
| Cytokeratin-10    | Abcam         | ab76318      | Rabbit mAb    | WB, IHC     | 1:10000, 1:250       |
| EGFR              | Abcam         | ab52894      | Rabbit mAb    | WB, Flow    | 1:5000, 1:100        |
| FLAG tag          | Sigma-Aldrich | F1804        | Mouse mAb     | WB, IF, IHC | 1:2000, 1:500, 1:300 |
| GAPDH             | SCBT          | sc-9996      | Mouse mAb     | WB          | 1:2000               |
| GFP               | SCBT          | sc-365062    | Mouse mAb     | WB          | 1:2000               |
| GM130             | CST           | 12480        | Rabbit mAb    | IF          | 1:3200               |
| HA tag            | Sigma-Aldrich | H9658        | Mouse mAb     | WB, IF      | 1:5000, 1:500        |

|             |   |           |               |        |                   |
|-------------|---|-----------|---------------|--------|-------------------|
| HPV-16 E6   | Genetex   | GTX132686 | Rabbit<br>pAb | WB     | 1:500             |
| HPV-16 E7   | SCBT  | sc-6981   | Mouse<br>mAb  | WB     | 1:250             |
| HPV-18 E6   | SCBT  | sc-365089 | Mouse<br>mAb  | WB     | 1:500             |
| HPV-18 E7   | Abcam   | ab100953  | Mouse<br>mAb  | WB     | 1:1000            |
| HPV-18E1^E4 | Kindly<br>provided by Dr.<br>Sally Roberts,<br>University of<br>Birmingham            | 1D11      | Mouse<br>mAb  | IHC    | 1:5               |
| Myc tag     | CST   | 2276      | Mouse<br>mAb  | WB, IF | 1:1000,<br>1:8000 |
| PARP        | CST   | 9542      | Rabbit<br>mAb | WB     | 1:2500            |
| PDI         | ThermoFisher<br>Scientific  | MA3019    | Mouse<br>mAb  | IF     | 1:100             |
| PRAF2       | Abcam   | ab53113   | Rabbit<br>pAb | WB, IF | 1:2500,<br>1:400  |
| PRAF2       | Abcam   | ab230420  | Rabbit<br>pAb | IHC    | 1:200             |
| TGN46       | Kindly<br>provided by Dr<br>Sreenivasan<br>Ponnambalam,<br>University of<br>Leeds, UK | N/A       | Sheep<br>pAb  | IF     | 1:100             |

**Table A. 5** *Secondary antibody reagents and fluorescent conjugates used in this study.*

Name, manufacturer, product code, host species (where appropriate), conjugation and dilution (or concentration) listed.

| Antibody           | Manufacturer            | Product code    | Host    | Conjugate         | Dilution |
|--------------------|-------------------------|-----------------|---------|-------------------|----------|
| Anti-mouse         | ThermoFisher Scientific | A-21200         | Chicken | AlexaFluor488     | 1:1000   |
| Anti-mouse         | "                       | A-21201         | Chicken | AlexaFluor594     | 1:1000   |
| Anti-mouse         | "                       | A-21203         | Donkey  | AlexaFluor594     | 1:1000   |
| Anti-Rabbit        | "                       | A-21441         | Chicken | AlexaFluor488     | 1:1000   |
| Anti-Rabbit        | "                       | A-21442         | Chicken | AlexaFluor594     | 1:1000   |
| Anti-Rabbit        | "                       | A-11012         | Goat    | AlexaFluor594     | 1:1000   |
| Anti-Sheep         | "                       | A-11015         | Donkey  | AlexaFluor488     | 1:1000   |
| Streptavidin       | "                       | S32354          | N/A     | AlexaFluor488     | 1:1000   |
| Anti-mouse         | Stratech                | JIR-115-035-174 | Goat    | HRP               | 1:5000   |
| Anti-rabbit        | Stratech                | JIR-211-032-171 | Mouse   | HRP               | 1:5000   |
| Streptavidin       | ThermoFisher Scientific | 21130           | N/A     | HRP               | 1:40000  |
| Mitotracker CMXRos | "                       | M7512           | N/A     | Excitation at 594 | 200 nM   |

**Table A. 6** *Cell lines used in this study*

| Cell line | Type                          | Species | Split ratio | Every  |
|-----------|-------------------------------|---------|-------------|--------|
| C33A      | Cervical cancer               | Human   | 1:3         | 3 days |
| HeLa      | Cervical cancer (HPV-18)      | Human   | 1:8         | 2 days |
| CaSki     | Cervical cancer (HPV-16)      | Human   | 1:3         | 4 days |
| SiHa      | Cervical cancer (HPV-16)      | Human   | 1:5         | 3 days |
| SW756     | Cervical cancer (HPV-16)      | Human   | 1:3         | 4 days |
| Phoenix A | Retroviral producer cell line | Human   | 1:5         | 3 days |

|   |  |       |          |               |
|---|--|-------|----------|---------------|
| HEK293  | Embryonic kidney transformed with sheared adenovirus 5 DNA                       | Human | 1:5      | 3 days        |
| HEK293T                                       | HEK293 cells containing a stably integrated SV40 genome. Express small T antigen | Human | 1:5      | 3 days        |
| HEK293TT                                      | HEK293T cells maintaining a plasmid expressing the SV40 large T antigen          | Human | 1:5      | 3 days        |
| J2 3T3  | Mouse fibroblasts  | Mouse | 1:10     | 4 days        |
| NHK (Primary, 2 donors)                       | Primary human foreskin keratinocytes   | Human | 1:5      | When required |
| HPV-18 positive keratinocytes (2 donors)      | Primary human foreskin keratinocytes stably maintaining episomal HPV-18          | Human | 1:5/1:10 | When required |
| HPV-18 E5KO positive keratinocytes (2 donors) | Primary human foreskin keratinocytes stably maintaining episomal HPV-18 E5KO     | Human | 1:5/1:10 | When required |

**Table A. 7**      *TMT sample labels*

| Sample number | Sample ID | TMT label  |
|---------------|-----------|------------|
| 1             | C33A 1    | TMT10_126  |
| 2             | C33A 2    | TMT10_127N |
| 3             | C33A 3    | TMT10_127C |
| 4             | BioID 1   | TMT10_128N |
| 5             | BioID 2   | TMT10_128C |
| 6             | BioID 3   | TMT10_129N |
| 7             | PRAF2_1   | TMT10_129C |
| 8             | PRAF2_2   | TMT10_130N |
| 9             | PRAF2_3   | TMT10_130C |

## **Appendix B Supplementary methods**

### **B.1 Mitochondrial staining with Mitotracker CMXRos**

15 minutes prior to fixation cell culture media was replaced with complete DMEM warmed to 37°C containing 200 nM of Mitotracker CMXRos (ThermoFisher Scientific, M7512). Cells were incubated at 37°C protected from light, then media removed and washed once with 37°C complete DMEM and then fixed with 4% paraformaldehyde prewarmed to 37°C, and incubated at 37°C for 15 minutes, briefly washed with PBS then permeabilised with 0.1% Triton X-100 for 10 minutes. Cells were then blocked and processed as per Chapter 2.7.3.

## Appendix C Supplementary figures

```

PRAF1      MAAQKDQOKDAEAEGLSGTLLPKLIPSGAGREWLERRRATIRPWSTFVD-QQRFS--RP
PRAF2      -----MSEVRLPPLRALDDFVLGSARLAAPDP
PRAF3      -----MDVNIAPLRAWDDFFPGSDRFARPDF

PRAF1      RNLGELCQRLVRRNVEYYQSNYVFVFLGLLILYCVVTSPELLVALAVFFGACYILYLRTLES
PRAF2      CDPQRWCHRVINNLLYYQTNYLLCFGIGLALAGYVRPLHTLLSALVVAVALGVLVWAAET
PRAF3      RDISKWNRRVVSNLLYYQTNYLVVAAMMISIVGFSLPFNMILGGIVVVLVFTGFVWAAHN

PRAF1      KLVL-FGREVSPA HQYALAGGISFPFFWLAGAGSAVFVWLGATLVVIGSHAAFHQIEAVD
PRAF2      RAAVRRRCRRSHPAACLA AVLAVGLLVLVWVAGGACTFLFSIAGPVLLILVHASLRLRNLKN
PRAF3      KDVLRRMKKRYPTTFVMVMLASYFLISMFGGVMVFVFGITFPLLLMFIHASLRLRNLKN

PRAF1      GEELQMEPV----- 185
PRAF2      KIENKIESIGLKRTPMGLLLEALGQEQEAGS----- 178
PRAF3      KLENKMEGIGLKRTPMGIVLDALEQQEEGINRLTDYISKVKE 188
    
```

**Figure A. 1 PRA family protein sequence alignment**

PRA family members PRAF1, PRAF2 and PRAF3 protein sequences were aligned using Clustal Omega. The conserved regions are highlighted in bold text and orange.

```

94-178      -----
34-178      -----MCHRVINNLLYYQTNYLLCFGIGLALAG
19-178      -----MSARLAAPDPCDPQRWCHRVINNLLYYQTNYLLCFGIGLALAG
WT          MSEVRLPPLRALDDFVLGSARLAAPDPCDPQRWCHRVINNLLYYQTNYLLCFGIGLALAG
1-165      MSEVRLPPLRALDDFVLGSARLAAPDPCDPQRWCHRVINNLLYYQTNYLLCFGIGLALAG
1-160      MSEVRLPPLRALDDFVLGSARLAAPDPCDPQRWCHRVINNLLYYQTNYLLCFGIGLALAG
1-135      MSEVRLPPLRALDDFVLGSARLAAPDPCDPQRWCHRVINNLLYYQTNYLLCFGIGLALAG

94-178      -----MCRRSHPAACLA AVLAVGLLVLVWVAGGA
34-178      YVRPLHTLLSALVVAVALGVLVWAAETRAAVRRCRRSHPAACLA AVLAVGLLVLVWVAGGA
19-178      YVRPLHTLLSALVVAVALGVLVWAAETRAAVRRCRRSHPAACLA AVLAVGLLVLVWVAGGA
WT          YVRPLHTLLSALVVAVALGVLVWAAETRAAVRRCRRSHPAACLA AVLAVGLLVLVWVAGGA
1-165      YVRPLHTLLSALVVAVALGVLVWAAETRAAVRRCRRSHPAACLA AVLAVGLLVLVWVAGGA
1-160      YVRPLHTLLSALVVAVALGVLVWAAETRAAVRRCRRSHPAACLA AVLAVGLLVLVWVAGGA
1-135      YVRPLHTLLSALVVAVALGVLVWAAETRAAVRRCRRSHPAACLA AVLAVGLLVLVWVAGGA
*****

94-178      CTFLFSIAGPVLLILVHASLRLRNLKNKIENKIESIGLKRTPMGLLLEALGQEQEAGS 86
34-178      CTFLFSIAGPVLLILVHASLRLRNLKNKIENKIESIGLKRTPMGLLLEALGQEQEAGS 146
19-178      CTFLFSIAGPVLLILVHASLRLRNLKNKIENKIESIGLKRTPMGLLLEALGQEQEAGS 161
WT          CTFLFSIAGPVLLILVHASLRLRNLKNKIENKIESIGLKRTPMGLLLEALGQEQEAGS 178
1-165      CTFLFSIAGPVLLILVHASLRLRNLKNKIENKIESIGLKRTPMGL----- 165
1-160      CTFLFSIAGPVLLILVHASLRLRNLKNKIENKIESIGLKR----- 160
1-135      CTFLFSIAGPVLLIL----- 135
*****
    
```

**Figure A. 2 Alignment of PRAF2 mutants against the WT PRAF2 sequence**

PRAF2 mutants were aligned against the WT PRAF2 sequence using Clustal Omega. Mutants 19-178, 34-178 and 94-178 are the N-termini truncation mutants tagged with 3xHA at their C-termini. Mutants 1-135, 1-160 and 1-165 are the C-termini truncation mutants tagged with 3xFLAG at their N-termini. The conserved regions NLLYYQTNY and HASLRLR are highlighted in the orange boxes. Total amino acid length is also shown.

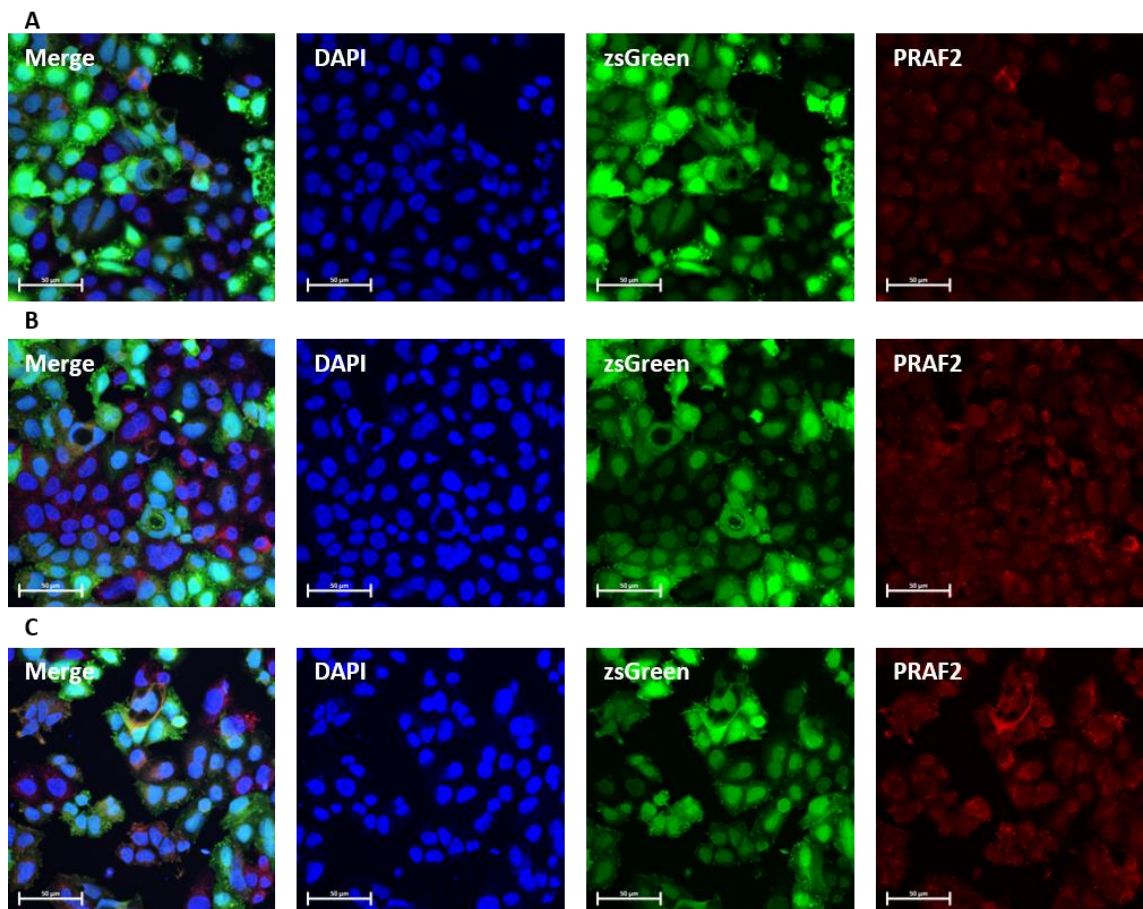


**Figure A. 3 Endogenous PRAF2 was not detected by immunofluorescence in a specific manner by the PRAF2 antibody**

C33A cells stably expressing either shNTC or shPRAF2, where the knockdown of PRAF2 had been validated by western blotting, were fixed, permeabilised and probed with an antibody to endogenous PRAF2, then stained with Alexa-594 conjugated secondary antibodies. zsGreen (green), PRAF2 (red). Nuclei counterstained with DAPI (blue), Scale bars 50 μm, images

representative. A. C33A-zsGreen-shNTC. B. C33A-zsGreen-shPRAF2. C. C33A-zsGreen-shPRAF2

n=1

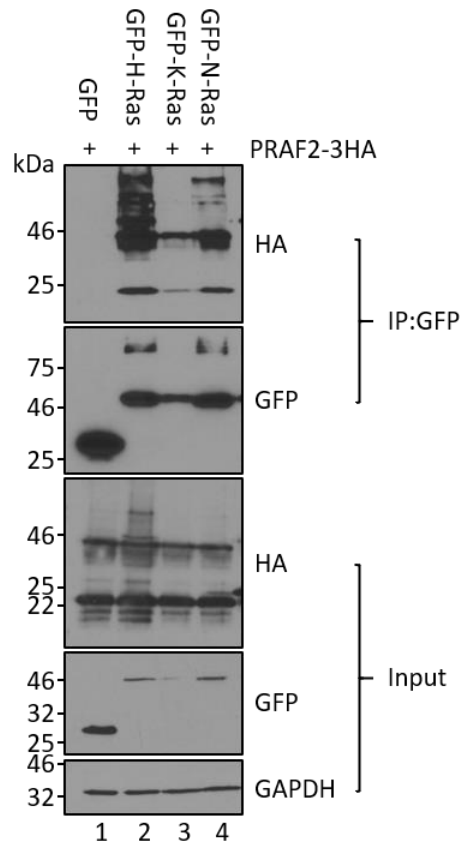


**Figure A. 4** Proteins from the Ras family could immunoprecipitate PRAF2

GFP-H-Ras, GFP-K-Ras and GFP-N-Ras were co-transfected with PRAF2-3HA into HEK293 cells with GFP as a negative control, immunoprecipitations were performed using GFP-trap magnetic agarose beads using equal amounts of protein. The resulting western blots were probed for GFP, HA and GAPDH. N=2

## Bibliography

- Abbate, E.A., Voitenleitner, C. and Botchan, M.R. 2006. Structure of the papillomavirus DNA-tethering complex E2:Brd4 and a peptide that ablates HPV chromosomal association. *Mol Cell*. **24**(6), pp.877-889.
- Abdul-Ghani, M., Gougeon, P.Y., Prosser, D.C., Da-Silva, L.F. and Ngsee, J.K. 2001. PRA isoforms are targeted to distinct membrane compartments. *J Biol Chem*. **276**(9), pp.6225-6233.
- Abe, F., Van Prooyen, N., Ladasky, J.J. and Edidin, M. 2009. Interaction of Bap31 and MHC class I molecules and their traffic out of the endoplasmic reticulum. *J Immunol*. **182**(8), pp.4776-4783.
- Akerman, G.S., Tolleson, W.H., Brown, K.L., Zyzak, L.L., Mourateva, E., Engin, T.S., Basaraba, A., Coker, A.L., Creek, K.E. and Pirisi, L. 2001. Human papillomavirus type 16 E6 and E7 cooperate to increase epidermal growth factor receptor (EGFR) mRNA levels, overcoming mechanisms by which excessive EGFR signaling shortens the life span of normal human keratinocytes. *Cancer Res*. **61**(9), pp.3837-3843.
- Alili, L., Diekmann, J., Giesen, M., Holtkötter, O. and Brenneisen, P. 2014. A drug-induced accelerated senescence (DIAS) is a possibility to study aging in time lapse. *Age (Dordr)*. **36**(3), p9658.
- Anderson, T.A., Schick, V., Herbenick, D., Dodge, B. and Fortenberry, J.D. 2014. A study of human papillomavirus on vaginally inserted sex toys, before and after cleaning, among women who have sex with women and men. *Sex Transm Infect*. **90**(7), pp.529-531.
- Antonsson, A. and Persson, J.L. 2009. Induction of apoptosis by staurosporine involves the inhibition of expression of the major cell cycle proteins at the G(2)/m checkpoint accompanied by alterations in Erk and Akt kinase activities. *Anticancer Res*. **29**(8), pp.2893-2898.
- Armbruster-Moraes, E., Ioshimoto, L.M., Leão, E. and Zugaib, M. 1994. Presence of human papillomavirus DNA in amniotic fluids of pregnant women with cervical lesions. *Gynecol Oncol*. **54**(2), pp.152-158.
- Ashrafi, G.H., Brown, D.R., Fife, K.H. and Campo, M.S. 2006a. Down-regulation of MHC class I is a property common to papillomavirus E5 proteins. *Virus Res*. **120**(1-2), pp.208-211.
- Ashrafi, G.H., Haghshenas, M., Marchetti, B. and Campo, M.S. 2006b. E5 protein of human papillomavirus 16 downregulates HLA class I and interacts with the heavy chain via its first hydrophobic domain. *Int J Cancer*. **119**(9), pp.2105-2112.
- Ashrafi, G.H., Haghshenas, M.R., Marchetti, B., O'Brien, P.M. and Campo, M.S. 2005. E5 protein of human papillomavirus type 16 selectively downregulates surface HLA class I. *Int J Cancer*. **113**(2), pp.276-283.
- Ashrafi, G.H., Tsirimonaki, E., Marchetti, B., O'Brien, P.M., Sibbet, G.J., Andrew, L. and Campo, M.S. 2002. Down-regulation of MHC class I by bovine papillomavirus E5 oncoproteins. *Oncogene*. **21**(2), pp.248-259.
- Auvinen, E., Alonso, A. and Auvinen, P. 2004. Human papillomavirus type 16 E5 protein colocalizes with the antiapoptotic Bcl-2 protein. *Arch Virol*. **149**(9), pp.1745-1759.

- Avila, J.R., Lee, J.S. and Torii, K.U. 2015. Co-Immunoprecipitation of Membrane-Bound Receptors. *Arabidopsis Book*. **13**, pe0180.
- Aydin, I., Villalonga-Planells, R., Greune, L., Bronnimann, M.P., Calton, C.M., Becker, M., Lai, K.Y., Campos, S.K., Schmidt, M.A. and Schelhaas, M. 2017. A central region in the minor capsid protein of papillomaviruses facilitates viral genome tethering and membrane penetration for mitotic nuclear entry. *PLoS Pathog*. **13**(5), pe1006308.
- Bachman, K.E. and Park, B.H. 2005. Dual nature of TGF-beta signaling: tumor suppressor vs. tumor promoter. *Curr Opin Oncol*. **17**(1), pp.49-54.
- Bai, J., Zhang, J., Wu, J., Shen, L., Zeng, J., Ding, J., Wu, Y., Gong, Z., Li, A., Xu, S., Zhou, J. and Li, G. 2010. JWA regulates melanoma metastasis by integrin alphaVbeta3 signaling. *Oncogene*. **29**(8), pp.1227-1237.
- Bassioukas, K., Danielides, V., Georgiou, I., Photos, E., Zagorianakou, P. and Skevas, A. 2000. Oral focal epithelial hyperplasia. *Eur J Dermatol*. **10**(5), pp.395-397.
- Bastian FB, P.G., Roux J, Moretti S, Laudet V, Robinson-Rechavi M. 2008. *Bgee: Integrating and Comparing Heterogeneous Transcriptome Data Among Species*. DILS: Data Integration in Life Sciences. **Lecture Notes in Computer Science**.: Springer. 5109. pp.124-131.
- Becker, M., Greune, L., Schmidt, M.A. and Schelhaas, M. 2018. Extracellular Conformational Changes in the Capsid of Human Papillomaviruses Contribute to Asynchronous Uptake into Host Cells. *J Virol*. **92**(11).
- Bellanger, S., Demeret, C., Goyat, S. and Thierry, F. 2001. Stability of the human papillomavirus type 18 E2 protein is regulated by a proteasome degradation pathway through its amino-terminal transactivation domain. *J Virol*. **75**(16), pp.7244-7251.
- Belleudi, F., Leone, L., Purpura, V., Cannella, F., Scrofani, C. and Torrisi, M.R. 2011. HPV16 E5 affects the KGFR/FGFR2b-mediated epithelial growth through alteration of the receptor expression, signaling and endocytic traffic. *Oncogene*. **30**(50), pp.4963-4976.
- Bergvall, M., Melendy, T. and Archambault, J. 2013. The E1 proteins. *Virology*. **445**(1-2), pp.35-56.
- Berk, J.M., Simon, D.N., Jenkins-Houk, C.R., Westerbeck, J.W., Grønning-Wang, L.M., Carlson, C.R. and Wilson, K.L. 2014. The molecular basis of emerin-emerin and emerin-BAF interactions. *J Cell Sci*. **127**(Pt 18), pp.3956-3969.
- Berk, J.M., Tiffit, K.E. and Wilson, K.L. 2013. The nuclear envelope LEM-domain protein emerin. *Nucleus*. **4**(4), pp.298-314.
- Bernard, H.U., Burk, R.D., Chen, Z., van Doorslaer, K., zur Hausen, H. and de Villiers, E.M. 2010. Classification of papillomaviruses (PVs) based on 189 PV types and proposal of taxonomic amendments. *Virology*. **401**(1), pp.70-79.
- Bharti, A.H., Chotaliya, K. and Marfatia, Y.S. 2013. An update on oral human papillomavirus infection. *Indian J Sex Transm Dis AIDS*. **34**(2), pp.77-82.

- Bienkowska-Haba, M., Williams, C., Kim, S.M., Garcea, R.L. and Sapp, M. 2012. Cyclophilins facilitate dissociation of the human papillomavirus type 16 capsid protein L1 from the L2/DNA complex following virus entry. *J Virol.* **86**(18), pp.9875-9887.
- Biryukov, J., Myers, J.C., McLaughlin-Drubin, M.E., Griffin, H.M., Milici, J., Doorbar, J. and Meyers, C. 2017. Mutations in HPV18 E1<sup>E4</sup> Impact Virus Capsid Assembly, Infectivity Competence, and Maturation. *Viruses.* **9**(12).
- Blanpain, C. and Fuchs, E. 2006. Epidermal stem cells of the skin. *Annu Rev Cell Dev Biol.* **22**, pp.339-373.
- Blanpain, C., Lowry, W.E., Pasolli, H.A. and Fuchs, E. 2006. Canonical notch signaling functions as a commitment switch in the epidermal lineage. *Genes Dev.* **20**(21), pp.3022-3035.
- Blenski, M. and Kehlenbach, R.H. 2019. Targeting of LRRC59 to the Endoplasmic Reticulum and the Inner Nuclear Membrane. *Int J Mol Sci.* **20**(2).
- Blom, N., Gammeltoft, S. and Brunak, S. 1999. Sequence and structure-based prediction of eukaryotic protein phosphorylation sites1 1Edited by F. E. Cohen. *Journal of Molecular Biology.* **294**(5), pp.1351-1362.
- Bolte, S. and Cordelières, F.P. 2006. A guided tour into subcellular colocalization analysis in light microscopy. *J Microsc.* **224**(Pt 3), pp.213-232.
- Boon, S.S. and Banks, L. 2013. High-risk human papillomavirus E6 oncoproteins interact with 14-3-3 $\zeta$  in a PDZ binding motif-dependent manner. *J Virol.* **87**(3), pp.1586-1595.
- Borbély, A.A., Murvai, M., Kónya, J., Beck, Z., Gergely, L., Li, F. and Veress, G. 2006. Effects of human papillomavirus type 16 oncoproteins on survivin gene expression. *J Gen Virol.* **87**(Pt 2), pp.287-294.
- Borsics, T., Lundberg, E., Geerts, D., Koomoa, D.L., Koster, J., Wester, K. and Bachmann, A.S. 2010. Subcellular distribution and expression of prenylated Rab acceptor 1 domain family, member 2 (PRAF2) in malignant glioma: Influence on cell survival and migration. *Cancer Sci.* **101**(7), pp.1624-1631.
- Bourgeois, B., Gilquin, B., Tellier-Lebègue, C., Östlund, C., Wu, W., Pérez, J., El Hage, P., Lallemand, F., Worman, H.J. and Zinn-Justin, S. 2013. Inhibition of TGF- $\beta$  signaling at the nuclear envelope: characterization of interactions between MAN1, Smad2 and Smad3, and PPM1A. *Sci Signal.* **6**(280), pra49.
- Bouvard, V., Baan, R., Straif, K., Grosse, Y., Secretan, B., El Ghissassi, F., Benbrahim-Tallaa, L., Guha, N., Freeman, C., Galichet, L., Coglianò, V. and Group, W.I.A.f.R.o.C.M.W. 2009. A review of human carcinogens--Part B: biological agents. *Lancet Oncol.* **10**(4), pp.321-322.
- Branon, T.C., Bosch, J.A., Sanchez, A.D., Udeshi, N.D., Svinkina, T., Carr, S.A., Feldman, J.L., Perrimon, N. and Ting, A.Y. 2018. Efficient proximity labeling in living cells and organisms with TurboID. *Nat Biotechnol.* **36**(9), pp.880-887.
- Bray, F., Ferlay, J., Soerjomataram, I., Siegel, R.L., Torre, L.A. and Jemal, A. 2018. Global cancer statistics 2018: GLOBOCAN estimates of incidence and mortality worldwide for 36 cancers in 185 countries. *CA Cancer J Clin.* **68**(6), pp.394-424.

- Briggs, M.W., Adam, J.L. and McCance, D.J. 2001. The human papillomavirus type 16 E5 protein alters vacuolar H(+)-ATPase function and stability in *Saccharomyces cerevisiae*. *Virology*. **280**(2), pp.169-175.
- Brotherton, J.M., Budd, A., Rompotis, C., Bartlett, N., Malloy, M.J., Andersen, R.L., Coulter, K.A., Couvee, P.W., Steel, N., Ward, G.H. and Saville, M. 2019. Is one dose of human papillomavirus vaccine as effective as three?: A national cohort analysis. *Papillomavirus Res.* **8**, p100177.
- Bucci, C., Chiariello, M., Lattero, D., Maiorano, M. and Bruni, C.B. 1999. Interaction cloning and characterization of the cDNA encoding the human prenylated rab acceptor (PRA1). *Biochem Biophys Res Commun.* **258**(3), pp.657-662.
- Bucci, C., De Gregorio, L. and Bruni, C.B. 2001. Expression analysis and chromosomal assignment of PRA1 and RILP genes. *Biochem Biophys Res Commun.* **286**(4), pp.815-819.
- Buck, C.B., Cheng, N., Thompson, C.D., Lowy, D.R., Steven, A.C., Schiller, J.T. and Trus, B.L. 2008. Arrangement of L2 within the papillomavirus capsid. *J Virol.* **82**(11), pp.5190-5197.
- Buck, C.B., Day, P.M. and Trus, B.L. 2013. The papillomavirus major capsid protein L1. *Virology*. **445**(1-2), pp.169-174.
- Buck, C.B., Van Doorslaer, K., Peretti, A., Geoghegan, E.M., Tisza, M.J., An, P., Katz, J.P., Pipas, J.M., McBride, A.A., Camus, A.C., McDermott, A.J., Dill, J.A., Delwart, E., Ng, T.F., Farkas, K., Austin, C., Kraberger, S., Davison, W., Pastrana, D.V. and Varsani, A. 2016. The Ancient Evolutionary History of Polyomaviruses. *PLoS Pathog.* **12**(4), pe1005574.
- Burd, E.M. 2003. Human papillomavirus and cervical cancer. *Clin Microbiol Rev.* **16**(1), pp.1-17.
- Butchbach, M.E., Lai, L. and Lin, C.L. 2002. Molecular cloning, gene structure, expression profile and functional characterization of the mouse glutamate transporter (EAAT3) interacting protein GTRAP3-18. *Gene.* **292**(1-2), pp.81-90.
- Bzhalava, D., Eklund, C. and Dillner, J. 2015. International standardization and classification of human papillomavirus types. *Virology.* **476**, pp.341-344.
- Campo, M.S., Graham, S.V., Cortese, M.S., Ashrafi, G.H., Araibi, E.H., Dornan, E.S., Miners, K., Nunes, C. and Man, S. 2010. HPV-16 E5 down-regulates expression of surface HLA class I and reduces recognition by CD8 T cells. *Virology.* **407**(1), pp.137-142.
- Campos, S.K. and Ozburn, M.A. 2009. Two highly conserved cysteine residues in HPV16 L2 form an intramolecular disulfide bond and are critical for infectivity in human keratinocytes. *PLoS One.* **4**(2), pe4463.
- Cardeal, L.B., Boccardo, E., Termini, L., Rabachini, T., Andreoli, M.A., di Loreto, C., Longatto Filho, A., Villa, L.L. and Maria-Engler, S.S. 2012. HPV16 oncoproteins induce MMPs/RECK-TIMP-2 imbalance in primary keratinocytes: possible implications in cervical carcinogenesis. *PLoS One.* **7**(3), pe33585.
- Cardone, G., Moyer, A.L., Cheng, N., Thompson, C.D., Dvoretzky, I., Lowy, D.R., Schiller, J.T., Steven, A.C., Buck, C.B. and Trus, B.L. 2014. Maturation of the human papillomavirus 16 capsid. *MBio.* **5**(4), pp.e01104-01114.

- Cartin, W. and Alonso, A. 2003. The human papillomavirus HPV2a E5 protein localizes to the Golgi apparatus and modulates signal transduction. *Virology*. **314**(2), pp.572-579.
- Castanon, A., Landy, R., Pesola, F., Windridge, P. and Sasieni, P. 2018. Prediction of cervical cancer incidence in England, UK, up to 2040, under four scenarios: a modelling study. *Lancet Public Health*. **3**(1), pp.e34-e43.
- Catarino, R., Petignat, P., Dongui, G. and Vassilakos, P. 2015. Cervical cancer screening in developing countries at a crossroad: Emerging technologies and policy choices. *World J Clin Oncol*. **6**(6), pp.281-290.
- Cerqueira, C., Samperio Ventayol, P., Vogeley, C. and Schelhaas, M. 2015. Kallikrein-8 Proteolytically Processes Human Papillomaviruses in the Extracellular Space To Facilitate Entry into Host Cells. *J Virol*. **89**(14), pp.7038-7052.
- Chang, J.L., Tsao, Y.P., Liu, D.W., Huang, S.J., Lee, W.H. and Chen, S.L. 2001. The expression of HPV-16 E5 protein in squamous neoplastic changes in the uterine cervix. *J Biomed Sci*. **8**(2), pp.206-213.
- Chang, S.W., Liu, W.C., Liao, K.Y., Tsao, Y.P., Hsu, P.H. and Chen, S.L. 2014. Phosphorylation of HPV-16 E2 at serine 243 enables binding to Brd4 and mitotic chromosomes. *PLoS One*. **9**(10), pe110882.
- Che, L.F., Shao, S.F. and Wang, L.X. 2016. Downregulation of CCR5 inhibits the proliferation and invasion of cervical cancer cells and is regulated by microRNA-107. *Exp Ther Med*. **11**(2), pp.503-509.
- Chen, H., Bai, J., Ye, J., Liu, Z., Chen, R., Mao, W., Li, A. and Zhou, J. 2007. JWA as a functional molecule to regulate cancer cells migration via MAPK cascades and F-actin cytoskeleton. *Cell Signal*. **19**(6), pp.1315-1327.
- Chen, R., Qiu, W., Liu, Z., Cao, X., Zhu, T., Li, A., Wei, Q. and Zhou, J. 2007. Identification of JWA as a novel functional gene responsive to environmental oxidative stress induced by benzo[a]pyrene and hydrogen peroxide. *Free Radic Biol Med*. **42**(11), pp.1704-1714.
- Chen, S.L. and Mounts, P. 1989. Detection by antibody probes of human papillomavirus type 6 E5 proteins in respiratory papillomata. *J Med Virol*. **29**(4), pp.273-283.
- Chen, X., Feng, J., Ge, Z., Chen, H., Ding, W., Zhu, W., Tang, X., Chen, Y., Tan, Y. and Ma, T. 2015. Effects of the JWA gene in the regulation of human breast cancer cells. *Mol Med Rep*. **11**(5), pp.3848-3853.
- Chen, Y., Huang, Y., Xia, X., Zhang, J., Zhou, Y., Tan, Y., He, S., Qiang, F., Li, A., Re, O.D., Li, G. and Zhou, J. 2014. JWA suppresses tumor angiogenesis via Sp1-activated matrix metalloproteinase-2 and its prognostic significance in human gastric cancer. *Carcinogenesis*. **35**(2), pp.442-451.
- Chien, W.M., Parker, J.N., Schmidt-Grimminger, D.C., Broker, T.R. and Chow, L.T. 2000. Casein kinase II phosphorylation of the human papillomavirus-18 E7 protein is critical for promoting S-phase entry. *Cell Growth Differ*. **11**(8), pp.425-435.

- Chiu, H.C., Hannemann, H., Heesom, K.J., Matthews, D.A. and Davidson, A.D. 2014. High-throughput quantitative proteomic analysis of dengue virus type 2 infected A549 cells. *PLoS One*. **9**(3), pe93305.
- Cifuentes-Diaz, C., Marullo, S. and Doly, S. 2016. Anatomical and ultrastructural study of PRAF2 expression in the mouse central nervous system. *Brain Struct Funct*. **221**(8), pp.4169-4185.
- Clayton, E., Doupé, D.P., Klein, A.M., Winton, D.J., Simons, B.D. and Jones, P.H. 2007. A single type of progenitor cell maintains normal epidermis. *Nature*. **446**(7132), pp.185-189.
- Clower, R.V., Fisk, J.C. and Melendy, T. 2006. Papillomavirus E1 protein binds to and stimulates human topoisomerase I. *J Virol*. **80**(3), pp.1584-1587.
- Collins, S.I., Constandinou-Williams, C., Wen, K., Young, L.S., Roberts, S., Murray, P.G. and Woodman, C.B. 2009. Disruption of the E2 gene is a common and early event in the natural history of cervical human papillomavirus infection: a longitudinal cohort study. *Cancer Res*. **69**(9), pp.3828-3832.
- Conrad, M., Bubb, V.J. and Schlegel, R. 1993. The human papillomavirus type 6 and 16 E5 proteins are membrane-associated proteins which associate with the 16-kilodalton pore-forming protein. *J Virol*. **67**(10), pp.6170-6178.
- Conrad, M., Goldstein, D., Andresson, T. and Schlegel, R. 1994. The E5 protein of HPV-6, but not HPV-16, associates efficiently with cellular growth factor receptors. *Virology*. **200**(2), pp.796-800.
- Cortese, M.S., Ashrafi, G.H. and Campo, M.S. 2010. All 4 di-leucine motifs in the first hydrophobic domain of the E5 oncoprotein of human papillomavirus type 16 are essential for surface MHC class I downregulation activity and E5 endomembrane localization. *Int J Cancer*. **126**(7), pp.1675-1682.
- Cox, J. and Mann, M. 2008. MaxQuant enables high peptide identification rates, individualized p.p.b.-range mass accuracies and proteome-wide protein quantification. *Nat Biotechnol*. **26**(12), pp.1367-1372.
- Crequer, A., Picard, C., Patin, E., D'Amico, A., Abhyankar, A., Munzer, M., Debré, M., Zhang, S.Y., de Saint-Basile, G., Fischer, A., Abel, L., Orth, G., Casanova, J.L. and Jouanguy, E. 2012a. Inherited MST1 deficiency underlies susceptibility to EV-HPV infections. *PLoS One*. **7**(8), pe44010.
- Crequer, A., Troeger, A., Patin, E., Ma, C.S., Picard, C., Pedergnana, V., Fieschi, C., Lim, A., Abhyankar, A., Gineau, L., Mueller-Fleckenstein, I., Schmidt, M., Taieb, A., Krueger, J., Abel, L., Tangye, S.G., Orth, G., Williams, D.A., Casanova, J.L. and Jouanguy, E. 2012b. Human RHOH deficiency causes T cell defects and susceptibility to EV-HPV infections. *J Clin Invest*. **122**(9), pp.3239-3247.
- Crosbie, E.J., Einstein, M.H., Franceschi, S. and Kitchener, H.C. 2013. Human papillomavirus and cervical cancer. *Lancet*. **382**(9895), pp.889-899.
- Cubie, H.A. 2013. Diseases associated with human papillomavirus infection. *Virology*. **445**(1-2), pp.21-34.

D'Souza, G. and Dempsey, A. 2011. The role of HPV in head and neck cancer and review of the HPV vaccine. *Prev Med.* **53 Suppl 1**, pp.S5-S11.

Davy, C.E., Jackson, D.J., Raj, K., Peh, W.L., Southern, S.A., Das, P., Sorathia, R., Laskey, P., Middleton, K., Nakahara, T., Wang, Q., Masterson, P.J., Lambert, P.F., Cuthill, S., Millar, J.B.A. and Doorbar, J. 2005. Human Papillomavirus Type 16 E1<sup>Δ</sup>-Induced G<sub>2</sub> Arrest Is Associated with Cytoplasmic Retention of Active Cdk1/Cyclin B1 Complexes. *Journal of Virology.* **79**(7), p3998.

Day, P.M. and Schelhaas, M. 2014. Concepts of papillomavirus entry into host cells. *Curr Opin Virol.* **4**, pp.24-31.

De Franceschi, N., Hamidi, H., Alanko, J., Sahgal, P. and Ivaska, J. 2015. Integrin traffic - the update. *J Cell Sci.* **128**(5), pp.839-852.

de Martel, C., Plummer, M., Vignat, J. and Franceschi, S. 2017. Worldwide burden of cancer attributable to HPV by site, country and HPV type. *Int J Cancer.* **141**(4), pp.664-670.

de Sanjose, S., Quint, W.G., Alemany, L., Geraets, D.T., Klaustermeier, J.E., Lloveras, B., Tous, S., Felix, A., Bravo, L.E., Shin, H.R., Vallejos, C.S., de Ruiz, P.A., Lima, M.A., Guimera, N., Clavero, O., Alejo, M., Llombart-Bosch, A., Cheng-Yang, C., Tatti, S.A., Kasamatsu, E., Iljazovic, E., Odida, M., Prado, R., Seoud, M., Grce, M., Usubutun, A., Jain, A., Suarez, G.A., Lombardi, L.E., Banjo, A., Menéndez, C., Domingo, E.J., Velasco, J., Nessa, A., Chichareon, S.C., Qiao, Y.L., Lerma, E., Garland, S.M., Sasagawa, T., Ferrera, A., Hammouda, D., Mariani, L., Pelayo, A., Steiner, I., Oliva, E., Meijer, C.J., Al-Jassar, W.F., Cruz, E., Wright, T.C., Puras, A., Llave, C.L., Tzardi, M., Agorastos, T., Garcia-Barriola, V., Clavel, C., Ordi, J., Andújar, M., Castellsagué, X., Sánchez, G.I., Nowakowski, A.M., Bornstein, J., Muñoz, N., Bosch, F.X. and Group, R.I.S.a.H.T.T.S. 2010. Human papillomavirus genotype attribution in invasive cervical cancer: a retrospective cross-sectional worldwide study. *Lancet Oncol.* **11**(11), pp.1048-1056.

de Villiers, E.M. 2013. Cross-roads in the classification of papillomaviruses. *Virology.* **445**(1-2), pp.2-10.

de Villiers, E.M., Fauquet, C., Broker, T.R., Bernard, H.U. and zur Hausen, H. 2004. Classification of papillomaviruses. *Virology.* **324**(1), pp.17-27.

Dedo, H.H. and Yu, K.C. 2001. CO(2) laser treatment in 244 patients with respiratory papillomas. *Laryngoscope.* **111**(9), pp.1639-1644.

Delury, C.P., Marsh, E.K., James, C.D., Boon, S.S., Banks, L., Knight, G.L. and Roberts, S. 2013. The role of protein kinase A regulation of the E6 PDZ-binding domain during the differentiation-dependent life cycle of human papillomavirus type 18. *J Virol.* **87**(17), pp.9463-9472.

Demetriadou, A., Morales-Sanfrutos, J., Nearchou, M., Baba, O., Kyriacou, K., Tate, E.W., Drousiotou, A. and Petrou, P.P. 2017. Mouse Stbd1 is. *J Cell Sci.* **130**(5), pp.903-915.

Deng, W., Lin, B.Y., Jin, G., Wheeler, C.G., Ma, T., Harper, J.W., Broker, T.R. and Chow, L.T. 2004. Cyclin/CDK regulates the nucleocytoplasmic localization of the human papillomavirus E1 DNA helicase. *J Virol.* **78**(24), pp.13954-13965.

Derkey, C.S. 2001. Recurrent respiratory papillomatosis. *Laryngoscope.* **111**(1), pp.57-69.

- Dhiman, G., Srivastava, N., Goyal, M., Rakha, E., Lothion-Roy, J., Mongan, N.P., Miftakhova, R.R., Khaiboullina, S.F., Rizvanov, A.A. and Baranwal, M. 2019. Metadherin: A Therapeutic Target in Multiple Cancers. *Front Oncol.* **9**, p349.
- Dho, S.H., Deverman, B.E., Lapid, C., Manson, S.R., Gan, L., Riehm, J.J., Aurora, R., Kwon, K.S. and Weintraub, S.J. 2013. Control of cellular Bcl-xL levels by deamidation-regulated degradation. *PLoS Biol.* **11**(6), pe1001588.
- Dickison, V.M., Richmond, A.M., Abu Irqeba, A., Martak, J.G., Hoge, S.C., Brooks, M.J., Othman, M.I., Khanna, R., Mears, A.J., Chowdhury, A.Y., Swaroop, A. and Ogilvie, J.M. 2012. A role for prenylated rab acceptor 1 in vertebrate photoreceptor development. *BMC Neurosci.* **13**, p152.
- Disbrow, G.L., Hanover, J.A. and Schlegel, R. 2005. Endoplasmic reticulum-localized human papillomavirus type 16 E5 protein alters endosomal pH but not trans-Golgi pH. *J Virol.* **79**(9), pp.5839-5846.
- Disbrow, G.L., Sunitha, I., Baker, C.C., Hanover, J. and Schlegel, R. 2003. Codon optimization of the HPV-16 E5 gene enhances protein expression. *Virology.* **311**(1), pp.105-114.
- Doghman-Bouguerra, M., Granatiero, V., Sbiera, S., Sbiera, I., Lacas-Gervais, S., Brau, F., Fassnacht, M., Rizzuto, R. and Lalli, E. 2016. FATE1 antagonizes calcium- and drug-induced apoptosis by uncoupling ER and mitochondria. *EMBO Rep.* **17**(9), pp.1264-1280.
- Doly, S., Shirvani, H., Gäta, G., Meye, F.J., Emerit, M.B., Enslin, H., Achour, L., Pardo-Lopez, L., Yang, S.K., Armand, V., Gardette, R., Giros, B., Gassmann, M., Bettler, B., Mameli, M., Darmon, M. and Marullo, S. 2016. GABAB receptor cell-surface export is controlled by an endoplasmic reticulum gatekeeper. *Mol Psychiatry.* **21**(4), pp.480-490.
- Dong, R., Liu, X., Zhang, Q., Jiang, Z., Li, Y., Wei, Y., Yang, Q., Liu, J., Wei, J.J., Shao, C., Liu, Z. and Kong, B. 2014. miR-145 inhibits tumor growth and metastasis by targeting metadherin in high-grade serous ovarian carcinoma. *Oncotarget.* **5**(21), pp.10816-10829.
- Dong, R., Saheki, Y., Swarup, S., Lucast, L., Harper, J.W. and De Camilli, P. 2016. Endosome-ER Contacts Control Actin Nucleation and Retromer Function through VAP-Dependent Regulation of PI4P. *Cell.* **166**(2), pp.408-423.
- Dong, X., Armstrong, S.D., Xia, D., Makepeace, B.L., Darby, A.C. and Kadowaki, T. 2017. Draft genome of the honey bee ectoparasitic mite, *Tropilaelaps mercedesae*, is shaped by the parasitic life history. *Gigascience.* **6**(3), pp.1-17.
- Doorbar, J. 2005. The papillomavirus life cycle. *J Clin Virol.* **32 Suppl 1**, pp.S7-15.
- Doorbar, J. 2006. Molecular biology of human papillomavirus infection and cervical cancer. *Clin Sci (Lond).* **110**(5), pp.525-541.
- Doorbar, J. 2013. The E4 protein; structure, function and patterns of expression. *Virology.* **445**(1-2), pp.80-98.
- Doorbar, J., Egawa, N., Griffin, H., Kranjec, C. and Murakami, I. 2015. Human papillomavirus molecular biology and disease association. *Rev Med Virol.* **25 Suppl 1**, pp.2-23.
- Doorbar, J., Quint, W., Banks, L., Bravo, I.G., Stoler, M., Broker, T.R. and Stanley, M.A. 2012. The biology and life-cycle of human papillomaviruses. *Vaccine.* **30 Suppl 5**, pp.F55-70.

- Drews, C.M., Case, S. and Vande Pol, S.B. 2019. E6 proteins from high-risk HPV, low-risk HPV, and animal papillomaviruses activate the Wnt/ $\beta$ -catenin pathway through E6AP-dependent degradation of NHERF1. *PLoS Pathog.* **15**(4), pe1007575.
- Dumesic, P.A., Scholl, F.A., Barragan, D.I. and Khavari, P.A. 2009. Erk1/2 MAP kinases are required for epidermal G2/M progression. *J Cell Biol.* **185**(3), pp.409-422.
- Dürst, M., Gissmann, L., Ikenberg, H. and zur Hausen, H. 1983. A papillomavirus DNA from a cervical carcinoma and its prevalence in cancer biopsy samples from different geographic regions. *Proc Natl Acad Sci U S A.* **80**(12), pp.3812-3815.
- Edwards, L., Ferenczy, A., Eron, L., Baker, D., Owens, M.L., Fox, T.L., Hougham, A.J. and Schmitt, K.A. 1998. Self-administered topical 5% imiquimod cream for external anogenital warts. HPV Study Group. Human PapillomaVirus. *Arch Dermatol.* **134**(1), pp.25-30.
- Egawa, N., Egawa, K., Griffin, H. and Doorbar, J. 2015. Human Papillomaviruses; Epithelial Tropisms, and the Development of Neoplasia. *Viruses.* **7**(7), pp.3863-3890.
- Egawa, N., Wang, Q., Griffin, H.M., Murakami, I., Jackson, D., Mahmood, R. and Doorbar, J. 2017. HPV16 and 18 genome amplification show different E4-dependence, with 16E4 enhancing E1 nuclear accumulation and replicative efficiency via its cell cycle arrest and kinase activation functions. *PLoS Pathog.* **13**(3), pe1006282.
- Elmore, S. 2007. Apoptosis: a review of programmed cell death. *Toxicol Pathol.* **35**(4), pp.495-516.
- Emdad, L., Sarkar, D., Su, Z.Z., Randolph, A., Boukerche, H., Valerie, K. and Fisher, P.B. 2006. Activation of the nuclear factor kappaB pathway by astrocyte elevated gene-1: implications for tumor progression and metastasis. *Cancer Res.* **66**(3), pp.1509-1516.
- Enemark, E.J., Stenlund, A. and Joshua-Tor, L. 2002. Crystal structures of two intermediates in the assembly of the papillomavirus replication initiation complex. *EMBO J.* **21**(6), pp.1487-1496.
- Enouf, V., Chwetzoff, S., Trugnan, G. and Cohen, J. 2003. Interactions of rotavirus VP4 spike protein with the endosomal protein Rab5 and the prenylated Rab acceptor PRA1. *J Virol.* **77**(12), pp.7041-7047.
- Ernst, W.L., Shome, K., Wu, C.C., Gong, X., Frizzell, R.A. and Aridor, M. 2016. VAMP-associated Proteins (VAP) as Receptors That Couple Cystic Fibrosis Transmembrane Conductance Regulator (CFTR) Proteostasis with Lipid Homeostasis. *J Biol Chem.* **291**(10), pp.5206-5220.
- Evans, D.T., Tillman, K.C. and Desrosiers, R.C. 2002. Envelope glycoprotein cytoplasmic domains from diverse lentiviruses interact with the prenylated Rab acceptor. *J Virol.* **76**(1), pp.327-337.
- Faber, M.T., Sand, F.L., Albieri, V., Norrild, B., Kjaer, S.K. and Verdoodt, F. 2017. Prevalence and type distribution of human papillomavirus in squamous cell carcinoma and intraepithelial neoplasia of the vulva. *Int J Cancer.* **141**(6), pp.1161-1169.
- Fan, X., Liu, Y., Heilman, S.A. and Chen, J.J. 2013. Human papillomavirus E7 induces rereplication in response to DNA damage. *J Virol.* **87**(2), pp.1200-1210.

- Fehrmann, F., Klumpp, D.J. and Laimins, L.A. 2003. Human papillomavirus type 31 E5 protein supports cell cycle progression and activates late viral functions upon epithelial differentiation. *J Virol.* **77**(5), pp.2819-2831.
- Ferlay, J., Ervik, M., Lam, F., Colombet, M., Mery, L., Piñeros, M., Znaor, A., Soerjomataram, I. and Bray, F. 2018. *Global Cancer Observatory: Cancer Today*. Lyon, France: International Agency for Research on Cancer. [Online]. [Accessed 02/09/2019]. Available from: <https://gco.iarc.fr/today>
- Figuroa, C., Taylor, J. and Vojtek, A.B. 2001. Prenylated Rab acceptor protein is a receptor for prenylated small GTPases. *J Biol Chem.* **276**(30), pp.28219-28225.
- Filippova, M., Parkhurst, L. and Duerksen-Hughes, P.J. 2004. The human papillomavirus 16 E6 protein binds to Fas-associated death domain and protects cells from Fas-triggered apoptosis. *J Biol Chem.* **279**(24), pp.25729-25744.
- Flores, E.R. and Lambert, P.F. 1997. Evidence for a switch in the mode of human papillomavirus type 16 DNA replication during the viral life cycle. *J Virol.* **71**(10), pp.7167-7179.
- Flores-Díaz, E., Serey, K.A., Ferreira, S., Sirak, B., Sobrinho, J.S., Baggio, M.L., Galan, L., Silva, R.C., Lazcano-Ponce, E., Giuliano, A.R., Villa, L.L., Sichero, L. and Group, T.H.S. 2017. HPV-11 variability, persistence and progression to genital warts in men: the HIM study. *J Gen Virol.* **98**(9), pp.2339-2342.
- Florin, L., Becker, K.A., Sapp, C., Lambert, C., Sirma, H., Müller, M., Streeck, R.E. and Sapp, M. 2004. Nuclear translocation of papillomavirus minor capsid protein L2 requires Hsc70. *J Virol.* **78**(11), pp.5546-5553.
- Florin, L., Sapp, C., Streeck, R.E. and Sapp, M. 2002. Assembly and Translocation of Papillomavirus Capsid Proteins. *Journal of Virology.* **76**(19), p10009.
- Fo, C.S., Coleman, C.S., Wallick, C.J., Vine, A.L. and Bachmann, A.S. 2006. Genomic organization, expression profile, and characterization of the new protein PRA1 domain family, member 2 (PRAF2). *Gene.* **371**(1), pp.154-165.
- Fox, S.H. and Elston, D.M. 2016. Epidermodysplasia verruciformis and the risk for malignancy. *Cutis.* **98**(4), pp.E10-E12.
- Fradet-Turcotte, A., Moody, C., Laimins, L.A. and Archambault, J. 2010. Nuclear export of human papillomavirus type 31 E1 is regulated by Cdk2 phosphorylation and required for viral genome maintenance. *J Virol.* **84**(22), pp.11747-11760.
- French, D., Belleudi, F., Mauro, M.V., Mazzetta, F., Raffa, S., Fabiano, V., Frega, A. and Torrisi, M.R. 2013. Expression of HPV16 E5 down-modulates the TGFbeta signaling pathway. *Mol Cancer.* **12**, p38.
- Fuchs, E. 2007. Scratching the surface of skin development. *Nature.* **445**(7130), pp.834-842.
- Fuchs, E. 2008. Skin stem cells: rising to the surface. *J Cell Biol.* **180**(2), pp.273-284.
- Galea, G., Bexiga, M.G., Panarella, A., O'Neill, E.D. and Simpson, J.C. 2015. A high-content screening microscopy approach to dissect the role of Rab proteins in Golgi-to-ER retrograde trafficking. *J Cell Sci.* **128**(13), pp.2339-2349.

Geerts, D., Wallick, C.J., Koomoa, D.L., Koster, J., Versteeg, R., Go, R.C. and Bachmann, A.S. 2007. Expression of prenylated Rab acceptor 1 domain family, member 2 (PRAF2) in neuroblastoma: correlation with clinical features, cellular localization, and cerulenin-mediated apoptosis regulation. *Clin Cancer Res.* **13**(21), pp.6312-6319.

Genther, S.M., Sterling, S., Duensing, S., Munger, K., Sattler, C. and Lambert, P.F. 2003a. Quantitative role of the human papillomavirus type 16 E5 gene during the productive stage of the viral life cycle. *Journal of Virology.* **77**(5), pp.2832-2842.

Genther, S.M., Sterling, S., Duensing, S., Münger, K., Sattler, C. and Lambert, P.F. 2003b. Quantitative role of the human papillomavirus type 16 E5 gene during the productive stage of the viral life cycle. *J Virol.* **77**(5), pp.2832-2842.

Genther Williams, S.M., Disbrow, G.L., Schlegel, R., Lee, D., Threadgill, D.W. and Lambert, P.F. 2005. Requirement of epidermal growth factor receptor for hyperplasia induced by E5, a high-risk human papillomavirus oncogene. *Cancer Res.* **65**(15), pp.6534-6542.

Georgopoulos, N.T., Proffitt, J.L. and Blair, G.E. 2000. Transcriptional regulation of the major histocompatibility complex (MHC) class I heavy chain, TAP1 and LMP2 genes by the human papillomavirus (HPV) type 6b, 16 and 18 E7 oncoproteins. *Oncogene.* **19**(42), pp.4930-4935.

Gheit, T. 2019. Mucosal and Cutaneous Human Papillomavirus Infections and Cancer Biology. *Front Oncol.* **9**, p355.

Gibson, J. 2018. Oral cancer - CPD and the GDC. *Br Dent J.* **225**(9), pp.884-888.

Gillison. 2008. Behavioral risk factors for head and neck cancers identified. *J Am Dent Assoc.* **139**(5), pp.540-541.

Gillison, M.L., Alemany, L., Snijders, P.J., Chaturvedi, A., Steinberg, B.M., Schwartz, S. and Castellsagué, X. 2012. Human papillomavirus and diseases of the upper airway: head and neck cancer and respiratory papillomatosis. *Vaccine.* **30 Suppl 5**, pp.F34-54.

Giroglou, T., Florin, L., Schäfer, F., Streeck, R.E. and Sapp, M. 2001. Human papillomavirus infection requires cell surface heparan sulfate. *J Virol.* **75**(3), pp.1565-1570.

Gkogkas, C., Middleton, S., Kremer, A.M., Wardrope, C., Hannah, M., Gillingwater, T.H. and Skehel, P. 2008. VAPB interacts with and modulates the activity of ATF6. *Hum Mol Genet.* **17**(11), pp.1517-1526.

Gorini, G., Ponomareva, O., Shores, K.S., Person, M.D., Harris, R.A. and Mayfield, R.D. 2010. Dynamin-1 co-associates with native mouse brain BKCa channels: proteomics analysis of synaptic protein complexes. *FEBS Lett.* **584**(5), pp.845-851.

Gottschling, M., Göker, M., Stamatakis, A., Bininda-Emonds, O.R., Nindl, I. and Bravo, I.G. 2011. Quantifying the phylodynamic forces driving papillomavirus evolution. *Mol Biol Evol.* **28**(7), pp.2101-2113.

Gottschling, M., Stamatakis, A., Nindl, I., Stockfleth, E., Alonso, A. and Bravo, I.G. 2007. Multiple evolutionary mechanisms drive papillomavirus diversification. *Mol Biol Evol.* **24**(5), pp.1242-1258.

- Gougeon, P.Y. and Ngsee, J.K. 2005. Purification and functional properties of prenylated Rab acceptor 2. *Methods Enzymol.* **403**, pp.799-807.
- Gougeon, P.Y., Prosser, D.C., Da-Silva, L.F. and Ngsee, J.K. 2002. Disruption of Golgi morphology and trafficking in cells expressing mutant prenylated rab acceptor-1. *J Biol Chem.* **277**(39), pp.36408-36414.
- Griffin, H., Wu, Z., Marnane, R., Dewar, V., Molijn, A., Quint, W., Van Hoof, C., Struyf, F., Colau, B., Jenkins, D. and Doorbar, J. 2012. E4 Antibodies Facilitate Detection and Type-Assignment of Active HPV Infection in Cervical Disease. *PLOS ONE.* **7**(12), pe49974.
- Grose, R., Fantl, V., Werner, S., Chioni, A.M., Jarosz, M., Rudling, R., Cross, B., Hart, I.R. and Dickson, C. 2007. The role of fibroblast growth factor receptor 2b in skin homeostasis and cancer development. *EMBO J.* **26**(5), pp.1268-1278.
- Gruener, M., Bravo, I.G., Momburg, F., Alonso, A. and Tomakidi, P. 2007. The E5 protein of the human papillomavirus type 16 down-regulates HLA-I surface expression in calnexin-expressing but not in calnexin-deficient cells. *Virology.* **4**, p116.
- Gräbel, L., Fast, L.A., Scheffer, K.D., Boukhallouk, F., Spoden, G.A., Tenzer, S., Boller, K., Bago, R., Rajesh, S., Overduin, M., Berditchevski, F. and Florin, L. 2016. The CD63-Syntenin-1 Complex Controls Post-Endocytic Trafficking of Oncogenic Human Papillomaviruses. *Sci Rep.* **6**, p32337.
- Guasch, G., Schober, M., Pasolli, H.A., Conn, E.B., Polak, L. and Fuchs, E. 2007. Loss of TGFbeta signaling destabilizes homeostasis and promotes squamous cell carcinomas in stratified epithelia. *Cancer Cell.* **12**(4), pp.313-327.
- Guo, X. and Wang, X.F. 2009. Signaling cross-talk between TGF-beta/BMP and other pathways. *Cell Res.* **19**(1), pp.71-88.
- Gupta, S., Kumar, P. and Das, B.C. 2018. HPV: Molecular pathways and targets. *Curr Probl Cancer.* **42**(2), pp.161-174.
- Halavaty, K.K., Regan, J., Mehta, K. and Laimins, L. 2014. Human papillomavirus E5 oncoproteins bind the A4 endoplasmic reticulum protein to regulate proliferative ability upon differentiation. *Virology.* **452**, pp.223-230.
- Hamidi, H. and Ivaska, J. 2018. Every step of the way: integrins in cancer progression and metastasis. *Nat Rev Cancer.* **18**(9), pp.533-548.
- Han, J., Alvarez-Breckenridge, C.A., Wang, Q.E. and Yu, J. 2015. TGF- $\beta$  signaling and its targeting for glioma treatment. *Am J Cancer Res.* **5**(3), pp.945-955.
- Han, Y., Loo, Y.M., Militello, K.T. and Melendy, T. 1999. Interactions of the papovavirus DNA replication initiator proteins, bovine papillomavirus type 1 E1 and simian virus 40 large T antigen, with human replication protein A. *J Virol.* **73**(6), pp.4899-4907.
- Haque, F., Mazzeo, D., Patel, J.T., Smallwood, D.T., Ellis, J.A., Shanahan, C.M. and Shackleton, S. 2010. Mammalian SUN protein interaction networks at the inner nuclear membrane and their role in laminopathy disease processes. *J Biol Chem.* **285**(5), pp.3487-3498.
- Harper, D.M. and DeMars, L.R. 2017. HPV vaccines - A review of the first decade. *Gynecol Oncol.* **146**(1), pp.196-204.

- Hasan, U.A., Bates, E., Takeshita, F., Biliato, A., Accardi, R., Bouvard, V., Mansour, M., Vincent, I., Gissmann, L., Iftner, T., Sideri, M., Stubenrauch, F. and Tommasino, M. 2007. TLR9 expression and function is abolished by the cervical cancer-associated human papillomavirus type 16. *J Immunol.* **178**(5), pp.3186-3197.
- Hassett, K.J., Meinerz, N.M., Semmelmann, F., Cousins, M.C., Garcea, R.L. and Randolph, T.W. 2015. Development of a highly thermostable, adjuvanted human papillomavirus vaccine. *Eur J Pharm Biopharm.* **94**, pp.220-228.
- Hatcher, R.A. 1982. Consider condoms for the woman at high risk of cervical cancer. *Contracept Technol Update.* **3**(4), pp.52-53.
- Hawley-Nelson, P., Androphy, E.J., Lowy, D.R. and Schiller, J.T. 1988. The specific DNA recognition sequence of the bovine papillomavirus E2 protein is an E2-dependent enhancer. *EMBO J.* **7**(2), pp.525-531.
- He, W., Staples, D., Smith, C. and Fisher, C. 2003. Direct activation of cyclin-dependent kinase 2 by human papillomavirus E7. *J Virol.* **77**(19), pp.10566-10574.
- He, W., Tang, J., Li, W., Li, Y., Mei, Y., He, L., Zhong, K. and Xu, R. 2019. Mutual regulation of JAG2 and PRAF2 promotes migration and invasion of colorectal cancer cells uncoupled from epithelial-mesenchymal transition. *Cancer Cell Int.* **19**, p160.
- Hebner, C.M. and Laimins, L.A. 2006. Human papillomaviruses: basic mechanisms of pathogenesis and oncogenicity. *Rev Med Virol.* **16**(2), pp.83-97.
- Heck, J.E., Berthiller, J., Vaccarella, S., Winn, D.M., Smith, E.M., Shan'gina, O., Schwartz, S.M., Purdue, M.P., Pilarska, A., Eluf-Neto, J., Menezes, A., McClean, M.D., Matos, E., Koifman, S., Kelsey, K.T., Herrero, R., Hayes, R.B., Franceschi, S., Wünsch-Filho, V., Fernández, L., Daudt, A.W., Curado, M.P., Chen, C., Castellsagué, X., Ferro, G., Brennan, P., Boffetta, P. and Hashibe, M. 2010. Sexual behaviours and the risk of head and neck cancers: a pooled analysis in the International Head and Neck Cancer Epidemiology (INHANCE) consortium. *Int J Epidemiol.* **39**(1), pp.166-181.
- Hehlgans, S., Haase, M. and Cordes, N. 2007. Signalling via integrins: implications for cell survival and anticancer strategies. *Biochim Biophys Acta.* **1775**(1), pp.163-180.
- Helt, A.M. and Galloway, D.A. 2001. Destabilization of the retinoblastoma tumor suppressor by human papillomavirus type 16 E7 is not sufficient to overcome cell cycle arrest in human keratinocytes. *J Virol.* **75**(15), pp.6737-6747.
- Herfs, M., Parra-Herran, C., Howitt, B.E., Laury, A.R., Nucci, M.R., Feldman, S., Jimenez, C.A., McKeon, F.D., Xian, W. and Crum, C.P. 2013. Cervical squamocolumnar junction-specific markers define distinct, clinically relevant subsets of low-grade squamous intraepithelial lesions. *Am J Surg Pathol.* **37**(9), pp.1311-1318.
- Herfs, M., Yamamoto, Y., Laury, A., Wang, X., Nucci, M.R., McLaughlin-Drubin, M.E., Münger, K., Feldman, S., McKeon, F.D., Xian, W. and Crum, C.P. 2012. A discrete population of squamocolumnar junction cells implicated in the pathogenesis of cervical cancer. *Proc Natl Acad Sci U S A.* **109**(26), pp.10516-10521.

Holmgren, S.C., Patterson, N.A., Ozburn, M.A. and Lambert, P.F. 2005. The minor capsid protein L2 contributes to two steps in the human papillomavirus type 31 life cycle. *J Virol.* **79**(7), pp.3938-3948.

Hong, S. and Laimins, L.A. 2013. The JAK-STAT transcriptional regulator, STAT-5, activates the ATM DNA damage pathway to induce HPV 31 genome amplification upon epithelial differentiation. *PLoS Pathog.* **9**(4), pe1003295.

Horev, L., Unger, S., Molho-Pessach, V., Meir, T., Maly, A., Stepensky, P., Zamir, M., Keller, B., Babay, S., Warnatz, K., Ramot, Y. and Zlotogorski, A. 2015. Generalized verrucosis and HPV-3 susceptibility associated with CD4 T-cell lymphopenia caused by inherited human interleukin-7 deficiency. *J Am Acad Dermatol.* **72**(6), pp.1082-1084.

Horton, E.R., Byron, A., Askari, J.A., Ng, D.H.J., Millon-Frémillon, A., Robertson, J., Koper, E.J., Paul, N.R., Warwood, S., Knight, D., Humphries, J.D. and Humphries, M.J. 2015. Definition of a consensus integrin adhesome and its dynamics during adhesion complex assembly and disassembly. *Nat Cell Biol.* **17**(12), pp.1577-1587.

Houlihan, C.F., Baisley, K., Bravo, I.G., Pavón, M.A., Changalucha, J., Kapiga, S., De Sanjosé, S., Ross, D.A., Hayes, R.J. and Watson-Jones, D. 2019. Human papillomavirus DNA detected in fingertip, oral and bathroom samples from unvaccinated adolescent girls in Tanzania. *Sex Transm Infect.* **95**(5), pp.374-379.

Huang, S., Shen, Q., Mao, W.G., Li, A.P., Ye, J., Liu, Q.Z., Zou, C.P. and Zhou, J.W. 2006a. JWA, a novel signaling molecule, involved in all-trans retinoic acid induced differentiation of HL-60 cells. *J Biomed Sci.* **13**(3), pp.357-371.

Huang, S., Shen, Q., Mao, W.G., Li, A.P., Ye, J., Liu, Q.Z., Zou, C.P. and Zhou, J.W. 2006b. JWA, a novel signaling molecule, involved in the induction of differentiation of human myeloid leukemia cells. *Biochem Biophys Res Commun.* **341**(2), pp.440-450.

Hubbert, N.L., Schiller, J.T., Lowy, D.R. and Androphy, E.J. 1988. Bovine papilloma virus-transformed cells contain multiple E2 proteins. *Proc Natl Acad Sci U S A.* **85**(16), pp.5864-5868.

Hughes, F.J. and Romanos, M.A. 1993. E1 protein of human papillomavirus is a DNA helicase/ATPase. *Nucleic Acids Res.* **21**(25), pp.5817-5823.

Huh, K., Zhou, X., Hayakawa, H., Cho, J.Y., Libermann, T.A., Jin, J., Harper, J.W. and Munger, K. 2007. Human papillomavirus type 16 E7 oncoprotein associates with the cullin 2 ubiquitin ligase complex, which contributes to degradation of the retinoblastoma tumor suppressor. *J Virol.* **81**(18), pp.9737-9747.

Hunter, M., Angelicheva, D., Tournev, I., Ingley, E., Chan, D.C., Watts, G.F., Kremensky, I. and Kalaydjieva, L. 2005. NDRG1 interacts with APO A-I and A-II and is a functional candidate for the HDL-C QTL on 8q24. *Biochem Biophys Res Commun.* **332**(4), pp.982-992.

Hutt, D.M., Da-Silva, L.F., Chang, L.H., Prosser, D.C. and Ngsee, J.K. 2000. PRA1 inhibits the extraction of membrane-bound rab GTPase by GDI1. *J Biol Chem.* **275**(24), pp.18511-18519.

Hwang, E.S., Nottoli, T. and Dimaio, D. 1995. The HPV16 E5 protein: expression, detection, and stable complex formation with transmembrane proteins in COS cells. *Virology.* **211**(1), pp.227-233.

- Ikemoto, M.J., Inoue, K., Akiduki, S., Osugi, T., Imamura, T., Ishida, N. and Ohtomi, M. 2002. Identification of adducin/GTRAP3-18 as a chronic morphine-augmented gene in amygdala. *Neuroreport*. **13**(16), pp.2079-2084.
- Ingle, E., Williams, J.H., Walker, C.E., Tsai, S., Colley, S., Sayer, M.S., Tilbrook, P.A., Sarna, M., Beaumont, J.G. and Klinken, S.P. 1999. A novel ADP-ribosylation like factor (ARL-6), interacts with the protein-conducting channel SEC61beta subunit. *FEBS Lett*. **459**(1), pp.69-74.
- Iwasawa, R., Mahul-Mellier, A.L., Datler, C., Pazarentzos, E. and Grimm, S. 2011. Fis1 and Bap31 bridge the mitochondria-ER interface to establish a platform for apoptosis induction. *EMBO J*. **30**(3), pp.556-568.
- Jacobs, C. and Pirson, I. 2003. Pitfalls in the use of transfected overexpression systems to study membrane proteins function: the case of TSH receptor and PRA1. *Mol Cell Endocrinol*. **209**(1-2), pp.71-75.
- Jensen, K.B. and Watt, F.M. 2006. Single-cell expression profiling of human epidermal stem and transit-amplifying cells: Lrig1 is a regulator of stem cell quiescence. *Proc Natl Acad Sci U S A*. **103**(32), pp.11958-11963.
- Jung, C.J., Lee, M.H., Min, M.K. and Hwang, I. 2011. Localization and trafficking of an isoform of the AtPRA1 family to the Golgi apparatus depend on both N- and C-terminal sequence motifs. *Traffic*. **12**(2), pp.185-200.
- Kachhap, S.K., Faith, D., Qian, D.Z., Shabbeer, S., Galloway, N.L., Pili, R., Denmeade, S.R., DeMarzo, A.M. and Carducci, M.A. 2007. The N-Myc down regulated Gene1 (NDRG1) Is a Rab4a effector involved in vesicular recycling of E-cadherin. *PLoS One*. **2**(9), pe844.
- Kalińska-Bienias, A., Kowalewski, C. and Majewski, S. 2016. The EVER genes - the genetic etiology of carcinogenesis in epidermodysplasia verruciformis and a possible role in non-epidermodysplasia verruciformis patients. *Postepy Dermatol Alergol*. **33**(2), pp.75-80.
- Kang, Y.J., Smith, M. and Canfell, K. 2019. Correction: Anal cancer in high-income countries: Increasing burden of disease. *PLoS One*. **14**(5), pe0216884.
- Karanam, B., Jagu, S., Huh, W.K. and Roden, R.B. 2009. Developing vaccines against minor capsid antigen L2 to prevent papillomavirus infection. *Immunol Cell Biol*. **87**(4), pp.287-299.
- Khan, J., Davy, C.E., McIntosh, P.B., Jackson, D.J., Hinz, S., Wang, Q. and Doorbar, J. 2011. Role of Calpain in the Formation of Human Papillomavirus Type 16 E1<sup>E4</sup> Amyloid Fibers and Reorganization of the Keratin Network. *Journal of Virology*. **85**(19), p9984.
- Khan, M.J. and Smith-McCune, K.K. 2014. Treatment of cervical precancers: back to basics. *Obstet Gynecol*. **123**(6), pp.1339-1343.
- Kidd, L.C., Chaing, S., Chipollini, J., Giuliano, A.R., Spiess, P.E. and Sharma, P. 2017. Relationship between human papillomavirus and penile cancer-implications for prevention and treatment. *Transl Androl Urol*. **6**(5), pp.791-802.
- Kim, D.I., Birendra, K.C., Zhu, W., Motamedchaboki, K., Doye, V. and Roux, K.J. 2014. Probing nuclear pore complex architecture with proximity-dependent biotinylation. *Proc Natl Acad Sci U S A*. **111**(24), pp.E2453-2461.

- Kim, D.I., Jensen, S.C., Noble, K.A., Kc, B., Roux, K.H., Motamedchaboki, K. and Roux, K.J. 2016. An improved smaller biotin ligase for BioID proximity labeling. *Mol Biol Cell*. **27**(8), pp.1188-1196.
- Kim, J.T., Cho, H.J., Cho, M.Y., Lim, J., Park, E.S., Lim, J.S. and Lee, H.G. 2019. Prenylated Rab acceptor RABAC1 inhibits anti-apoptotic protein BCL2A1 and induces apoptosis. *Biochem Biophys Res Commun*. **513**(4), pp.940-946.
- Kim, J.T., Cho, M.Y., Choi, S.C., Kim, J.W., Chae, S.K., Yoon, D.Y. and Lim, J.S. 2006. Prenylated Rab acceptor 1 (PRA1) inhibits TCF/beta-catenin signaling by binding to beta-catenin. *Biochem Biophys Res Commun*. **349**(1), pp.200-208.
- Kim, J.T., Kim, J.W., Kang, Y.H., Kim, K.D., Lee, S.J., Choi, S.C., Kim, K.S., Chae, S.K., Lim, J.S. and Lee, H.G. 2012. NDRG2 and PRA1 interact and synergistically inhibit T-cell factor/ $\beta$ -catenin signaling. *FEBS Lett*. **586**(22), pp.3962-3968.
- Kiyono, T., Hiraiwa, A., Fujita, M., Hayashi, Y., Akiyama, T. and Ishibashi, M. 1997. Binding of high-risk human papillomavirus E6 oncoproteins to the human homologue of the Drosophila discs large tumor suppressor protein. *Proc Natl Acad Sci U S A*. **94**(21), pp.11612-11616.
- Kmietowicz, Z. 2018. Boys in England to get HPV vaccine from next year. *BMJ*. **362**, pk3237.
- Knapp, A.A., McManus, P.M., Bockstall, K. and Moroianu, J. 2009. Identification of the nuclear localization and export signals of high risk HPV16 E7 oncoprotein. *Virology*. **383**(1), pp.60-68.
- Knight, G.L., Pugh, A.G., Yates, E., Bell, I., Wilson, R., Moody, C.A., Laimins, L.A. and Roberts, S. 2011. A cyclin-binding motif in human papillomavirus type 18 (HPV18) E1<sup>E4</sup> is necessary for association with CDK-cyclin complexes and G2/M cell cycle arrest of keratinocytes, but is not required for differentiation-dependent viral genome amplification or L1 capsid protein expression. *Virology*. **412**(1), pp.196-210.
- Kobayashi, K., Hisamatsu, K., Suzui, N., Hara, A., Tomita, H. and Miyazaki, T. 2018. A Review of HPV-Related Head and Neck Cancer. *J Clin Med*. **7**(9).
- Kolev, V., Mandinova, A., Guinea-Viniegra, J., Hu, B., Lefort, K., Lambertini, C., Neel, V., Dummer, R., Wagner, E.F. and Dotto, G.P. 2008. EGFR signalling as a negative regulator of Notch1 gene transcription and function in proliferating keratinocytes and cancer. *Nat Cell Biol*. **10**(8), pp.902-911.
- Koomoa, D.L., Go, R.C., Wester, K. and Bachmann, A.S. 2008. Expression profile of PRA2 in the human brain and enrichment in synaptic vesicles. *Neurosci Lett*. **436**(2), pp.171-176.
- Koonin, E.V., Krupovic, M. and Yutin, N. 2015. Evolution of double-stranded DNA viruses of eukaryotes: from bacteriophages to transposons to giant viruses. *Ann N Y Acad Sci*. **1341**, pp.10-24.
- Koster, M.I., Dai, D., Marinari, B., Sano, Y., Costanzo, A., Karin, M. and Roop, D.R. 2007. p63 induces key target genes required for epidermal morphogenesis. *Proc Natl Acad Sci U S A*. **104**(9), pp.3255-3260.
- Kou, C., Zhou, T., Han, X., Zhuang, H. and Qian, H. 2015. LRIG1, a 3p tumor suppressor, represses EGFR signaling and is a novel epigenetic silenced gene in colorectal cancer. *Biochem Biophys Res Commun*. **464**(2), pp.519-525.

- Krawczyk, E., Hanover, J.A., Schlegel, R. and Suprynowicz, F.A. 2008. Karyopherin beta 3: A new cellular target for the HPV-16 E5 oncoprotein. *Biochemical and Biophysical Research Communications*. **371**(4), pp.684-688.
- Krawczyk, E., Suprynowicz, F.A., Hebert, J.D., Kamonjoh, C.M. and Schlegel, R. 2011. The Human Papillomavirus Type 16 E5 Oncoprotein Translocates Calpactin I to the Perinuclear Region. *Journal of Virology*. **85**(21), pp.10968-10975.
- Kreimer, A.R., Clifford, G.M., Boyle, P. and Franceschi, S. 2005. Human papillomavirus types in head and neck squamous cell carcinomas worldwide: a systematic review. *Cancer Epidemiol Biomarkers Prev*. **14**(2), pp.467-475.
- Krupovic, M. 2013. Networks of evolutionary interactions underlying the polyphyletic origin of ssDNA viruses. *Curr Opin Virol*. **3**(5), pp.578-586.
- Kumar, S., Biswas, M. and Jose, T. 2015. HPV vaccine: Current status and future directions. *Med J Armed Forces India*. **71**(2), pp.171-177.
- Kämper, N., Day, P.M., Nowak, T., Selinka, H.C., Florin, L., Bolscher, J., Hilbig, L., Schiller, J.T. and Sapp, M. 2006. A membrane-destabilizing peptide in capsid protein L2 is required for egress of papillomavirus genomes from endosomes. *J Virol*. **80**(2), pp.759-768.
- Laurikkala, J., Mikkola, M.L., James, M., Tummers, M., Mills, A.A. and Thesleff, I. 2006. p63 regulates multiple signalling pathways required for ectodermal organogenesis and differentiation. *Development*. **133**(8), pp.1553-1563.
- LeBleu, V.S., Macdonald, B. and Kalluri, R. 2007. Structure and function of basement membranes. *Exp Biol Med (Maywood)*. **232**(9), pp.1121-1129.
- Lechler, T. and Fuchs, E. 2005. Asymmetric cell divisions promote stratification and differentiation of mammalian skin. *Nature*. **437**(7056), pp.275-280.
- Lee, B., Lee, T.H. and Shim, J. 2017. Emerin suppresses Notch signaling by restricting the Notch intracellular domain to the nuclear membrane. *Biochim Biophys Acta Mol Cell Res*. **1864**(2), pp.303-313.
- Lee, C. and Laimins, L.A. 2004. Role of the PDZ domain-binding motif of the oncoprotein E6 in the pathogenesis of human papillomavirus type 31. *J Virol*. **78**(22), pp.12366-12377.
- Lee, H.J., Kang, S.J., Lee, K. and Im, H. 2011. Human  $\alpha$ -synuclein modulates vesicle trafficking through its interaction with prenylated Rab acceptor protein 1. *Biochem Biophys Res Commun*. **412**(4), pp.526-531.
- Lee, M.H., Jung, C., Lee, J., Kim, S.Y., Lee, Y. and Hwang, I. 2011. An Arabidopsis prenylated Rab acceptor 1 isoform, AtPRA1.B6, displays differential inhibitory effects on anterograde trafficking of proteins at the endoplasmic reticulum. *Plant Physiol*. **157**(2), pp.645-658.
- Lee, S.G., Su, Z.Z., Emdad, L., Sarkar, D., Franke, T.F. and Fisher, P.B. 2008. Astrocyte elevated gene-1 activates cell survival pathways through PI3K-Akt signaling. *Oncogene*. **27**(8), pp.1114-1121.

- Leechanachai, P., Banks, L., Moreau, F. and Matlashewski, G. 1992. The E5 gene from human papillomavirus type 16 is an oncogene which enhances growth factor-mediated signal transduction to the nucleus. *Oncogene*. **7**(1), pp.19-25.
- Lehto, M., Mäyränpää, M.I., Pellinen, T., Ihalmo, P., Lehtonen, S., Kovanen, P.T., Groop, P.H., Ivaska, J. and Olkkonen, V.M. 2008. The R-Ras interaction partner ORP3 regulates cell adhesion. *J Cell Sci*. **121**(Pt 5), pp.695-705.
- Lewis, C., Baro, M.F., Marques, M., Grüner, M., Alonso, A. and Bravo, I.G. 2008. The first hydrophobic region of the HPV16 E5 protein determines protein cellular location and facilitates anchorage-independent growth. *Virology*. **5**, p30.
- Li, C.P., Zhu, Y.J., Chen, R., Wu, W., Li, A.P., Liu, J., Liu, Q.Z., Wei, Q.Y., Zhang, Z.D. and Zhou, J.W. 2007. Functional polymorphisms of JWA gene are associated with risk of bladder cancer. *J Toxicol Environ Health A*. **70**(11), pp.876-884.
- Li, H., Zhan, T., Li, C., Liu, M. and Wang, Q.K. 2009. Repression of MHC class I transcription by HPV16E7 through interaction with a putative RXRbeta motif and NF-kappaB cytoplasmic sequestration. *Biochem Biophys Res Commun*. **388**(2), pp.383-388.
- Li, L.Y., Shih, H.M., Liu, M.Y. and Chen, J.Y. 2001. The cellular protein PRA1 modulates the anti-apoptotic activity of Epstein-Barr virus BHRF1, a homologue of Bcl-2, through direct interaction. *J Biol Chem*. **276**(29), pp.27354-27362.
- Li, S.X., Liu, L.J., Dong, L.W., Shi, H.G., Pan, Y.F., Tan, Y.X., Zhang, J., Zhang, B., Ding, Z.W., Jiang, T.Y., Hu, H.P. and Wang, H.Y. 2014a. CKAP4 inhibited growth and metastasis of hepatocellular carcinoma through regulating EGFR signaling. *Tumour Biol*. **35**(8), pp.7999-8005.
- Li, S.X., Tang, G.S., Zhou, D.X., Pan, Y.F., Tan, Y.X., Zhang, J., Zhang, B., Ding, Z.W., Liu, L.J., Jiang, T.Y., Hu, H.P., Dong, L.W. and Wang, H.Y. 2014b. Prognostic significance of cytoskeleton-associated membrane protein 4 and its palmitoyl acyltransferase DHHC2 in hepatocellular carcinoma. *Cancer*. **120**(10), pp.1520-1531.
- Li, Y., Wang, Y., Kim, E., Beemiller, P., Wang, C.Y., Swanson, J., You, M. and Guan, K.L. 2007. Bnip3 mediates the hypoxia-induced inhibition on mammalian target of rapamycin by interacting with Rheb. *J Biol Chem*. **282**(49), pp.35803-35813.
- Liang, C., Ding, J., Yang, Y., Deng, L. and Li, X. 2017. MicroRNA-433 inhibits cervical cancer progression by directly targeting metadherin to regulate the AKT and  $\beta$ -catenin signalling pathways. *Oncol Rep*. **38**(6), pp.3639-3649.
- Liang, Y.J., Chang, H.S., Wang, C.Y. and Yu, W.C. 2008. DYRK1A stabilizes HPV16E7 oncoprotein through phosphorylation of the threonine 5 and threonine 7 residues. *Int J Biochem Cell Biol*. **40**(11), pp.2431-2441.
- Liang, Z. and Li, G. 2000. Mouse prenylated Rab acceptor is a novel Golgi membrane protein. *Biochem Biophys Res Commun*. **275**(2), pp.509-516.
- Liang, Z., Veeraprame, H., Bayan, N. and Li, G. 2004. The C-terminus of prenylin is important in forming a dimer conformation necessary for endoplasmic-reticulum-to-Golgi transport. *Biochem J*. **380**(Pt 1), pp.43-49.

- Lin, C.I., Orlov, I., Ruggiero, A.M., Dykes-Hoberg, M., Lee, A., Jackson, M. and Rothstein, J.D. 2001. Modulation of the neuronal glutamate transporter EAAC1 by the interacting protein GTRAP3-18. *Nature*. **410**(6824), pp.84-88.
- Lin, F., Morrison, J.M., Wu, W. and Worman, H.J. 2005. MAN1, an integral protein of the inner nuclear membrane, binds Smad2 and Smad3 and antagonizes transforming growth factor-beta signaling. *Hum Mol Genet*. **14**(3), pp.437-445.
- Lin, J., Liang, Z., Zhang, Z. and Li, G. 2001. Membrane topography and topogenesis of prenylated Rab acceptor (PRA1). *J Biol Chem*. **276**(45), pp.41733-41741.
- Liu, H.P., Wu, C.C. and Chang, Y.S. 2006. PRA1 promotes the intracellular trafficking and NF-kappaB signaling of EBV latent membrane protein 1. *EMBO J*. **25**(17), pp.4120-4130.
- Liu, H.P., Wu, C.C., Kao, H.Y., Huang, Y.C., Liang, Y., Chen, C.C., Yu, J.S. and Chang, Y.S. 2011. Proteome-wide dysregulation by PRA1 depletion delineates a role of PRA1 in lipid transport and cell migration. *Mol Cell Proteomics*. **10**(3), pM900641MCP900200.
- Liu, J., Wang, C., Ma, X., Tian, Y., Fu, Y. and Luo, Y. 2019. High expression of CCR5 in melanoma enhances epithelial-mesenchymal transition and metastasis via TGFβ1. *J Pathol*. **247**(4), pp.481-493.
- Longworth, M.S. and Laimins, L.A. 2004. Pathogenesis of human papillomaviruses in differentiating epithelia. *Microbiol Mol Biol Rev*. **68**(2), pp.362-372.
- Lu, J., Chew, E.H. and Holmgren, A. 2007. Targeting thioredoxin reductase is a basis for cancer therapy by arsenic trioxide. *Proc Natl Acad Sci U S A*. **104**(30), pp.12288-12293.
- Lu, J., Tang, Y., Farshidpour, M., Cheng, Y., Zhang, G., Jafarnejad, S.M., Yip, A., Martinka, M., Dong, Z., Zhou, J., Xu, J. and Li, G. 2013. JWA inhibits melanoma angiogenesis by suppressing ILK signaling and is an independent prognostic biomarker for melanoma. *Carcinogenesis*. **34**(12), pp.2778-2788.
- López-Bueno, A., Mavian, C., Labella, A.M., Castro, D., Borrego, J.J., Alcami, A. and Alejo, A. 2016. Concurrence of Iridovirus, Polyomavirus, and a Unique Member of a New Group of Fish Papillomaviruses in Lymphocystis Disease-Affected Gilthead Sea Bream. *J Virol*. **90**(19), pp.8768-8779.
- Machleidt, T., Geller, P., Schwandner, R., Scherer, G. and Krönke, M. 1998. Caspase 7-induced cleavage of kinectin in apoptotic cells. *FEBS Lett*. **436**(1), pp.51-54.
- Maier, S., Reiterer, V., Ruggiero, A.M., Rothstein, J.D., Thomas, S., Dahm, R., Sitte, H.H. and Farhan, H. 2009. GTRAP3-18 serves as a negative regulator of Rab1 in protein transport and neuronal differentiation. *J Cell Mol Med*. **13**(1), pp.114-124.
- Mammas, I.N., Sourvinos, G. and Spandidos, D.A. 2014. The paediatric story of human papillomavirus (Review). *Oncol Lett*. **8**(2), pp.502-506.
- Mansharamani, M. and Wilson, K.L. 2005. Direct binding of nuclear membrane protein MAN1 to emerin in vitro and two modes of binding to barrier-to-autointegration factor. *J Biol Chem*. **280**(14), pp.13863-13870.

- Mao, D., Lin, G., Tepe, B., Zuo, Z., Tan, K.L., Senturk, M., Zhang, S., Arenkiel, B.R., Sardiello, M. and Bellen, H.J. 2019. VAMP associated proteins are required for autophagic and lysosomal degradation by promoting a PtdIns4P-mediated endosomal pathway. *Autophagy*. **15**(7), pp.1214-1233.
- Mao, W.G., Liu, Z.L., Chen, R., Li, A.P. and Zhou, J.W. 2006. JWA is required for the antiproliferative and pro-apoptotic effects of all-trans retinoic acid in Hela cells. *Clin Exp Pharmacol Physiol*. **33**(9), pp.816-824.
- Markiewicz, E., Tilgner, K., Barker, N., van de Wetering, M., Clevers, H., Dorobek, M., Hausmanowa-Petrusewicz, I., Ramaekers, F.C., Broers, J.L., Blankesteyn, W.M., Salpingidou, G., Wilson, R.G., Ellis, J.A. and Hutchison, C.J. 2006. The inner nuclear membrane protein emerin regulates beta-catenin activity by restricting its accumulation in the nucleus. *EMBO J*. **25**(14), pp.3275-3285.
- Martin, L.G., Demers, G.W. and Galloway, D.A. 1998. Disruption of the G1/S transition in human papillomavirus type 16 E7-expressing human cells is associated with altered regulation of cyclin E. *J Virol*. **72**(2), pp.975-985.
- Martincic, I., Peralta, M.E. and Ngsee, J.K. 1997. Isolation and characterization of a dual prenylated Rab and VAMP2 receptor. *J Biol Chem*. **272**(43), pp.26991-26998.
- Marur, S., D'Souza, G., Westra, W.H. and Forastiere, A.A. 2010. HPV-associated head and neck cancer: a virus-related cancer epidemic. *Lancet Oncol*. **11**(8), pp.781-789.
- Massa, S., Paolini, F., Marino, C., Franconi, R. and Venuti, A. 2019. Bioproduction of a Therapeutic Vaccine Against Human Papillomavirus in Tomato Hairy Root Cultures. *Front Plant Sci*. **10**, p452.
- Matsuo, Y., Akiyama, N., Nakamura, H., Yodoi, J., Noda, M. and Kizaka-Kondoh, S. 2001. Identification of a novel thioredoxin-related transmembrane protein. *J Biol Chem*. **276**(13), pp.10032-10038.
- Maufort, J.P., Williams, S.M., Pitot, H.C. and Lambert, P.F. 2007. Human papillomavirus 16 E5 oncogene contributes to two stages of skin carcinogenesis. *Cancer Res*. **67**(13), pp.6106-6112.
- McBride, A.A. 2013. The papillomavirus E2 proteins. *Virology*. **445**(1-2), pp.57-79.
- McCune, B.T., Tang, W., Lu, J., Eaglesham, J.B., Thorne, L., Mayer, A.E., Condiff, E., Nice, T.J., Goodfellow, I., Krezel, A.M. and Virgin, H.W. 2017. Noroviruses Co-opt the Function of Host Proteins VAPA and VAPB for Replication via a Phenylalanine-Phenylalanine-Acidic-Tract-Motif Mimic in Nonstructural Viral Protein NS1/2. *MBio*. **8**(4).
- McIntosh, P.B., Laskey, P., Sullivan, K., Davy, C., Wang, Q., Jackson, D.J., Griffin, H.M. and Doorbar, J. 2010. E1<sup>E4</sup>-mediated keratin phosphorylation and ubiquitylation: a mechanism for keratin depletion in HPV16-infected epithelium. *Journal of Cell Science*. **123**(16), p2810.
- McIntosh, P.B., Martin, S.R., Jackson, D.J., Khan, J., Isaacson, E.R., Calder, L., Raj, K., Griffin, H.M., Wang, Q., Laskey, P., Eccleston, J.F. and Doorbar, J. 2008. Structural Analysis Reveals an Amyloid Form of the Human Papillomavirus Type 16 E1<sup>E4</sup> Protein and Provides a Molecular Basis for Its Accumulation. *Journal of Virology*. **82**(16), p8196.

- Mechali, F., Hsu, C.Y., Castro, A., Lorca, T. and Bonne-Andrea, C. 2004. Bovine papillomavirus replicative helicase E1 is a target of the ubiquitin ligase APC. *J Virol.* **78**(5), pp.2615-2619.
- Mehanna, H., Beech, T., Nicholson, T., El-Hariry, I., McConkey, C., Paleri, V. and Roberts, S. 2013. Prevalence of human papillomavirus in oropharyngeal and nonoropharyngeal head and neck cancer--systematic review and meta-analysis of trends by time and region. *Head Neck.* **35**(5), pp.747-755.
- Melar-New, M. and Laimins, L.A. 2010. Human papillomaviruses modulate expression of microRNA 203 upon epithelial differentiation to control levels of p63 proteins. *J Virol.* **84**(10), pp.5212-5221.
- Menon, S., Rossi, R., Kariisa, M. and Callens, S. 2018. Determining the HPV vaccine schedule for a HIV-infected population in sub Saharan Africa, a commentary. *Viol J.* **15**(1), p129.
- Meshher, D., Panwar, K., Thomas, S.L., Edmundson, C., Choi, Y.H., Beddows, S. and Soldan, K. 2018. The Impact of the National HPV Vaccination Program in England Using the Bivalent HPV Vaccine: Surveillance of Type-Specific HPV in Young Females, 2010-2016. *J Infect Dis.* **218**(6), pp.911-921.
- Metsalu, T. and Vilo, J. 2015. ClustVis: a web tool for visualizing clustering of multivariate data using Principal Component Analysis and heatmap. *Nucleic Acids Res.* **43**(W1), pp.W566-570.
- Meyers, J., Ryndock, E., Conway, M.J., Meyers, C. and Robison, R. 2014. Susceptibility of high-risk human papillomavirus type 16 to clinical disinfectants. *J Antimicrob Chemother.* **69**(6), pp.1546-1550.
- Mills, A.A., Zheng, B., Wang, X.J., Vogel, H., Roop, D.R. and Bradley, A. 1999. p63 is a p53 homologue required for limb and epidermal morphogenesis. *Nature.* **398**(6729), pp.708-713.
- Miura, S., Kawana, K., Schust, D.J., Fujii, T., Yokoyama, T., Iwasawa, Y., Nagamatsu, T., Adachi, K., Tomio, A., Tomio, K., Kojima, S., Yasugi, T., Kozuma, S. and Taketani, Y. 2010. CD1d, a sentinel molecule bridging innate and adaptive immunity, is downregulated by the human papillomavirus (HPV) E5 protein: a possible mechanism for immune evasion by HPV. *J Virol.* **84**(22), pp.11614-11623.
- Moll, U.M. and Petrenko, O. 2003. The MDM2-p53 interaction. *Mol Cancer Res.* **1**(14), pp.1001-1008.
- Montecucco, A., Zanetta, F. and Biamonti, G. 2015. Molecular mechanisms of etoposide. *EXCLI J.* **14**, pp.95-108.
- Moody, C.A., Fradet-Turcotte, A., Archambault, J. and Laimins, L.A. 2007. Human papillomaviruses activate caspases upon epithelial differentiation to induce viral genome amplification. *Proc Natl Acad Sci U S A.* **104**(49), pp.19541-19546.
- Moreno-Layseca, P., Icha, J., Hamidi, H. and Ivaska, J. 2019. Integrin trafficking in cells and tissues. *Nat Cell Biol.* **21**(2), pp.122-132.
- Morgan, E.L. and Macdonald, A. 2019. Autocrine STAT3 activation in HPV positive cervical cancer through a virus-driven Rac1-NFκB-IL-6 signalling axis. *PLoS Pathog.* **15**(6), pe1007835.

- Morgan, E.L., Wasson, C.W., Hanson, L., Kealy, D., Pentland, I., McGuire, V., Scarpini, C., Coleman, N., Arthur, J.S.C., Parish, J.L., Roberts, S. and Macdonald, A. 2018. STAT3 activation by E6 is essential for the differentiation-dependent HPV18 life cycle. *PLoS Pathog.* **14**(4), pe1006975.
- Moscicki, A.B., Schiffman, M., Burchell, A., Albero, G., Giuliano, A.R., Goodman, M.T., Kjaer, S.K. and Palefsky, J. 2012. Updating the natural history of human papillomavirus and anogenital cancers. *Vaccine.* **30 Suppl 5**, pp.F24-33.
- Muller, M., Wasson, C.W., Bhatia, R., Boxall, S., Millan, D., Goh, G.Y.S., Haas, J., Stonehouse, N.J. and Macdonald, A. 2015. YIP1 family member 4 (YIPF4) is a novel cellular binding partner of the papillomavirus E5 proteins. *Scientific Reports.* **5**, p14.
- Muslimović, A., Nyström, S., Gao, Y. and Hammarsten, O. 2009. Numerical analysis of etoposide induced DNA breaks. *PLoS One.* **4**(6), pe5859.
- Mühr, L.S.A., Eklund, C. and Dillner, J. 2018. Towards quality and order in human papillomavirus research. *Virology.* **519**, pp.74-76.
- Müller, F. and Sapp, M. 1996. Domains of the E1 protein of human papillomavirus type 33 involved in binding to the E2 protein. *Virology.* **219**(1), pp.247-256.
- Müller, M.P. and Goody, R.S. 2018. Molecular control of Rab activity by GEFs, GAPs and GDI. *Small GTPases.* **9**(1-2), pp.5-21.
- Nakagawa, S. and Huibregtse, J.M. 2000. Human scribble (Vartul) is targeted for ubiquitin-mediated degradation by the high-risk papillomavirus E6 proteins and the E6AP ubiquitin-protein ligase. *Mol Cell Biol.* **20**(21), pp.8244-8253.
- Ng, I.C., Pawijit, P., Teo, L.Y., Li, H., Lee, S.Y. and Yu, H. 2016. Kinectin-dependent ER transport supports the focal complex maturation required for chemotaxis in shallow gradients. *J Cell Sci.* **129**(13), pp.2660-2672.
- Nguyen, B.C., Lefort, K., Mandinova, A., Antonini, D., Devgan, V., Della Gatta, G., Koster, M.I., Zhang, Z., Wang, J., Tommasi di Vignano, A., Kitajewski, J., Chiorino, G., Roop, D.R., Missero, C. and Dotto, G.P. 2006. Cross-regulation between Notch and p63 in keratinocyte commitment to differentiation. *Genes Dev.* **20**(8), pp.1028-1042.
- Nishimura, A.L., Mitne-Neto, M., Silva, H.C., Richieri-Costa, A., Middleton, S., Cascio, D., Kok, F., Oliveira, J.R., Gillingwater, T., Webb, J., Skehel, P. and Zatz, M. 2004. A mutation in the vesicle-trafficking protein VAPB causes late-onset spinal muscular atrophy and amyotrophic lateral sclerosis. *Am J Hum Genet.* **75**(5), pp.822-831.
- Oshikane, H., Watabe, M., Kikuchi-Utsumi, K. and Nakaki, T. 2018. Rab1a rescues the toxicity of PRAF3. *Biochem Biophys Rep.* **14**, pp.16-19.
- Ozbun, M.A. and Meyers, C. 1997. Characterization of late gene transcripts expressed during vegetative replication of human papillomavirus type 31b. *Journal of Virology.* **71**(7), p5161.
- Ozden, B., Gunduz, K., Gunhan, O. and Ozden, F.O. 2011. A Case Report of Focal Epithelial Hyperplasia (Heck's disease) with PCR Detection of Human Papillomavirus. *J Maxillofac Oral Surg.* **10**(4), pp.357-360.

- Pacini, L., Ceraolo, M.G., Venuti, A., Melita, G., Hasan, U.A., Accardi, R. and Tommasino, M. 2017. UV Radiation Activates Toll-Like Receptor 9 Expression in Primary Human Keratinocytes, an Event Inhibited by Human Papillomavirus 38 E6 and E7 Oncoproteins. *J Virol.* **91**(19).
- Palom, Y., Suresh Kumar, G., Tang, L.Q., Paz, M.M., Musser, S.M., Rockwell, S. and Tomasz, M. 2002. Relative toxicities of DNA cross-links and monoadducts: new insights from studies of decarbamoyl mitomycin C and mitomycin C. *Chem Res Toxicol.* **15**(11), pp.1398-1406.
- Parish, J.L., Bean, A.M., Park, R.B. and Androphy, E.J. 2006a. ChlR1 is required for loading papillomavirus E2 onto mitotic chromosomes and viral genome maintenance. *Mol Cell.* **24**(6), pp.867-876.
- Parish, J.L., Kowalczyk, A., Chen, H.T., Roeder, G.E., Sessions, R., Buckle, M. and Gaston, K. 2006b. E2 proteins from high- and low-risk human papillomavirus types differ in their ability to bind p53 and induce apoptotic cell death. *J Virol.* **80**(9), pp.4580-4590.
- Park, H., Lee, S.W., Lee, I.H., Ryu, H.M., Cho, A.R., Kang, Y.S., Hong, S.R., Kim, S.S., Seong, S.J., Shin, S.M. and Kim, T.J. 2012. Rate of vertical transmission of human papillomavirus from mothers to infants: relationship between infection rate and mode of delivery. *Virol J.* **9**, p80.
- Partridge, M.A. and Marcantonio, E.E. 2006. Initiation of attachment and generation of mature focal adhesions by integrin-containing filopodia in cell spreading. *Mol Biol Cell.* **17**(10), pp.4237-4248.
- Patel, D., Huang, S.M., Baglia, L.A. and McCance, D.J. 1999. The E6 protein of human papillomavirus type 16 binds to and inhibits co-activation by CBP and p300. *EMBO J.* **18**(18), pp.5061-5072.
- PaVE. 2016. *Papillomavirus Episteme (PaVE)*. [Online]. Available from: <http://pave.niaid.nih.gov/#home>
- Paz, M.M., Zhang, X., Lu, J. and Holmgren, A. 2012. A new mechanism of action for the anticancer drug mitomycin C: mechanism-based inhibition of thioredoxin reductase. *Chem Res Toxicol.* **25**(7), pp.1502-1511.
- Peralta-Zaragoza, O., Bermúdez-Morales, V.H., Pérez-Plasencia, C., Salazar-León, J., Gómez-Cerón, C. and Madrid-Marina, V. 2012. Targeted treatments for cervical cancer: a review. *Oncol Targets Ther.* **5**, pp.315-328.
- Peto, J., Gilham, C., Fletcher, O. and Matthews, F.E. 2004. The cervical cancer epidemic that screening has prevented in the UK. *Lancet.* **364**(9430), pp.249-256.
- PHE. 2016. *Cervical screening: programme and colposcopy management*. [Online]. [Accessed 03.09.2019]. Available from: <https://www.gov.uk/government/publications/cervical-screening-programme-and-colposcopy-management>
- PHE. 2019. *Cervical screening: coverage by CCG and GP practice March 2019*. [Online]. [Accessed 02.09.2019]. Available from: <https://www.gov.uk/government/publications/cervical-screening-coverage-and-data>
- Pim, D., Collins, M. and Banks, L. 1992. HUMAN PAPILOMAVIRUS TYPE-16 E5 GENE STIMULATES THE TRANSFORMING ACTIVITY OF THE EPIDERMAL GROWTH-FACTOR RECEPTOR. *Oncogene.* **7**(1), pp.27-32.

- Pisoni, G.B., Ruddock, L.W., Bulleid, N. and Molinari, M. 2015. Division of labor among oxidoreductases: TMX1 preferentially acts on transmembrane polypeptides. *Mol Biol Cell*. **26**(19), pp.3390-3400.
- Pizarro, L., Leibman-Markus, M., Schuster, S., Bar, M., Meltz, T. and Avni, A. 2018. Tomato Prenylated RAB Acceptor Protein 1 Modulates Trafficking and Degradation of the Pattern Recognition Receptor LeEIX2, Affecting the Innate Immune Response. *Front Plant Sci*. **9**, p257.
- Pohthipornthawat, N., Feldman, S., Granter, S.R., Laga, A.C., Crum, C.P. and Herfs, M. 2018. Epidermodysplasia Verruciformis-like HPV Infection of the Vulva in Immunosuppressed Women. *Int J Gynecol Pathol*. **37**(3), pp.233-238.
- Popa, A., Zhang, W., Harrison, M.S., Goodner, K., Kazakov, T., Goodwin, E.C., Lipovsky, A., Burd, C.G. and DiMaio, D. 2015. Direct binding of retromer to human papillomavirus type 16 minor capsid protein L2 mediates endosome exit during viral infection. *PLoS Pathog*. **11**(2), pe1004699.
- Przybyszewska, J., Zlotogorski, A. and Ramot, Y. 2017. Re-evaluation of epidermodysplasia verruciformis: Reconciling more than 90 years of debate. *J Am Acad Dermatol*. **76**(6), pp.1161-1175.
- Purpura, V., Belleudi, F., Caputo, S. and Torrisi, M.R. 2013. HPV16 E5 and KGFR/FGFR2b interplay in differentiating epithelial cells. *Oncotarget*. **4**(2), pp.192-205.
- Qi, R., Xu, N., Wang, G., Ren, H., Li, S., Lei, J., Lin, Q., Wang, L., Gu, X., Zhang, H., Jiang, Q. and Zhang, C. 2015. The lamin-A/C-LAP2 $\alpha$ -BAF1 protein complex regulates mitotic spindle assembly and positioning. *J Cell Sci*. **128**(15), pp.2830-2841.
- Qian, Z., Wei, B., Zhou, Y., Wang, Q., Wang, J., Sun, Y., Gao, Y. and Chen, X. 2019. PRAF2 overexpression predicts poor prognosis and promotes tumorigenesis in esophageal squamous cell carcinoma. *BMC Cancer*. **19**(1), p585.
- Quinlan, E.J., Culleton, S.P., Wu, S.Y., Chiang, C.M. and Androphy, E.J. 2013. Acetylation of conserved lysines in bovine papillomavirus E2 by p300. *J Virol*. **87**(3), pp.1497-1507.
- Raff, A.B., Woodham, A.W., Raff, L.M., Skeate, J.G., Yan, L., Da Silva, D.M., Schelhaas, M. and Kast, W.M. 2013. The evolving field of human papillomavirus receptor research: a review of binding and entry. *J Virol*. **87**(11), pp.6062-6072.
- Raikhy, G., Woodby, B.L., Scott, M.L., Shin, G., Myers, J.E., Scott, R.S. and Bodily, J.M. 2019. Suppression of stromal interferon signaling by human papillomavirus type 16. *J Virol*.
- Raimondi, A., Ferguson, S.M., Lou, X., Armbruster, M., Paradise, S., Giovedi, S., Messa, M., Kono, N., Takasaki, J., Cappello, V., O'Toole, E., Ryan, T.A. and De Camilli, P. 2011. Overlapping role of dynamin isoforms in synaptic vesicle endocytosis. *Neuron*. **70**(6), pp.1100-1114.
- Ranieri, D., Belleudi, F., Magenta, A. and Torrisi, M.R. 2015. HPV16 E5 expression induces switching from FGFR2b to FGFR2c and epithelial-mesenchymal transition. *Int J Cancer*. **137**(1), pp.61-72.
- Rector, A., Lemey, P., Tachezy, R., Mostmans, S., Ghim, S.J., Van Doorslaer, K., Roelke, M., Bush, M., Montali, R.J., Joslin, J., Burk, R.D., Jenson, A.B., Sundberg, J.P., Shapiro, B. and Van Ranst, M. 2007. Ancient papillomavirus-host co-speciation in Felidae. *Genome Biol*. **8**(4), pR57.

- Rector, A. and Van Ranst, M. 2013. Animal papillomaviruses. *Virology*. **445**(1-2), pp.213-223.
- Regan, J.A. and Laimins, L.A. 2008. Bap31 Is a Novel Target of the Human Papillomavirus E5 Protein. *Journal of Virology*. **82**(20), pp.10042-10051.
- Rodríguez, M.I., Finbow, M.E. and Alonso, A. 2000. Binding of human papillomavirus 16 E5 to the 16 kDa subunit c (proteolipid) of the vacuolar H<sup>+</sup>-ATPase can be dissociated from the E5-mediated epidermal growth factor receptor overactivation. *Oncogene*. **19**(33), pp.3727-3732.
- Rodríguez, M.I., Finbow, M.E. and Alonso, A. 2000. Binding of human papillomavirus 16 E5 to the 16 kDa subunit c (proteolipid) of the vacuolar H<sup>+</sup>-ATPase can be dissociated from the E5-mediated epidermal growth factor receptor overactivation. *Oncogene*. **19**(33), pp.3727-3732.
- Rogers, H.D., Macgregor, J.L., Nord, K.M., Tyring, S., Rady, P., Engler, D.E. and Grossman, M.E. 2009. Acquired epidermodysplasia verruciformis. *J Am Acad Dermatol*. **60**(2), pp.315-320.
- Rollison, D.E., Viarasio, D., Amorrortu, R.P., Gheit, T. and Tommasino, M. 2019. An Emerging Issue in Oncogenic Virology: the Role of Beta Human Papillomavirus Types in the Development of Cutaneous Squamous Cell Carcinoma. *J Virol*. **93**(7).
- Roman, A. and Munger, K. 2013. The papillomavirus E7 proteins. *Virology*. **445**(1-2), pp.138-168.
- Romano, R.A., Smalley, K., Magraw, C., Serna, V.A., Kurita, T., Raghavan, S. and Sinha, S. 2012.  $\Delta$ Np63 knockout mice reveal its indispensable role as a master regulator of epithelial development and differentiation. *Development*. **139**(4), pp.772-782.
- Roux, K.J., Kim, D.I. and Burke, B. 2013. BioID: a screen for protein-protein interactions. *Curr Protoc Protein Sci*. **74**, pUnit 19.23.
- Roux, K.J., Kim, D.I., Raida, M. and Burke, B. 2012. A promiscuous biotin ligase fusion protein identifies proximal and interacting proteins in mammalian cells. *J Cell Biol*. **196**(6), pp.801-810.
- Rozenblatt-Rosen, O., Deo, R.C., Padi, M., Adelmant, G., Calderwood, M.A., Rolland, T., Grace, M., Dricot, A., Askenazi, M., Tavares, M., Pevzner, S.J., Abderazzaq, F., Byrdsong, D., Carvunis, A.R., Chen, A.A., Cheng, J., Correll, M., Duarte, M., Fan, C., Feltkamp, M.C., Ficarro, S.B., Franchi, R., Garg, B.K., Gulbahce, N., Hao, T., Holthaus, A.M., James, R., Korkhin, A., Litovchick, L., Mar, J.C., Pak, T.R., Rabello, S., Rubio, R., Shen, Y., Singh, S., Spangle, J.M., Tasan, M., Wanamaker, S., Webber, J.T., Roecklein-Canfield, J., Johannsen, E., Barabási, A.L., Beroukhim, R., Kieff, E., Cusick, M.E., Hill, D.E., Münger, K., Marto, J.A., Quackenbush, J., Roth, F.P., DeCaprio, J.A. and Vidal, M. 2012. Interpreting cancer genomes using systematic host network perturbations by tumour virus proteins. *Nature*. **487**(7408), pp.491-495.
- Ruggiero, A.M., Liu, Y., Vidensky, S., Maier, S., Jung, E., Farhan, H., Robinson, M.B., Sitte, H.H. and Rothstein, J.D. 2008. The endoplasmic reticulum exit of glutamate transporter is regulated by the inducible mammalian Yip6b/GTRAP3-18 protein. *J Biol Chem*. **283**(10), pp.6175-6183.
- Ryndock, E.J. and Meyers, C. 2014. A risk for non-sexual transmission of human papillomavirus? *Expert Rev Anti Infect Ther*. **12**(10), pp.1165-1170.
- Sabeena, S., Bhat, P., Kamath, V. and Arunkumar, G. 2017. Possible non-sexual modes of transmission of human papilloma virus. *J Obstet Gynaecol Res*. **43**(3), pp.429-435.

- Sahab, Z., Sudarshan, S.R., Liu, X., Zhang, Y., Kirilyuk, A., Kamonjoh, C.M., Simic, V., Dai, Y., Byers, S.W., Doorbar, J., Suprynowicz, F.A. and Schlegel, R. 2012. Quantitative measurement of human papillomavirus type 16 e5 oncoprotein levels in epithelial cell lines by mass spectrometry. *J Virol.* **86**(17), pp.9465-9473.
- Sales, K.J., Adefuye, A., Nicholson, L. and Katz, A.A. 2014. CCR5 expression is elevated in cervical cancer cells and is up-regulated by seminal plasma. *Mol Hum Reprod.* **20**(11), pp.1144-1157.
- Sanclemente, G. and Gill, D.K. 2002. Human papillomavirus molecular biology and pathogenesis. *J Eur Acad Dermatol Venereol.* **16**(3), pp.231-240.
- Santesso, N., Mustafa, R.A., Schünemann, H.J., Arbyn, M., Blumenthal, P.D., Cain, J., Chirenje, M., Denny, L., De Vuyst, H., Eckert, L.O., Forhan, S.E., Franco, E.L., Gage, J.C., Garcia, F., Herrero, R., Jeronimo, J., Lu, E.R., Luciani, S., Quek, S.C., Sankaranarayanan, R., Tsu, V., Broutet, N. and Group, G.S. 2016. World Health Organization Guidelines for treatment of cervical intraepithelial neoplasia 2-3 and screen-and-treat strategies to prevent cervical cancer. *Int J Gynaecol Obstet.* **132**(3), pp.252-258.
- Santos, M.F., Rappa, G., Karbanová, J., Kurth, T., Corbeil, D. and Lorico, A. 2018. VAMP-associated protein-A and oxysterol-binding protein-related protein 3 promote the entry of late endosomes into the nucleoplasmic reticulum. *J Biol Chem.* **293**(36), pp.13834-13848.
- Sapp, M. and Bienkowska-Haba, M. 2009. Viral entry mechanisms: human papillomavirus and a long journey from extracellular matrix to the nucleus. *FEBS J.* **276**(24), pp.7206-7216.
- Sarkar, D., Park, E.S., Emdad, L., Lee, S.G., Su, Z.Z. and Fisher, P.B. 2008. Molecular basis of nuclear factor-kappaB activation by astrocyte elevated gene-1. *Cancer Res.* **68**(5), pp.1478-1484.
- Scheffer, K.D., Gawlitza, A., Spoden, G.A., Zhang, X.A., Lambert, C., Berditchevski, F. and Florin, L. 2013. Tetraspanin CD151 mediates papillomavirus type 16 endocytosis. *J Virol.* **87**(6), pp.3435-3446.
- Scheffner, M., Huibregtse, J.M., Vierstra, R.D. and Howley, P.M. 1993. The HPV-16 E6 and E6-AP complex functions as a ubiquitin-protein ligase in the ubiquitination of p53. *Cell.* **75**(3), pp.495-505.
- Schembri, L., Dalibart, R., Tomasello, F., Legembre, P., Ichas, F. and De Giorgi, F. 2007. The HA tag is cleaved and loses immunoreactivity during apoptosis. *Nat Methods.* **4**(2), pp.107-108.
- Schiller, J.T. and Müller, M. 2015. Next generation prophylactic human papillomavirus vaccines. *Lancet Oncol.* **16**(5), pp.e217-225.
- Schneider, M.A., Spoden, G.A., Florin, L. and Lambert, C. 2011. Identification of the dynein light chains required for human papillomavirus infection. *Cell Microbiol.* **13**(1), pp.32-46.
- Schrevel, M., Gorter, A., Kolkman-Uljee, S.M., Trimbos, J.B., Fleuren, G.J. and Jordanova, E.S. 2011. Molecular mechanisms of epidermal growth factor receptor overexpression in patients with cervical cancer. *Mod Pathol.* **24**(5), pp.720-728.
- Schuck, S. and Stenlund, A. 2005. Role of papillomavirus E1 initiator dimerization in DNA replication. *J Virol.* **79**(13), pp.8661-8664.

- Schuck, S. and Stenlund, A. 2011. Mechanistic analysis of local ori melting and helicase assembly by the papillomavirus E1 protein. *Mol Cell*. **43**(5), pp.776-787.
- Schweizer, A., Ericsson, M., Bächli, T., Griffiths, G. and Hauri, H.P. 1993. Characterization of a novel 63 kDa membrane protein. Implications for the organization of the ER-to-Golgi pathway. *J Cell Sci*. **104 ( Pt 3)**, pp.671-683.
- Schweneker, M., Bachmann, A.S. and Moelling, K. 2005. JM4 is a four-transmembrane protein binding to the CCR5 receptor. *FEBS Lett*. **579**(7), pp.1751-1758.
- Scott, M.L., Coleman, D.T., Kelly, K.C., Carroll, J.L., Woodby, B., Songcock, W.K., Cardelli, J.A. and Bodily, J.M. 2018. Human papillomavirus type 16 E5-mediated upregulation of Met in human keratinocytes. *Virology*. **519**, pp.1-11.
- Selinka, H.C., Giroglou, T., Nowak, T., Christensen, N.D. and Sapp, M. 2003. Further evidence that papillomavirus capsids exist in two distinct conformations. *J Virol*. **77**(24), pp.12961-12967.
- Selvey, L.A., Dunn, L.A., Tindle, R.W., Park, D.S. and Frazer, I.H. 1994. Human papillomavirus (HPV) type 18 E7 protein is a short-lived steroid-inducible phosphoprotein in HPV-transformed cell lines. *J Gen Virol*. **75 ( Pt 7)**, pp.1647-1653.
- Shah, S.D., Doorbar, J. and Goldstein, R.A. 2010. Analysis of host-parasite incongruence in papillomavirus evolution using importance sampling. *Mol Biol Evol*. **27**(6), pp.1301-1314.
- Shao, J.B., Gao, Z.M., Huang, W.Y. and Lu, Z.B. 2017. The mechanism of epithelial-mesenchymal transition induced by TGF- $\beta$ 1 in neuroblastoma cells. *Int J Oncol*. **50**(5), pp.1623-1633.
- Shen, L., Xu, W., Li, A., Ye, J. and Zhou, J. 2011. JWA enhances As<sub>2</sub>O<sub>3</sub>-induced tubulin polymerization and apoptosis via p38 in HeLa and MCF-7 cells. *Apoptosis*. **16**(11), pp.1177-1193.
- Shi, G.Z., Yuan, Y., Jiang, G.J., Ge, Z.J., Zhou, J., Gong, D.J., Tao, J., Tan, Y.F. and Huang, S.D. 2012. PRAF3 induces apoptosis and inhibits migration and invasion in human esophageal squamous cell carcinoma. *BMC Cancer*. **12**, p97.
- Shin, H.J., Kwon, H.K., Lee, J.H., Anwar, M.A. and Choi, S. 2016. Etoposide induced cytotoxicity mediated by ROS and ERK in human kidney proximal tubule cells. *Sci Rep*. **6**, p34064.
- Shin, J.Y., Méndez-López, I., Wang, Y., Hays, A.P., Tanji, K., Lefkowitz, J.H., Schulze, P.C., Worman, H.J. and Dauer, W.T. 2013. Lamina-associated polypeptide-1 interacts with the muscular dystrophy protein emerin and is essential for skeletal muscle maintenance. *Dev Cell*. **26**(6), pp.591-603.
- Shin, M.K., Balsitis, S., Brake, T. and Lambert, P.F. 2009. Human papillomavirus E7 oncoprotein overrides the tumor suppressor activity of p21Cip1 in cervical carcinogenesis. *Cancer Res*. **69**(14), pp.5656-5663.
- Shinno, N., Kimura, H., Sada, R., Takiguchi, S., Mori, M., Fumoto, K., Doki, Y. and Kikuchi, A. 2018. Activation of the Dickkopf1-CKAP4 pathway is associated with poor prognosis of esophageal cancer and anti-CKAP4 antibody may be a new therapeutic drug. *Oncogene*. **37**(26), pp.3471-3484.

- Sicoli, D., Jiao, X., Ju, X., Velasco-Velazquez, M., Ertel, A., Addya, S., Li, Z., Andò, S., Fatatis, A., Paudyal, B., Cristofanilli, M., Thakur, M.L., Lisanti, M.P. and Pestell, R.G. 2014. CCR5 receptor antagonists block metastasis to bone of v-Src oncogene-transformed metastatic prostate cancer cell lines. *Cancer Res.* **74**(23), pp.7103-7114.
- Siddiqā, A., Broniarczyk, J. and Banks, L. 2018. Papillomaviruses and Endocytic Trafficking. *Int J Mol Sci.* **19**(9).
- Sivars, U., Aivazian, D. and Pfeffer, S.R. 2003. Yip3 catalyses the dissociation of endosomal Rab-GDI complexes. *Nature.* **425**(6960), pp.856-859.
- Skjerpén, C.S., Wesche, J. and Olsnes, S. 2002. Identification of ribosome-binding protein p34 as an intracellular protein that binds acidic fibroblast growth factor. *J Biol Chem.* **277**(26), pp.23864-23871.
- Smola-Hess, S., Pahne, J., Mauch, C., Zigrino, P., Smola, H. and Pfister, H.J. 2005. Expression of membrane type 1 matrix metalloproteinase in papillomavirus-positive cells: role of the human papillomavirus (HPV) 16 and HPV8 E7 gene products. *J Gen Virol.* **86**(Pt 5), pp.1291-1296.
- Song, H., Tian, Z., Qin, Y., Yao, G., Fu, S. and Geng, J. 2014. Astrocyte elevated gene-1 activates MMP9 to increase invasiveness of colorectal cancer. *Tumour Biol.* **35**(7), pp.6679-6685.
- Stanley, M. 2010. Pathology and epidemiology of HPV infection in females. *Gynecol Oncol.* **117**(2 Suppl), pp.S5-10.
- Stanley, M. 2016. Preventing cervical cancer and genital warts - How much protection is enough for HPV vaccines? *J Infect.* **72** Suppl, pp.S23-28.
- Stewart, D., Ghosh, A. and Matlashewski, G. 2005. Involvement of nuclear export in human papillomavirus type 18 E6-mediated ubiquitination and degradation of p53. *J Virol.* **79**(14), pp.8773-8783.
- Stier, E.A., Chigurupati, N.L. and Fung, L. 2016. Prophylactic HPV vaccination and anal cancer. *Hum Vaccin Immunother.* **12**(6), pp.1348-1351.
- Straight, S.W., Herman, B. and McCance, D.J. 1995. The E5 Oncoprotein Of Human Papillomavirus Type-16 Inhibits The Acidification Of Endosomes In Human Keratinocytes. *Journal of Virology.* **69**(5), pp.3185-3192.
- Straight, S.W., Hinkle, P.M., Jewers, R.J. and McCance, D.J. 1993. The E5 oncoprotein of human papillomavirus type 16 transforms fibroblasts and effects the downregulation of the epidermal growth factor receptor in keratinocytes. *Journal of Virology.* **67**(8), pp.4521-4532.
- Stratton, K.L. and Culkin, D.J. 2016. A Contemporary Review of HPV and Penile Cancer. *Oncology (Williston Park).* **30**(3), pp.245-249.
- Stray-Pedersen, A., Jouanguy, E., Crequer, A., Bertuch, A.A., Brown, B.S., Jhangiani, S.N., Muzny, D.M., Gambin, T., Sorte, H., Sasa, G., Metry, D., Campbell, J., Sockrider, M.M., Dishop, M.K., Scollard, D.M., Gibbs, R.A., Mace, E.M., Orange, J.S., Lupski, J.R., Casanova, J.L. and Noroski, L.M. 2014. Compound heterozygous CORO1A mutations in siblings with a mucocutaneous-immunodeficiency syndrome of epidermodysplasia verruciformis-HPV,

molluscum contagiosum and granulomatous tuberculoid leprosy. *J Clin Immunol.* **34**(7), pp.871-890.

Stubenrauch, F. and Laimins, L.A. 1999. Human papillomavirus life cycle: active and latent phases. *Semin Cancer Biol.* **9**(6), pp.379-386.

Supryniewicz, F.A., Krawczyk, E., Hebert, J.D., Sudarshan, S.R., Simic, V., Kamonjoh, C.M. and Schlegel, R. 2010. The human papillomavirus type 16 E5 oncoprotein inhibits epidermal growth factor trafficking independently of endosome acidification. *J Virol.* **84**(20), pp.10619-10629.

Tang, W.Y., Wang, L., Li, C., Hu, Z.B., Chen, R., Zhu, Y.J., Shen, H.B., Wei, Q.Y. and Zhou, J.W. 2007. Identification and functional characterization of JWA polymorphisms and their association with risk of gastric cancer and esophageal squamous cell carcinoma in a Chinese population. *J Toxicol Environ Health A.* **70**(11), pp.885-894.

Tang, Y., Liu, X., Su, B., Zhang, Z., Zeng, X., Lei, Y., Shan, J., Wu, Y., Tang, H. and Su, Q. 2015. microRNA-22 acts as a metastasis suppressor by targeting metadherin in gastric cancer. *Mol Med Rep.* **11**(1), pp.454-460.

Tatematsu, M., Funami, K., Ishii, N., Seya, T., Obuse, C. and Matsumoto, M. 2015. LRRC59 Regulates Trafficking of Nucleic Acid-Sensing TLRs from the Endoplasmic Reticulum via Association with UNC93B1. *J Immunol.* **195**(10), pp.4933-4942.

*The Scottish HPV Archive.* [Online]. Available from:

<https://www.ed.ac.uk/pathology/research/scottish-hpv-archive>

Thirkettle, H.J., Girling, J., Warren, A.Y., Mills, I.G., Sahadevan, K., Leung, H., Hamdy, F., Whitaker, H.C. and Neal, D.E. 2009. LYRIC/AEG-1 is targeted to different subcellular compartments by ubiquitinylation and intrinsic nuclear localization signals. *Clin Cancer Res.* **15**(9), pp.3003-3013.

Thomas, M. and Banks, L. 1998. Inhibition of Bak-induced apoptosis by HPV-18 E6. *Oncogene.* **17**(23), pp.2943-2954.

Thomas, M., Glaunsinger, B., Pim, D., Javier, R. and Banks, L. 2001. HPV E6 and MAGUK protein interactions: determination of the molecular basis for specific protein recognition and degradation. *Oncogene.* **20**(39), pp.5431-5439.

Thomas, M., Myers, M.P., Massimi, P., Guarnaccia, C. and Banks, L. 2016. Analysis of Multiple HPV E6 PDZ Interactions Defines Type-Specific PDZ Fingerprints That Predict Oncogenic Potential. *PLoS Pathog.* **12**(8), pe1005766.

Thomas, M.C. and Chiang, C.M. 2005. E6 oncoprotein represses p53-dependent gene activation via inhibition of protein acetylation independently of inducing p53 degradation. *Mol Cell.* **17**(2), pp.251-264.

Thul, P.J., Åkesson, L., Wiking, M., Mahdessian, D., Geladaki, A., Ait Blal, H., Alm, T., Asplund, A., Björk, L., Breckels, L.M., Bäckström, A., Danielsson, F., Fagerberg, L., Fall, J., Gatto, L., Gnann, C., Hober, S., Hjelmare, M., Johansson, F., Lee, S., Lindskog, C., Mulder, J., Mulvey, C.M., Nilsson, P., Oksvold, P., Rockberg, J., Schutten, R., Schwenk, J.M., Sivertsson, Å., Sjöstedt, E., Skogs, M., Stadler, C., Sullivan, D.P., Tegel, H., Winsnes, C., Zhang, C., Zwahlen, M., Mardinoglu, A., Pontén, F., von Feilitzen, K., Lilley, K.S., Uhlén, M. and Lundberg, E. 2017. A subcellular map of the human proteome. *Science.* **356**(6340).

- Titolo, S., Brault, K., Majewski, J., White, P.W. and Archambault, J. 2003. Characterization of the minimal DNA binding domain of the human papillomavirus e1 helicase: fluorescence anisotropy studies and characterization of a dimerization-defective mutant protein. *J Virol.* **77**(9), pp.5178-5191.
- Titolo, S., Pelletier, A., Sauvé, F., Brault, K., Wardrop, E., White, P.W., Amin, A., Cordingley, M.G. and Archambault, J. 1999. Role of the ATP-binding domain of the human papillomavirus type 11 E1 helicase in E2-dependent binding to the origin. *J Virol.* **73**(7), pp.5282-5293.
- Tiwari, S., Askari, J.A., Humphries, M.J. and Bulleid, N.J. 2011. Divalent cations regulate the folding and activation status of integrins during their intracellular trafficking. *J Cell Sci.* **124**(Pt 10), pp.1672-1680.
- Tomaić, V. 2016. Functional Roles of E6 and E7 Oncoproteins in HPV-Induced Malignancies at Diverse Anatomical Sites. *Cancers (Basel).* **8**(10).
- Tomaić, V., Pim, D. and Banks, L. 2009. The stability of the human papillomavirus E6 oncoprotein is E6AP dependent. *Virology.* **393**(1), pp.7-10.
- Tomakidi, P., Cheng, H., Kohl, A., Komposch, G. and Alonso, A. 2000. Modulation of the epidermal growth factor receptor by the human papillomavirus type 16 E5 protein in raft cultures of human keratinocytes. *Eur J Cell Biol.* **79**(6), pp.407-412.
- Tungteakkhun, S.S., Filippova, M., Fodor, N. and Duerksen-Hughes, P.J. 2010. The full-length isoform of human papillomavirus 16 E6 and its splice variant E6\* bind to different sites on the procaspase 8 death effector domain. *J Virol.* **84**(3), pp.1453-1463.
- Tusnády, G.E. and Simon, I. 1998. Principles governing amino acid composition of integral membrane proteins: application to topology prediction. *J Mol Biol.* **283**(2), pp.489-506.
- Tusnády, G.E. and Simon, I. 2001. The HMMTOP transmembrane topology prediction server. *Bioinformatics.* **17**(9), pp.849-850.
- Uhlen, M., Zhang, C., Lee, S., Sjöstedt, E., Fagerberg, L., Bidkhori, G., Benfeitas, R., Arif, M., Liu, Z., Edfors, F., Sanli, K., von Feilitzen, K., Oksvold, P., Lundberg, E., Hober, S., Nilsson, P., Mattsson, J., Schwenk, J.M., Brunnström, H., Glimelius, B., Sjöblom, T., Edqvist, P.H., Djureinovic, D., Micke, P., Lindskog, C., Mardinoglu, A. and Ponten, F. 2017. A pathology atlas of the human cancer transcriptome. *Science.* **357**(6352).
- Uhlén, M., Fagerberg, L., Hallström, B.M., Lindskog, C., Oksvold, P., Mardinoglu, A., Sivertsson, Å., Kampf, C., Sjöstedt, E., Asplund, A., Olsson, I., Edlund, K., Lundberg, E., Navani, S., Szgyarto, C.A., Odeberg, J., Djureinovic, D., Takanen, J.O., Hober, S., Alm, T., Edqvist, P.H., Berling, H., Tegel, H., Mulder, J., Rockberg, J., Nilsson, P., Schwenk, J.M., Hamsten, M., von Feilitzen, K., Forsberg, M., Persson, L., Johansson, F., Zwahlen, M., von Heijne, G., Nielsen, J. and Pontén, F. 2015. Proteomics. Tissue-based map of the human proteome. *Science.* **347**(6220), p1260419.
- V'kovski, P., Gerber, M., Kelly, J., Pfaender, S., Ebert, N., Braga Lagache, S., Simillion, C., Portmann, J., Stalder, H., Gaschen, V., Bruggmann, R., Stoffel, M.H., Heller, M., Dijkman, R. and Thiel, V. 2019. Determination of host proteins composing the microenvironment of coronavirus replicase complexes by proximity-labeling. *Elife.* **8**.
- Valdembri, D. and Serini, G. 2012. Regulation of adhesion site dynamics by integrin traffic. *Curr Opin Cell Biol.* **24**(5), pp.582-591.

- Van Doorslaer, K. 2013. Evolution of the papillomaviridae. *Virology*. **445**(1-2), pp.11-20.
- Van Doorslaer, K., Li, Z., Xirasagar, S., Maes, P., Kaminsky, D., Liou, D., Sun, Q., Kaur, R., Huyen, Y. and McBride, A.A. 2017. The Papillomavirus Episteme: a major update to the papillomavirus sequence database. *Nucleic Acids Res.* **45**(D1), pp.D499-D506.
- Van Itallie, C.M., Tietgens, A.J., Aponte, A., Fredriksson, K., Fanning, A.S., Gucek, M. and Anderson, J.M. 2014. Biotin ligase tagging identifies proteins proximal to E-cadherin, including lipoma preferred partner, a regulator of epithelial cell-cell and cell-substrate adhesion. *J Cell Sci.* **127**(Pt 4), pp.885-895.
- van Steensel, B. and Henikoff, S. 2000. Identification of in vivo DNA targets of chromatin proteins using tethered dam methyltransferase. *Nat Biotechnol.* **18**(4), pp.424-428.
- Vande Pol, S.B. and Klingelutz, A.J. 2013. Papillomavirus E6 oncoproteins. *Virology*. **445**(1-2), pp.115-137.
- Velasco-Velázquez, M., Jiao, X., De La Fuente, M., Pestell, T.G., Ertel, A., Lisanti, M.P. and Pestell, R.G. 2012. CCR5 antagonist blocks metastasis of basal breast cancer cells. *Cancer Res.* **72**(15), pp.3839-3850.
- Vento, M.T., Zazzu, V., Loffreda, A., Cross, J.R., Downward, J., Stoppelli, M.P. and Iaccarino, I. 2010. Praf2 is a novel Bcl-xL/Bcl-2 interacting protein with the ability to modulate survival of cancer cells. *PLoS One.* **5**(12), pe15636.
- Viarisio, D., Müller-Decker, K., Accardi, R., Robitaille, A., Dürst, M., Beer, K., Jansen, L., Flechtenmacher, C., Bozza, M., Harbottle, R., Voegelé, C., Ardin, M., Zavadil, J., Caldeira, S., Gissmann, L. and Tommasino, M. 2018. Beta HPV38 oncoproteins act with a hit-and-run mechanism in ultraviolet radiation-induced skin carcinogenesis in mice. *PLoS Pathog.* **14**(1), pe1006783.
- Vignal, E., Blangy, A., Martin, M., Gauthier-Rouvière, C. and Fort, P. 2001. Kinectin is a key effector of RhoG microtubule-dependent cellular activity. *Mol Cell Biol.* **21**(23), pp.8022-8034.
- Vuillier, F., Gaud, G., Guillemot, D., Commere, P.H., Pons, C. and Favre, M. 2014. Loss of the HPV-infection resistance EVER2 protein impairs NF-κB signaling pathways in keratinocytes. *PLoS One.* **9**(2), pe89479.
- Wakefield, L.M. and Stuelten, C. 2007. Keeping order in the neighborhood: new roles for TGFβ in maintaining epithelial homeostasis. *Cancer Cell.* **12**(4), pp.293-295.
- Wang, C.H., Liu, L.L., Liao, D.Z., Zhang, M.F., Fu, J., Lu, S.X., Chen, S.L., Wang, H., Cai, S.H., Zhang, C.Z., Zhang, H.Z. and Yun, J.P. 2018. PRAF2 expression indicates unfavorable clinical outcome in hepatocellular carcinoma. *Cancer Manag Res.* **10**, pp.2241-2248.
- Wang, G.L., Shi, X., Salisbury, E. and Timchenko, N.A. 2008. Regulation of apoptotic and growth inhibitory activities of C/EBPα in different cell lines. *Exp Cell Res.* **314**(7), pp.1626-1639.
- Wang, J.W. and Roden, R.B. 2013. L2, the minor capsid protein of papillomavirus. *Virology*. **445**(1-2), pp.175-186.

- Wang, N.P., Zhou, J.W., Li, A.P., Cao, H.X. and Wang, X.R. 2003. [The mechanism of JWA gene involved in oxidative stress of cells]. *Zhonghua Lao Dong Wei Sheng Zhi Ye Bing Za Zhi*. **21**(3), pp.212-215.
- Wang, Q., Chen, Q., Zhu, L., Chen, M., Xu, W., Panday, S., Wang, Z., Li, A., Røe, O.D., Chen, R., Wang, S., Zhang, R. and Zhou, J. 2017. JWA regulates TRAIL-induced apoptosis via MARCH8-mediated DR4 ubiquitination in cisplatin-resistant gastric cancer cells. *Oncogenesis*. **6**(7), pe353.
- Wang, Q., Kennedy, A., Das, P., McIntosh, P.B., Howell, S.A., Isaacson, E.R., Hinz, S.A., Davy, C. and Doorbar, J. 2009. Phosphorylation of the Human Papillomavirus Type 16 E1<sup>E4</sup> Protein at T57 by ERK Triggers a Structural Change That Enhances Keratin Binding and Protein Stability. *Journal of Virology*. **83**(8), p3668.
- Wang, S., Gong, Z., Chen, R., Liu, Y., Li, A., Li, G. and Zhou, J. 2009. JWA regulates XRCC1 and functions as a novel base excision repair protein in oxidative-stress-induced DNA single-strand breaks. *Nucleic Acids Res*. **37**(6), pp.1936-1950.
- Wang, X., Meyers, C., Wang, H.K., Chow, L.T. and Zheng, Z.M. 2011. Construction of a full transcription map of human papillomavirus type 18 during productive viral infection. *J Virol*. **85**(16), pp.8080-8092.
- Wang, Y., Pennock, S., Chen, X. and Wang, Z. 2002. Endosomal signaling of epidermal growth factor receptor stimulates signal transduction pathways leading to cell survival. *Mol Cell Biol*. **22**(20), pp.7279-7290.
- Wasson, C.W., Morgan, E.L., Müller, M., Ross, R.L., Hartley, M., Roberts, S. and Macdonald, A. 2017. Human papillomavirus type 18 E5 oncogene supports cell cycle progression and impairs epithelial differentiation by modulating growth factor receptor signalling during the virus life cycle. *Oncotarget*. **8**(61), pp.103581-103600.
- Watabe, M., Aoyama, K. and Nakaki, T. 2007. Regulation of glutathione synthesis via interaction between glutamate transport-associated protein 3-18 (GTRAP3-18) and excitatory amino acid carrier-1 (EAAC1) at plasma membrane. *Mol Pharmacol*. **72**(5), pp.1103-1110.
- Watt, F.M. 1983. Involucrin and other markers of keratinocyte terminal differentiation. *J Invest Dermatol*. **81**(1 Suppl), pp.100s-103s.
- Weber-Boyvat, M., Kentala, H., Lilja, J., Vihervaara, T., Hanninen, R., Zhou, Y., Peränen, J., Nyman, T.A., Ivaska, J. and Olkkonen, V.M. 2015. OSBP-related protein 3 (ORP3) coupling with VAMP-associated protein A regulates R-Ras activity. *Exp Cell Res*. **331**(2), pp.278-291.
- Wechsler, E.I., Tugizov, S., Herrera, R., Da Costa, M. and Palefsky, J.M. 2018. E5 can be expressed in anal cancer and leads to epidermal growth factor receptor-induced invasion in a human papillomavirus 16-transformed anal epithelial cell line. *J Gen Virol*. **99**(5), pp.631-644.
- Weir, M.L., Xie, H., Klip, A. and Trimble, W.S. 2001. VAP-A binds promiscuously to both v- and tSNAREs. *Biochem Biophys Res Commun*. **286**(3), pp.616-621.
- Wetherill, L.F., Holmes, K.K., Verow, M., Müller, M., Howell, G., Harris, M., Fishwick, C., Stonehouse, N., Foster, R., Blair, G.E., Griffin, S. and Macdonald, A. 2012. High-risk human papillomavirus E5 oncoprotein displays channel-forming activity sensitive to small-molecule inhibitors. *J Virol*. **86**(9), pp.5341-5351.

- Wetherill, L.F., Wasson, C.W., Swinscoe, G., Kealy, D., Foster, R., Griffin, S. and Macdonald, A. 2018. Alkyl-imino sugars inhibit the pro-oncogenic ion channel function of human papillomavirus (HPV) E5. *Antiviral Res.* **158**, pp.113-121.
- Whelan, F., Stead, J.A., Shkumatov, A.V., Svergun, D.I., Sanders, C.M. and Antson, A.A. 2012. A flexible brace maintains the assembly of a hexameric replicative helicase during DNA unwinding. *Nucleic Acids Res.* **40**(5), pp.2271-2283.
- Wigle, J., Coast, E. and Watson-Jones, D. 2013. Human papillomavirus (HPV) vaccine implementation in low and middle-income countries (LMICs): health system experiences and prospects. *Vaccine.* **31**(37), pp.3811-3817.
- Williams, S.E., Beronja, S., Pasolli, H.A. and Fuchs, E. 2011. Asymmetric cell divisions promote Notch-dependent epidermal differentiation. *Nature.* **470**(7334), pp.353-358.
- Winer, R.L., Kiviat, N.B., Hughes, J.P., Adam, D.E., Lee, S.K., Kuypers, J.M. and Koutsky, L.A. 2005. Development and duration of human papillomavirus lesions, after initial infection. *J Infect Dis.* **191**(5), pp.731-738.
- Witchev, D.J., Witchev, N.B., Roth-Kauffman, M.M. and Kauffman, M.K. 2018. Plantar Warts: Epidemiology, Pathophysiology, and Clinical Management. *J Am Osteopath Assoc.* **118**(2), pp.92-105.
- Wu, X., Chen, H., Gao, Q., Bai, J., Wang, X., Zhou, J., Qiu, S., Xu, Y., Shi, Y. and Fan, J. 2014. Downregulation of JWA promotes tumor invasion and predicts poor prognosis in human hepatocellular carcinoma. *Mol Carcinog.* **53**(4), pp.325-336.
- Wu, Y., Wang, M., Peng, Y., Ding, Y., Deng, L. and Fu, Q. 2015. Overexpression of Arl6ip5 in osteoblast regulates RANKL subcellular localization. *Biochem Biophys Res Commun.* **464**(4), pp.1275-1281.
- Wu, Y., Yang, M., Fan, J., Peng, Y., Deng, L., Ding, Y., Yang, R., Zhou, J., Miao, D. and Fu, Q. 2014. Deficiency of osteoblastic Arl6ip5 impaired osteoblast differentiation and enhanced osteoclastogenesis via disturbance of ER calcium homeostasis and induction of ER stress-mediated apoptosis. *Cell Death Dis.* **5**, pe1464.
- Wu, Y.C., Bian, X.L., Heaton, P.R., Deyrieux, A.F. and Wilson, V.G. 2009. Host cell sumoylation level influences papillomavirus E2 protein stability. *Virology.* **387**(1), pp.176-183.
- Xian, H., Yang, S., Jin, S., Zhang, Y. and Cui, J. 2019. LRRC59 modulates type I interferon signaling by restraining the SQSTM1/p62-mediated autophagic degradation of pattern recognition receptor DDX58/RIG-I. *Autophagy.* pp.1-11.
- Xu, G., Xin, X. and Zheng, C. 2013. GPS2 is required for the association of NS5A with VAP-A and hepatitis C virus replication. *PLoS One.* **8**(11), pe78195.
- Xu, L., Cheng, L., Yang, F., Pei, B., Liu, X., Zhou, J., Zhu, Y. and Wang, S. 2018. JWA suppresses the invasion of human breast carcinoma cells by downregulating the expression of CXCR4. *Mol Med Rep.* **17**(6), pp.8137-8144.
- Xu, W., Chen, Q., Wang, Q., Sun, Y., Wang, S., Li, A., Xu, S., Røe, O.D., Wang, M., Zhang, R., Yang, L. and Zhou, J. 2014. JWA reverses cisplatin resistance via the CK2-XRCC1 pathway in human gastric cancer cells. *Cell Death Dis.* **5**, pe1551.

- Yanofsky, V.R., Patel, R.V. and Goldenberg, G. 2012. Genital warts: a comprehensive review. *J Clin Aesthet Dermatol.* **5**(6), pp.25-36.
- Yco, L.P., Geerts, D., Koster, J. and Bachmann, A.S. 2013. PRAF2 stimulates cell proliferation and migration and predicts poor prognosis in neuroblastoma. *Int J Oncol.* **42**(4), pp.1408-1416.
- Ye, F., Snider, A.K. and Ginsberg, M.H. 2014. Talin and kindlin: the one-two punch in integrin activation. *Front Med.* **8**(1), pp.6-16.
- Yoh, K. and Prywes, R. 2015. Pathway Regulation of p63, a Director of Epithelial Cell Fate. *Front Endocrinol (Lausanne).* **6**, p51.
- Yoo, B.K., Emdad, L., Su, Z.Z., Villanueva, A., Chiang, D.Y., Mukhopadhyay, N.D., Mills, A.S., Waxman, S., Fisher, R.A., Llovet, J.M., Fisher, P.B. and Sarkar, D. 2009. Astrocyte elevated gene-1 regulates hepatocellular carcinoma development and progression. *J Clin Invest.* **119**(3), pp.465-477.
- Yu, J.H., Lin, B.Y., Deng, W., Broker, T.R. and Chow, L.T. 2007. Mitogen-activated protein kinases activate the nuclear localization sequence of human papillomavirus type 11 E1 DNA helicase to promote efficient nuclear import. *J Virol.* **81**(10), pp.5066-5078.
- Zanier, K., Charbonnier, S., Sidi, A.O., McEwen, A.G., Ferrario, M.G., Poussin-Courmontagne, P., Cura, V., Brimer, N., Babah, K.O., Ansari, T., Muller, I., Stote, R.H., Cavarelli, J., Vande Pol, S. and Travé, G. 2013. Structural basis for hijacking of cellular LxxLL motifs by papillomavirus E6 oncoproteins. *Science.* **339**(6120), pp.694-698.
- Zerfass, K., Schulze, A., Spitkovsky, D., Friedman, V., Henglein, B. and Jansen-Dürr, P. 1995. Sequential activation of cyclin E and cyclin A gene expression by human papillomavirus type 16 E7 through sequences necessary for transformation. *J Virol.* **69**(10), pp.6389-6399.
- Zerfass-Thome, K., Zwerschke, W., Mannhardt, B., Tindle, R., Botz, J.W. and Jansen-Dürr, P. 1996. Inactivation of the cdk inhibitor p27KIP1 by the human papillomavirus type 16 E7 oncoprotein. *Oncogene.* **13**(11), pp.2323-2330.
- Zhang, B., Li, P., Wang, E., Brahmi, Z., Dunn, K.W., Blum, J.S. and Roman, A. 2003. The E5 protein of human papillomavirus type 16 perturbs MHC class II antigen maturation in human foreskin keratinocytes treated with interferon-gamma. *Virology.* **310**(1), pp.100-108.
- Zhang, B., Srirangam, A., Potter, D.A. and Roman, A. 2005. HPV16 E5 protein disrupts the c-Cbl-EGFR interaction and EGFR ubiquitination in human foreskin keratinocytes. *Oncogene.* **24**(15), pp.2585-2588.
- Zhang, S., Liu, L., Lv, Z., Li, Q., Gong, W. and Wu, H. 2017. MicroRNA-342-3p Inhibits the Proliferation, Migration, and Invasion of Osteosarcoma Cells by Targeting Astrocyte-Elevated Gene-1 (AEG-1). *Oncol Res.* **25**(9), pp.1505-1515.
- Zhang, X., Tee, Y.H., Heng, J.K., Zhu, Y., Hu, X., Margadant, F., Ballestrem, C., Bershady, A., Griffiths, G. and Yu, H. 2010. Kinectin-mediated endoplasmic reticulum dynamics supports focal adhesion growth in the cellular lamella. *J Cell Sci.* **123**(Pt 22), pp.3901-3912.
- Zhao, L., Wang, Y., Xue, Y., Lv, W., Zhang, Y. and He, S. 2015. Critical roles of chemokine receptor CCR5 in regulating glioblastoma proliferation and invasion. *Acta Biochim Biophys Sin (Shanghai).* **47**(11), pp.890-898.

Zheng, Z.M. and Baker, C.C. 2006. Papillomavirus genome structure, expression, and post-transcriptional regulation. *Front Biosci.* **11**, pp.2286-2302.

Zhou, C.X., Wang, C.L., Yu, A.L., Wang, Q.Y., Zhan, M.N., Tang, J., Gong, X.F., Yin, Q.Q., He, M., He, J.R., Chen, G.Q. and Zhao, Q. 2016. MiR-630 suppresses breast cancer progression by targeting metadherin. *Oncotarget.* **7**(2), pp.1288-1299.

Zhou, J., Doorbar, J., Sun, X.Y., Crawford, L.V., McLean, C.S. and Frazer, I.H. 1991. Identification of the nuclear localization signal of human papillomavirus type 16 L1 protein. *Virology.* **185**(2), pp.625-632.

Zhou, J., Ge, Z., Tan, Y., Jiang, G., Feng, J., Wang, H. and Shi, G. 2012. Downregulation of JWA expression in human esophageal squamous cell carcinoma and its clinical significance. *Oncol Res.* **20**(4), pp.157-162.

Zhou, J., Ye, J., Zhao, X. and Li, A. 2008. JWA is required for arsenic trioxide induced apoptosis in HeLa and MCF-7 cells via reactive oxygen species and mitochondria linked signal pathway. *Toxicol Appl Pharmacol.* **230**(1), pp.33-40.

Zhu, K., Dai, Z., Pan, Q., Wang, Z., Yang, G.H., Yu, L., Ding, Z.B., Shi, G.M., Ke, A.W., Yang, X.R., Tao, Z.H., Zhao, Y.M., Qin, Y., Zeng, H.Y., Tang, Z.Y., Fan, J. and Zhou, J. 2011. Metadherin promotes hepatocellular carcinoma metastasis through induction of epithelial-mesenchymal transition. *Clin Cancer Res.* **17**(23), pp.7294-7302.

Zhu, T., Chen, R., Li, A.P., Liu, J., Liu, Q.Z., Chang, H.C. and Zhou, J.W. 2005. Regulation of a novel cell differentiation-associated gene, JWA during oxidative damage in K562 and MCF-7 cells. *J Biomed Sci.* **12**(1), pp.219-227.

Zi, Z., Chapnick, D.A. and Liu, X. 2012. Dynamics of TGF- $\beta$ /Smad signaling. *FEBS Lett.* **586**(14), pp.1921-1928.

Zimmermann, H., Degenkolbe, R., Bernard, H.U. and O'Connor, M.J. 1999. The human papillomavirus type 16 E6 oncoprotein can down-regulate p53 activity by targeting the transcriptional coactivator CBP/p300. *J Virol.* **73**(8), pp.6209-6219.